# Exosome-Mediated Macrophage Reprogramming and Immune Regulation During Colorectal Cancer Progression

**Ph.D. Thesis**

By

**Khandu Wadhonkar**




**Mehta Family School of Biosciences and Biomedical Engineering**

**INDIAN INSTITUTE OF TECHNOLOGY INDORE**

**June, 2026**

# Exosome-Mediated Macrophage Reprogramming and Immune Regulation During Colorectal Cancer Progression

**A THESIS**

*Submitted in partial fulfillment of the*
*requirements for the award of the degree*
***of***
**DOCTOR OF PHILOSOPHY**

*by*

**Khandu Wadhonkar**

**Mehta Family School of Biosciences and Biomedical Engineering**
**INDIAN INSTITUTE OF TECHNOLOGY INDORE**

**June, 2026**

# INDIAN INSTITUTE OF TECHNOLOGY INDORE

I hereby certify that the work which is being presented in the thesis entitled **Exosome-Mediated Macrophage Reprogramming and Immune Regulation During Colorectal Cancer Progression** in the partial fulfillment of the requirements for the award of the degree of **DOCTOR OF PHILOSOPHY** and submitted in the **Mehta Family School of Biosciences and Biomedical Engineering, Indian Institute of Technology Indore**, is an authentic record of my own work carried out during the time period from May, 2021 to June, 2026, under the supervision of Dr. Mirza S Baig, Professor, Mehta Family School of Biosciences and Biomedical Engineering, IIT Indore.

The matter presented in this thesis has not been submitted by me for the award of any other degree of this or any other institute.

12.10.2026

**Signature of the student with date**
**Khandu Wadhonkar**

---

This is to certify that the above statement made by the candidate is correct to the best of my/our knowledge.

12-10-26

Signature of Thesis Supervisor with date
**Prof. (Dr.) Mirza S Baig**

---

**Khandu Wadhonkar** has successfully given his Ph.D. Oral Examination held on **12/10/2026**.

12-10-26

Signature of Thesis Supervisor with date
**Prof. (Dr.) Mirza S Baig**

---

-

# ACKNOWLEDGEMENTS

Behind every successful journey lies the guidance, encouragement, and support of many wonderful individuals. This thesis is not only the outcome of my academic effort, but also a reflection of the kindness, motivation, and constant support of everyone who walked beside me through every challenge and milestone of this journey. Today, I feel deeply privileged to express my gratitude and acknowledge all the people whose presence and support made this journey meaningful and memorable.

First and foremost, I express my deepest gratitude to my respected supervisor, **Prof. (Dr.) Mirza S. Baig,** for his constant guidance, encouragement, and belief in me throughout this journey. Working with Prof. Baig has been one of the most valuable experiences of my academic life. His approach to research and passion for science have left a lasting impact on me. When I joined the Indian Institute of Technology Indore as a Ph.D. scholar, I was very naive and uncertain about my abilities, but his guidance and belief in me helped me to grow as a researcher. I still remember his words that "we are fortunate to work in a field where science goes beyond discovery- allowing us to understand the challenges and suffering faced by society and use our research to contribute toward meaningful solutions." Those words influenced my prospects towards research and life. However, his continuous belief in my potential motivated me to overcome challenges, improve myself, and move forward with determination. His encouragement and trust played a significant role in giving me the confidence to complete this thesis successfully. I will be thankful for his mentorship and unwavering support throughout this memorable journey.

Further, I would also like to express my sincere thanks to my PSPC members - **Prof. Kiran Bala** and **Prof. Parimal Kar**- for their valuable insights, productive suggestions, and encouragement throughout my research. My heartfelt gratitude goes to the **Head of the Department** and the **DPGC convener** for their continuous support, academic

guidance, and encouragement. I am also extremely thankful to the **MFS-BSBE office staff - Mr. Amit Mishra**, **Mr. Arif Patel**, **and Mr. Gaurav Singh** - for their unfailing administrative support and timely help with all official procedures and documentation. I would like to express my special thanks to **Dr. Ravindra Kumar** from the **SIC Facility** for his expert assistance and guidance with confocal microscopy.

I remain grateful to **all my teachers** whose support and guidance accompanied me through my educational path, from my early schooling years to the present stage of my academic career.

I sincerely acknowledge my lab members, who have been an integral part of my PhD journey. I will always remain grateful to my senior, **Dr. Sajjan Rajpoot,** for his guidance, encouragement, and support during the early phase of my research journey. I would also like to acknowledge my lab colleagues, **Dr. Kundan Solanki** and **Mr. Pramod Patidar**, for their insightful discussions and valuable suggestions during the experimental work. A special mention goes to **Dr. Rajat Atre**, who joined the lab as my junior but gradually became like a younger brother to me. Hearing him call me "Bhau" has always been very special and close to my heart. Throughout my academic journey, I learned many things from him, not only in research but also in life. His constant support and encouragement during difficult times meant a lot to me, and I will always cherish the bond and memories we shared in the lab.

I also extend my sincere thanks to my lab fellows - **Mr. Rameez**, **Ms. Krishma**, **Mr. Anil**, **Mr. Shubham**, **Ms. Shreya**, **Mr. Rohit**, **Mr. Manveer**, and **Ms. Faaiza** for creating a friendly, cooperative, and joyful working environment. A special mention to **Ms. Faaiza** for her valuable collaborative support and teamwork during the research work. I am deeply thankful to **Mr. Lateefur Rehman Khan** and **Ms. Bushra** for their assistance and support in the lab. Their cooperative nature, technical help, and positive encouragement contributed to maintaining a productive research environment throughout my journey.

A special Thanks to **Dr. Suman Koirala** and **Mr. Sunanda Samanta** for always taking care of me and being like a true best friend throughout my journey. I want to thank my friends here at IIT Indore, **Mr. Kapil Ursal, Mr. Sibi Kartik, Ms. Sushma**, **Mrs. Raveena**, **Mrs. Sayali**, **Ms. Surbhi**, **Mr. Tileshwar Sahare**, **Mr. Pranit Bagde**, **Mr. Lekhnath**, **Mrs. Anshul**, **Ms. Meenakshi**, **Mr. Aritra Chakrabarty**, **Mr. Akshay Jangam**, **Mr. Satyam Sing**, and **Mr. Sayan Poddar**. They are more than friends; they are the ones who made my journey at IIT Indore truly memorable. I am also happy to acknowledge **Ms. Neha**, **Ms. Rigzin**, and **Mr. Abhishek,** who carried out their M.Sc. dissertation work with me. It was a wonderful experience and a pleasure to have the opportunity to train and work with them. Furthermore, I would like to acknowledge **Ms. Yashi**, **Mr. Soumalya**, **Ms. Ayushi**, **Ms. Shubhi**, **Mr. Rahul**, **Ms. Shivani**, **Mr. Shivmuni, Mr. Javed**, **Ms. Niharika,** and **Ms. Yusra.** I am thankful to each of them for being such an integral part of my life. Whenever I think about IIT Indore, their names are the first that come to mind, and they will always hold a special place in my heart.

Outside the boundary of academia, every journey is shaped by the silent strength of those who stand beside us. Mine would not have been possible without the support of my family. I want to express my deepest gratitude to my beloved family. I am especially grateful to my mother, **Mrs. Saraswati Wadhonkar,** and my father, **Mr. Digambar Wadhonkar**. Their relentless efforts, hard work, silent sacrifices, and lifelong dedication helped me to achieve my dreams and gave me the strength to reach this milestone. They never forced anything on me and allowed me to explore whatever I wanted to do. I hope I could do justice to all their hard work, patience, and love, which they poured into me, and never expected anything in return except my happiness. I would especially like to mention my brother, **Mr. Anil Wadhonkar,** to whom I am deeply indebted. His unwavering support ensured that no hardship or difficulty at home reached me, allowing me to remain focused on my academic journey. He is younger than me, but handled responsibilities

with the care and maturity of an elder brother. His silent support has been one of the greatest strengths behind this journey.

I love to express my heartfelt gratitude to my grandmother, **Mrs. Sarubai,** my sister, **Mrs. Seema**, my nephew, **Mr. Daksh,** and my brother-in-law, **Mr. Avinash Kakde**, for their love, care, and support.

During this Ph.D. journey, life gifted me some of its most beautiful moments. I got married to my wife, **Mrs. Shubhangi**, whose patience, understanding, and unconditional support stood beside me through every high and low of this journey. In 2025, we were blessed with our son, **Mr. Adway**, who brought immense happiness, peace, and new meaning to my life. No matter how stressful or difficult the days became, his innocent smile had the power to make everything feel lighter. He became my little source of joy, peace, and strength, reminding me why every struggle was worth it.

This journey would have been incomplete without the support of my best friends, **Mr. Shrikant Wakade**, **Mr. Shivdas Kadam**, **Mr. Bharat Trimukhe**, **Mr. Prasad Jadhav**, and **Mr. Motiram Borkar**. These people are the strongest pillars of my life, and without their support, love, and encouragement, I could never reach this milestone.

Finally, I would like to sincerely thank everyone who, directly or indirectly, supported me throughout this journey. Even if I have not mentioned here, their kindness, encouragement, and presence have always meant a lot to me. Their belief in me gave me strength and motivation whenever I needed it the most. This achievement is as much yours as it is mine. Thank you for everything.

**-KHANDU WADHONKAR**

***Dedicated***
***To***
***My Family,***
***For Their Endless Love and Support,***
***And to the Loving Memory of My Late Grandfather***

# SYNOPSIS

## Introduction:

Colorectal cancer (CRC) is one of the deadliest cancer types and arises at the inner lining of the colon or rectum, typically starting as a non-cancerous polyp. In the early stages, initiation occurs in normal colonic mucosa due to mutations in the adenomatous polyposis coli (APC) gene, leading to early tumor formation (stage I) [1]. At the same time, subsequent progression involves mutations in the RAS oncogene, which promotes tumor growth and local invasion (stage II) [2]. additional genetic mutation, especially in tumor protein 53 (TP53), allows the cancer to reach lymph nodes in (stage III) and ultimately facilitates distant metastasis (stage IV) [3]. Regardless of ongoing significant advancements in diagnosis and treatment, the survival rate of advanced CRC patients remains poor due to metastasis, recurrence, and immune evasion [4].

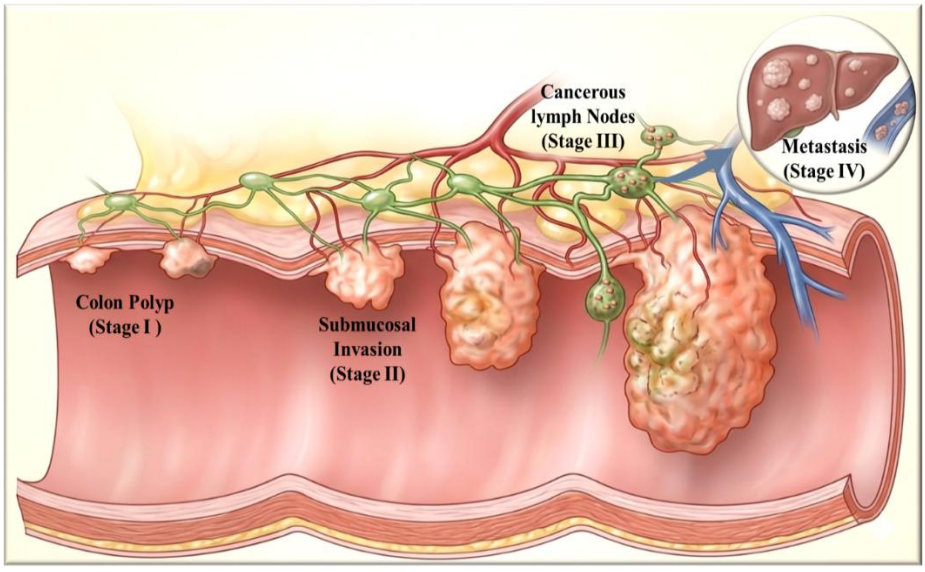



**Figure 1: Schematic representation of CRC progression from Stage I to Stage IV.** Stage I-II CRC remains localized to the colon or rectal wall without lymph node involvement, whereas Stage III-IV involves lymph node spread and distant metastasis to organs such as the liver or lungs. Figure prepared using Microsoft PowerPoint with icons obtained from Servier Medical Art.

Globally, the incidence rate of CRC varies widely across different regions of the world, with a higher rate typically observed in developed countries compared to developing countries [5]. A high incidence rate was observed in North America, Australia, New Zealand, and Europe, while countries in Africa and South Asia have the lowest incidence rate [6,7]. However, these trends are now shifting towards low-risk regions because of the adaptation of a westernized lifestyle, changes in dietary patterns, as well as a lack of advancement in screening patterns and treatment.

According to the Global Cancer Observatory data in India, the annual incidence rates (AARs) for CRC were 40,430 cases in males and 24,433 cases in females in 2022 [8]. An alarming rise in early-onset CRC has been observed, underscoring the need to deepen understanding of its underlying mechanisms and to improve strategies for early diagnosis. Traditionally, it was believed that CRC progression was primarily driven by genetic alteration within epithelial cells of the colon or rectum; however, growing evidence suggests that tumor progression is not determined only by the genetic alterations within cancer cells. Importantly, the surrounding tumor microenvironment (TME) plays a crucial role in shaping disease progression and therapeutic response.

**Role of TME in Macrophage Reprogramming During CRC Progression:**

The TME contains a complex network of stromal cells and immune cells that continuously interact with tumor cells through the release of soluble factors as well as extracellular vesicles. Among the immune cells present within the TME, macrophages are particularly abundant and functionally diverse and can adopt different activation states depending on the signals they receive from their surroundings. In the TME, macrophages undergo reprogramming and adopt a pro- or anti-tumor phenotype see **Figure 2** [9]. The signaling molecules include soluble cytokines, growth factors, and extracellular vesicles as important mediators of intercellular communication during cancer progression.

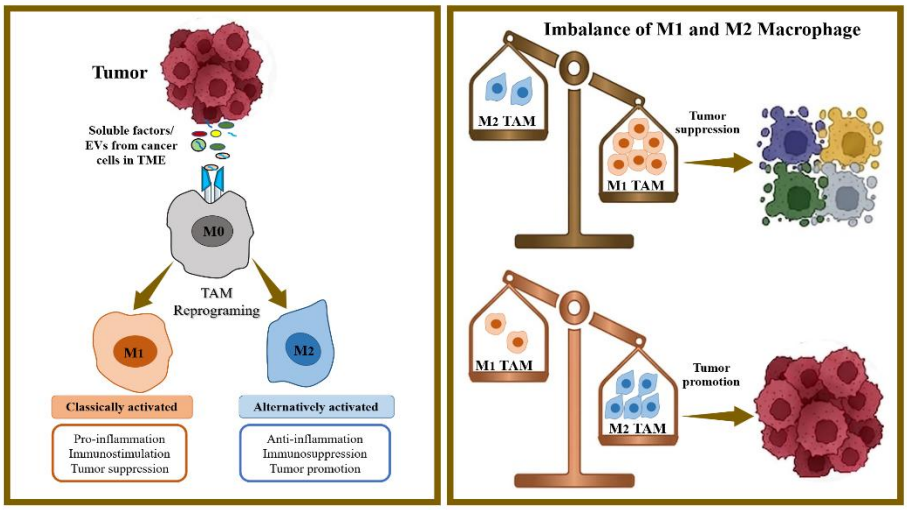



**Figure 2: Overview of tumor-associated macrophage reprogramming within the tumor microenvironment in CRC**. Macrophages within TME adopt either an antitumor M1 like TAMs or protumor phenotype M2 like TAMs. A predominance of M1 like TAMs suppresses tumor growth, whereas M2 like TAMs supports cancer progression and metastasis. Figure prepared using Microsoft PowerPoint with icons obtained from BioRender.

## CRC Exosomes in Immune Modulation and Tumor Progression:

The EVs are a broad class of membrane vesicles important for intercellular communication and can serve as disease biomarkers, including cancer. Based on their size and place of origin, they can be divided into several categories, such as apoptotic bodies (1,000 to 5,000 nm), microvesicles (100 to 1,000 nm), and the smallest exosomes (40 to 120 nm) size [10]. Among these vesicles, exosomes have received particular attention due to their ability to transfer biologically active molecules from donor to recipient cells and emerge as a key regulator of tumor progression and immunomodulation. However, most studies have focused on exosome-containing nucleic acid and protein cargo see **Figure 3**, while determinants of immune recognition and signaling remain largely unexplored.

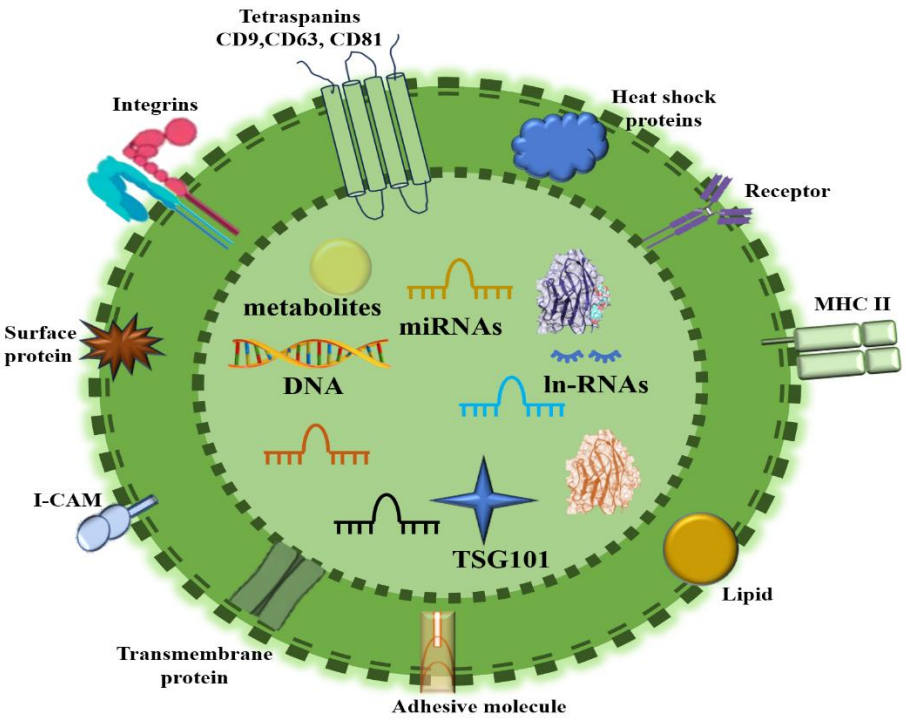



**Figure 3: The structure and composition of exosomes**. Exosomes are composed of biomolecules such as proteins, tetraspanins (CD9, CD63, CD81), membrane transport and fusion protein, integrin, heat shock protein (HSP70/90), endosomal sorting complex proteins (Alix, TSG101. Additionally, nucleic acids, including DNA, coding and non-coding RNAs, and lipid components

Although few recent studies have demonstrated that exosomal miRNAs and proteins secreted by CRC cells control macrophage polarization and regulate tumor growth, targeting these miRNAs and proteins has yielded promising results. Many other miRNAs and proteins involved in CRC progression remain unidentified. The ongoing investigation is focused on understanding their role and how they contribute to tumor progression and metastasis. Given the growing recognition of exosome-mediated communication in cancer and the critical role of macrophages in the TME, investigating the composition and role of CRC-derived exosomes represents an important research opportunity.

**Mechanistic Insights into CRC-Derived Exosome Function:**

Considering the understanding of TME, macrophage reprogramming, and exosome biology. It is equally important to explore the mechanistic role of CRC-derived exosomes in intracellular communication within TME. The exosomal cargo is known to regulate several oncogenic signaling pathways. These pathways mainly include PI3K-AKT, JAK-STAT, TGF-β, MAPK, and Wnt/β-catenin signalling. Exosome-mediated activation of these pathways alters the functional behaviour of the recipient cells within TME and contributes to immune suppression, angiogenesis, epithelial-mesenchymal transition, invasion, and metastasis. In the present study, we selected colorectal cancer as a disease model to investigate exosome-induced macrophage reprogramming because macrophages are among the most abundant populations in the CRC microenvironment. Collectively, this study aims to provide mechanistic insight into exosome-mediated immune regulation. Furthermore, targeting exosome-mediated macrophage interaction may offer a new opportunity in CRC for therapeutic intervention.

**Hypothesis and Objectives of the Study:**

This work focuses on identifying exosome-mediated molecular mechanisms that drive macrophage phenotypic switching during CRC progression. Here, we hypothesize that CRC-derived exosomes play a critical role in reprogramming macrophages toward an M2-like, tumor-supportive phenotype. Accordingly, we propose a disease model illustrating CRC cell- macrophage interactions; **see Figure 4**. To gain a more detailed understanding of this mechanism, we propose the following objectives.

## Hypothesis

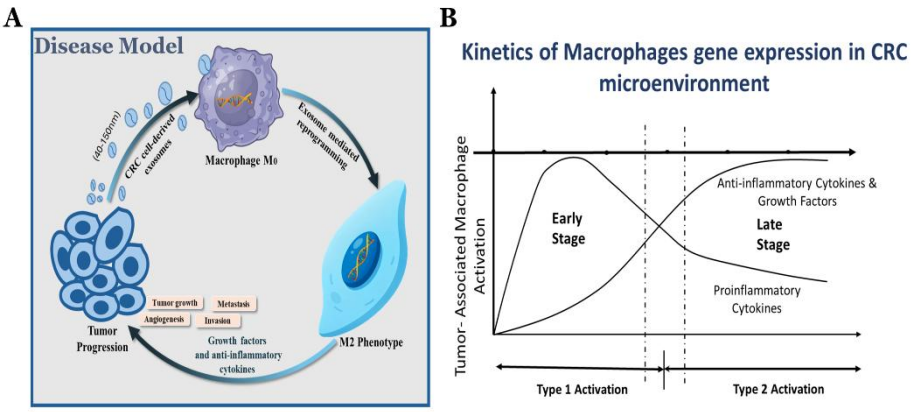



**Figure 4: A)** Disease model illustrating CRC cell-derived exosome-mediated macrophage reprogramming. **B)** Kinetics study of macrophages gene expression in CRC microenvironment

### Objectives of the study

1. Investigating macrophage morphological changes in response to CRC cells co-culture conditions.
2. Dissecting the signaling mechanism of macrophage polarization in response to CRC cells-derived exosomes.
3. Designing therapeutic interventions (anti-miRNAs, small molecules, or peptides) targeting the identified signaling molecules.

### Thesis Organization

The thesis is systematically organized into the following chapters to provide in-depth and mechanistic insights into CRC progression. Each chapter addresses a specific aspect of the study and collectively contributes to a comprehensive understanding of the overall study.

### Chapter 1: Introduction

This chapter provides an idea of the research area, focusing on CRC and what are underlying molecular mechanisms. It also highlights the role of exosome-mediated communication between CRC cells and tumor-

associated macrophages within TME. Additionally, it outlines the fundamental concept of CRC, emphasizing the global burden, molecular pathogenesis, significance, research gap, hypothesis, and objectives of the study.

**Chapter 2: Literature Review**

This chapter sheds light on the review of existing literature relevant to the composition of exosomes released from cancer cells and their role in TAMs polarization. Here, we discuss how exosomal cargo, including proteins, glycoproteins, and miRNAs, influences key signaling pathways involved in macrophage polarization within TME. Furthermore, it highlights the current understanding of exosomes' composition, function, and therapeutic approaches. It also points out gaps in existing studies that need further investigation in this area.

**Chapter 3: CRC Exosome-Induced Macrophage Reprogramming**

This chapter presents the key findings of the study, focusing on the interaction between CRC-derived exosomes and macrophages. It further investigates the molecular mechanisms involved in this interaction, with particular emphasis on the NF-κB signaling pathway, and how it ultimately promotes the aggressive behaviour and metastatic progression of CRC cells. Using in vitro and in vivo immune-relevant models, we demonstrate that CRC-derived exosomes are internalized by macrophages and initially activate inflammatory signaling. However, prolonged exposure induces macrophage reprogramming toward an anti-inflammatory, tumor-supportive phenotype. Mechanistically, in an in vitro study, we proved that exosome-mediated signaling activates the NF-κB pathway, resulting in upregulation of PD-L1 expression in macrophages and suppression of anti-tumor immune responses.

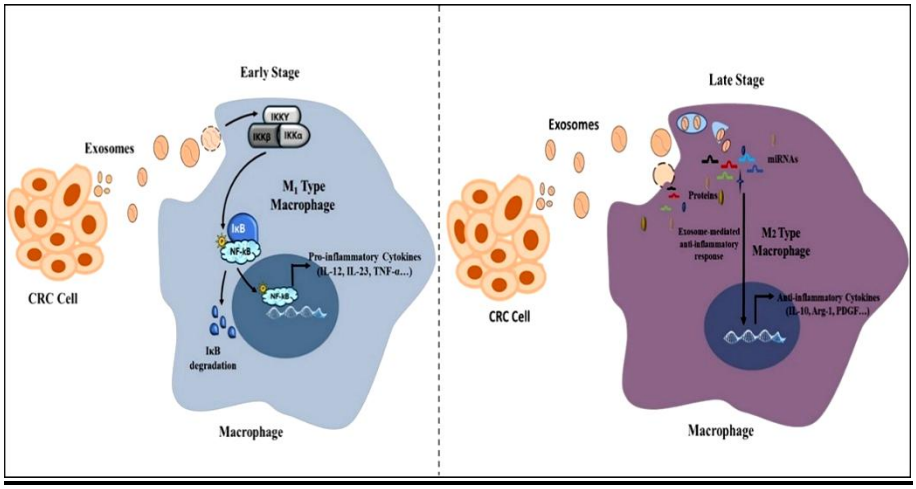



**Figure 5: Cross-Talk Between CRC Cells and Macrophages in the Colorectal Cancer Microenvironment**. Exosome-mediated early-stage macrophage activation and exosomal miRNAs mediated late-stage M2 reprogramming of macrophages in TME

## Chapter 4: Therapeutic Targeting of Tumor-Supportive Macrophages in CRC

This chapter mainly discusses the importance of PD-L1 as a potential therapeutic target in CRC, focusing on how it helps tumor cells escape immune surveillance and how its expression is regulated within the TME. In our study, we observed, in response to CRC exosomes, upregulation of PD-L1 expression in macrophages. These activated macrophages further enhance PD-L1 expression in CRC cells, resulting in T cell apoptosis. To counter PD-L1-mediated immune evasion, we identified a marine-derived natural inhibitor targeting PD-L1 through in silico screening, with molecular dynamics simulations supporting stable interactions at the PD-L1 interface. This suggests its potential to modulate PD-L1–dependent regulatory signaling in T cells.

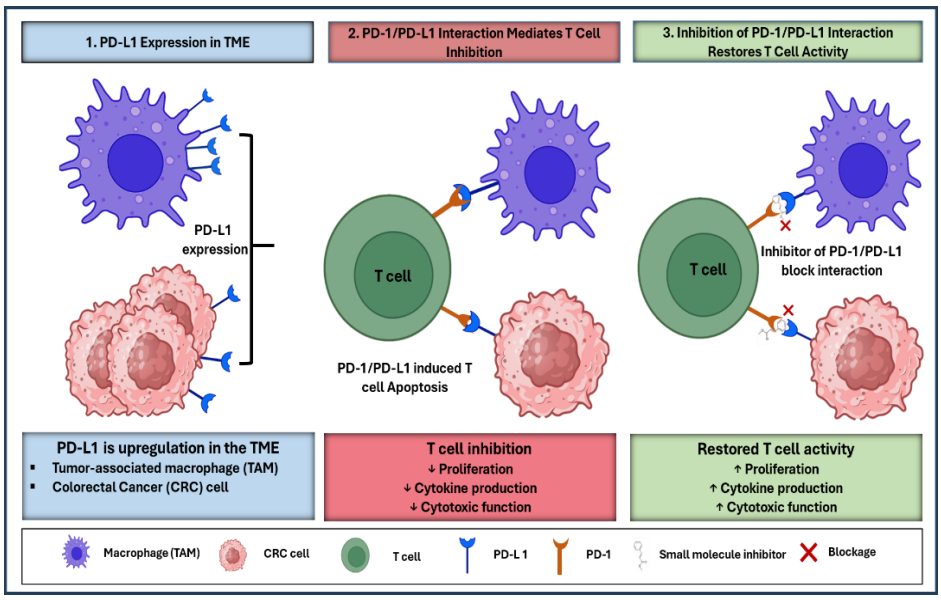



**Figure 6: PD-1/PD-L1-mediated immune suppression and therapeutic intervention in CRC.** PD-L1 is expressed on TAMs and CRC cells, where it binds to PD-1 expressed on T cells, resulting in T cell exhaustion and immunosuppression. Small-molecule inhibitors of the PD-1/PD-L1 interaction block this immune checkpoint, restoring T cell proliferation and cytotoxic activity, thereby enhancing anti-tumor immune responses. Figure prepared using Microsoft PowerPoint with icons obtained from BioRender.

## Chapter 5: In silico Targeting of Glycoproteins Fucosylation for Therapeutic Intervention in CRC

In this chapter, we focused on glycoprotein which influence tumor development; while targeting the carcinoembryonic antigen (CEA), we identified fucosyltransferase 8 (FUT8) as a promising therapeutic target in CRC. In silico screening of marine natural compounds reveals promising FUT8 inhibitors with favorable binding affinity, stability, and pharmacokinetic properties. This finding suggests that targeting FUT8 could mitigate CEA function and may represent a potential therapeutic intervention for CRC treatment.

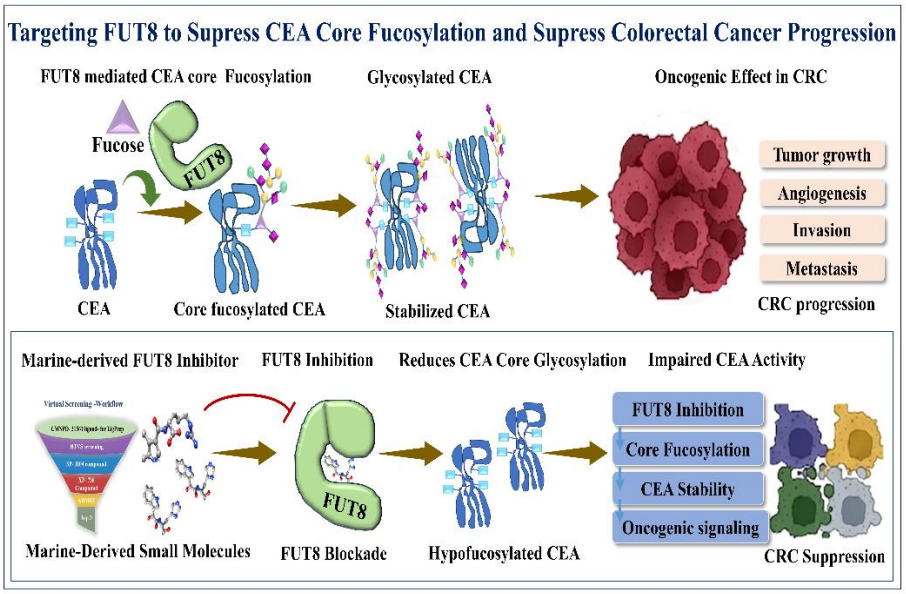



**Figure 7: Targeting FUT8-mediated core fucosylation of CEA in CRC.** Proposed mechanism illustrating FUT8-mediated core fucosylation of CEA and identification of marine-derived FUT8 inhibitor through an in-silico approach to suppress colorectal cancer progression.

## Chapter 6: Summary

This chapter summarizes the key findings of the study, focusing on how CRC cell-derived exosomes contribute to macrophage reprogramming through NF-κB-mediated signaling. It also discusses the importance of targeting PD-L1 and FUT8-mediated core fucosylation of CEA to counter immune evasion by tumor cells, thereby highlighting its potential in improving cancer immunotherapy strategies.

## Chapter 7: Future Prospects

It outlines possible future directions for further research based on the findings of this study. It focuses on gaining deeper insight into exosome-mediated communication and understanding the detailed mechanism of macrophage polarization within the TME condition. Exploring the key components of this TME, especially exosomes, glycoproteins, and immune checkpoints, which may serve as a therapeutic intervention for CRC treatment.

## References

[1] H. Lamlum, A. Papadopoulou, M. Ilyas, A. Rowan, C. Gillet, A. Hanby, I. Talbot, W. Bodmer, I. Tomlinson, *APC* mutations are sufficient for the growth of early colorectal adenomas, Proc. Natl. Acad. Sci. U.S.A. 97 (2000) 2225–2228. https://doi.org/10.1073/pnas.040564697.

[2] J.B.E. Janssen, J.P. Medema, E.C. Gootjes, D.V.F. Tauriello, H.M.W. Verheul, Mutant RAS and the tumor microenvironment as dual therapeutic targets for advanced colorectal cancer, Cancer Treatment Reviews 109 (2022) 102433. https://doi.org/10.1016/j.ctrv.2022.102433.

[3] T. Mizutani, M. Boretto, S. Lim, J. Drost, D.M. González, R. Oka, M.H. Geurts, H. Begthel, J. Korving, J.H. Van Es, R. Van Boxtel, H. Clevers, Recapitulating the adenoma–carcinoma sequence by selection of four spontaneous oncogenic mutations in mismatch-repair-deficient human colon organoids, Nat Cancer 5 (2024) 1852–1867. https://doi.org/10.1038/s43018-024-00841-x.

[4] Q. Tang, Z. Su, W. Gu, A.K. Rustgi, Mutant p53 on the Path to Metastasis, Trends in Cancer 6 (2020) 62–73. https://doi.org/10.1016/j.trecan.2019.11.004.

[5] A. Mohammadain, S. Kheiri, D. Darmadi, Global Disparities in Colorectal Cancer: Unveiling the Present Landscape of Incidence and Mortality Rates, Analyzing Geographical Variances, and Assessing the Human Development Index, Journal of Preventive Medicine and Hygiene (2025) E499 Pages. https://doi.org/10.15167/2421-4248/JPMH2024.65.4.3071.

[6] B. Yao, Y. Zhang, S. Li, Y. Tian, M. Ashrafizadeh, H. Rastin, M. Tang, Y. Li, Colorectal cancer epidemiology (1990–2050): lessons from the Australasian experience, J Transl Med 23 (2025) 855. https://doi.org/10.1186/s12967-025-06630-z.

[7] P. Rawla, T. Sunkara, A. Barsouk, Epidemiology of colorectal cancer: incidence, mortality, survival, and risk factors, Pg 14 (2019) 89–103. https://doi.org/10.5114/pg.2018.81072.

[8] S. Shivshankar, P.S. Patil, K. Deodhar, A.M. Budukh, Epidemiology of colorectal cancer: A review with special emphasis on India, Indian J Gastroenterol (2025). https://doi.org/10.1007/s12664-024-01726-8.

[9] T.A. Wynn, A. Chawla, J.W. Pollard, Macrophage biology in development, homeostasis and disease, Nature 496 (2013) 445–455. https://doi.org/10.1038/nature12034.

[10] F. Ciregia, A. Urbani, G. Palmisano, Extracellular Vesicles in Brain Tumors and Neurodegenerative Diseases, Front. Mol. Neurosci. 10 (2017) 276. https://doi.org/10.3389/fnmol.2017.00276.

# LIST OF PUBLICATIONS

**A. Publications from Ph.D. Thesis Work**

1. **Wadhonkar, K.,** Das D., Kant Chittela R., Obukhov AG., & Baig, M. S. (2026). Role of Colorectal Cancer-Derived Exosomes in Modulating Macrophage Phenotypes During Tumor Development. ***Carcinogenesis***. DOI: 10.1093/carcin/bgag003

**2. Wadhonkar, K.,** Siddiqi, F., Rughetti, A., & Baig, M. S. (2026). Structure-Based Prioritization of Marine Natural Products as Candidate FUT8 Binders. ***In Silico Research in Biomedicine*** DOI: 10.1016/j.insi.2026.100657

3. **Wadhonkar, K.,** Siddiqi, F., & Baig, M. S. (2026). Identification of Marine-Derived Small Molecules Targeting the PD-1/PD-L1 Immune Checkpoint Using Molecular Docking and Molecular Dynamics Simulations. ***Journal of Molecular Structure*** (Revised *Manuscript Submitted*) DOI: 10.21203/rs.3.rs-8751886/v1

4. **Wadhonkar, K.,** Ohishi T., & Baig, M. S. (2026). Adaptor Proteins Regulating Tumor-Associated Macrophage Polarization During Cancer Progression. ***Oncoscience***. DOI: 10.18632/oncoscience.661

5**. Wadhonkar, K.,** Singh, Y., Rughetti, A., Das, S., Yangdol, R., Sk, M. H., & Baig, M. S. (2025). Role of cancer cell-derived exosomal glycoproteins in macrophage polarization. ***Molecular Biology Reports***. DOI: 10.1007/s11033-025-10535-x

6. **Wadhonkar, K.,** Das, S., Subramanian, R., Sk, M. H., Singh, Y., & Baig, M. S. (2024). The effect of cancer cell-derived exosomal proteins on macrophage polarization: An in-depth review. ***Experimental Cell Research***, DOI: 10.1016/j.yexcr.2024.114393

7. **Wadhonkar, K.,** Singh, N., Heralde III, F. M., Parihar, S. P., Hirani, N., & Baig, M. S. (2023). Exosome-derived miRNAs regulate macrophage-colorectal cancer cell cross-talk during aggressive tumor development. ***Colorectal Cancer***, DOI: 10.2217/crc-2022-0012

**B. Other Publications During Ph.D. Work**

1. Yamalakonda, S., **Wadhonkar, K.,** Kumbhar, N. K., Baig, M.S., Hosmani, S. S. (2026). Biological Response of ZX50 Mg Alloy: The Role of Surface Microstructure. ***ACS Biomaterials Science & Engineering***, DOI: 10.1021/acsbiomaterials.6c00753

2. Kumbhar, N. K., Yamamoto, A., **Wadhonkar, K**., Baig, M. S., & Hosmani, S. S. (2025). The effect of severe surface deformation on microstructure refinement, corrosion, and biocompatibility of Mg5Zn0. 2Ca alloy. ***Journal of Alloys and Compounds***, DOI: 10.1016/j.jallcom.2024.178259

3. Raizada, S., Obukhov, A. G., Bharti, S., **Wadhonkar, K**., & Baig, M. S. (2024). Pharmacological targeting of adaptor proteins in chronic inflammation. ***Inflammation Research***, DOI: 10.1007/s00011-024-01921-5

4. Atre, R., Sharma, R., Vadim, G., Solanki, K., **Wadhonkar, K**., Singh, N., Patidar, P., et al. (2023). The indispensability of macrophage adaptor proteins in chronic inflammatory diseases. ***International Immunopharmacology***, DOI: 10.1016/j.intimp.2023.110176

5. Solanki, K., Rajpoot, S., Kumar, A., Zhang, K. Y. J., Ohishi, T., Hirani, N., **Wadhonkar, K**., et al. (2022). Structural analysis of spike proteins from SARS-CoV-2 variants of concern highlighting their functional alterations. ***Future Virology***, DOI: 10.2217/fvl-2022-000

**Awards**

- Received **First Prize in Oral Presentation** at the **International Conference IALS 2026**, organized by the **Swami Ramanand Teerth Marathwada University at Nanded**
- Received **Best Poster Award** at the In-House Symposium 2024, organized by the Department of Biosciences and Biomedical Engineering (BSBE), **IIT Indore**
- Received **Travel Award** at the **EVOLVE 2025** conference, organized by the Indian Society for Extracellular Vesicles (InSEV) at **AIIMS, New Delhi**

# TABLE OF CONTENTS


**ACKNOWLEDGEMENT** I

**SYNOPSIS** VII

**LIST OF PUBLICATIONS** XIX

**TABLE OF CONTENTS** XXIII

**LIST OF FIGURES** XXIX

**LIST OF TABLES** XXXIX

**NOMENCLATURE** XLI

**ACRONYMS** XLIII

**Chapter 1 Introduction**……. 1

1.1 Overview of colorectal cancer (CRC)……..... 3

1.2 Epidemiology and risk factors of CRC……. 4

1.2.1 Epidemiology……..... 4

1.2.2 Risk factors associated with CRC……..... 5

1.3 Molecular pathogenesis of colorectal cancer…….. 7

1.3.1Chromosomal instability (CSI)……..... 7

1.3.2 Defective DNA repair mechanism…….. 7

1.3.3 Abnormal DNA hypermethylation……. 8

1.4 Tumor microenvironment in CRC…….. 8

1.4.1 Tumor-associated macrophages in CRC…… 9

1.4.2 Role of CRC-derived exosomes……. 12

1.5 Diagnosis: current scenario and recent advancement……. 14

1.6 Rationale and objective of the study……... 15

1.7 Novel findings and limitations of this study……... 16

1.8 Thesis organization……. 17

1.9 References……..... 19

**Chapter 2: Literature Review**…… 31

2.1 Tumor-derived exosomal protein role in macrophage polarization……... 33

2.1.1 Exosomal proteins driving M2 macrophage polarization……..... 34
2.1.2 Tumor-derived exosomal proteins driving M1 macrophage polarization……..... 47
2.1.3 Exosomal proteins driving macrophage polarization towards both M1 and M2……..... 52
2.2 Tumor-Derived exosomal glycoproteins in macrophage phenotypic change……..... 55
2.2.1 Cancer-derived exosomal glycoproteins as drivers of macrophage polarization within TME……..... 57
2.3 Exosome-derived miRNAs regulate macrophage-CRC cell cross-talk during aggressive tumor development…… 67
2.3.1 General Overview of MicroRNAs…… 67
2.3.2 CRC-derived exosomal miRNA in the regulation of macrophage polarization……..... 68
2.3.3 Macrophage-derived exosomal miRNAs……..... 74
2.3.4 miRNAs-based therapeutic approach……... 75
2.4 References……..... 80

**Chapter 3: Role of Colorectal Cancer-Derived Exosomes in Modulating Macrophage Phenotypes During Tumor Development……** 125
3.1 Graphical abstract…… 127
3.2 Overview…… 127
3.3 Introduction…… 128
3.4 Method…… 130
3.4.1 Cell lines and culture…… 130
3.4.2 Exosome extraction and characterization……. 130
3.4.2.1 Nanoparticle tracking analysis……... 131
3.4.2.2 Scanning electron microscopy (SEM)…… 131
3.4.2.3 Western blot analysis of exosome markers…… 131
3.4.3 Exosomes labelling and uptake analysis…….. 132

3.4.4 RNA isolation and quantitative real-time PCR (qRT-PCR)……. 132
3.4.5 Western Blotting of THP-1 cell lysates……. 133
3.4.6 Immunofluorescence…… 133
3.4.7 Measurement of macrophage phagocytic capacity…… 134
3.4.8 In vivo tumor development and immunohistochemical analysis in Swiss albino mice…… 134
3.4.9 Statistical analysis……. 135
3.5 Results……. 135
3.5.1 Molecular and phenotypic alterations in macrophages induced by CRC cell conditioned media…… 135
3.5.2 CRC cell-derived exosome isolation and characterization…… 137
3.5.3 Fluorescent labelling and confocal analysis reveal efficient uptake of PKH67-labelled CRC cell-derived exosomes by macrophages…… 137
3.5.4 CRC cell-derived exosome treatment altered phenotype and cytokine production in macrophages……. 138
3.5.5 Exposure to CRC-derived exosomes initially increased the rate of phagocytosis in THP-1-derived macrophages but then decreased macrophage phagocytic function over time…..... 140
3.5.6 CRC-exosome treatment activates the NF-κB signaling and promotes expression of M1 type markers in macrophages… 141
3.5.7 IKK inhibitor treatment attenuated NF-κB signaling activation induced by CRC exosomes in macrophages……... 144
3.5.8 CRC-derived exosome-treated macrophages upregulate the EMT marker and PD-L1 expression in CRC cells……. 145
3.5.9 CT-26 exosome-treated macrophages promote tumor progression with increased adhesion and angiogenic markers… 146
3.6 Discussion…….. 148
3.7 Conclusion……. 154
3.8 References…… 155

**Chapter 4: Identification of small-molecule inhibitors targeting the PD-1/PD-L1 interaction in CRC: insights from docking and molecular dynamics simulations……...** 163
4.1 Graphical Abstract…… 165
4.2 Overview…….. 166
4.3 Introduction…….. 167
4.4 Materials and methods…….. 169
4.4.1Cell lines and culture……... 169
4.4.2 Exosome isolation and characterization…….. 169
4.4.2.1 Nanoparticle tracking analysis…… 169
4.4.2.2 Scanning electron microscopy (SEM)…….. 169
4.4.3 RNA isolation and quantitative real-time PCR (qRT-PCR)…… 170
4.4.4 Target structure preparation……. 170
4.4.5 Ligand library processing…… 171
4.4.6 Virtual screening and ADMET predictions…….. 171
4.4.7 Protein–protein docking……... 172
4.4.8 Molecular dynamics simulations…….. 172
4.4.9 Trajectory analysis……. 173
4.4.10 Binding free energy calculations and data visualization. 174
4.5 Results……... 175
4.5.1 Exosome-mediated upregulation of PD-L1 in macrophages and CRC cells…… 175
4.5.2 Site-directed docking reveals high-affinity marine natural products engaging the PD-L1- PD-1 interface……. 176
4.5.3 Protein–protein docking suggests inhibitor-mediated modulation of PD 1/PD L1 binding……. 178
4.5.4 Marine database-derived ligands enhance PD-L1 structural stability and binding persistence…….. 180
4.5.5 Root-mean-square fluctuation analysis reveals PD-L1 stabilization by marine database-derived ligands…… 183
4.5.6 Protein compactness and solvent exposure validate structural integrity of ligand-bound PD-L1 complexes……... 183

4.5.7 Hydrogen bonding patterns indicate stable and selective ligand anchoring at the PD-L1 interface…….. 185
4.5.8 End-state free energy decomposition identifies CMNPD3605 as the most thermodynamically favourable PD-L1 binder……. 186
4.5.9 Residue-level MM/PBSA analysis pinpoints key anchoring residues and confirms CMNPD3605 as the most stabilizing ligand……. 188
4.6 Discussion and conclusion…… 189
4.7 References……. 192

**Chapter 5: Structure-Based Prioritization of Marine Natural Products as Candidate FUT8 Binders……** 201
5.1 Graphical Abstract…… 203
5.2 Overview…….. 203
5.3 Introduction…….. 204
5.4 Materials and methods…….. 207
5.4.1 Expression analysis of CEACAM5 and FUT8 in human cancers……. 207
5.4.2 Target preparation……... 207
5.4.3 Ligand library preparation……... 208
5.4.4 Virtual screening……. 209
5.4.5 ADMET prediction…….. 209
5.4.6 Molecular dynamics simulations……. 210
5.4.7 Trajectory analysis…….. 211
5.4.8 Binding free energy calculations and data visualization. 211
5.5 Results……... 212
5.5.1 Expression analysis supports CEACAM5 and FUT8 as relevant targets in CRC…… 212
5.5.2 Structure-based virtual screening identifies potential FUT8 inhibitors……... 214
5.5.3 ADMET analysis supports drug-like properties of the selected FUT8 inhibitors……. 215

5.5.4 RMSD analysis indicates stable binding of marine-derived compounds to FUT8……... 216
5.5.5 Residue flexibility analysis indicates active-site stability 218
5.5.6 Ligand binding preserves FUT8 compactness and solvent accessibility…… 219
5.5.7 Persistent hydrogen bonding stabilizes FUT8-ligand interactions……... 220
5.5.8 MM/PBSA analysis reveals favorable binding energies for the selected compounds…….. 222
5.5.9 Residue decomposition analysis highlights key binding determinants……. 223
5.6 Discussion and conclusion…… 225
5.7 References……. 227

**Chapter 6: Summary……** 235
**Chapter 7: Future prospects……** 243
**APPENDIX** 241
Appendix A: Supplementary Figures……... 249
Appendix B: Supplementary Tables……. 254

# LIST OF FIGURES

**Chapter 1**

**Figure 1.1: Schematic representation of CRC progression from Stage I to Stage IV.** Stage I-II CRC remains localized to the colon or rectal wall without lymph node involvement, whereas Stage III-IV involves lymph node spread and distant metastasis to organs such as the liver or lungs…….3

**Figure 1.2 Epidemiological burden of colorectal cancer**. (A) Global distribution of major cancer types in the human population, highlighting the prominence of breast, lung, and colorectal cancers. (B) Global incidence of colorectal cancer (CRC) with a ten-year forecast (2017–2027), illustrating the projected increase in CRC cases worldwide. (C) Regional growth forecast of CRC incidence, showing differential trends across geographic regions……5

**Figure 1.3. Overview of tumor-associated macrophage reprogramming within the tumor microenvironment in CRC**. A) The macrophage polarization into TAM1 (anti-tumor) and TAM2 (pro-tumor) phenotypes within TME. B) The imbalance between these populations determines disease outcome, where TAM1 dominance promotes anti-tumor immune responses, while TAM2 enrichment supports tumor growth, immune suppression, and progression……...11

**Figure 1.4: The structure and composition of exosomes.** Exosomes consist of various biomolecules such as proteins, tetraspanins (CD9, CD63, CD81), membrane transport and fusion protein, integrin, heat shock protein (HSP70/90), endosomal sorting complex proteins (Alix, TSG101. Additionally, nucleic acids, including DNA, coding and non-coding RNAs, and lipid components……...13

**Figure 1.5 A)** Disease model illustrating CRC cell-derived exosome-mediated macrophage reprogramming. **B)** Kinetics study of macrophages gene expression in CRC microenvironment……...15

**Chapter 2:**

**Figure 2.1**: Schematic diagram of macrophage polarization in response to exosomal protein content…….34

**Figure 2.1.1*:*** Represent various cancer cell-derived exosomes containing proteins that significantly contribute to macrophage polarization towards an anti-inflammatory phenotype during cancer progression…….47

**Figure 2.1.2:** Depicts cancer cell-derived exosomes containing proteins that play a crucial role in inducing macrophages to switch to a pro-inflammatory phenotype during cancer……54

**Figure 2.2.1** Cancer cell–derived exosomal glycoprotein-mediated signaling pathways regulating macrophage polarization: This schematic illustrates the molecular mechanisms underlying macrophage polarization. M2 polarization is driven by CD44–GP130 and IL-10–mediated STAT3 activation, NID1-induced ERK signaling, GPC3-induced β-catenin signaling, and ICAM-1–dependent PI3K/AKT signaling. In contrast, M1 polarization is promoted by FetA–MyD88/TRIF–mediated NF-κB activation and THBS1-induced MAPK/AP-1 activation……57

**Figure 2.2.2:** Cancer cell-derived exosomal glycoproteins in macrophage M1/M2 polarization through the modulation of distinct signaling pathways……...59

**Figure 2.3.1.** Representing exosome-mediated effect, the CRC cell secreted exosomes miR-25-3p, miR-425-5p, miR-130-3p, miR-934, miR-200a and miR-21-5p promote M2 polarization via PI3K/AKT mediated signaling, miR-203 and miR-145 mediated M2 polarization via STAT3 dimerization, and miR-21-5p and miR-29b promote M1 polarization which further increases miR-21 and leads to M1 to M2 reprogramming. The M2-polarized macrophages also secrete the exosome miR-21-5p, miR-155-5p, and miR-183-5p, which mediate

tumor growth, invasion, metastasis, angiogenesis, and cancer progression……..68

**Figure 2.3.2** Representation of exosome-mediated macrophage polarization into M1 phenotype and M2 phenotype. In an early-stage colorectal cancer cell, secreted exosome promotes M1 polarization with a proinflammatory response, and in the later stage, the exosomal miRNA mediates reprogramming toward an M2 phenotype…….76

**Figure 2.3.3** Representation of THP-1 cell morphology in normal RPMI media and 48 h of Colo 205 CRC cells condition media isolated exosome and treated conditions after 24 and 72 h**.** The THP-1 cells were treated with PMA (25 ng/ml) for 48 h before the experiment for their differentiation into monocytes. The images were taken under a bright-field microscope at 20× magnification. EXO: Exosomes; PMA: Phorbol 12-myristate 13-acetate……..……78

**Chapter 3:**

**Figure 3.1:** Interplay between CRC cells and macrophages gene expression in Colorectal cancer microenvironment: Exosome-mediated early-stage macrophage activation and Exosomal miRNAs mediated late-stage M2-like reprogramming of macrophages in TME……127

**Figure 3.2** Morphology of THP-1 cells treated with Colo205 conditioned media and exosomes. (a) Morphological changes in THP-1 cells incubated with Colo205 cell culture-derived conditioned media for 24, 48, 72, and 96 hours. Images captured using a 20× magnification (scale bar = 20 μm). (b) Western blot analysis for the detection of exosome-specific markers. (c) Nanoparticle tracking analysis (NTA) to determine the concentration and average size of the exosomes. (d) Scanning electron microscopy (SEM) images showing the morphology and size of the exosomes. (e) Time-dependent macrophage polarization induced by colorectal cancer (CRC) cell-derived exosomes. Images captured using a confocal microscope at 100× magnification (scale bar = 30 μm) …….136

**Figure 3.3:** Uptake of PKH67-labeled exosomes by macrophages. THP-1 cells were co-cultured with PKH67-labeled exosomes (green) derived from *CRC (Colo-205) cells* and subsequently fixed for Confocal microscopy. Cells were incubated with PKH67-labeled exosomes for 30 minutes, 4, 12, and 24 hours. Cell nuclei were counterstained with DAPI (blue). Red arrows denote exosomes internalized by THP-1 macrophage cells, magnification 100× (scale bar = 20μm)…….138

**Figure 3.4:** Morphological changes and phagocytic activity of THP-1 macrophages treated with Colo205-derived exosomes. (a) Morphology of THP-1 cells treated with Colo205-derived exosomes. PMA-treated THP-1 cells were grouped as follows: Control, N.M. exo (exosomes isolated from normal complete media with FBS), and Colo exo (exosomes isolated from Colo205 cell-conditioned media). Cells were incubated for 24, 48, 72, and 96 hours. Images were taken at 20× magnification (scale bar = 20 μm). (b) Phagocytic activity of THP-1 macrophages treated with Colo205-derived exosomes for 12, 24, and 72 hours. Phagocytosis was assessed using FITC-labeled *E. coli*. (c) Bar graph showing the relative fluorescence intensity of FITC-labeled *E. coli* uptake, quantified from the images in (B), and Supplementary Figure S1 documents the phagocytic activity of THP-1 macrophages treated with CRC cell-derived exosomes, assessed by Oil Red O staining. Images were acquired using a confocal microscope at 100× (scale bar = 20 μm). *$P < 0.05$, **$P < 0.005$, ***$P < 0.0005$, ****$P < 0.00005$……..139

**Figure 3.5:** Time-dependent cytokine and immunomodulatory factor expression in macrophages treated with CRC cell-derived exosomes: THP-1 macrophages were treated with exosomes isolated from CRC cells, and the expression levels of pro-inflammatory (IL-23, IL-12, TNF-α) and anti-inflammatory (IL-10, ARG-1) cytokines, along with PDGF, were analyzed at 24, 72, and 96 hours. Gene expression was measured using RT-qPCR. *$P < 0.05$, **$P < 0.005$, ***$P < 0.0005$, ****$P < 0.00005$……..…….140

**Figure 3.6:** p65 Expression in THP-1 Cells Treated with COLO-205-Derived Exosomes (A-B) Immunoblot analysis of NF-κB (p65) and its quantification demonstrate a significant downregulation of p65 phosphorylation in THP-1 macrophage cells following treatment with COLO-205-derived exosomes. THP-1 cells were incubated with exosomes for 30 min, 4, 12, 24, and 72 hrs. Western blot analysis revealed an initial increase in phosphorylated NF-κB (p-NF-κB) levels at 30 minutes, followed by a gradual decline at subsequent time points (4, 12, 24, and 72 hours). (C-D) The nuclear translocation of NF-κB (p65) was assessed using confocal microscopy. The accompanying graph represents the quantitative analysis of protein levels. Statistical significance is indicated as follows: $p < 0.05$, **p** < 0.01, ***p** < 0.001, ****p** < 0.0001 compared to the control group. Scale bar=10μm……142

**Figure 3.7:** IκB degradation in macrophage cells treated with CRC cell-derived exosomes: (A and B) Immunoblot analysis and quantification show that CRC-derived exosomes modulate total IκB level in macrophages. Cand D) Immunofluorescence analysis confirm change in IκB expression (E and F) confirms the kinetics of iκb degradation at 10, 20 30,40, 50,60 min, 2, 3, 4hrs. Significance: *p < 0.05, **p < 0.01, ***p < 0.001, ****p < 0.0001 vs. control, Scale bar=10μm……..143

**Figure 3.8:** IKK inhibitor treatment attenuated NF-κB signaling induced by CRC exosomes in macrophages: (A-B) Immunoblot analysis and quantification indicate that CRC exosomes modulate the p-IKK phosphorylation in macrophages, with an initial increase at 30 minutes followed by a gradual decrease at 4-72 hours. (C-D) Immunofluorescence analysis further confirms p-IKK expression in macrophages. (E-G) Treatment with the IKK inhibitor TPCA-1 attenuates exosome-induced changes p-IKK and IκB expression level compared to control conditions. Significance: *p < 0.05, **p < 0.01, ***p < 0.001, ****p < 0.0001 vs. control, Scale bar=10μm……144

**Figure 3.9:** CRC-derived exosomes-treated macrophages promote EMT, PD-L1 expression, and migration in colorectal cancer cells: (a) Assessment of cell migration in Colo-205 colorectal cancer cells using the scratch assay; COLO-205 cells were seeded in 6-well plates and cultured to ∼50% confluence. A straight-line scratch was created using a sterile pipette tip, and detached cells were removed by gentle washing with PBS. Cells were exposed to conditioned media from untreated macrophages (MΦ CM), LPS-stimulated macrophages (LPS CM), IL-4-stimulated macrophages (IL-4 CM), and exosome-stimulated macrophages for 24 and 72 hours (Exo 24 hours CM, Exo 72 hours CM). Images were captured at 0, 24, and 48 hours post-scratch using a phase-contrast microscope, magnification: 10× (scale bar = 200 μm). (b) Macrophages exposed to CRC-derived exosomes exhibited an enhanced expression of snail, fibronectin, AKR1B1, and PD-L1 in CRC cells, as confirmed through qRT-PCR. **p* < 0.05, **p** < 0.01, ***p** < 0.001, ****p** < 0.0001……..……146

**Figure 3.10A:** Subcutaneous tumor development and histopathological characterization in a murine allograft model of CRC. Representative images showing subcutaneous tumor development, excised tumor morphology, and H&E-stained tumor sections from different treatment groups…….……147

**Figure 3.10B:** Enhanced expression of cell adhesion and angiogenic factor during CRC progression. Immunohistochemical staining shows evaluated expression of ICAM-1 and VE-cadherin in tumor tissues from mice co-injected with CT-26 cells and exosome-treated macrophages for a 72-hour treatment condition, compared to the control group. Images taken under 100X confocal microscope…….148

**Figure 3.11:** Kinetics study of macrophage gene expression during early and late stages of CRC-derived exosome treatment. The figure illustrates temporal changes in the expression of macrophage-associated genes, highlighting their dynamic regulation during tumor progression……...…..149

**Chapter 4:**

**Figure 4.1:** Graphical Abstract: Mechanism of Blocking PD-1/PD-L1 Axis in Tumor Immunity. The figure illustrates PD-1 expression on cytotoxic T cells interacting with PD-L1 on cancer cells and tumor-associated macrophages, suppressing T-cell activity. Blocking this interaction with small-molecule inhibitors can restore and enhance anti-tumor T-cell-mediated immunity……165

**Figure 4.2** Exosome characterization and PD-L1 expression analysis. Colo-205–derived exosomes were isolated by ultracentrifugation and characterized by (A) nanoparticle tracking analysis (NTA) and (B) scanning electron microscopy (SEM).(C) CRC cells-derived exosomes induced PD-L1 expression in macrophages and conditioned media (CM) obtained from exosome-stimulated macrophages subsequently elevated PD-L1 expression in CRC cells was quantified by RT-PCR **p<0.05, **p<0.005, ***p<0.0005, ****p<0.00005* ……..…176

**Figure 4.3:** Structural visualization and residue-level analysis of the PD-1/PD-L1 complex (PDB: 4ZQK), highlighting interface residues within 3Å proximity. Identified contact residues were used to define the PD-L1 binding grid for virtual screening……177

**Figure 4.4:** Virtual screening workflow and molecular interaction of small-molecule inhibitors with PD-L1. (A) Schematic representation of the virtual screening workflow used to identify potential PD-L1 inhibitors, including ligand selection, docking, and pharmacokinetic evaluation steps. (B) Two-dimensional interaction diagrams illustrating the binding modes of selected small-molecule inhibitors within the PD-L1 binding pocket, highlighting key residues involved in hydrogen bonding and hydrophobic interactions……...……178

**Figure 4.5.** Molecular docking of PD-1/PD-L1 complex with control and top ligands. (A) Structural alignment of the PD-1/PD-L1 protein–protein complex (PDB ID: 4ZQK) is shown, with the redocking of the

native interface (PPI) serving as reference. B) Docking scores (mean ± SD) are summarized in the accompanying table, indicating relative protein-protein binding affinities compared to the native redock and control ligand. C) The control ligand INCB086550 is depicted in blue, while three candidate ligands are shown bound at the interface: CMNPD16477 (orange), CMNPD21979 (green), and CMNPD3605 (pink)……..……179

**Figure 4.6.** Molecular dynamics trajectory analysis. (A) RMSD showing overall structural stability during the simulation. (B) RMSF depicting residue-wise flexibility. (C) The radius of gyration (Rg) indicates protein compactness. (D) Solvent-accessible surface area (SASA) reflects changes in solvent exposure over time……....180

**Figure 4.7.** Molecular dynamics analysis of PD-L1 complexes with INCB086550, CMNPD16477, CMNPD21979, and CMNPD3605. **(A)** Ligand RMSD **(B)** Binding pocket RMSD **(C)** Ligand–pocket distance and **(D)** Ligand–protein distance plotted as a function of simulation time. These traces illustrate the degree of ligand stability, pocket rigidity, and spatial fluctuations for each system, allowing for direct comparison of binding persistence and conformational dynamics…181

**Figure 4.8:** Protein–ligand hydrogen bond formation during 200 ns molecular dynamics simulations for PD-L1 complexes with INCB086550, CMNPD16477, CMNPD21979, and CMNPD3605. (A) Moving-average number of hydrogen bonds quantifies persistence and fluctuation of polar contacts, and (B) total hydrogen bonds at each timestep reveal the overall temporal pattern and differences in anchoring strategy among ligands……..…….186

**Figure 4.9:** MM/PBSA binding free energy decomposition for PD-L1 complexes with INCB086550, CMNPD16477, CMNPD21979, and CMNPD3605. Bars depict the contributions (kcal/mol) of van der Waals (ΔE_vdW), electrostatic (ΔE_elec), polar solvation (ΔG_pol), and nonpolar (ΔG_np) terms, as well as total binding free energy (ΔG_bind),

highlighting differences in the thermodynamic drivers of binding across ligand systems……..……..187

**Chapter 5:**

**Figure 5.1**. Graphical abstract: proposed mechanism illustrating FUT8-mediated core fucosylation of CEA and identification of marine-derived FUT8 inhibitor through an in-silico approach to suppress colorectal cancer progression……..203

**Figure 5.2**. Expression analysis of CEACAM5 and FUT8 in colorectal cancer. (A) HPA protein expression profile of CEACAM5 across human cancers. (B) HPA RNA expression profile of CEACAM5. (C) GEPIA2 comparison of CEACAM5 transcript levels between tumor (T) and normal (N) tissues in colon adenocarcinoma (COAD) and rectum adenocarcinoma (READ). (D) HPA protein expression profile of FUT8 across human cancers. (E) HPA RNA expression profile of FUT8. CEACAM5 and FUT8 were both expressed in colorectal cancer tissues, with higher transcript levels observed in tumor samples than in corresponding normal tissues. (F) GEPIA2 comparison of FUT8 transcript levels between tumor and normal tissues in COAD and READ…….…213

**Figure 5.3**. Virtual Screening Workflow and 2D interactions of FUT8 with small molecule inhibitors……...215

**Figure 5.4**. Molecular dynamics analysis of FUT8 complexes with the control ligand and selected marine-derived compounds. (A) Protein backbone RMSD, (B) residue-wise RMSF, (C) radius of gyration (Rg), and (D) solvent-accessible surface area (SASA) over 200 ns simulations……..…218

**Figure 5.5**. Hydrogen-bond analysis of FUT8 complexes during 200 ns molecular dynamics simulations. (A) Moving average of protein–ligand

hydrogen bonds and (B) distribution of hydrogen bonds over time for the control ligand and selected marine-derived compounds……..222

**Figure 5.6**. MM/PBSA binding free energy decomposition of FUT8–ligand complexes. Average van der Waals (ΔE_vdW), electrostatic (ΔE_elec), polar solvation (ΔG_pol), nonpolar solvation (ΔG_np), and total binding free energies (ΔG_bind) calculated from MD trajectories for the control ligand and selected compounds. Negative values indicate favorable contributions to binding……...……222

**Chapter 6:**

**Figure 6.1**. Cancer cells and secreted exosomes upregulate PD-L1 in macrophages, targeting PD-1/PD-L1 interaction and restoring T-Cell-mediated response in CRC…….240

**Chapter 7:**

**Figure 7.1** Potential future directions from the current research work……245

# LIST OF TABLES

## Chapter 2:

**Table 2.1.1.** List of cancer cells derived exosomes containing protein involved in M2 type of macrophage polarization……46

**Table 2.1.2.** List of cancer cells derived exosome containing protein involved in M1 type of macrophage polarization……53

**Table 2.2.1** List of cancer-derived exosomes containing glycoproteins involved in macrophage polarization……..65

**Table 2.3.1** List of CRC cell and macrophage-derived exosomal miRNA involved in CRC progression……69

**Table 2.3.2** Table of microRNA-based clinical studies in a different cancer type……..76

**Table 5.1.** Predicted ADMET profiles of CMNPD23062, CMNPD23066, and CMNPD8620 were generated using pkCSM…216

## NOMENCLATURE

kDa- Kilo Dalton

µg/ml- Microgram per milliliter

ng/ml- Nanogram per milliliter

µM- Micro molar

U/ml- Unit per milliliter

°C- degrees Centigrade

%- Percentage

ns- Nano second

min- Minutes

hr- Hour

mM- Milli molar

xg- Gravitational force

µg- Microgram

ng-Nanogram

rpm- Revolutions per minute

# ACRONYMS

| Acronym | Full Form |
|---|---|
| AKT | Protein Kinase B |
| APC | Adenomatous Polyposis Coli |
| ARG1 | Arginase 1 |
| CEA | Carcinoembryonic Antigen |
| CRC | Colorectal Cancer |
| CTLA-4 | Cytotoxic T-Lymphocyte-Associated Protein 4 |
| CXCL | C-X-C Motif Chemokine Ligand |
| DAPI | 4',6-diamidino-2-phenylindole |
| DMEM | Dulbecco's Modified Eagle Medium |
| DNA | Deoxyribonucleic acid |
| EGFR | Epidermal Growth Factor Receptor |
| EMT | Epithelial–Mesenchymal Transition |
| EV | Extracellular Vesicle |
| FAP | Fibroblast Activation Protein |
| FBS | Fetal bovine serum |
| FUT8 | Fucosyl Transferase 8 |
| H&E | Hematoxylin and eosin |
| HIF-1α | Hypoxia-Inducible Factor 1 Alpha |
| IFN-γ | Interferon Gamma |
| ICAM | Intercellular adhesion molecule |
| IL | Interleukin |
| JAK | Janus Kinase |
| KRAS | Kirsten Rat Sarcoma Viral Oncogene Homolog |
| MAPK | Mitogen-Activated Protein Kinase |

| | |
|---|---|
| MD | Molecular dynamics |
| MHC | Major Histocompatibility Complex |
| mi-RNAs | Micro RNAs |
| MMP | Matrix Metalloproteinase |
| MM-PBSA | Molecular Mechanics Poisson–Boltzmann Surface Area |
| MSI | Microsatellite Instability |
| mTOR | Mammalian Target of Rapamycin |
| NF-κB | Nuclear Factor Kappa B |
| NK cell | Natural Killer Cell |
| PBS | Phosphate Buffer Saline |
| PDB | Protein Data Bank |
| PD-1 | Programmed Cell Death Protein 1 |
| PD-L1 | Programmed Death Ligand 1 |
| PI3K | Phosphoinositide 3-Kinase |
| PMA | Phorbol 12-Myristate 13-Acetate |
| PPI | Protein–Protein Interaction |
| RT-PCR | Real-Time Quantitative Reverse Transcription PCR |
| RMSD | Root mean square deviation |
| RMSF | Root mean square fluctuation |
| RNA | Ribonucleic acid |
| ROS | Reactive Oxygen Species |
| RPMI | Roswell Park Memorial Institute Medium |
| SHP1 | Src Homology Region 2 Domain-Containing Phosphatase 1 |
| SHP2 | Src Homology Region 2 Domain-Containing Phosphatase 2 |
| STAT3 | Signal Transducer and Activator of Transcription 3 |
| TAM | Tumor-Associated Macrophage |

| | |
|---|---|
| T-Cells | T-Cytotoxic cells |
| TGF-β | Transforming Growth Factor Beta |
| THP-1 | Human Monocytic Leukemia Cell Line |
| TIM3 | T-cell Immunoglobulin and Mucin-domain Containing-3 |
| TLR | Toll-like receptors |
| TME | Tumor Microenvironment |
| TNF-α | Tumor Necrosis Factor Alpha |
| VEGF | Vascular Endothelial Growth Factor |
| Wnt | Wingless/Integrated Signaling Pathway |

# Chapter 1

## Introduction

# Chapter 1: Introduction

## 1.1 OVERVIEW OF COLORECTAL CANCER

Colorectal cancer (CRC) is one of the deadliest, commonly diagnosed cancer types worldwide, and one of the key contributors to cancer-related mortality [1]. It develops at the site of the epithelial lining of the colon and rectum, part of the large intestine, and becomes prominent through a gradual, multistep process involving the accumulation of multiple mutations [2]. In the earlier stages, it arises in normal colonic mucosa due to a mutation in the *adenomatous polyposis coli (APC)* gene, leading to initial tumor formation (Stage I) [3]. Subsequently, progression involves mutation in the *RAS* oncogene, which further promotes growth and local invasion (stage II) [4]. In addition, genetic mutations, especially in tumor protein 53 (TP53), allow tumor cells to reach lymph nodes in stage III and ultimately facilitate distant metastasis in stage IV [5,6] **See Figure 1.1**. The development of CRC is not a rapid process; it generally takes 10-15 years from initial polyp formation to malignancy, which allows opportunity for prevention through initial screening and treatment [7]. An alarming rise in the early onset of CRC is observed, underscoring the need for a better understanding of its underlying mechanisms and improved strategies for early diagnosis.

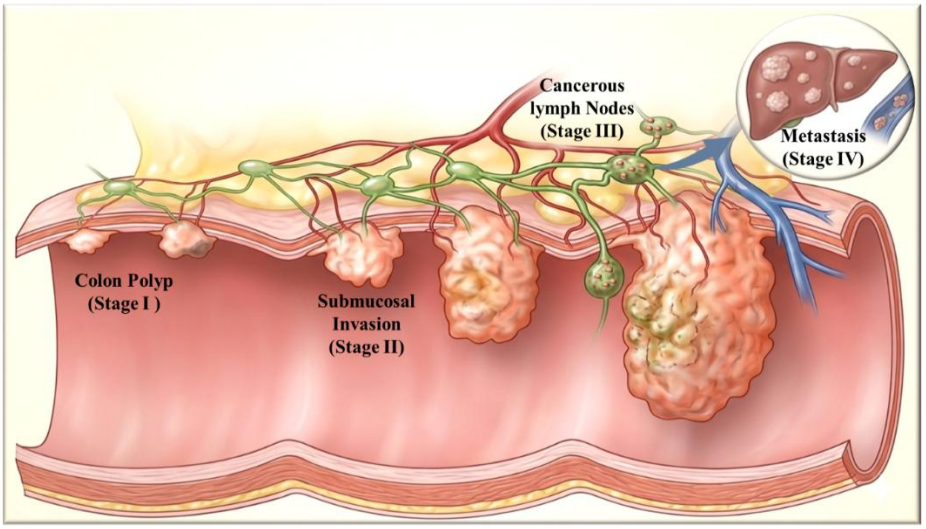


**Figure 1.1: Schematic representation of CRC progression from Stage I to Stage IV.** Stage I-II CRC remains localized to the colon or rectal wall without lymph node involvement, whereas Stage III-IV involves lymph node spread and distant metastasis to organs such as the liver. Figure prepared using Microsoft PowerPoint with icons obtained from Servier Medical Art.

## 1.2 EPIDEMIOLOGY AND RISK FACTORS OF CRC:

**1.2.1 Epidemiology:** Globally, CRC remains a significant health challenge and is ranked as the third most commonly diagnosed cancer [8]. The incidence rate of CRC varies widely across different regions of the world, with a higher rate typically observed in developed countries compared to developing countries [9]. A high incidence rate was observed in North America, Australia, New Zealand, and Europe, while countries in Africa and South Asia have the lowest incidence rate [10,11]. However, these trends are now shifting towards low-risk regions because of the adaptation of westernized lifestyle, changes in dietary patterns, as well as a lack of advancement in screening patterns and treatment [12]. This is further supported by data from the International Agency for Research on Cancer (GLOBCAN) indicate the CRC incidence is expected to increase substantially from approximately 1.8 million to over 3 million cases in the coming decade, with the fastest growth observed in low and middle-income regions undergoing rapid epidemiological transition **See Figure 1.2**. Despite advances in detection and treatment, CRC continues to be the second leading cause of cancer-related deaths only in the United States, with ~153,000 cases and ~52,000 deaths expected in 2025 [13]. As global disease patterns change, India is also reflecting these global shifts, where the burden of CRC is gradually emerging as a significant health concern. Traditionally, India has been considered a low-incidence region for cancer compared to western countries [14].

According to the Global Cancer Observatory data in India, the annual incidence rates (AARs) for CRC were 40,430 cases in males and 24,433 cases in females in 2022 [15,16]. The ratio of CRC incidence in males (AAR

5.7) is greater than in females (AAR 3.4) and contributes to more than 4% of India's cancer incidence and mortality [16]. Based on histological evaluations, approximately 93% cases of CRC patients observed in India are adenocarcinomas. In addition, 45% of colon and 55% of rectal cancer patients are detected at the locoregional stage https://ncdirindia.org/All_Reports/HBCR_2021/Default.aspx. Since a significant proportion of CRC cases are linked to preventable risk factors, highlighting the urgent need for comprehensive population-based prevention and early detection strategies. Addressing these risk factors through targeted interventions will offer a practical approach to mitigate the rising incidence of CRC in India.

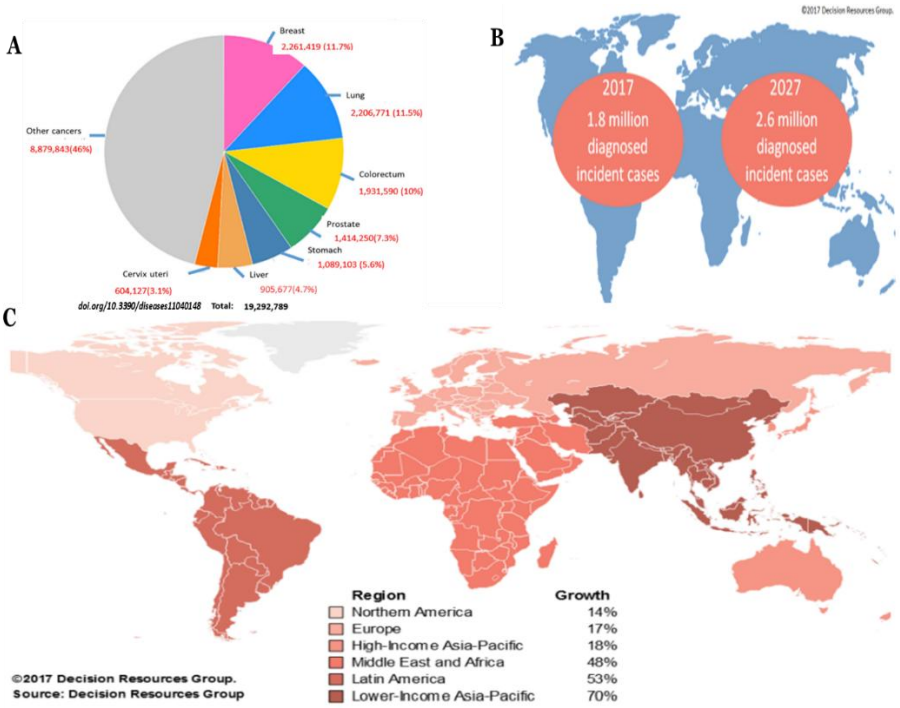



**Figure 1.2 Epidemiological burden of colorectal cancer**. (A) Global distribution of major cancer types in the human population, highlighting the prominence of breast, lung, and colorectal cancers. (B) Global incidence of colorectal cancer (CRC) with a ten-year forecast (2017–2027), illustrating the projected increase in

CRC cases worldwide. (C) Regional growth forecast of CRC incidence, showing differential trends across geographic regions.

**1.2.2 Risk Factors Associated with CRC:** The incidence rate of CRC varies worldwide due to differences in the distribution of risk factors. Among all the risk factors, increasing age is the primary driver of tumor progression, and the most pronounced increase in susceptibility begins after the age of 50 years [17]. The key risk factors include lifestyle-associated factors, medical, genetic, and surrounding environmental factors, which contribute significantly to tumor development [18].

**1.2.2.1 Lifestyle Associated Risk Factors:** Unhealthy diet and lifestyle habits contribute significantly to CRC development. Frequent consumption of red and processed meat, insufficient intake of fibre, fruits, vegetables, excessive alcohol consumption, and tobacco smoking are all well-established risk factors for CRC [19]. In addition, sedentary behaviour, such as prolonged sitting or sleeping, promotes metabolic dysfunction and increases the risk of obesity and diabetes, which favours CRC development [20].

**1.2.2.2 Clinical and biological Risk Factors:** Besides lifestyle, host-related biological factors and pre-existing medical history also plays a crucial role, such as chronic inflammatory bowel disease (IBD), ulcerative colitis, or Crohn's disease plays equally important roles in CRC progression [21]. Furthermore, obesity, diabetes, and personal history of colorectal polyps or related disorders may enhance the chances of CRC diagnosis. Recent studies also highlight the role of gut microbiota dysbiosis and environmental exposure in the development of CRC progression [22].

**1.2.2.3 Genetic and Environmental Risk Factors:** Genetic predisposition contributes to 5-10% of cases with conditions such as familial adenomatous polyposis and Lynch syndrome, which markedly increase the risk of CRC

[23]. Additionally, environmental exposure to harmful chemicals, pollutants, and other carcinogenic reagents further promotes tumorigenesis.

Collectively, CRC arises from a combination of factors and needs to focus on reducing the disease burden, although many of the risk factors contributing to tumor development are within our control and can be reduced through simple and effective lifestyle changes.

## 1.3 MOLECULAR PATHOGENESIS OF CRC:

The major cause of CRC development includes primarily chromosomal instability (CSI), which involves mutations in oncogene KRAS and tumor suppressor genes (APC, TP53, SMAD) [24]. Another mechanism involves a defect in the DNA repair system, resulting in errors accumulating during DNA replication [25]. Similarly, abnormal DNA hypermethylation silences genes that normally help regulate cell function and prevent tumor development [26].

**1.3.1 Chromosomal instability (CSI):** Among these mechanisms, the CSI pathway is most well characterized and represents the classical route of CRC development [27]. This process begins with a mutation in the APC gene, which interferes with the normal regulation of β-catenin in the Wnt-β-catenin signalling, leading to its accumulation in the nucleus and activating genes that promote cell growth [28]. Additionally, a mutation in TP53, observed in about 70% of cases, allows these abnormal cells to survive and continue dividing infinitely [29].

**1.3.2 Defective DNA repair mechanism:** Another major reason for CRC development is a defect in the DNA repair gene, particularly the mismatch repair (MMP) proteins [30]. When these proteins are mutated, they fail to correct errors that occur during DNA replication, such as single base mismatches, short insertions or deletions, even in 1-6 base pair long repeating microsatellite sequences [31].

**1.3.3 Abnormal DNA hypermethylation:** An additional mechanism involves hypermethylation of tumor suppressor genes' promoters, or proto-oncogenes such as BRAF mutation, where DNA methyltransferase enzyme adds a methyl group to the CPG site, leading to gene silencing and contributing to CRC progression [32].

Besides this important molecular alteration, other molecular-level signaling mechanisms also play an equally important role during CRC progression. However, these alterations are central to the initiation and progression, but they do not fully explain the heterogeneity in tumor behaviour, disease progression, and therapeutic response among CRC patients. This knowledge gap highlights the need to investigate additional regulatory mechanisms beyond the tumor cell intrinsic processes. Nowadays, this traditional view has been changed, and CRC progression is considered a complex and dynamic disease influenced not only by genetic alteration within tumor cells but also by the interaction with the surrounding TME [33]. Therefore, the TME emerged as a crucial contributor to shaping tumor progression through complex cellular interactions.

## 1.4 TUMOR MICROENVIRONMENT IN CRC:

The advancement of CRC relies on the multifaceted dynamics of the TME [34]. The TME is a composite and dynamic network comprising cancer cells and a variety of immune cells, including tumor-associated macrophages, T-cells, B-cells, natural killer cells, along with various other tissue-resident cell types [33]. Among them, cancer cells and immune cells crosstalk with each other and contribute to the overall behaviour of cancer. The TME is responsible for the more aggressive proliferation of tumor cells by recruiting immunosuppressive cells, rejuvenating the extracellular matrix, and promoting angiogenesis, ultimately promoting tumor proliferation and metastasis [35]. The communication between immune cells and cancer cells occurs through the secretion of soluble factors, such as cytokines,

chemokines, metalloproteins, and growth factors, as well as the release of extracellular vesicles within TME [36]; **see Figure 1.3A**. TME-containing cytokines, chemokines, and extracellular vesicles activate different signalling pathways and promote or inhibit cancer progression [37]. These inflammatory mediators, such as TNF-α, IL-1β, IL-6, and reactive oxygen species (ROS), contribute to DNA damage, genomic instability, and aberrant cell proliferation [38]. Similarly, matrix metalloproteinases facilitate remodelling of the extracellular matrix and enable tumor invasion and metastasis [39]. Pro-angiogenic factors, such as vascular endothelial growth factor (VEGF), increase new blood vessels required for tumor growth and dissemination [40]. TME-containing factors also activate oncogenic signalling, such as Wnt-β-catenin, NF-κB, which further enhance tumor cell proliferation, survival, and resistance to apoptosis [41,42]. Furthermore, an inflammatory TME helps cancer cells to avoid the immune attack and bypass immune surveillance, which leads to persistent tumor growth and therapy resistance. These processes collectively contribute to aggressive tumor development and metastasis. Overall, understanding and targeting TME in CRC is a promising approach for improving therapeutic outcomes.

### 1.4.1 TUMOR-ASSOCIATED MACROPHAGES IN CRC

Cancer progression is strongly influenced by complex interactions between cancer cells and the surrounding immune microenvironment, where tumor-associated macrophages (TAMs) represent one of the most abundant and functionally adaptable immune cell populations [43]. In general, macrophages are present in distinct populations defined by both phenotypic markers and developmental origin. Monocyte-derived macrophages express high levels of CD11b, MHC class II, and CCR2 and originate from adult hematopoietic stem cells (HSC) via circulating monocytes [44]. On the other hand, tissue-resident macrophages are marked by elevated F4/80 and CX3CR1 expression and arise from embryonic progenitors,

maintaining their populations predominantly through self-renewal within tissues [44]. Macrophages can switch into distinct phenotypes depending on stimuli. They have the potential to polarize into classically activated, pro-inflammatory, known as antitumorigenic M1 phenotype, and inhibit cancer progression, while on the other hand can also be polarized into alternatively activated anti-inflammatory tumor-promoting M2 like phenotype, suppressing the immune response and making cancer more aggressive by secreting growth factors [45]. Macrophages exhibit considerable plasticity that cannot be fully explained by the M1/M2 framework [46]. Advances in single-cell technologies, including single-cell RNA sequencing and mass cytometry, have transformed our understanding of macrophage heterogeneity [47]. This concept is reinforced by single-cell RNA-seq analysis from Xue et al., which uncovered 49 transcriptionally distinct macrophage states across 28 different activation stimuli [48]. Instead of a fixed polarization state, TAMs display adoptable functional behaviors and are continuously reshaped by tumor-derived clues, including soluble factors, extracellular vesicles (EVs), and damage-associated molecular patterns secreted by cancer cells [49,50]. In the tumor microenvironment (TME), macrophages undergo reprogramming and adopt a pro- or anti-tumor phenotype [51] See in **figure 1.3B**. Anti-tumoral type of macrophages can destroy tumor cells and prevent malignancy, whereas pro-tumoral type of macrophages support tumor growth by suppressing the immune response and facilitating angiogenesis and metastasis [52]. Macrophage responses to stimuli within TME are governed by intracellular signaling networks that link receptor activation to coordinated transcriptional regulation [53].

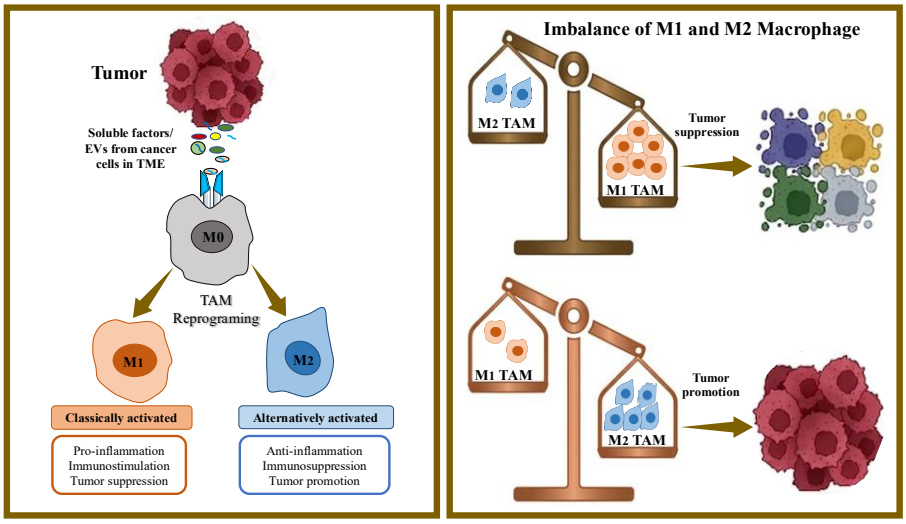



**Figure 1.3. Overview of tumor-associated macrophage reprogramming within the tumor microenvironment in CRC**. A) The macrophage polarization into TAM1 (anti-tumor) and TAM2 (pro-tumor) phenotypes within TME. B) The imbalance between these populations determines disease outcome, where TAM1 dominance promotes anti-tumor immune responses, while TAM2 enrichment supports tumor growth, immune suppression, and progression. Figure prepared using Microsoft PowerPoint with icons obtained from BioRender.

Notably, both pro- and anti-tumor types of TAMs can reprogram into each other in response to changes within the TME, and this switching is controlled by cytokines, chemokines, and other factors released by CRC cells [54]. For example, CCL2 chemokine, overexpressed by cancer cells, plays a crucial role in the recruitment of immune cells, particularly TAMs, via CCL2/CCR2 signaling [55]. Studies have already reported that CCL2/CCR2 interaction recruits TAMs and switches them into a pro-tumoral type and contributes to liver metastasis of CRC in a mouse model [56]. Colony-stimulating factor (CSF-1) and IL-34 share a common receptor CSF-1R, which is known for recruiting and converting them into tumor supportive type [57]. In contrast, the COX-2 inhibitor celecoxib reprograms macrophages from tumor supportive M2 to anti -tumor M1 type in an IFN-γ-dependent mechanism and helps to reduce intestinal tumor

growth [58]. Similarly, miR-148a and lncRNA-NBR2 polarize macrophages from tumor-promoting to anti-tumor type and suppress CRC progression [59,60]. The STAT-3 transcription factor is a key regulator of TAMs polarization, and inhibition of the JAK-STAT3 signaling reduces the tumor-supporting nature of macrophages, ultimately inhibiting metastasis of CRC cells [61,62]. Collectively, evidence suggests that signals generated within TME activate key pathways such as JAK-STAT, PI3K-AKT, NF-κB, along with various cytokines and chemokines, which together regulate macrophage polarization. The ability of TAMs to switch between different phenotypes reflects their adaptability and their role in controlling disease severity. The ability of TAMs to interchange between M1-like and M2-like phenotypes underscores their functional plasticity and their role in controlling disease outcome. Regardless of considerable progress, the molecular mechanism governing macrophage polarization in CRC remains incompletely understood. The identification of molecular mechanisms underlying macrophage phenotypic change during CRC progression is essential for advancing our understanding of disease progression and developing more effective therapeutic interventions.

### 1.4.2 ROLE OF CRC-DERIVED EXOSOMES

To advance our understanding of how CRC arises and spreads across the body, it is necessary to look beyond cancer cells. The cross-talk between CRC cells and surrounding immune and normal growing cells plays a crucial role in driving tumor growth and metastasis. This communication is achieved through the release of soluble factors, as discussed in the earlier section, such as cytokines, chemokines, and extracellular vesicles (EVs), including exosomes. The exosomes collectively facilitate the transfer of regulatory signaling molecules as well as bioactive molecular cargo to recipient cells [63]. In this regard, we specifically focus on the role of tumor-derived exosomes in macrophage polarization during CRC

progression. To highlight how CRC cell-derived exosomes contribute to macrophage reprogramming and support tumor progression.

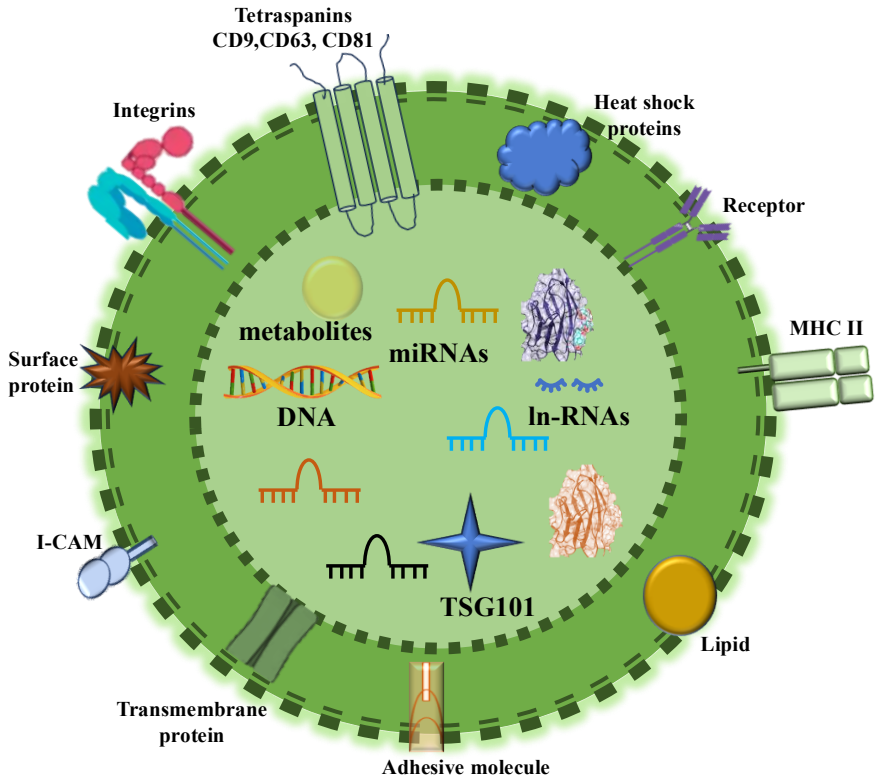



**Figure 1.4: The structure and composition of exosomes.** Exosomes consist of various biomolecules such as proteins, tetraspanins (CD9, CD63, CD81), membrane transport and fusion protein, integrin, heat shock protein (HSP70/90), endosomal sorting complex proteins (Alix, TSG101. Additionally, nucleic acids, including DNA, coding and non-coding RNAs, and lipid components

Exosomes are nanosized (40-150 nm) small vesicles, made up of lipid bilayers and enriched with bioactive cargos such as nucleic acids, proteins that reflect their cellular origin and can influence recipient cells and disease status [64,65]. CRC-derived exosomes are now recognized as key mediators of intracellular communication and are capable of transferring functional molecules that alter gene expression in recipient cells and contribute to tumor progression. Although few recent literatures demonstrated that CRC cells released exosomal miR-203a-3p regulate PTEN and activate PI3K/Akt

signaling axis, and switch macrophages towards a tumor-promoting type [66]. Similarly, CRC- exosome-containing proteins also control macrophage polarization and regulate tumor growth [67] Another interesting study reported that CRC cells derive exosomes containing miRNAs miR-21-5p and miR-200a synergistically switch macrophages towards tumor supportive phenotype and enhances the PD-L1 expression in macrophages [68]. Although the field of exosome research is still relatively new and underlying molecular mechanisms remains largely unexplored in cancer progression. Limited number of literatures is available regarding the specific role CRC derived exosomal miRNAs and proteins in macrophage polarization and functional reprogramming. Therefore, investigations in these directions offer substantial scope for further research.

## 1.5 DIAGNOSIS: CURRENT SCENARIO AND RECENT ADVANCEMENT

Currently, the diagnosis of CRC has evolved significantly, combining conventional clinical approaches with advanced molecular and imaging techniques. The conventional diagnostic approach includes colonoscopy, which remains the gold standard for early detection and permits direct visualization and removal of precancerous lesions. The other commonly used test for population-based screening includes non-invasive fecal-based tests like fecal occult blood test (FOBT) and fecal immunochemical test (FIT) [69]. Currently, cancer cells secrete circulating DNA, proteins, and exosomes that also hold the potential to improve early detection, prognosis, and therapeutic monitoring [70]. However, these methods work fine but still have some limitations in terms of sensitivity, patient comfort, and early-stage detection.

To get rid of these challenges, modern-day techniques have increasingly focused on the development of less invasive and highly sensitive diagnostic tools. These techniques, including liquid biopsy, offer the advantages of real-time disease monitoring and improved patient comfort during disease

assessment. Similarly, advancements in therapeutic approaches, including next-generation sequencing and proteomics, enable researchers to achieve more accurate molecular characterization of CRC cells. This helps early detection as well as personalized therapies in CRC. Collectively, we can say these advancements represent a major shift from traditional invasive and diagnostic methods to more precise, sensitive, non-invasive, and real-time strategies for diagnosis and CRC management.

## 1.6 RATIONALE AND OBJECTIVE OF THE STUDY

**1.6.1 Rationale:** Given the growing recognition of exosome-mediated communication in cancer and the critical role of macrophages in the TME, investigating the composition and role of CRC-derived exosomes represents an important research opportunity. This work focuses on identifying exosome-mediated molecular mechanisms that drive macrophage phenotypic switching during colorectal cancer progression. Here, we hypothesize that CRC-derived exosomes play a critical role in reprogramming macrophages toward an M2-like, tumor-supportive phenotype. Accordingly, we propose a disease model illustrating CRC-macrophage interactions see **Figure 1.5**.

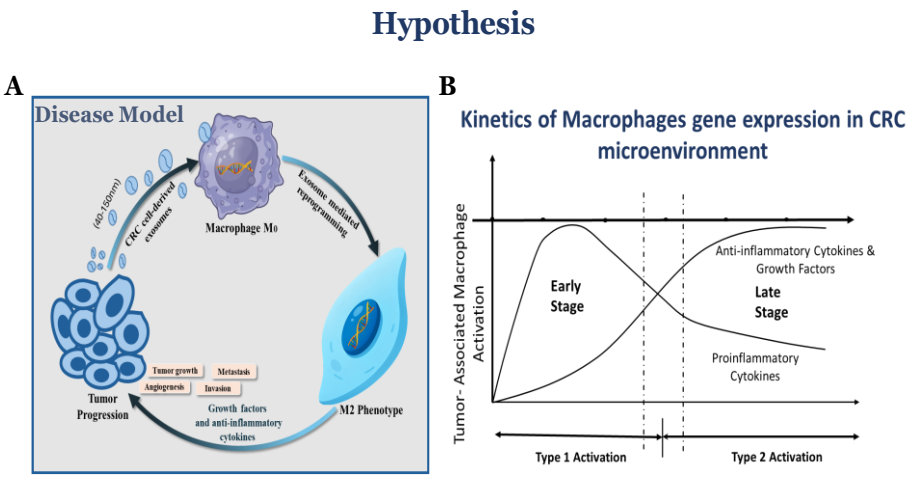


**Figure 1.5 A)** Disease model illustrating CRC cell-derived exosome-mediated macrophage reprogramming. **B)** Kinetics study of macrophages gene expression in CRC microenvironment

**1.6.2 Objective:** To gain a more detailed understanding of this mechanism, we propose the following objectives.

4. **Investigating macrophage morphological changes in response to CRC cells co-culture conditions**
5. **Dissecting the signaling mechanism of macrophage polarization in response to CRC cells-derived exosomes**
6. **Designing therapeutic interventions (Anti-miRNA/ small molecules/ peptide) against the identified target molecule**

## 1.7 NOVEL FINDINGS AND LIMITATIONS OF THIS STUDY

**1.7.1 Novelty:** This study establishes for the first time, the temporal kinetics of macrophage gene expression and functional reprogramming after CRC-exosome treatment. To the best of our knowledge, this concept was lacking in existing studies. We further uncovered a previously unexplored mechanism by which exosomes activate NF-κB signalling in CRC. In addition, we explored the response of macrophages to CRC-derived exosomes and observed a significant upregulation of PD-L1 expression. Notably, our findings reveal for the first time that exosome-educated macrophages enhance PD-L1 expression in CRC cells, contributing to suppression of T-cell-mediated response. To address this, we proposed a potential PD-L1 inhibitor, which shows encouraging results in our *in-silico* studies compared to existing small-molecule inhibitors in clinical trials.

**1.7.2 Limitation:** The limitations of this study include the lack of in vivo validation of NF-κB involvement and PD-L1-mediated immunosuppression. Further mechanistic and experimental validation of the proposed PD-L1 inhibitor is needed for clinical translation.

## 1.8 THESIS ORGANIZATION

The thesis is systematically organized into the following chapters to provide in-depth and mechanistic insights into CRC progression. Each chapter addresses a specific aspect of the study and collectively contributes to a comprehensive understanding of the overall study.

**Chapter 1:** It provides an overview of the research area, focusing on CRC and its underlying molecular mechanism. It also highlights the role of exosome-mediated communication between CRC cells and tumor-associated macrophages within TME. Additionally, it outlines the fundamental concept of CRC, emphasizing the global burden, molecular pathogenesis, significance, research gap, hypothesis, and objectives of the study.

**Chapter 2:** This chapter sheds light on the review of existing literature relevant to the composition of exosomes released from cancer cells and their role in TAMs polarization. Here, we discuss how exosomal cargo, including proteins, glycoproteins, and miRNAs, influences key signalling pathways involved in macrophage polarization within TME. Furthermore, it highlights the current understanding of exosomes' composition, function, and therapeutic approaches. It also points out gaps in existing studies that need further investigation in this area.

**Chapter 3:** This chapter includes the key findings from the research work, highlighting the interaction between CRC-exosomes and macrophages. It also explores the underlying molecular mechanism involved, especially through NF-κB signalling pathways, which further supports the more aggressive growth and metastasis of CRC cells.

**Chapter 4:** This chapter focuses on PD-L1 as a therapeutic target, describing its role in immune evasion in CRC and its regulation within TME. It further explores targeting PD-1/PD-L1 axis in an *in-silico* approach, particularly molecular docking and computational screening to

identify potential inhibitors. This approach included the utilization of a marine natural product database to screen for compounds that can target PD-L1, and to develop new strategies for cancer immunotherapy.

**Chapter 5:** In this chapter, we focused on glycoprotein which influence tumor development. While targeting the carcinoembryonic antigen (CEA), we identified Fucosyltransferase 8 (FUT8) as a promising therapeutic target in CRC. In silico screening of marine natural compounds reveals promising FUT8 inhibitors with favorable binding affinity, stability, and pharmacokinetic properties. This finding suggested that targeting FUT8 could mitigate CEA function and may represent a potential therapeutic intervention for CRC treatment.

**Chapter 6:** This chapter concludes the thesis with the key findings of the study, highlighting the role of CRC cells-derived exosomes in macrophage reprogramming and NF-κB mediated signalling. In addition, it discusses the importance of targeting PD-L1 and FUT8-mediated core fucosylation of CEA to overcome the problem of immune evasion.

**Chapter 7:** This chapter discusses possible new future directions for further research based on the findings of this study. We also explore the key components of this TME, especially exosomes, which may serve as a therapeutic intervention for CRC treatment. It also provides inputs about what are possible ways to inhibit cancer progression by targeting macrophage polarization, immune checkpoints, glycoproteins within TME, and reprogramming of pro-tumoral macrophages towards an anti-tumor phenotype.

## 1.9 REFERENCES

[1] K. Mani, D. Deng, C. Lin, M. Wang, M.L. Hsu, N.G. Zaorsky, Causes of death among people living with metastatic cancer, Nat. Commun. 15 (2024) 1519. https://doi.org/10.1038/s41467-024-45307-x.

[2] K. Bardhan, K. Liu, Epigenetics and Colorectal Cancer Pathogenesis, Cancers 5 (2013) 676–713. https://doi.org/10.3390/cancers5020676.

[3] H. Lamlum, A. Papadopoulou, M. Ilyas, A. Rowan, C. Gillet, A. Hanby, I. Talbot, W. Bodmer, I. Tomlinson, *APC* mutations are sufficient for the growth of early colorectal adenomas, Proc. Natl. Acad. Sci. 97 (2000) 2225–2228. https://doi.org/10.1073/pnas.040564697.

[4] J.B.E. Janssen, J.P. Medema, E.C. Gootjes, D.V.F. Tauriello, H.M.W. Verheul, Mutant RAS and the tumor microenvironment as dual therapeutic targets for advanced colorectal cancer, Cancer Treat. Rev. 109 (2022) 102433. https://doi.org/10.1016/j.ctrv.2022.102433.

[5] T. Mizutani, M. Boretto, S. Lim, J. Drost, D.M. González, R. Oka, M.H. Geurts, H. Begthel, J. Korving, J.H. Van Es, R. Van Boxtel, H. Clevers, Recapitulating the adenoma–carcinoma sequence by selection of four spontaneous oncogenic mutations in mismatch-repair-deficient human colon organoids, Nat. Cancer 5 (2024) 1852–1867. https://doi.org/10.1038/s43018-024-00841-x.

[6] Q. Tang, Z. Su, W. Gu, A.K. Rustgi, Mutant p53 on the Path to Metastasis, Trends Cancer 6 (2020) 62–73. https://doi.org/10.1016/j.trecan.2019.11.004.

[7] Md.S. Hossain, H. Karuniawati, A.A. Jairoun, Z. Urbi, D.J. Ooi, A. John, Y.C. Lim, K.M.K. Kibria, A.K.M. Mohiuddin, L.C. Ming, K.W. Goh, M.A. Hadi, Colorectal Cancer: A Review of Carcinogenesis, Global Epidemiology, Current Challenges, Risk Factors, Preventive and Treatment

Strategies, Cancers 14 (2022) 1732. https://doi.org/10.3390/cancers14071732.

[8] G. Roshandel, F. Ghasemi-Kebria, R. Malekzadeh, Colorectal Cancer: Epidemiology, Risk Factors, and Prevention, Cancers 16 (2024) 1530. https://doi.org/10.3390/cancers16081530.

[9] A. Mohammadain, S. Kheiri, D. Darmadi, Global Disparities in Colorectal Cancer: Unveiling the Present Landscape of Incidence and Mortality Rates, Analyzing Geographical Variances, and Assessing the Human Development Index, J. Prev. Med. Hyg. (2025) E499 Pages. https://doi.org/10.15167/2421-4248/JPMH2024.65.4.3071.

[10] B. Yao, Y. Zhang, S. Li, Y. Tian, M. Ashrafizadeh, H. Rastin, M. Tang, Y. Li, Colorectal cancer epidemiology (1990–2050): lessons from the Australasian experience, J. Transl. Med. 23 (2025) 855. https://doi.org/10.1186/s12967-025-06630-z.

[11] P. Rawla, T. Sunkara, A. Barsouk, Epidemiology of colorectal cancer: incidence, mortality, survival, and risk factors, Gastroenterol. Rev. 14 (2019) 89–103. https://doi.org/10.5114/pg.2018.81072.

[12] J. Zhao, D. Miao, T. Yang, J. Chen, X. Lai, Trend analysis and epidemiological forecasting of colorectal Cancer mortality among reproductive-age women in sub-Saharan Africa, Prev. Med. Rep. 56 (2025) 103167. https://doi.org/10.1016/j.pmedr.2025.103167.

[13] R.L. Siegel, N.S. Wagle, J. Star, T.B. Kratzer, R.A. Smith, A. Jemal, Colorectal cancer statistics, 2026, CA. Cancer J. Clin. 76 (2026) e70067. https://doi.org/10.3322/caac.70067.

[14] G. Patel, P. Patil, Worrisome Trends in Young-Onset Colorectal Cancer: Now Is the Time for Action, Indian J. Surg. Oncol. 13 (2022) 446–452. https://doi.org/10.1007/s13193-022-01496-9.

[15] A. Loomba, J. Hundal, D. Patel, S602 Colorectal Cancer Screening in India: A Neglected Priority, Am. J. Gastroenterol. 120 (2025) S129–S129. https://doi.org/10.14309/01.ajg.0001129868.12188.51.

[16] S. Shivshankar, P.S. Patil, K. Deodhar, A.M. Budukh, Epidemiology of colorectal cancer: A review with special emphasis on India, Indian J. Gastroenterol. (2025). https://doi.org/10.1007/s12664-024-01726-8.

[17] T.A. Zaki, A.G. Singal, F.P. May, C.C. Murphy, Increasing Incidence Rates of Colorectal Cancer at Ages 50–54 Years, Gastroenterology 162 (2022) 964-965.e3. https://doi.org/10.1053/j.gastro.2021.10.039.

[18] G. Roshandel, F. Ghasemi-Kebria, R. Malekzadeh, Colorectal Cancer: Epidemiology, Risk Factors, and Prevention, Cancers 16 (2024) 1530. https://doi.org/10.3390/cancers16081530.

[19] Q. Yuan, J. Liu, X. Wang, C. Du, Y. Zhang, L. Lin, C. Wang, Z. Hong, Deciphering the impact of dietary habits and behavioral patterns on colorectal cancer, Int. J. Surg. 111 (2025) 2603–2612. https://doi.org/10.1097/JS9.0000000000002229.

[20] Y. Yang, Z. Han, X. Li, A. Huang, J. Shi, J. Gu, Key Laboratory of Carcinogenesis and Translational Research (Ministry of Education/Beijing), Center of Gastrointestinal Surgery, Peking University Cancer Hospital & Institute, Beijing 100142, China, Key Laboratory of Carcinogenesis and Translational Research (Ministry of Education/Beijing), Department of Gastrointestinal Oncology, Peking University Cancer Hospital & Institute, Beijing 100142, China, Peking-Tsinghua Center for Life Science, Peking University International Cancer Center, Beijing 100142, China, Department of Gastrointestinal Surgery, Peking University Shougang Hospital, Beijing 100144, China, Epidemiology and risk factors of colorectal cancer in China, Chin. J. Cancer

Res. 32 (2020) 729–741. https://doi.org/10.21147/j.issn.1000-9604.2020.06.06.

[21] Y. Sato, S. Tsujinaka, T. Miura, Y. Kitamura, H. Suzuki, C. Shibata, Inflammatory Bowel Disease and Colorectal Cancer: Epidemiology, Etiology, Surveillance, and Management, Cancers 15 (2023) 4154. https://doi.org/10.3390/cancers15164154.

[22] D.N. Paduraru, A.C. Palcau, V.G. Dinca, D.M. Ciuc, A. Constantinescu, The Role of Gut Microbiota in Colorectal Cancer Pathogenesis: A Comprehensive Literature Review, Int. J. Mol. Sci. 26 (2025) 11870. https://doi.org/10.3390/ijms262411870.

[23] M. Mahdouani, D. Zhuri, F. Dusenkalkan, H. Gurkan, S. Yalcintepe, Genomic characterization of patients with colorectal cancer, Hered. Cancer Clin. Pract. 23 (2025) 21. https://doi.org/10.1186/s13053-025-00322-x.

[24] H. Nguyen, H. Duong, The molecular characteristics of colorectal cancer: Implications for diagnosis and therapy (Review), Oncol. Lett. (2018). https://doi.org/10.3892/ol.2018.8679.

[25] L.H. Nguyen, A. Goel, D.C. Chung, Pathways of Colorectal Carcinogenesis, Gastroenterology 158 (2020) 291–302. https://doi.org/10.1053/j.gastro.2019.08.059.

[26] A. Agrawal, R.F. Murphy, D.K. Agrawal, DNA methylation in breast and colorectal cancers, Mod. Pathol. 20 (2007) 711–721. https://doi.org/10.1038/modpathol.3800822.

[27] M.S. Pino, D.C. Chung, The Chromosomal Instability Pathway in Colon Cancer, Gastroenterology 138 (2010) 2059–2072. https://doi.org/10.1053/j.gastro.2009.12.065.

[28] T.W. Parker, K.L. Neufeld, APC controls Wnt-induced β-catenin destruction complex recruitment in human colonocytes, Sci. Rep. 10 (2020) 2957. https://doi.org/10.1038/s41598-020-59899-z.

[29] S. Yan, F. Zhan, Y. He, Y. Zhu, Z. Ma, p53 in colorectal cancer: from a master player to a privileged therapy target, J. Transl. Med. 23 (2025) 684. https://doi.org/10.1186/s12967-025-06566-4.

[30] J. Taieb, M. Svrcek, R. Cohen, D. Basile, D. Tougeron, J.-M. Phelip, Deficient mismatch repair/microsatellite unstable colorectal cancer: Diagnosis, prognosis and treatment, Eur. J. Cancer 175 (2022) 136–157. https://doi.org/10.1016/j.ejca.2022.07.020.

[31] G.L. de' Angelis, L. Bottarelli, C. Azzoni, N. de' Angelis, G. Leandro, F. Di Mario, F. Gaiani, F. Negri, Microsatellite instability in colorectal cancer, Acta Bio Medica Atenei Parm. 89 (2018) 97–101. https://doi.org/10.23750/abm.v89i9-S.7960.

[32] D.J. Weisenberger, K.D. Siegmund, M. Campan, J. Young, T.I. Long, M.A. Faasse, G.H. Kang, M. Widschwendter, D. Weener, D. Buchanan, H. Koh, L. Simms, M. Barker, B. Leggett, J. Levine, M. Kim, A.J. French, S.N. Thibodeau, J. Jass, R. Haile, P.W. Laird, CpG island methylator phenotype underlies sporadic microsatellite instability and is tightly associated with BRAF mutation in colorectal cancer, Nat. Genet. 38 (2006) 787–793. https://doi.org/10.1038/ng1834.

[33] K.E. De Visser, J.A. Joyce, The evolving tumor microenvironment: From cancer initiation to metastatic outgrowth, Cancer Cell 41 (2023) 374–403. https://doi.org/10.1016/j.ccell.2023.02.016.

[34] T.L. Whiteside, The tumor microenvironment and its role in promoting tumor growth, Oncogene 27 (2008) 5904–5912. https://doi.org/10.1038/onc.2008.271.

[35] N. Zafari, F. Khosravi, Z. Rezaee, S. Esfandyari, M. Bahiraei, A. Bahramy, G.A. Ferns, A. Avan, The role of the tumor microenvironment in colorectal cancer and the potential therapeutic approaches, J. Clin. Lab. Anal. 36 (2022) e24585. https://doi.org/10.1002/jcla.24585.

[36] J. Pörschke, S. Heidemann, H.P. Nehring, A. Lluch, W. Szymański, F. Finkernagel, C. Preußer, A.M. Bhagwat, T.J. Stamm, L. Sommerfeld, F. Helmprobst, R. Müller, S. Reinartz, J. Graumann, E. Pogge Von Strandmann, M. Gómez-Serrano, Tumor-associated macrophages display differential protein cargo sorting in extracellular vesicles associated with poor survival in ovarian cancer, Mol. Med. 32 (2026) 16. https://doi.org/10.1186/s10020-025-01416-x.

[37] P. Hou, H. Chen, Extracellular vesicles in the tumor immune microenvironment, Cancer Lett. 516 (2021) 48–56. https://doi.org/10.1016/j.canlet.2021.05.032.

[38] N. Rembiałkowska, Z. Kocik, A. Kłosińska, M. Kübler, A. Pałkiewicz, W. Rozmus, M. Sędzik, H. Wojciechowska, A. Gajewska-Naryniecka, Inflammation-Driven Genomic Instability: A Pathway to Cancer Development and Therapy Resistance, Pharmaceuticals 18 (2025) 1406. https://doi.org/10.3390/ph18091406.

[39] G.A. Cabral-Pacheco, I. Garza-Veloz, C. Castruita-De La Rosa, J.M. Ramirez-Acuña, B.A. Perez-Romero, J.F. Guerrero-Rodriguez, N. Martinez-Avila, M.L. Martinez-Fierro, The Roles of Matrix Metalloproteinases and Their Inhibitors in Human Diseases, Int. J. Mol. Sci. 21 (2020) 9739. https://doi.org/10.3390/ijms21249739.

[40] H. Mahaki, S. Nobari, H. Tanzadehpanah, A. Babaeizad, G. Kazemzadeh, M. Mehrabzadeh, A. Valipour, N. Yazdinezhad, H. Manoochehri, P. Yang, M. Sheykhhasan, Targeting VEGF signaling for tumor microenvironment remodeling and metastasis inhibition: Therapeutic

strategies and insights, Biomed. Pharmacother. 186 (2025) 118023. https://doi.org/10.1016/j.biopha.2025.118023.

[41] P. Yang, X. Li, L. Yang, N. Xiao, L. Ren, M. Ji, H. Yang, NF-κB signaling in hepatocellular carcinoma: Mechanisms of tumor progression, immune evasion, and therapeutic resistance, Transl. Oncol. 67 (2026) 102760. https://doi.org/10.1016/j.tranon.2026.102760.

[42] Y. Ruan, H. Ogana, E. Gang, H.N. Kim, Y.-M. Kim, Wnt Signaling in the Tumor Microenvironment, in: A. Birbrair (Ed.), Tumor Microenviron., Springer International Publishing, Cham, 2021: pp. 107–121. https://doi.org/10.1007/978-3-030-47189-7_7.

[43] M.J. Pittet, O. Michielin, D. Migliorini, Clinical relevance of tumour-associated macrophages, Nat. Rev. Clin. Oncol. 19 (2022) 402–421. https://doi.org/10.1038/s41571-022-00620-6.

[44] E. Mass, I. Ballesteros, M. Farlik, F. Halbritter, P. Günther, L. Crozet, C.E. Jacome-Galarza, K. Händler, J. Klughammer, Y. Kobayashi, E. Gomez-Perdiguero, J.L. Schultze, M. Beyer, C. Bock, F. Geissmann, Specification of tissue-resident macrophages during organogenesis, Science 353 (2016) aaf4238. https://doi.org/10.1126/science.aaf4238.

[45] Y. Yao, X.-H. Xu, L. Jin, Macrophage Polarization in Physiological and Pathological Pregnancy, Front. Immunol. 10 (2019) 792. https://doi.org/10.3389/fimmu.2019.00792.

[46] W. Zhao, Z. Zhang, M. Xie, F. Ding, X. Zheng, S. Sun, J. Du, Exploring tumor-associated macrophages in glioblastoma: from diversity to therapy, Npj Precis. Oncol. 9 (2025) 126. https://doi.org/10.1038/s41698-025-00920-x.

[47] L. Yan, J. Wang, X. Cai, Y. Liou, H. Shen, J. Hao, C. Huang, G. Luo, W. He, Macrophage plasticity: signaling pathways, tissue repair, and regeneration, MedComm 5 (2024) e658. https://doi.org/10.1002/mco2.658.

[48] J. Xue, S.V. Schmidt, J. Sander, A. Draffehn, W. Krebs, I. Quester, D. De Nardo, T.D. Gohel, M. Emde, L. Schmidleithner, H. Ganesan, A. Nino-Castro, M.R. Mallmann, L. Labzin, H. Theis, M. Kraut, M. Beyer, E. Latz, T.C. Freeman, T. Ulas, J.L. Schultze, Transcriptome-Based Network Analysis Reveals a Spectrum Model of Human Macrophage Activation, Immunity 40 (2014) 274–288. https://doi.org/10.1016/j.immuni.2014.01.006.

[49] J. Zhao, B. Wang, X. Li, C. Wei, Y. Min, D. Wang, Single-cell transcriptomic analysis reveals the heterogeneity and functional characteristics of macrophage subpopulations in colon cancer, Discov. Oncol. 17 (2025) 101. https://doi.org/10.1007/s12672-025-04002-z.

[50] J. Xu, L. Ding, J. Mei, Y. Hu, X. Kong, S. Dai, T. Bu, Q. Xiao, K. Ding, Dual roles and therapeutic targeting of tumor-associated macrophages in tumor microenvironments, Signal Transduct. Target. Ther. 10 (2025) 268. https://doi.org/10.1038/s41392-025-02325-5.

[51] T.A. Wynn, A. Chawla, J.W. Pollard, Macrophage biology in development, homeostasis and disease, Nature 496 (2013) 445–455. https://doi.org/10.1038/nature12034.

[52] S. Gordon, Alternative activation of macrophages, Nat. Rev. Immunol. 3 (2003) 23–35. https://doi.org/10.1038/nri978.

[53] M. Li, M. Wang, Y. Wen, H. Zhang, G. Zhao, Q. Gao, Signaling pathways in macrophages: molecular mechanisms and therapeutic targets, MedComm 4 (2023) e349. https://doi.org/10.1002/mco2.349.

[54] X. Zhong, B. Chen, Z. Yang, The Role of Tumor-Associated Macrophages in Colorectal Carcinoma Progression, Cell. Physiol. Biochem. 45 (2018) 356–365. https://doi.org/10.1159/000486816.

[55] X. Zhong, B. Chen, Z. Yang, The Role of Tumor-Associated Macrophages in Colorectal Carcinoma Progression, Cell. Physiol. Biochem. 45 (2018) 356–365. https://doi.org/10.1159/000486816.

[56] W. Tu, J. Gong, Z. Zhou, D. Tian, Z. Wang, TCF4 enhances hepatic metastasis of colorectal cancer by regulating tumor-associated macrophage via CCL2/CCR2 signaling, Cell Death Dis. 12 (2021) 882. https://doi.org/10.1038/s41419-021-04166-w.

[57] C. Gao, W. Hu, J. Zhao, X. Ni, Y. Xu, LncRNA HCG18 promotes M2 macrophage polarization to accelerate cetuximab resistance in colorectal cancer through regulating miR-365a-3p/FOXO1/CSF-1 axis, Pathol. - Res. Pract. 240 (2022) 154227. https://doi.org/10.1016/j.prp.2022.154227.

[58] Y. Nakanishi, M. Nakatsuji, H. Seno, S. Ishizu, R. Akitake-Kawano, K. Kanda, T. Ueo, H. Komekado, M. Kawada, M. Minami, T. Chiba, COX-2 inhibition alters the phenotype of tumor-associated macrophages from M2 to M1 in ApcMin/+ mouse polyps, Carcinogenesis 32 (2011) 1333–1339. https://doi.org/10.1093/carcin/bgr128.

[59] F. Lai, H. Zhang, B. Xu, Y. Xie, H. Yu, Long non-coding RNA NBR2 suppresses the progress of colorectal cancer in vitro and in vivo by regulating the polarization of TAM, Bioengineered 12 (2021) 5462–5475. https://doi.org/10.1080/21655979.2021.1958558.

[60] D. Ma, Y. Zhang, G. Chen, J. Yan, miR-148a Affects Polarization of THP-1-Derived Macrophages and Reduces Recruitment of Tumor-Associated Macrophages via Targeting SIRPα, Cancer Manag. Res. Volume 12 (2020) 8067–8077. https://doi.org/10.2147/CMAR.S238317.

[61] H. Zhang, B. Zhao, H. Wei, H. Zeng, D. Sheng, Y. Zhang, Cucurbitacin B controls M2 macrophage polarization to suppresses metastasis via targeting JAK-2/STAT3 signalling pathway in colorectal

cancer, J. Ethnopharmacol. 287 (2022) 114915. https://doi.org/10.1016/j.jep.2021.114915.

[62] T. Xia, M. Zhang, W. Lei, R. Yang, S. Fu, Z. Fan, Y. Yang, T. Zhang, Advances in the role of STAT3 in macrophage polarization, Front. Immunol. 14 (2023) 1160719. https://doi.org/10.3389/fimmu.2023.1160719.

[63] F.A. Pelissier Vatter, M. Cioffi, S.J. Hanna, I. Castarede, S. Caielli, V. Pascual, I. Matei, D. Lyden, Extracellular vesicle– and particle-mediated communication shapes innate and adaptive immune responses, J. Exp. Med. 218 (2021) e20202579. https://doi.org/10.1084/jem.20202579.

[64] F. Ciregia, A. Urbani, G. Palmisano, Extracellular Vesicles in Brain Tumors and Neurodegenerative Diseases, Front. Mol. Neurosci. 10 (2017) 276. https://doi.org/10.3389/fnmol.2017.00276.

[65] E.R. Abels, X.O. Breakefield, Introduction to Extracellular Vesicles: Biogenesis, RNA Cargo Selection, Content, Release, and Uptake, Cell. Mol. Neurobiol. 36 (2016) 301–312. https://doi.org/10.1007/s10571-016-0366-z.

[66] W. Pei, K. Wei, Y. Wu, Q. Qiu, H. Zhu, L. Mao, X. Shi, S. Zhang, Y. Shi, S. Tao, H. Mao, S. Pang, J. Wang, M. Liu, W. Wang, Q. Yang, C. Chen, Colorectal cancer tumor cell-derived exosomal miR-203a-3p promotes CRC metastasis by targeting PTEN-induced macrophage polarization, Gene 885 (2023) 147692. https://doi.org/10.1016/j.gene.2023.147692.

[67] K. Wadhonkar, Y. Singh, A. Rughetti, S. Das, R. Yangdol, M.H. Sk, M.S. Baig, Role of cancer cell-derived exosomal glycoproteins in macrophage polarization, Mol. Biol. Rep. 52 (2025) 451. https://doi.org/10.1007/s11033-025-10535-x.

[68] Y. Yin, B. Liu, Y. Cao, S. Yao, Y. Liu, G. Jin, Y. Qin, Y. Chen, K. Cui, L. Zhou, Z. Bian, B. Fei, S. Huang, Z. Huang, Colorectal Cancer-Derived Small Extracellular Vesicles Promote Tumor Immune Evasion by Upregulating PD-L1 Expression in Tumor-Associated Macrophages, Adv. Sci. 9 (2022) 2102620. https://doi.org/10.1002/advs.202102620.

[69] L. Tang, X. Zhao, G. Wang, J. Huang, M. Zhang, W. Xu, Advances in colorectal cancer screening: technological innovations, guideline discrepancies, and individualized strategies, Front. Oncol. 15 (2025) 1723546. https://doi.org/10.3389/fonc.2025.1723546.

[70] L. Ma, H. Guo, Y. Zhao, Z. Liu, C. Wang, J. Bu, T. Sun, J. Wei, Liquid biopsy in cancer: current status, challenges and future prospects, Signal Transduct. Target. Ther. 9 (2024) 336. https://doi.org/10.1038/s41392-024-02021-w.

# Chapter 2

## Review literature

# Chapter 2: Literature Review

As discussed in Chapter 1, the TME is a highly dynamic milieu in which continuous crosstalk occurs between tumor cells and immune cells via the release of soluble factors and extracellular vesicles (EVs). Among the different types of EVs, exosomes have emerged as key cargo transporters from donor cells to recipient cells. Considering their crucial role in cellular response regulation within TME, our research study mainly focuses on exosome-mediated communication between CRC cells and TAMs. This chapter provides a comprehensive review of the existing literature related to exosome contents and their role in macrophage polarization and cancer progression-associated signaling. In this context, we initially summarized the role of exosomal proteins in the regulation of macrophage polarization within TME.

## 2.1 Tumor-derived exosomal protein role in macrophage polarization

Exosomal protein overexpression in various cancer cells leads to the polarization of Macrophages [1]. The effect of different exosomal proteins on recipient macrophages in the TME leads to multiple downstream signaling pathways that determine the fate of the macrophages (M1 or M2) [2]. Therefore, identifying the role of different exosomal proteins in various types of cancer and understanding their effect on macrophage polarization is vital for comprehending the molecular basis of cancer progression. This knowledge can aid in developing novel therapeutic strategies against different types of cancer.

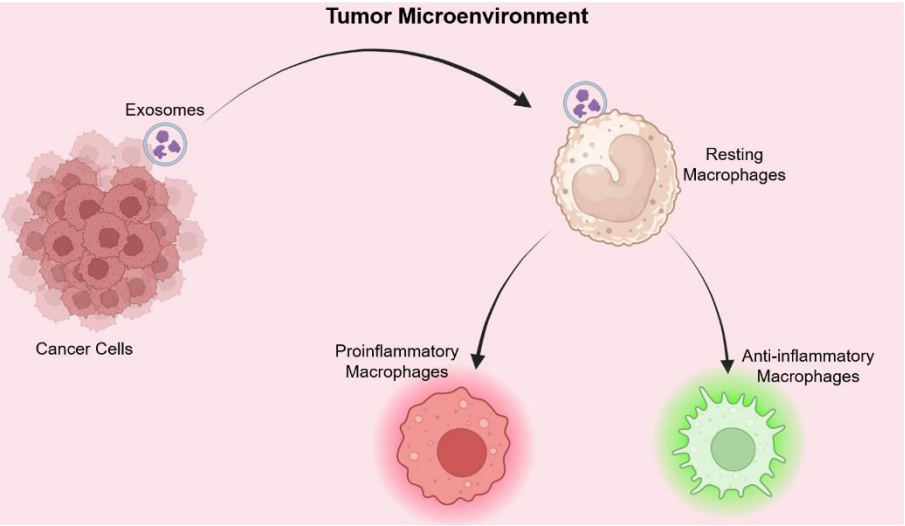



**Figure 2.1**: Schematic diagram of macrophage polarization in response to exosomal protein content. Created using Bio Render software (https://biorender.com).

**2.1.1 Exosomal proteins driving M2 macrophage polarization-** Exosomal proteins are pivotal in the intricate communication between cancer cells and macrophages. These proteins exert their influence through diverse signaling pathways, including the JAK (Janus Kinase)-STAT (Signal Transducer and Activator of Transcription), and PI3K(Phosphoinositide 3-Kinase)-AKT (Protein Kinase) signaling pathway. The activation of the JAK/STAT signaling occurs when a ligand binds to surface receptors, which leads to JAK phosphorylation and STAT activation [3]. Upon phosphorylation, STAT proteins migrate to the nucleus, where they specifically bind to DNA, and modulate gene expression [4]. Similarly, the PI3K-AKT signaling pathway is activated through receptors like TLR and IL-R, triggering PI3K activation that generates PIP3 which leads to AKT recruitment and phosphorylation, which initiates downstream signaling, including transcription factor NF-κB inhibition or STAT activation [5–7]. Their collective impact typically induces the polarization of macrophages towards the alternatively activated M2 phenotype, characterized by anti-inflammatory properties and pro-

tumorigenic effects. This shift in macrophages further facilitates the progression of cancer.

***Leptin-*** Leptin, encoded by the lep gene, is a crucial adipokine involved in signal transduction pathways (AMPK, PI3K/AKT, ERK1/2, STAT3) influencing energy balance, metabolism, immune response, tumorigenesis, and cancer metastasis. It plays an essential role in macrophage polarization and is associated with the invasion as well as migration of gallbladder cancer (GBC) cells. Zhao et al. reported that leptin is abundantly present in exosomes derived from GBC cells, where it can be transferred to macrophages, promoting M2 polarization [8]. When leptin binds to the leptin receptor (tyrosine kinase-associated receptor) on the plasma membrane, it forms complexes of ligand-receptor and immediately triggers the phosphorylation of the JAK. The phosphorylated tyrosine site on JAK help to recruit STAT3 with the SH2 structural domain for phosphorylation modification [9]. Upon phosphorylation, STAT3 (p-STAT) undergoes dimerization and enters inside the nucleus. Subsequently, it interacts with specific genes and regulates expression, and promotes macrophage polarization into the M2 phenotype, enhancing cancer cell invasion and migration [8,10]. is
known as an anti-inflammatory cytokine and involved in the regulation of inflammatory response [11] and is also responsible for skewing macrophages into a pro-tumorigenic phenotype [12]. IL-10 is detected in exosomes of non-small cell lung cancer (NSCLC) and small cell lung cancer (SCLC) [13]. Studies revealed that it is also upregulated in breast cancer [14]. The Binding of IL-10 dimerizes the receptor, i.e., JAK1 dimerizes with TYK 2 [12], and then the JAKs are activated by interactive tyrosine phosphorylation. Subsequently, the activated JAKs catalyze the phosphorylation of tyrosine residues on the dimerized receptors, facilitating the recruitment of STAT3. These recruited STAT3 then bind to the receptors and undergo phosphorylation by the activated JAKs. Then, the phosphorylated STAT3 detaches from the receptor, forming dimers within

the cytoplasm, and subsequently translocates inside the nucleus. These dimers bind with the promoter of the specific gene, leading to the expression of M2-related genes (Arg-1, CD 206, IL-6) [15], and contribute to the advancement of cancer.

***Glucose-regulated protein-78 (GRP78)***- GRP78, a 78KDa protein, also known as BiP and HSP5a, exhibits multifunctional properties that extend beyond its established involvement in the unfolded protein response (UPR) activated during endoplasmic reticulum (ER) stress. GRP78 plays a significant role in tumor cells' survival, proliferation, and chemoresistance development. GRP78 influences how cancer cells survive, proliferate, and develop chemoresistance [16]. The expression of GRP78 is elevated in lung cancer [17]. Additionally, GRP78 is identified as a protein found in exosomes derived from gastric cancer cells[18]. Upon stimulation with IGF-1, GRP78 binds to IGF-1R, activating the JAK/STAT pathway in macrophages. This interaction likely induces the phosphorylation of JAK1 and JAK2, subsequently leading to the recruitment and phosphorylation of STAT3 and STAT6. Phosphorylated STAT3 and STAT6 then form homodimers, migrate toward the nucleus, and attach to specific promoters, inducing the expression of M2-associated genes. Notably, the knockdown of GRP78 or PERK in breast cancer promotes M1 polarization. Furthermore, GRP78 may regulate macrophage polarization through downstream PERK (Protein Kinase RNA-Like ER Kinase) or IRE1 (Inositol-requiring enzyme type 1) signaling, independently of the IGF-1/IGF-1R pathway [19], and thus fostering the progression of cancer.

***Plasminogen activator inhibitor-1 (PAI-1)***- PAI-1 or SERPINE1, a multiple myeloma cell-derived exosomal protein [20], has a tumor-supportive role via its pro-angiogenic and anti-apoptotic activities further; it is also reported that PAI-1 supports M2 polarization [21]. It is also overexpressed in pancreatic cancer, glioma, and melanoma [22]. Kubala et

al. reported that PAI-1 polarizes macrophages through the uPA domain that interacts with uPAR, a GPI-anchored protein in the surface of macrophages, that leads to the phosphorylation of p38MAPK followed by phosphorylation (Ser536) of the p65 subunit of NF-kB which is responsible for the transcriptional activation of IL-6. This IL-6 acts in an autocrine manner and binds its receptor present on the surface of the macrophage; this binding leads to the phosphorylation of STAT3, which further forms dimer and enters the nucleus. Then, it binds to the specific promoter and induces the expression of M2-associated markers, [21] thus leading to the advancement of cancer.

***S100 calcium-binding protienA9 (S100A9)-*** S100A9 is a protein that binds calcium and zinc, significantly influencing the regulation of inflammatory processes and immune responses [23]. Overexpressed in chronic lymphocytic leukemia [24], colon, lung, melanoma, gastric, prostate, ovarian, breast, head and neck cancers [25]. S100A9 switches macrophages into a tumor-promoting phenotype via activation of the PI3K/Akt signaling [26]. The activation of the PI3K/Akt pathway plays a crucial role in dampening proinflammatory responses. Upon activation of PI3K by S100A9, it phosphorylates phosphatidylinositol 4, 5-bisphosphate (PIP2) - generating phosphatidylinositol 3, 4, 5-triphosphate (PIP3) at the plasma membrane. PIP3 recruits Akt and the mTORC 2 - facilitating Akt activation by mTORC2 [27]. This activation in turn inhibits NF-kB activation, resulting in a significant upregulation of IL-10, transforming growth factor-beta (TGF-β), and other markers associated with the M2 anti-inflammatory phenotype[26,27], this supports the development of cancer.

***Growth and differentiation factor15 (GDF15)-*** GDF15(Growth and differentiation factor 15) is a unique member of the TGF-β superfamily, and crucial in various physiological processes and cellular activities. Numerous studies have linked GDF15 to various health conditions such as cancer, inflammation, cardiovascular diseases, and dyserythropoietic diseases [28]. GDF15 is a protein found in exosomes released from colon cancer cells

[29]. It also shows overexpression in cervical cancer [30], breast cancer, CRC [31], prostate cancer, endometrial cancer, and osteosarcoma [32]. GDF15 can activate the PI3K/Akt signaling, leading to the polarization of macrophages into the M2 phenotype. GDF15 binding to the GDF15 receptor leads to the phosphorylation of PI3K, which in turn leads to phosphorylation of Akt which activates various transcription factors. This results in elevated expression of the M2 phenotype gene (Arg1 and IL-4) expression [33] leading to metastasis and advancement of cancer.

***Hepatocyte Growth Factor (HGF)-*** Hepatocyte Growth Factor is a protein that interacts with the hepatocyte growth factor receptor, influencing growth, motility, as well as morphogenesis across various cell and tissue types [34]. Multiple myeloma cell-derived exosomes contain Hepatocyte Growth Factor (HGF)[20]. Recent studies have reported that HGF binds with tyrosine-protein kinase Met (c-MET), which leads to M2 polarization by the downstream signaling process. Binding HGF to MET leads to the activation of PI3K, activating AKT in its downstream. This activated AKT phosphorylates and then activates GSK3β. which phosphorylate and activate cAMP-responsive element-binding protein (CREB). Further, this activated CREB in the nucleus activates CCAAT/enhancer-binding protein beta (C/EBPβ), which acts as a transcription factor that specifically binds to promoters and leads to the expression of M2 phenotype-associated genes. This leads to a shift in the phenotype of macrophages towards M2-type [34–36] that drives cancer progression.

***Annexin-A1 (ANXA1)-*** ANXA1 is a 37 kDa phospholipid-binding protein, is abundantly expressed in different tissues. Initially identified for mediating the anti-inflammatory effects of glucocorticoids, it plays diverse roles in health and disease [37]. Elevated levels of ANXA1 are observed in various cancers, including breast, melanoma, hepatocellular carcinoma, colorectal, glioma, lung adenocarcinoma, and prostate cancer [38]. Additionally, pancreatic cancer cells release ANXA1 via exosomes [39]. ANXA1, through its interaction with the FPR2 receptor, likely facilitates

macrophage polarization. The FPR2-ERK signaling axis downstream of ANXA1 is likely to play a key role in the process of macrophage polarization [40], which contributes further to the progression of cancer.

***CKLF-like MARVEL transmembrane domain-containing 6 (CMTM6)-*** CKLF-like MARVEL transmembrane domain-containing 6 (CMTM6), a protein located at the plasma membrane, has emerged as a potential player in cancer progression. Across various cancer types, CMTM6 is consistently overexpressed, including in cervical squamous cell carcinoma, esophageal cancer, lung squamous cell carcinoma, and head and neck squamous cell carcinoma (HNSCC) [41]. CTMN6 is expressed in exosomes derived from OSCC (Oral squamous cell carcinoma) [41]. As reported by Pang and colleagues, CMTM6 within oral squamous cell carcinoma (OSCC) cells regulates the polarization of anti-inflammatory-type macrophages in the TME. This modulation occurs through the activation of ERK1/2, contributing to signaling pathways associated with cancer progression. However, the precise signaling pathway remains undisclosed [41].

***Transforming growth factor beta (TGF-β)-*** TGF-β is a family of secreted signaling proteins which are participate in cellular differentiation, proliferation, and apoptosis [42], which is found in exosomes of NSCLC and SCLC[43]. Further upregulated expression of TGF-β reported in different cancers such as colon, breast, liver, esophagus, stomach, pancreas, prostate, lung, kidney, brain, and malignant melanoma, as well as certain hematological malignancies[44]. Zhang et al. experimentally showed that TGF-β enhances the expression of Transcription factor SNAIL and facilitates M2 polarization. It upregulates SNAIL's mRNA and protein levels by SMAD2/3 and PI3K/Akt pathway [45]. The interaction of TGF-β with the TGF-β receptor induces phosphorylation of R-Smads leading to binding with SMAD2/3 in cytoplasm. Further, Phosphorylated Smads form a complex with SMAD4 that moves into the nucleus and interacts with various transcription factors. [46] and promotes the transcription of SNAIL mRNA. In the case of the PI3K/Akt signaling mechanism, the binding of

TGF-β to the receptor causes the activation of PI3K. Activated PI3K leads to the conversion of PIP2 to PIP3, which phosphorylates Akt, further activated Akt activates mTORC1, and then mTORC1 activates p70s6k, which gets translocated into the nucleus and initiates the expression of SNAIL [47]. SNAIL acts as a transcription factor, increasing anti-inflammatory cytokine IL-10 and CD-206 expression and metastatic progression of cancer [48].

***Intercellular Adhesion Molecule 1 (ICAM-1)-***ICAM-1 promotes various immune responses that rely on close cell-to-cell interactions and cooperation[49]. Recent studies have shown that it is overexpressed in breast, prostate cancer, and myeloma, and it is also found in many human cancer cell-derived exosomes [50] as well as in melanoma cell-derived exosomes[51]. This protein is also involved in skewing macrophages via the ICAM-1/miR-124/MCP-1 pathway. ICAM-1 increases the expression of SP1 (specificity protein 1), which acts as a transcription factor and binds to the promoter of miR-124, increasing its expression. Further, miR-124 directly binds to the 3'UTR of MCP-1, inhibiting the monocyte chemotactic protein 1 (MCP-1) mRNA and protein expression. That leads to increased expression of M2 markers such as ym-1, (Mannose receptor C-type 1) Mrc-1, and IL-10 [52] and contributes to cancer progression.

***Fibroblast-specific protein 1 (Fsp1)-*** Fsp1 also known as S100A4, a member of the S100 family, significantly contributes to tumor cell metastasis by controlling adhesion, extracellular matrix remodeling as well as cellular motility [53]. Further, it is overexpressed in the lungs [54] and pancreatic cancer [55]. It is also reported that exosomes derived from hepatocellular carcinoma cells carry S100A4 [56]. Mechanistically, S100A4 activates peroxisome proliferator-activated receptor γ (PPAR-γ), required for fatty acid oxidation (FAO) induction during tumor-associated macrophage (TAM) into pro-tumorigenic M2 polarization. Moreover, experimental observations reveal that TAMs expressing S100A4 exhibit elevated levels of PD-L1, arginase 1, and TGF-β. This observation indicates

that it has a role in immune suppression and promotion of cancer progression [57].

***Nod -Like Receptor Pyrin domain-containing protein 6 (NLRP6)-*** The NLRP6 is an exosomal protein known to be highly expressed in gastric cancer [58] and small-cell lung cancer [59]. It is a member of the nod-like receptor family of pattern recognition receptors (PRRs) that consists of a PYD (N-terminal pyrin domain), a central NOD domain, and a C-terminal leucine-rich repeats (LRPs) [58].The exosomes derived from SCLC containing NLRP6 protein polarize macrophages into M2 phenotype by negatively regulating the NF-kB signaling pathway. In the presence of NLRP6, the levels of phosphorylated P65 and phosphorylated IkB decrease significantly [59]. As a result, NF-kB (heterodimer) remains bound to IkB and inactive in the cytoplasm. This ultimately results in a significantly increased expression of M2 markers, arginase-1 (Arg-1), CD206, and IL-10, leading to the progression of cancer [59].

***Integrin αvβ6-*** Integrin αvβ6 has a tripeptide RGD (Arg-Gly-Asp) motif, which is highly specialized for adhesion to extracellular ligands; both the subunits act collectively and recognize ligands at the interface between their extracellular domains. These proteins are essential in regulating biological signaling paths that control multiple processes, such as cell survival, migration, proliferation, differentiation, metastasis, and tumor invasion [60]. αvβ6 is known to be upregulated in breast, prostate, cervical, and CRC, which significantly influences the microenvironment. Specifically, prostate cancer cell-derived αvβ6-positive exosomes are transferred to monocytes, promoting the M2 phenotype by inhibiting the activation of the STAT1/MX1/2(Myxovirus 1/2) signaling pathway. Uptake of αvβ6 causes inhibition of STAT1. The impact of αvβ6 is crucial, given STAT1's pivotal role in tumorigenesis, regulating diverse cellular activities. Additionally, αvβ6 significantly influences MX1/2 as MX 1 expression depends on STAT1 signaling, and MX2, a member of the dynamin-like GTPase family, is interferon-inducible, highlighting its role in the immune response. Hence,

inhibition of STAT1 by αvβ6 leads to the inhibition of the STAT1/MX1/2 pathway; thus, promoting polarization of macrophage into the M2 phenotype and cancer progression [61].

***T-cell immunoglobulin and mucin domain-containing protein 3(TIM-3)-*** TIM-3 is an immune checkpoint receptor found on various immune cells. Its differential expression in diverse cancers has made it a prognostic indicator [62]. TIM-3 displays increased expression in various cancers, including CRC (CRC), gastric cancer (GC), hepatocellular carcinoma (HCC), non-small cell lung cancer (NSCLC), clear cell renal cell carcinomas (RCC), bladder urothelial carcinoma (BUC), prostate cancer, and leukemic stem cells [63]. Furthermore, it is identified to be upregulated in human melanoma cells [64]. Jiang et al. reported TIM-3 leads to M2 macrophage polarization by interacting with STAT1, which leads to the inhibition of the STAT1-miR-155-SOCS1 signaling axis. Tim-3 interacts with STAT1, specifically binding to residues Y256 and Y263, inhibiting STAT1 phosphorylation and nuclear translocation. STAT1, functioning as an adaptor, mediates Tim-3-induced suppression of miR-155 expression. Consequently, this leads to increased SOCS1 activity and elevated expression of Arg-1 and IL-10 [65], resulting in the promotion of cancer advancement.

***Phosphoribosyl-pyrophosphate synthetase 2 (PRPS2)-*** PRPS2 a member of the phosphoribosyl pyrophosphate synthetase (PRS) family, is crucial for synthesizing purine and pyrimidine nucleotides [66]. Recent studies have identified the expression of PRPS2 in prostate cancer, CRC, and neuroblastoma [67]. Furthermore, it was seen that exosomes derived from NSCLC contain PRPS2 which significantly increases the expression of both mRNA and protein of IL-10, Arg-1, CD163, and CD206 in macrophages. These findings indicate that exosomes derived from NSCLC containing PRPS2 promote the M2 polarization of macrophages, contributing to the progression of cancer [41,67].

***Lysyl oxidase-like 4 (LOXL4)-*** LOXL4 is a crucial member of the LOX family [68] that is extensively involved in tumor proliferation, metastasis, angiogenesis, and immunity [69]. LOXL4 is a hepatocellular carcinoma cell-derived exosomal protein [70] which is also upregulated in head and neck squamous cell carcinoma and [71] breast cancer [72]. Exosome-derived LOXL4 promotes immunosuppressive M2 phenotype in macrophages, leading to immune evasion and tumor growth [73].

***Cathepsin B-*** Cathepsin B belongs to the cysteine protease family, initially synthesized as a pre-proenzyme with an estimated molecular weight is around 38 kDa. The presence and function of cathepsin B have been associated with various pathological conditions, like cancer, pancreatitis, arthritis, cardiovascular disease, and Alzheimer's disease. In cancer conditions, cathepsin B has been observed to be overexpressed in a range of malignancies such as prostate, breast, brain, lung, esophageal, gastric, ovarian, thyroid, colon, and skin cancers [74]. Cathepsin B is upregulated in melanoma-derived exosomes [75]. The precise intracellular role of these cathepsins in TAM polarization, particularly in the development or maintenance of the M2-like phenotype, remains largely unclear. Further, it is seen that cathepsin inhibition leads to a switch towards a pro-inflammatory phenotype of macrophage [76].

***Insulin-like growth factor 1 receptor (IGF-1R)-*** IGF-1R exhibits a strong affinity for insulin-like growth factor and possesses tyrosine kinase activity. Its expression is notably elevated in most malignant tissues, where it acts as an anti-apoptotic agent promoting cell survival [77]. Recent studies have shown that cancer cell-derived exosomes contain IGF-IR [78] as well as its overexpression is observed in several malignant tumors that include lung cancer, breast cancer, prostate cancer, glioma, and gastrointestinal cancers [79]. According to Spadaro et al., IGF-1R is responsible for directing macrophages towards the M2 phenotype. Additionally, the elimination of IGF-1R decreased in the transcription associated with the activation of M2-like macrophages [19,80].

***Collagen type V alpha 2 (COL5A2)-*** COL5A2, a member of the collagen family, has diverse roles in modulating the immune system, promoting angiogenesis, and facilitating tumor metastasis[81], which is found to be overexpressed in Colorectal [82], breast [83] and gastric cancer[81]. Recent studies have also shown that Collagen type V alpha 2 is observed in ovarian cancer-derived exosomes [84]. Upon further exploration, it was found that the expression levels of the M2 macrophage markers, CD163 and Mannose receptor C-type 1 (MRC-1 or CD206), exhibit a positive correlation with COL5A2 expression. Consequently, these findings suggest that COL5A2 may contribute to the differentiation of M2 macrophages [84].

***Cytoskeleton-Centric Protein-*** Cytoskeleton-centric proteins are a group of proteins which is known to take part in the progression of various cancers. Further studies have revealed that these proteins are overexpressed in various cancer types such as liver cancer, melanoma, and myeloma [85] and also found to be transported through exosomes which are derived from CRC. Chen et al. experimentally showed that these cytoskeleton-centric proteins are involved in skewing macrophages into pro-tumorigenic M2 phenotype. It is also found that the exosome could significantly promote the NFκB expression, but the exact mechanism is unclear yet [86].

***Vascular endothelial growth factor (VEGF)-*** VEGF is a critical regulator in diverse physiological processes, and is involved in angiogenesis conditions such as tumors and intraocular neovascular disorders. Multiple studies have evaluated the efficacy of different VEGF inhibitors across several malignancies [87]. Its overexpression is also associated with several cancers, such as colorectal carcinoma, gastric carcinoma, pancreatic carcinoma, breast cancer, lung cancer, prostate cancer, and melanoma. Further, it is reported that many cancer cell-derived exosomes contain VEGF [88].VEGF treatment alters macrophage polarization by suppressing M1 markers and inducing M2 markers, as evidenced by higher VEGFR1 expression in M1 cells. Recent Studies have revealed that VEGF induces a

significant shift from M1 to M2 phenotype, indicating a potential regulatory role of VEGF in macrophage phenotype [89,90].

***Cyclooxygenase-2 (COX-2)-*** COX-2 a pivotal enzyme in prostaglandin synthesis, plays a significant role in tumor invasiveness, angiogenesis, and progression. Additionally, COX-2 contributes to immune evasion and resistance to cancer immunotherapy, impacting both type innate as well as adaptive immune responses [91,92]. COX-2 exhibits overexpression in lung, breast, and cervical cancers [93] and is also upregulated in exosomes derived from lung cancer [94]. It is reported that a positive correlation has been reported between COX-2 and M2 macrophage polarization [95].

***CD63-*** Exosomes derived from triple-negative breast cancer cells (TNBC), gastric cancer cells [96] and hepatocellular carcinoma cells contain CD63 protein. In co-culture experiments, macrophages activated by TNBC exosomes exhibited elevated expression of CD206, a marker associated with the M2 macrophage phenotype, decreasing the expression of NOS2, an M1-associated marker. These results indicate that exosomal CD63 can potentially polarize macrophages toward the M2 phenotype (54,110)

**Table 2.1.1.** List of cancer cells derived exosomes containing protein involved in M2 type of macrophage polarization.

| Sr. no. | Protein Name | Source of Exosomes | Mechanism/pathway | Reference |
|---|---|---|---|---|
| 1 | **Leptin** | Gallbladder cancer | JAK/STAT3 | [8] |
| 2 | **IL-10** | Lung cancer | JAK/STAT3 | [13] |
| 3 | **GRP78** | Lung, Gastric Cancer | JAK/STAT3 | [18] |
| 4 | **PA-1** | Multiple myeloma | p38MAPK/NF-kB/ IL-6/STAT3 | [20] |
| 5 | **S100A9** | Chronic lymphocytic leukemia | PI3K/AKT | [24] |
| 6 | **GDF15** | Colon cancer | PI3K/Akt | [29] |
| 7 | **HGF** | Multiple myeloma | By PI3K/AKT/ GSK3β/ CREB | [20] |
| 8 | **Annexin-A1** | Pancreatic cancer | FPR2-ERK | [39,40] |
| 9 | **CMTM6** | OSCC | ERK1/2 | [41] |
| 10 | **TGF-β** | Lung cancer | SNAIL via SMAD2/3 and PI3K/Akt | [45,48] |

| | | | | |
|---|---|---|---|---|
| 11 | **ICAM-1** | Melanoma | ICAM-1/ SP1/miR-124/MCP-1 | [52] |
| 12 | **S100A4** | Hepatocellular carcinoma | PPAR-γ | [56] |
| 13 | **NLRP6** | Gastric cancer | negatively regulate NF-kB | [58] |
| 14 | **Integrin α1β6** | Prostate cancer | STAT1/MX1/2 | [61] |
| 15 | **TIM-3** | Human melanoma | STAT1-miR-155-SOCS1 | [64,65] |
| 16 | **PRPS2** | prostate, colorectal, and neuroblastoma | - | [41,67] |
| 17 | **LOXL4** | Hepatocellular carcinoma | - | [70] |
| 18 | **IGF-1R** | Lung, breast, prostate, glioma | - | [79] |
| 19 | **COL5A2** | Ovarian cancer | - | [83] |
| 20 | **Cytoskeleton-centric protein** | Colorectal cancer | - | [86] |
| 21 | **VEGF** | colorectal, gastric, pancreatic, breast, lung, prostate, and melanoma | - | [88] |
| 22 | **COX-2** | Lung cancer cells | - | [93,94] |
| 23 | **CD63** | Triple-negative breast, Gastric, Hepatocellular carcinoma | - | [96,98] |

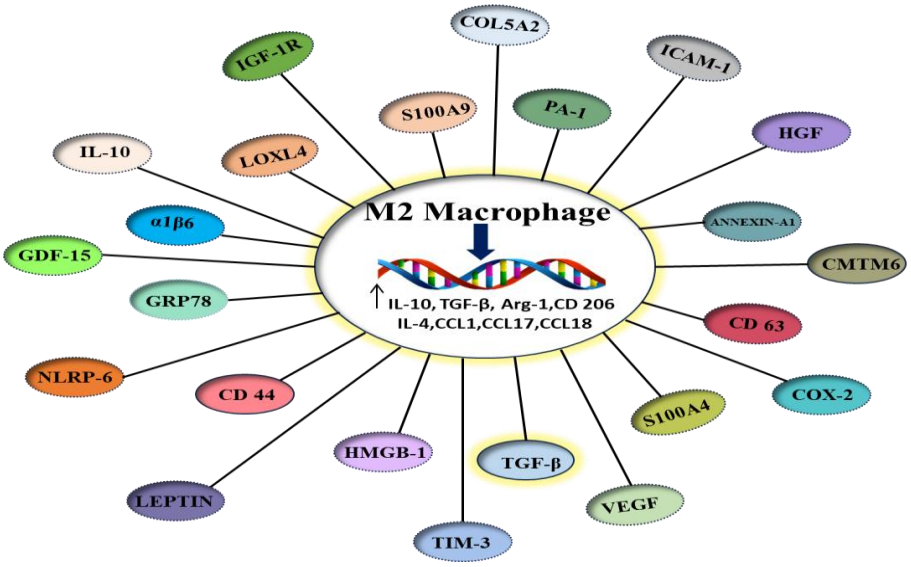


**Figure 2.1.1*:*** Represent various cancer cell-derived exosomes containing proteins that significantly contribute to macrophage polarization towards an anti-inflammatory phenotype during cancer progression.

**2.1.2 Tumor-derived Exosomal proteins driving M1 macrophage polarization -** Exosomal proteins are critical messengers during intricate communication networks between macrophages and cancer cells within the TME. Once released, exosomes can traverse to neighboring or distant cells, influencing their behavior and functions. In the cancer context, these exosomal proteins actively contribute to the cross-talk between macrophages and cancer cells, significantly shaping the immune response, tumor development, and metastasis. These proteins can modulate macrophage polarization, steering them toward the tumor-promoting M2 phenotype. Interestingly, numerous proteins have been identified with the capacity to polarize macrophages into the M1 phenotype by activating or inhibiting various signaling pathways that lead to the inhibition of cancer progression.

***Cyclase-associated protein 1 (CAP 1)-*** CAP 1 is the predominantly expressed isoform of a conserved actin-regulating protein, CAP (adenylyl cyclase-associated protein), involved in cancer cell migration and invasiveness [99]. It is an exosomal protein that is overexpressed in breast cancer, lung cancer, esophageal squamous cell carcinoma, pancreatic cancer [100], and hepatocellular carcinoma [101], which is involved in polarizing macrophages into M1 phenotype [102]. Upon being taken up by macrophages, CAP1 on the membrane of macrophages binds to its ligand molecule (e.g., resistin), which activates adenylyl cyclase (AC). Further, the AC, in turn, converts ATP into cAMP, which acts as a secondary messenger and activates PKA [103]. Then likely the catalytic sub-unit of PKA gets

bound to IKB and p65 inactive complex. After the phosphorylation and degradation of IKB by the IKK complex, PKA phosphorylates p65 which triggers a conformational change in p65 and increases its transcriptional activity [104]. This results into the increased expression of pro-inflammatory cytokines such as IL -6, TNF-α, IL-1β and which switch macrophages towards the M1 type and inhibit cancer progression [103].

***Cluster of differentiation 147 (CD147)-*** CD147 part of the immunoglobulin super-family, performs diverse functions, particularly in heart disease, Alzheimer's, stroke, and cancer[105]. CD147 exhibits elevated expression in several cancer types, including lung, breast, prostate, stomach, and genitourinary cancers [106]. Furthermore, CD147 is present in exosomes derived from epithelial ovarian cancer cells [107]. The CD147-mediated impact on macrophage polarization operates through the TRAF6-IKK-IRF5 signaling pathway. CD147 binding directly activates TRAF6, initiating a phosphorylation cascade that activates IKK and subsequently triggering the activation of IRF5 in its downstream. This activation results in an enhanced expression of pro-inflammatory M1-associated markers, contributing to cancer progression. Furthermore, Lv et al. also showed that CD147 knockout exhibited a phenotype shift from pro-inflammatory to anti-inflammatory macrophage [108].

***Pigment epithelium-derived factor (PEDF)-*** PEDF a 50-kDa glycoprotein encoded by the *SERPINF1* gene, a member of the serpin super-family that regulates vital biological processes like coagulation of blood, inflammation, angiogenesis, and protein folding. literature suggested that PEDF may hinder cancer progression [109] and also plays a pivotal role in skewing macrophages towards pro-inflammatory M1 phenotype [110,111]. Recent findings suggest that specific tumor cells release exosomes with PEDF into the pre-metastatic niche, promoting immunosuppression and aiding the spread of cancer. It is demonstrated that breast cancer cell-derived exosomes are rich in PEDF [111] as well as PDEF mRNAs are also found in osteosarcoma cell-derived exosomes [109] Marin et al. experimentally

showed that PEDF-mediated signaling promotes M1 polarization by upregulating PNPLA2 in macrophages [112]. Finally PEDF enhanced the expression of iNOS, IL-12, and TNF-α while suppressing IL-10 and arginase-1 in both mouse and human macrophages, confirming M1-type polarization [113]. Further, Moradi-Chaleshtori and colleagues experimentally demonstrated that treating M2 macrophages with exosomes containing PEDF from transfected cells resulted in significant reprogramming towards an M1 phenotype. This process was evidenced by increased expression of M1-associated genes, including CD80, IRF5, and MCP1, and decreased levels of M2-associated genes, such as CD206, Arg, and TGM2 [111].

***Protein tyrosine phosphatase receptor type O (PTPRO)-*** PTPRO is part of the family of receptor-type protein tyrosine phosphatases [114] that is found to be expressed in lung [115] and CRC [116]. Furthermore, PTPRO is found in breast cancer cell-derived exosomes [114]. Dong et al. experimentally illustrated that exosomes expressing PTPRO derived from tumors lead to the differentiation of macrophages into the M1 phenotype, shown by a notable increase in the count of M1-phenotype expressing iNOS. In contrast, the proportion of M2-phenotype expressing CD206 was comparatively reduced in macrophages. PTPRO within tumor cell-derived exosomes plays an important role in promoting the polarization of macrophages into an M1-like phenotype, likely by deactivating STAT signaling through its dephosphorylation function. The phosphatase activity of PTPRO is crucial to control STAT3/STAT6 signaling in macrophages. Moreover, studies have also shown that exosomes originating from PTPRO knockout cells were found to enhance STAT3/STAT6 signaling in macrophages[114].

***Heat shock protein 70 (HSP70)-*** HSP70 is a unique protein that helps cells deal with stress. It has essential roles in folding proteins, moving them around the cell, forming complexes, and breaking them down. HSP70 is involved in various diseases, including cancer, neurodegeneration, rejection

of transplanted organs, and infections [117]. Interestingly, HSP70 is found in exosomes originating from cancer cells [118]. It has a significant impact on promoting M1 polarization[119]. Zhu et al. experimentally showed that the introduction of an antibody against HSP70 reduces the levels of certain substances like TNF-α, CD206, and CCL2 while increasing the levels of molecules (such as Arg-1, iNOS, and IL-10) that suppress the immune response. Similarly, there was a notable increase in the levels of cytokines like CXCL10 and IL-12 in macrophages. At the same time, the expression of molecules that suppress the immune response in macrophages, such as Arg-1, iNOS, and IL-10, showed a significant decrease[119] that indicates a shift towards a pro-inflammatory M1 phenotype.

***Crystallin- Alpha B (CRYAB)-*** The human αB-crystallin (CRYAB) is a 20.2 kDa protein containing 175 amino acids [120]. Recent research findings indicate that elevated levels of CRYAB expression correlate with increased invasiveness in various solid tumor cells, highlighting its potential role in fostering metastasis [121]. It is also reported that expression of CRYAB is observed in various cancers such as renal cell carcinoma, osteosarcoma, colorectal, hepatocellular carcinoma, gastric, ovarian, NSCLC [122], and laryngeal squamous cell carcinoma (LSCC) [123]. Additionally, exosomes derived from Glioma cells exhibit upregulated levels of CRYAB [124]. Furthermore, Lim et al. experimentally showed that the expression of CRYAB is responsible for activating pro-inflammatory(M1) macrophages [125], which leads to the inhibition of cancer progression.

***Programmed-death ligand 1 (PDL-1)-*** PD-L1 or CD279/B7-H1) is a transmembrane protein that is commonly present in macrophages, specific T and B cells, dendritic cells (DCs), and certain epithelial cells, especially during inflammatory conditions. It plays a critical role in immune regulation and is a key player in tumor cells' evasion strategies [126]. Furthermore, elevated PD-L1 expression is observed in various cancers, including hepatocellular, gastric, esophageal, pancreatic, ovarian, bladder cancer and

renal cell carcinoma [127]. Elevated levels of PD-L1 are also found in exosomes derived from Head and neck squamous cell carcinomas (HNSCC) cancer cell [128] and lung cancer cells [129]. It is experimentally shown by Liu and colleagues that there is a positive feedback mechanism wherein PD-L1 exosomes released by tumor cells enhance the expression of PD-L1 in macrophages, promoting the M2 polarization of tumor-associated macrophages (TAMs) that leads to cancer progression [130].

***Caveolin 1 (CAV 1) -*** Caveolin-1 serves as a primary structural element of caveolae and functions as a binding protein for fatty acids and cholesterol. It is involved in diverse biological processes including endocytosis, transcytosis, signal transduction, and lipid metabolism [131]. Cav-1 which is closely associated with liver cancer [132], and found to be upregulated in pancreatic, colon, lung, breast, and prostate cancer [133]. Recent studies have demonstrated that Cav1 regulates macrophage polarization toward the M1 phenotype [134]. It is also reported that deletion of cav1 skews macrophages towards the M2 phenotype by regulating TGF-β signaling [135], which suggests the role of Cav1 in the suppression of cancer.

**2.1.3 Exosomal proteins driving macrophage polarization towards both M1 and M2-**

There are some proteins from exosomes that are capable of switching macrophages towards M1 or M2 phenotypes during their presence in specific pathophysiological conditions. The ability of exosomal proteins to modulate macrophage polarization in specific pathophysiological conditions highlights the important role of these extracellular vesicles in regulating immune responses and tissue homeostasis and could have implications for the development of targeted therapeutic strategies.

***High Mobility Group Box1 (HMGB1)-*** HMGB1 is a non-histone chromatin-associated protein upregulated in exosomes derived from gastric cancer cell [136]. HMGB1 is highly conserved and present in all cell types, functioning intracellularly and extracellularly. Its diverse roles contribute to its significance in diverse cellular processes[137], and is evident through its

overexpression observed in various tumor cells, including gastrointestinal stromal tumors, colon cancer, and cervical carcinomas. Increased HMGB1 mRNA expression is also noted in prostate cancer [138]. Recent studies have shown the dual role of HMBG1 in skewing macrophages into M1 phenotype as well as M2 phenotype by different signaling pathways. HMGB1 binds to RAGE (receptor for advanced glycation end products), leading to NF-kB pathway activation [139]. Upon binding of HMGB1, RAGE phosphorylates and activates its downstream p38 MAPK protein, which phosphorylates IkB [140] and P65 [141] leading to its dissociation from NF-kB. The free-activated NF-kB then enters the nucleus and regulates the transcriptional expression of various factors such as TNF-ALPHA and IL-1beta [142], which leads to a change in the phenotype of macrophages towards the M1 phenotype. HMGB1 containing exosomes derived from gastric cancer cells drives M2-like macrophage polarization suppressing the NF-κB signaling pathway[143].

***CD44-*** CD44 is recognized as a type I transmembrane protein that plays a significant role as a cell surface receptor. Several ligands have been recognized for CD44, with hyaluronan, an extracellular matrix constituent, as a primary binding partner [144]. CD44 is identified in ovarian [145], gastric [146], and breast [147] cancer cell-derived exosomes, exhibiting overexpression across diverse cancer types such as prostate, triple-negative breast, lung, and pancreatic cancers [148]. Recent research indicates that CD44 plays a dual role in influencing macrophage polarization, promoting both M1-type [149] and M2 phenotypes [150] through distinct signaling pathways. Whenever CD44 interacts with hyaluronic acid mediates M2 polarization of macrophages via STAT3 signaling otherwise STAT1 signaling remains active and switches macrophages into M1 type during glioblastoma progression [151].

**Table 2.1.2.** List of cancer cell-derived exosomes containing protein involved in M1 type of macrophage polarization.

| Sr. no. | Protein Name | Source of Exosomes | Mechanism | Reference |
|---|---|---|---|---|
| 1 | **CAP 1** | Hepatocellular carcinoma | cAMP/PKA/NF-kB | [100,101,104] |
| 2 | **CD147** | Epithelial ovarian cancer | CD147/ TRAF6/IKK/IRF5 | [106,107] |
| 3 | **PEDF** | Breast cancer | PNPLA2 up-regulation | [109,111,112] |
| 4 | **PTPRO** | Breast cancer | Deactivating STAT signaling | [114–116] |
| 5 | **HSP70** | Solid tumor | - | [118] |
| 6 | **CRYAB** | Glioma | - | [122–125] |
| 7 | **PD-L1** | HNSC and Lung cancer | - | [127–130] |
| 8 | **Caveolin 1** | Liver cancer | - | [132–134] |
| **Exosomal proteins perform a dual role in macrophage polarization (M1 or M2 )** | | | | |
| 9 | **HMBG1** | Gastric cancer | HMBG1/RAGE/p38 MAPK/NF-kB | [138,139,141-143] |
| 10 | **CD44** | Breast,ovarian, pancreatic, Gastric | STAT1/STAT3 | [146-148,150,151] |

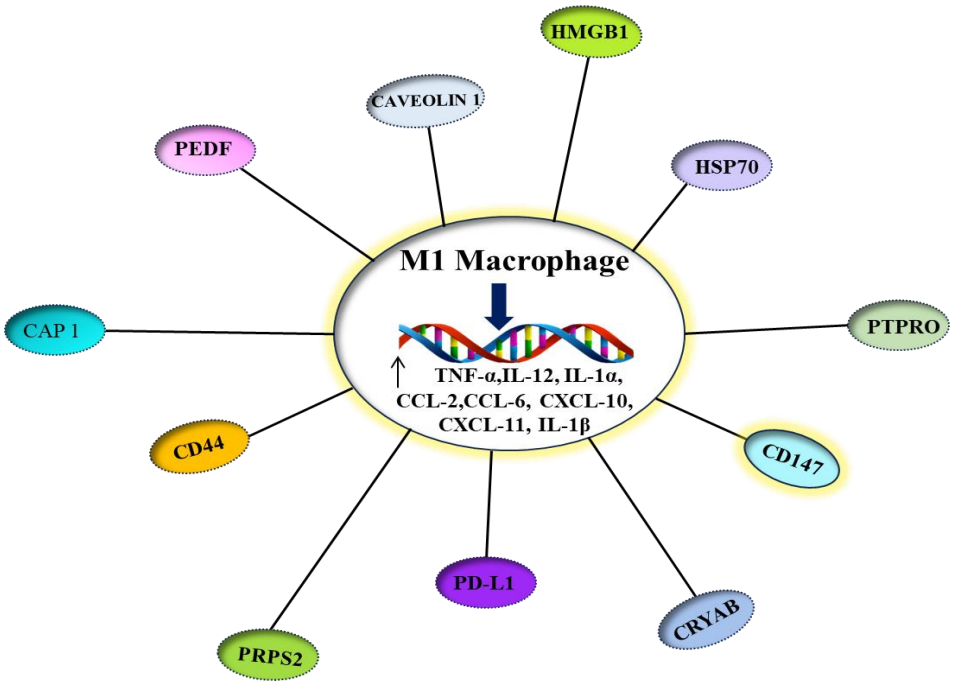



**Figure 2.1.2:** Depicts cancer cell-derived exosomes containing proteins that play a crucial role in inducing macrophages to switch to a pro-inflammatory phenotype during cancer.

Collectively, existing evidence suggests that tumor-derived exosomal proteins have an influence on macrophage polarization. Exploring exosomal proteins from various cancer cells represents an ongoing field that is rapidly advancing our knowledge of their role in gene expression regulation. For Example, Connexin 43 (Cx43) is a gap junction protein, widely expressed in most of the cancer cells derived exosomes and has various regulatory functions in the transfer of bioactive material from exosomes to the recipient cell[152] and recent studies demonstrate CX43 might be potential target to regulate M1 and M2 phenotype of macrophages[153]. These insights can potentially guide the development of innovative therapeutic strategies against diverse cancer types. Recent studies demonstrate that FAP-activated liposomes target pancreatic stellate cells to reverse desmoplasia and siATG5-loaded membrane-fused liposomes suppress autophagy and enhance chemotherapeutic uptake and efficacy in pancreatic cancer treatment[154,155]. Numerous approaches can be considered to impede the polarization of macrophages into the pro-tumorigenic M2 phenotype, thereby inhibiting cancer progression. Thymosin α1 reverses oncolytic adenovirus-induced M2 polarization of macrophages, shifting them to an M1 phenotype to enhance antitumor immunity and improve the efficacy of cancer therapy[156]. Specific targeting of exosomal proteins responsible for M2 polarization using drugs or small molecules is one avenue. Studies suggest, cobalt nanoparticles induce cytotoxicity in THP-1 macrophages by stabilizing hypoxia-inducible factor 1α, promoting oxidative stress, inflammation, and metabolic dysregulation[157]. Alternatively, targeting the mRNAs of these proteins through miRNA or siRNA can be explored, or delivering factors/proteins responsible for M1 polarization to counteract cancer progression. Studies have highlighted the role of exosomal membrane proteins in macrophage polarization towards the M2 phenotype, suggesting the potential for novel therapies targeting these surface proteins.

## 2.2 Tumor-Derived Exosomal Glycoproteins in Macrophage Phenotypic Change:

Following the literature survey on the functional significance of exosomal proteins in tumor progression and macrophage polarization. Then we focus towards exosome containg glycoproteins. Recently, exosome-derived proteins, including glycoproteins, are gaining attention in TAM switching towards tumor supportive types in TME [158]. Therefore, in this section we will discuss the emerging role of cancer cells-derived exosome containg glycoproteins in macrophage polarization and tumor promotion. The glycoproteins are the proteins which undergo glycosylation by the addition of carbohydrate moiety at the post-translational level. Several types of glycosylation occur on the amino acids of protein. For example, (i) N-glycosylation links complex glycans to asparagine, (ii) O-glycosylation appends single sugars or glycans to tyrosine, serine, and threonine. C-glycosylation and S-glycosylation that modify tryptophan and cysteine respectively are rarely found. P-glycosylation, identified in lower eukaryotes, utilizes a phospho-sugar to link with serine or threonine [159–163]. The majority of protein glycosylation in eukaryotes occurs within the Golgi apparatus and starts inside the endoplasmic reticulum (ER) along the secretory pathway [161]. Several glycosylation-associated enzymes including fucosyltransferases (FUTs), sialyltransferases (STs), N-acetylglucosaminyltransferases (MGATs), etc and contributes to aberrant glycosylation of proteins in cancer. During cancer transformation, aberrant glycosylation occurs thus generating novel glycoforms that are tumor-associated and do impacting the immunogenicity of cancer cells as well as interaction with immune cells [15–17], and the tumor glycoproteins are cargo components of EVs.[164,165]. Exosomal glycoproteins undergo various post-translational modifications (PTMs) that are crucial for their sorting, stability, and functional roles in intercellular communication, ultimately influencing disease progression [166–168]. Understanding the mechanisms of cargo loading and sorting in exosomes is essential for

elucidating their physiological and pathological functions, as well as for advancing their clinical applications in diagnostics and therapeutics[169]. Exosome biogenesis and trafficking of proteins to exosomes involve both ESCRT-dependent and ESCRT-independent pathways, although the detailed mechanisms remain incompletely understood [170]. In particular, macrophages do express lectin receptors specialized in the recognition of altered carbohydrate structures and glycan-lectin interactions trigger macrophage reprogramming.[163,171,172] As per our knowledge, for the first time, we are summarized the function of cancer cell-derived exosomes contained glycoproteins on TAM polarization. Glycoprotein-mediated switching of macrophages plays a crucial role in cancer progression or inhibition. Targeting this glycoprotein-mediated reprogramming of macrophages towards tumor-supportive phenotype may be a promising anti-cancer strategy.

### 2.2.1 Cancer-Derived Exosomal Glycoproteins as Drivers of Macrophage Polarization within TME:

Glycoproteins influence macrophage polarization via activation of JAK-STAT, PI3K-AKT, ERK, and NF-kB, etc signaling[173–176]. Cancer cells derived exosomal glycoproteins upon reaching the TAMs start reprogramming them towards proinflammatory M1 or anti-inflammatory M2 phenotype. M1 macrophages release pro-inflammatory cytokines and cancer-suppressive molecules that inhibit cancer cell proliferation and metastasis, while M2 types of macrophages release anti-inflammatory cytokines and growth factors that make cancer more aggressive [177,178]. The following exosomal glycoproteins, illustrated in a schematic figure (**Figure 2.2.1)**, play pivotal roles in driving macrophage polarization within the TME. These glycoproteins on the surface or within exosomes interact with macrophage receptors and trigger signaling pathways that drive polarization

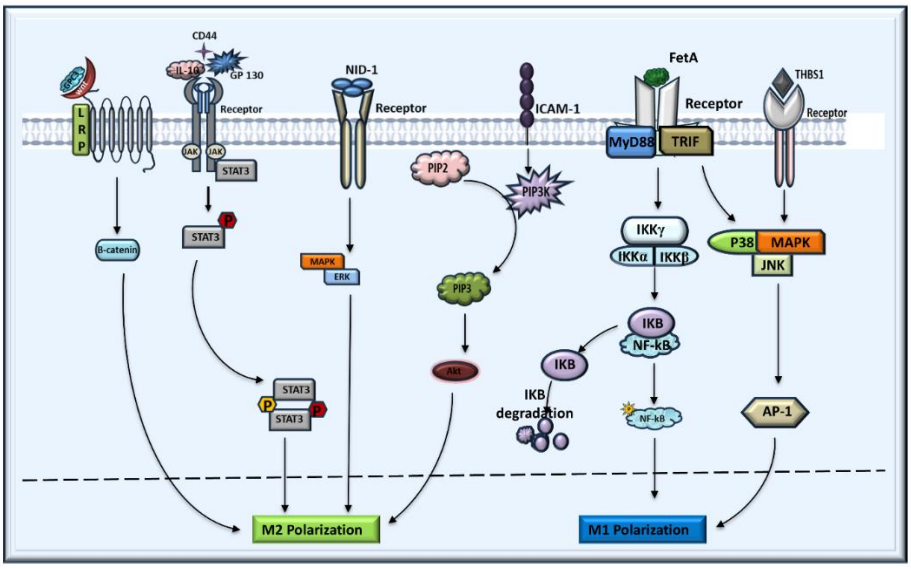



**Figure 2.2.1 Cancer cell–derived exosomal glycoprotein-mediated signaling pathways regulating macrophage polarization:** This schematic illustrates the molecular mechanisms underlying macrophage polarization. M2 polarization is driven by CD44–GP130 and IL-10–mediated STAT3 activation, NID1-induced ERK signaling, GPC3-induced β-catenin signaling, and ICAM-1–dependent PI3K/AKT signaling. In contrast, M1 polarization is promoted by FetA–MyD88/TRIF–mediated NF-κB activation and THBS1-induced MAPK/AP-1 activation. Image prepared in Microsoft powerPoint.

***Glypican-3-*** Glypican-3 (GPC-3) is an exosomal glycoprotein having heparan sulphate glycosaminoglycan chains covalently attached to core protein [179,180]. High expression of GPC-3 is found in hepatocellular carcinoma (HCC) as well as other cancers, types like lung squamous cell cancer, gastric cancer, ovarian cancer, melanomas, and pediatric embryonal cancer [175,181–186]. Experimentally, it has been proved that GPC-3 is involved in M2 macrophage polarisation and promotes cancer [187]. GPC-3 undergoes a Wnt/β-catenin axis which is inappropriately activated in cancers [188]. In the absence of Wnt signals, a complex of proteins, including APC, AXIN, CK1, and GSK3 forms a degradation complex that phosphorylates β-catenin to undergo degradation. When the Wnt signal is available, the destruction complex is recruited to the cell membrane,

preventing β-catenin degradation. Additionally, GPC3 form a complex with Wnt in the presence of an enzyme called SULF-2 and avoid β-catenin degradation. This stabilizes β-catenin and allows it to translocate into the nucleus and activate gene transcription, directing the growth of liver cancer cells[175]. Moreover, GPC3 helps in the expression of the fibroblast growth factor 2 (FGF2) which promotes cancer growth [189]. GPC-3 anchors the surface of cells with the help of a GPI (glycosylphosphatidylinositol), and serves as a diagnostic marker as well as a therapeutic target, particularly in hepatocellular carcinoma, where it is highly expressed in over 70% of cases. Reports reveal that the activation of Wnt/β-catenin pathway helps in the proliferation, metastasis, and angiogenesis of cancer cells [190] See **figure 2.2.2**. This increased expression of GPC-3 serves as a promising target for cancer treatment [187]. Recently, Chimeric antigen receptor (CAR) modified macrophage targeting GPC-3 have been proposed has possible anti-cancer therapeutic strategy see (**table 2.2.1**).

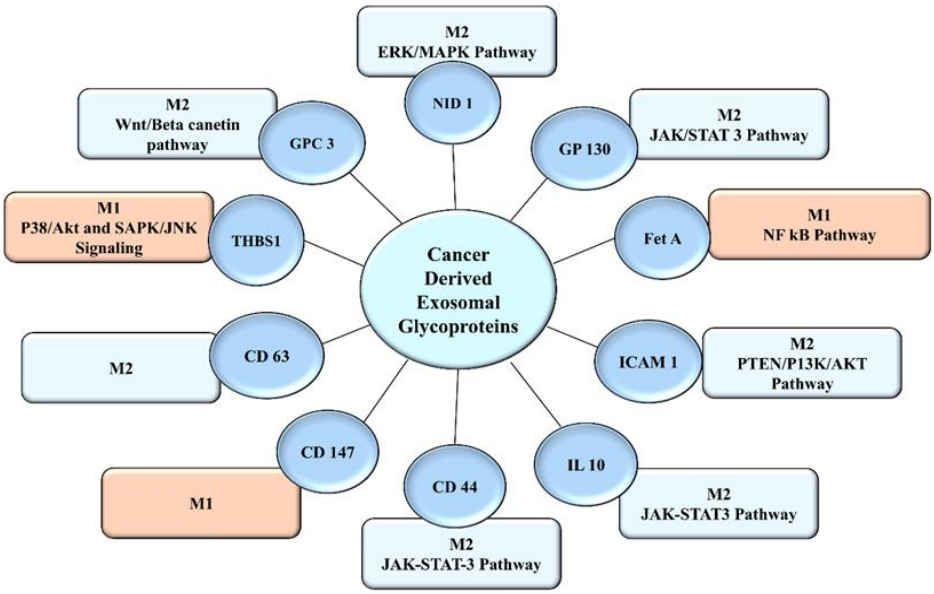



**Figure 2.2.2:** Cancer cell-derived exosomal glycoproteins in macrophage M1/M2 polarization through the modulation of distinct signaling pathways

***Nidogen- 1-***Nidogen-1 (NID), also called entactin, is a 150 KD glycoprotein and belongs to the Nidogen family [191]. In HCC (hepatocellular carcinoma), a high level of Nidogen-1 is expressed in cancer cell-derived exosomes, and promote metastatic niche formation in the lung thus increasing extrahepatic metastatization.[192] Nidogen-1 directs macrophages to adopt the M2 phenotype during polarization [193,194]. NID1 triggers the ERK/MAPK signaling axis, and enhances epithelial-mesenchymal transition (EMT) in cells of ovarian cancer which is activated by the protein kinase ERK+ [195]. When the amount of NID1 is increased in cells, the activated form of ERK1/2 which is a part of the MAPK (Mitogen-Activated Protein Kinase) signaling rises. ERK1/2 gets phosphorylated and enters into the nucleus and helps in the transcription of genes that are essential in cell growth and proliferation which leads to cancer progression [196]. When the amount of NID1 is decreased, the activated ERK1/2 slightly decreases. NID1 influences the MAPK pathway, specifically ERK1/2, to make cancer cells change shape. Increasing NID1 levels activates this pathway while reducing NID1 levels has the opposite effect. Understanding these changes based on NIS1 levels could provide insights into how to control cancer growth [195].

***Glycoprotein 130 (GP130)-*** Glycoprotein 130, (GP130) is a crucial signal-transducing-membrane-associated receptor [197]. GP-130 is involved in breast cancer, where it serves as an exosomal glycoprotein. It leads to the release of interleukin-6 (IL-6) by Bone Marrow-Derived Macrophages (BMDM) via the JAK-STAT-3 signaling mechanism which skews macrophage polarization into an alternative type (M2). This process can be reversed by targeting GP130, which offers a potential therapeutic approach [198]. Indeed, GP130 is a crucial molecule in the amplification of IL-6 signalling resulting in the triggering of the signalling cascade. Recently, it has been shown that GP130 can be transferred via EVs to acceptor cells that do not express the receptor, making them sensitive to the IL-6 effects [199]. This is particularly relevant for the moulding of TME for several cancer

contexts: regulated expression of GP130 is several cancers besides breast cancers as such as bladder cancer [200], pancreatic cancer [201], cholangiocarcinoma [44]. Exploring how GP130 and JAK-STAT-3 pathways work together helps us understand the working principle of diseases, especially inflammation and cancer. To dig more in this direction will help to find effective treatments [44,45]

***Fetuin-A*** **-** Fetuin-A (Fet-A) is a tumor-derived exosomal glycoprotein made up of two parts: an A-chain containing 282 amino acid residues and a B-chain consisting of 27 amino acid residues. These two chains are connected by a single inter-disulfide bond [202]. Fet-A is overexpressed in metastatic prostate cancer[203]. When free fatty acids (FFA) activate a pathway known as NF-κB, it interacts with the part of the DNA that manages the production of Fet-A. This interaction enhances the activity of the *Fet-A gene* and upregulates expression**.** The rise in Fet-A release from adipocytes results in an increase in markers related to pro-inflammatory M1-type macrophages, including TNFα, IL-6, and MCP-1. Simultaneously, there was a significant decrease in markers associated with the M2 phenotype of macrophages, specifically PPARγ as well as IL-10. Fet-A induced macrophage polarization from M2 to M1 type can be a useful strategy to improve the activity of TAM against tumor and inhibit tumor progression [204].

***Intercellular cell adhesion molecule-1 (ICAM-1)-*** ICAM-1 (Intercellular cell adhesion molecule-1) is a transmembrane glycoprotein [51]. It is a part of the immunoglobulin supergene family and the ligand for *β*2 integrin molecules expressed on leukocytes [205]. ICAM-1 is expressed in numerous cancer cells, such as melanoma, CRC, and lymphoma [206]. Cells with ICAM-1 on their surface are easily destroyed by immune cells as ICAM-1 sensitizes cancer cells to cytotoxic T lymphocytes (CTLs), which are a type of immune cell capable of killing cancer cells [207]. Other cells with low surface ICAM-1 can easily escape the immune system. [208]. The

absence of ICAM-1 changes macrophage behaviour, pushing them toward the pro-tumor M2 phenotype that facilitates tumor spread[209]. When the concentration of ICAM-1 is less, PTEN becomes free and gets phosphorylated, and activates PTEN/PI3K/AKT signaling axis which results in cancer progression via PTEN/PI3K/AKT pathway [210]. It has recently been reported that the Pancreatic Ductal Adenocarcinoma (PDAC) derived EVs containing ICAM-1 and arachidonic acid can trigger macrophages switching towards M2 phenotype resulting in secretion of tumor supportive cytokine and growth factor[211]. Interfering with such biological mechanism might be envisaged as efficient strategy to block this signaling to prevent the cancer cells from spreading.

***Interleukin-10 (IL-10)-*** Interleukin-10 (IL-10) acts as an anti-inflammatory to resolve inflammation and was originally characterized as a cytokine derived from T helper 2 (Th2) cells. However, it is generally acknowledged IL-10 is not only limited to specific T cell subsets but also produced by nearly all leukocytes [212,213]. IL-10 is a cancer-derived exosomal glycoprotein (18 KDa) plays an important role in macrophage-mediated signaling [43,214]. Cancer cells secrete IL-10 that binds the IL-10 receptor of macrophage leading to the phosphorylation of STAT3 through JAK-STAT signaling [215,216]. Phosphorylated STAT3 become dimerised and translocate into the nucleus where its drives expression of anti-inflammatory marker as well as growth factors which helps cancer progression [217]. Targeting IL-10 mediated signaling could be a potential therapeutic strategy that may restore macrophages into $M_0$ or $M_1$ type for therapeutic potential.

***Cluster of differentiation-44 (CD44)-*** Cluster of differentiation-44 (CD44) is a transmembrane glycoprotein having a molecular weight of 80-85 KDa, encoded by the CD44 gene located on the short arm of chromosome 11p13, initially known as Hermes antigen [218,219]. The expression of CD44 has been reported in the exosomes released from breast, ovarian, and pancreatic

cancer cells [220]. CD44 plays a crucial role in M2 macrophage polarization [221]. The JAK-STAT3 pathway has been identified as a key mechanism through which CD44 promotes the expression of M2 phenotype in TME. Upon signaling, Janus kinase (JAK) phosphorylates the receptor, leading to subsequent STAT3 phosphorylation. The phosphorylated STAT3 forms a dimer and translocates inside nucleus, initiating the genes expression associated with the M2 phenotype [222]. Yan et al. al (2022) reported that the suppression of hyaluronic acid (HA) signaling by interrupting glioblastoma hyaluronic acid synthesis or hindering the binding of hyaluronic acid to its receptor CD44 on macrophages has a role in polarization towards M1 phenotype. This occurs through the upregulation of signal regulatory protein α (SIRPα) on macrophages. SIRPα is a receptor found on monocytes, macrophages, neutrophils, dendritic cells, and microglia [223]. Upregulation of SIRPα leads to enhanced phosphorylation of STAT 1 and suppressed phosphorylation of STAT3 in the macrophages [222]. The modulation of this pathway is potentially an anti-cancer therapeutic strategy.

***CD147(Cluster of differentiation-147)-*** Basigin, also called as CD147(Cluster of differentiation-147) or EMMPRIN, is a glycoprotein found on cell surfaces, and it belongs to the immunoglobulin superfamily. It has different forms, with one having two immunoglobulin domains (basigin-2) and another having three (basigin-1) domains (basigin-1) [224]. CD147 has been identified as a glycoprotein present in exosomes [225]. The number of studies made it evident that CD147 plays a role in resistance to drugs, especially during cancer. The CD147/CD98hc complex, found in many tumor cells, is often overexpressed in cancers that are resistant to the drug cisplatin [226]. Overall, CD147 appears to have diverse roles, including potential implications in drug resistance and immune responses. Jian et.al (2024) reported that in atherosclerosis, macrophages sequestered from myeloid-specific CD147 knockout mice showed a phenotypic shift toward the anti-inflammatory (M2) type in response to LPS/ IFN-γ [227].

Kim et al reported that CD147 stimulation increases MMP-9 expression in macrophages through the ERK and NF-κB pathways, contributing to atherosclerosis[228]. Another study reported that CD147 was highly expressed in all breast cancer cell lines and activates MAPK/ERK phosphorylation, contributing to epithelial-mesenchymal transition and regulating the expression of E-cadherin, Vimentin, Snail1, and MMP-9[229]. To investigate the CD147-mediated mechanism during cancer progression could be of interest for formulating novel therapeutic strategies.

***Cluster of differentiation-63 (CD63)-*** Cluster of differentiation-63 (CD63) is an exosomal, transmembrane glycoprotein, also present on cancer cell-derived exosomes [230]. CD63 is highly expressed in breast cancer [230], CRC [231], gastric cancer [232] and gastrointestinal stromal tumor [233]. It is interesting to note that the modulation of glycosylation of CD63 impacts breast cancer cell malignancy [230]. Triple-negative breast cancer (TNBC) cells release CD63-containing extracellular vesicles, causing macrophage polarization toward alternatively activated macrophages (M2 phenotype) [211]. This polarization contributes to metastasis in breast cancer [211]. Nonetheless, the signaling pathway responsible for switching of macrophage towards M2 type is still unknown.

***Thrombospondin-1 (THBS1)-*** THBS1 belongs to a family of glycoproteins having molecular mass ranging from 150 to 180 kilodaltons (kDa). The structure consists of *N*-linked glycans (nearly 12 asparagine-linked), a variable number of *C*-mannosylated tryptophan residues in the type 1 repeats, and *O*-fucosylated residues [234]. Thrombospondin-1 is a multifaceted protein that plays various roles in the TME such as inhibition of angiogenesis, regulation of antitumor immunity, enhanced migration of tumor cells, and regulate extracellular proteases and growth factors activity [234]. The studies reported in mice lacking glycoprotein thrombospondin-1 or its receptors have highlighted its importance as an immune response regulator in infection, autoimmune diseases, as well as in antitumor

immunity [235]. In oral squamous cell carcinoma (OSCC), the glycoprotein thrombospondin-1 (THBS1) is transferred to macrophages through tumor Extracellular Vesicles, upon which they cause induction towards the M1 phenotype[211]. Further, in a Xiao et al. (2018) study, exosomes packed with THBS1 derived from OSCC were shown to hike in the transcription and successively the protein secretion of M1-associated markers, IL-6, IL-1β, and TNF-α [211]. The intake of exosomes by macrophages in OSCC leads to their activation via p38, Akt, and SAPK/JNK signaling pathways in the early phase[236]. In the study, the condition media-derived exosomes induced M1-like TAMs and significantly promoted the migration of OSCC cells[211]. Therefore, targeting M1-like Tumor-Associated Macrophages (TAMs) polarized by exosomes holds potential as a therapeutic approach for controlling cancer cells migration in OSCC.

**Table 2.2.1** List of cancer-derived exosomes containing glycoproteins involved in macrophage polarization

| Glycoprotein | Pathway/ Mechanism | TAMs Type | Cancers | References |
|---|---|---|---|---|
| **Glypican 3** | Wnt/ β-catenin | M2 | HCC, squamous, gastric, ovarian, and melanomas | [181–189] |
| **Nidogen 1** | ERK/ MAPK | M2 | HCC, ovarian cancer | [193,195,237] |
| **GP 130** | JAK/ STAT 3 p | M2 | Breast cancer | [198,200,201] |
| **Fetuin A** | NF-κB | M1 | Metastatic prostate cancer | [202–204] |
| **ICAM** | PTEN/ P13K/ AKT | M2 | Melanoma, colorectal cancer and lymphoma | [51,206,209–211] |
| **IL 10** | JAK1-STAT 3 | M2 | Negative breast carcinoma | [43,215–217] |
| **CD 44** | JAK –STAT 3 | M2/ M1 | Breast, ovarian, and pancreatic cancer, glioblastoma | [220–223] |
| **CD 147** | - | M1 | - | [224–227] |
| **CD 63** | - | M2 | HCC, breast cancer | [211,230] |

| | | | | |
|---|---|---|---|---|
| **Thrombospondin-1** | p38MAPK, Akt, SAPK/JNK | M1 | Oral squamous carcinoma | [211,234,236] |

In this section, we summarize various cancer cell-derived exosomal glycoproteins and their role in the polarization of the macrophages in the TME. The cancer cell-derived exosomes containing glycoproteins play a key role in switching of macrophages into alternatively M2 (anti-inflammatory) or classically M1 (pro-inflammatory) activated states, thus promoting or inhibiting cancer, respectively. Glycoproteins' involvement in M2 polarization has been more widely studied, but there is evidence suggesting that they can also influence M1 polarization, which requires further research. Researchers have already started to target glycoproteins in cancer therapy[238,239]. A therapeutic strategy targeting cancer cell-derived exosomal glycoproteins, such as CD147, CD44, and CD63, to modulate macrophage polarization to enhance anti-tumor response will be effective in inhibiting tumor progression. Direct targeting of glycoproteins is not feasible in most of the cases because its heavly glycosylated nature. Instead of this can be target its biosynthesis maschinary of glycoproteins such as fucosyltransferase 8 (FUT8). Currently, no ongoing clinical trials have been reported in this direction. Further studies are necessary to identify specific glycoprotein roles in macrophage switching and its impact on TME to prevent cancer. Future studies need to concentrate on the response of macrophage to exosomal glycoproteins in vivo models for immunotherapeutic approaches. Altogether, this review enhances our understanding of how exosomal glycoproteins influence macrophage phenotype changes, emphasizing their pivotal role in cancer progression.

**2.3 Exosome-derived miRNAs regulate macrophage-CRC cell cross-talk during aggressive tumor development:** In addition to proteins and glycoproteins, exosomes are enriched with nucleic acid cargo, including microRNAs (miRNAs), and play a functional role in post-transcriptional regulation of gene expression. These miRNAs gained significant attention due to their capability to control different signaling pathways that are closely associated with tumor progression, metastasis, and macrophage polarization. Continuation of the previous section on exosomal proteins and glycoproteins, now in this section we focus on exosomal miRNAs mediated macrophage polarization and tumor progression. Furthermore, this section narrows the discussion towards CRC-derived exosomes containing miRNAs and their functions in macrophage polarization.

**2.3.1 General Overview of MicroRNAs:** MicroRNAs are a type of non-coding RNA with a short length made up of 18-25 nucleotides [240]. They are involved in post-transcriptional alterations, which play a crucial function in inflammatory response regulation. They interact with the 3'-end of untranslated regions of messenger RNA (mRNA) to regulate gene expression. Translational repression or mRNA breakdown occurs as a result of this binding. MicroRNAs are single-stranded and highly conserved [241]. They are transcribed by RNA polymerase II or III, and their initial processing is via RNAase Drosha inside the nucleus. After that, the precursor of miRNA is transported into the cytoplasm, where it is digested by RNAase III, which is assisted by DICER. The resulting mature miRNA is integrated into the RNA-induced Silencing Complex (RISC), which further regulates protein transcription and translation [242]. Many cells express miRNAs, which regulate both pro-and anti-inflammatory responses [243]. Numerous human diseases, including cancer and inflammatory

disorders, are linked to excessive miRNA expression. Controlling the expression of SOCS3 and HDAC11 at the post-transcriptional level increases miR-203 and miR-145, respectively, and promotes polarization of macrophages toward M2 phenotype which suppresses the immune response and supports metastasis of CRC [244–246]. miR-25-3p, miR-425-5p and miR-130-3p target common sites of PTEN and modulate macrophages towards an anti-inflammatory type [247].

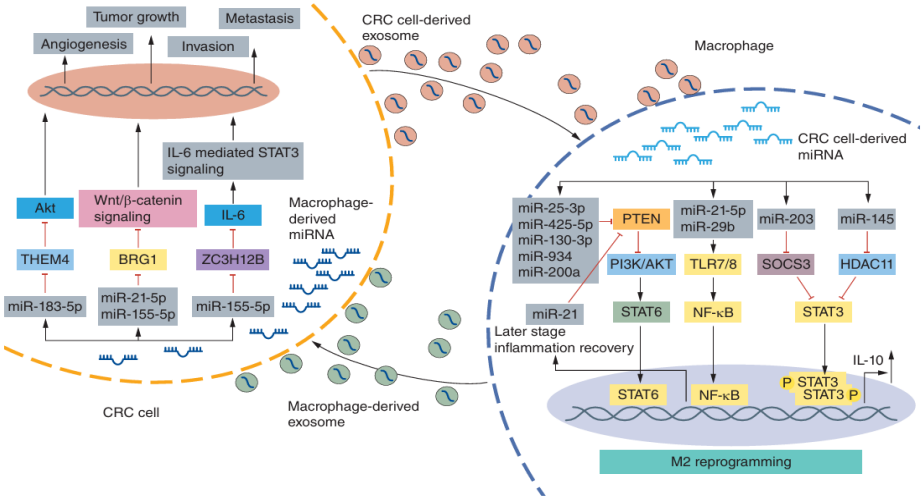



**Figure 2.3.1.** Representing exosome-mediated effect, the CRC cell secreted exosomes miR-25-3p, miR-425-5p, miR-130-3p, miR-934, miR-200a and miR-21-5p promote M2 polarization via PI3K/AKT mediated signaling, miR-203 and miR-145 mediated M2 polarization via STAT3 dimerization, and miR-21-5p and miR-29b promote M1 polarization which further increases miR-21 and leads to M1 to M2 reprogramming. The M2-polarized macrophages also secrete the exosome miR-21-5p, miR-155-5p, and miR-183-5p, which mediate tumor growth, invasion, metastasis, angiogenesis, and cancer progression.

**2.3.2 CRC-derived exosomal miRNA in the regulation of macrophage polarization:** Over the past few years, convincing evidence has emerged that macrophages have a tumor-promoting function in the TME. Consequently, the modification and migration of TAMs at the tumor site, for example through miRNAs, are crucial. The key miRNAs relevant to

miRNA-mediated crosstalk between CRC cells and TAMs in TME are listed in **TABLE 2.3.1**. Targeting major transcriptional networks that regulate the reprogramming of the M2 polarization state of macrophages to control cancer proliferation would be a novel therapeutic strategy.

**Table 2.3.1** List of CRC cell and macrophage-derived exosomal miRNA involved in CRC progression.

| CRC cell-derived miRNAs | | | | |
|---|---|---|---|---|
| **S.No.** | **miRNA** | **Target** | **Function** | **References** |
| **1** | **miR-203** | SOCS3 | Monocytes to M2 polarization, Immune suppression and metastasis. | [248] |
| **2** | **miR-145** | HDAC11 | M2 polarization and tumor growth. | [245,249] |
| **3** | **miR-934** | PTEN | M2 polarization and liver metastasis. | [250] |
| **4** | **miR-1246** | **-** | Reprogramming of TAMs. | [251,252] |
| **5** | **miR-25-5p, miR-130b-3p, and miR-425-5p** | PTEN | M2 polarization. | [247,253] |
| **6** | **miR-21-5p, miR-29b, and miR-200a** | PTEN | SOCS1/STAT1 mediated M2 And TLR7/8 mediated M1 polarization. | [254–256] |
| **7** | **Let-7d** | CCL7 | M2 polarization. | [257] |
| **Macrophage-derived** | | | | |
| **1** | **miR-155-5p** | ZC3H1B, BRG1 | Cancer proliferation and antiapoptotic. | [253,258,259] |
| **2** | **miR-21-5p** | BRG1 | CRC metastasis. | [259] |
| **3** | **miR-185-5p** | THEM4 | Cancer proliferation. | [260] |

**1. miR-203-** miRNA-203 plays an essential role in the progression of CRC by supporting tumor growth, immune suppression, and metastasis [248]. miR-203 has been found to promote a M2 (alternative) macrophage phenotype in the pre-metastasis niche [248]. miRNA-203 targets SOCS3, which results in an increase in STAT3 expression and therefore promotes M2 macrophage polarization [244]. The intravenous transfer of miR-203-rich CRC cells in the xenograft liver tumor model has been shown to promote tumour growth [248].

**2. miR-145-** miRNA-145, released from the CRC cells, is taken up by the macrophages, where it suppresses the expression level of the histone deacetylase HDAC11. miR-145 targets the 3' UTR sequence of HDAC11, which promotes the acetylation of histone H3 and H4, followed by recruitment of the transcription factor sp1 and STAT3, which upregulates the IL-10 [249]. To confirm the M2 polarization, the CRC cell line DLD-1 was co-cultured with the macrophage-like cell THP-1 and NOMO-1 which has shown an increase in the mRNAs level of IL-10 and VEGF, along with the increased surface markers CD11b+, CD68+ and CD206+ on the macrophage. *In vivo* miR-145 promotes tumor growth and enlargement of tumor volume [245,246]. It was also found that another target of miR-145 is TLR4, which diminishes the production of pro-inflammatory cytokines and inhibits M1 polarization. TLR4 transduces its signal through several adaptor molecules, including TIRAP, which has been reported as the target of miR-145; by inhibiting TLR4 or TIRAP, pro-inflammatory cytokines are decreased, and may be necessary for the production of anti-inflammatory cytokines in TAMs [261].

**3. miR-934-** miR-934 has a role in tumor growth, migration, angiogenesis, and liver metastasis by producing various growth factors, cytokines and chemokines. This miRNA is encapsulated in the exosome with the help of hnRNPA2B1, RNA binding protein through the GGAG sequence motif binding. The hnRNPA2B1 guides the transportation and post-transcriptional regulation of miRNA [262]. As exosomes are released from tumor-derived cells, they are transported to macrophages and release their content within them. Intracellular miR-934 is released from the binding protein and subsequently binds to the 3'UTR sequence of PTEN and downregulates its expression. This leads to the activation of PI3K/AKT signaling pathway [250], where activated PI3K initiates the conversion of PIP2 into PIP3, and the PIP3 which phosphorylates and activates AKT and polarization of the macrophage into the M2 (alternative) phenotype [263]. Differentiated M2 macrophages release a high amount of CXCL13

chemoattractant, which binds to the CXCR5 receptor present on CRC cells [264] and promotes the CRC liver metastasis. The CXCL13/CXCR5 axis promotes tumor progression by activating NF-kB/p65 signaling pathway in CRC cells and, thus, provokes a positive feedback loop with the TAM [250]. Along with this, TAMs promote the liver metastasis of CRC. It has been found that miR-934 targets Dickkopf-related protein 2 (DDK2) and negatively regulates the Wnt signaling pathway, and regulates the CRC cell proliferation [265].

**4. miR-1246-** Oncogenic miR-1246 was reported in CRC and involved proliferation, invasion, and metastasis [266]. It plays a critical role in reprogramming TAM towards an anti-inflammatory phenotype and modifies the tumor microenvironment. This miRNA action is closely associated with the presence of p53 mutant in colon cancer cells, which is the most common molecular mutation associated with cancer development in humans [251]. Mutation in p53 in cancer cells is responsible for reprogramming TAM towards tumor-supportive and anti-inflammatory phenotypes through increasing expression of TGF-β in CRC. This pathway also occurs in other cancers such as glioblastoma, wherein hypoxic glioma-derived extracellular vesicle containing miR-1246 converts macrophages towards anti-inflammatory phenotype via activation of STAT-3 signaling pathway and prohibiting the NF-kB signaling [252]. Huang et al. found that increased expression of miR-1246 was associated with higher risk and lower survival rate in CRC patients mainly associated with KRAS and PI3K signaling cascade [267]. CRC secreted mir-1246 is taken up by endothelial cells where it activates Smad 1/5/8 signaling via directly targeting promyelocytic leukaemia (PML) mRNA which results in boosting of angiogenesis [268]. As miR-1246 plays a pivotal role in TME modification by targeting macrophage polarization, it may be a target for antitumor immunotherapy.

**5. miR-25-5-p, miR-130b-3p and miR-425-5p-** These cluster of miRNAs regulates macrophage polarization transferred from CRC to TAM. miR-25-3p, miR-130b-3p and miR-425-5p are upregulated in CRC, and mainly responsible for the skewing of macrophages towards an anti-inflammatory phenotype via the PTEN/PI3K/Akt mediated signaling [253]. Exosomal miR-25-3p, miR-130b-3p, and miR-425-5p facilitated the M2 polarization. PTEN controls the phosphorylation of AKT by inhibiting PI3K, which results in the reprogramming of TAM to M2 type [269]. This M2 type enhances CRC cell-secreted VEGF and EMT, ultimately resulting in angiogenesis and metastasis. These *in vivo* studies also reported macrophages (THP-1 or Raw264.7) transfected with miR-25-3p, miR-130b-3p, and miR-425-5p mimic mixed with CRC (HCT116 and MC38) injected into the flanks of nude mice. The tumor size rapidly increased in mice transfected with macrophages which excessively express these miRNAs upon stimulation with IL-4 [247]. Targeting miR-25-3p, miR-130b-3p, and miR-425-5p will be a novel approach to designing drugs to inhibit the interaction with their specific receptor molecule, which favour a more proinflammatory macrophage phenotype in CRC.

**6. miR-21-5p, miR-29b and miR-200a-** CRC-derived exosomal miRNAs have the potential to transform macrophages into M1 or M2 macrophages, depending upon the conditions. miR-21-5p (miR-21) has a significant role in CRC at the primary and secondary sites. Initially, it was known for its pro-inflammatory phenotype; a study by Ying Kuan Shao et al. has shown that miR-21-5p promotes the liver pro-inflammatory phenotype in macrophage and liver metastasis in CRC [254]. The investigators incubated miR-21 rich exosomes derived from SW480 and SW620 cell lines with RAW264.7 and THP-1 for 24hr and found increase in IL-6 and TNF- mRNA while the anti-inflammatory cytokines showed no changes. The tail vein exosomal transfer also confirmed miR-21-5p localization predominantly in the liver. miR-21-5p has a GU motif in its nucleotide region, which plays an important role in modulating TLR-mediated

signaling and activating NF-kB. Thus, in the liver, these CRC cell-derived miRNA phagocytosed by the exosome and mediated signaling through TLR7/8 leads to the M1 phenotype, which further shows the high expression of IL-6 [254]. IL-6 plays a major role in macrophage polarization and also promotes macrophages to release IL-6 and miR-21, which target STAT3 in CRC cells creating positive feedback [255,270]. Interestingly miR-21-5p with miR-29b also shows a similar effect and promotes tumor growth and invasion [255]. A recent study by Yuan Yin et al. had shown a miR-21 role in polarization towards the M2 phenotype. At the primary site of the tumor, the subpopulation of macrophages was found to be polarized into CD206+ macrophages. miR-21-5p and miR-200a showed the synergistic effect on specific TAM, i.e., CD206 macrophages where they target the PTEN/AKT axis and SOCS1/STAT1, and lead to polarization of macrophages towards an M2 phenotype with increased PDL-1. The expression of PDL-1 inhibits the CD8 T-cells and promotes tumor immune escape and progression [256]**.**

**7. miR-Let-7d-** This miRNA targets the C-C motif chemokine CCL7, secreted by the cancer-associated macrophages (CAFs) and downregulates its expression. CCL7 promotes macrophage polarization toward the M2 phenotype, which inhibits monocyte migration and other functions like tumor growth, progression, and metastasis [257].

**2.3.3 Macrophage-derived exosomal miRNAs:** Not only do cancer cell-derived exosomal miRNAs support cancer proliferation but macrophage-derived miRNAs also promote CRC proliferation and metastasis (Table 1). miRNAs play a crucial role in cancer development, particularly invasion, metastasis, and drug resistance, and hence could be used as prominent biomarkers in cancer treatment and detection.

**1. miR-155-5p and miR-21-5p-** The miR-155-5p released from the M2 macrophages derive exosomes to CRC cells and support colon cancer

proliferation and antiapoptotic ability. Recent findings suggest the miR-155-5p target Zinc-finger-type-containing 12B (ZC3H12B) and upregulate the IL-6 expression, which results in CRC escape from the immune system [258]. ZC3H12 family proteins are mainly known for their involvement in inflammation, binding with IL-6 mRNA, and downregulating the IL-6 protein expression. It can be concluded that in CRC cells, the ZC3H12B protein plays a crucial part in controlling the predominant role of IL-6 in cancer to increase tumor growth. IL-6 induces the IL-6-dependent STAT3 activation through the phosphorylation of tyrosine residues of STAT3, which result in subsequent transcription of target genes that play a crucial role in cancer development [271]. The report also suggested that TAM-secreted exosomal miR-21-5p and miR-155-5p suppress BRG-1 expression, which is a key molecule for the proliferation of metastasis and involved in cancer progression [253]. *In vitro* and *in vivo* experiments showed downregulation of BRG-1 is involved in CRC metastasis through the activation of the Wnt/ b-catenin signaling pathway [259]. In CRC patients, it is feasible that exosomal miR-21-5p and miR-155-3p can be transferred from TAM to CRC perhaps via surrounding vessels. Preventing this transfer by designing therapeutic molecules may be an approach to inhibiting CRC metastasis and proliferation. Macrophages-derived exosomal miR-21-5p and miR-155-5p transfer to colon cancer cells is not a fully described mechanism, and more studies are needed in this direction.

**2. miR-183-5p-** The level of miR-183-5p was markedly elevated in M2-TAM and exosomes generated from M2-TAM, which enhanced colon cancer cell invasion and proliferation while reducing apoptosis [260]. This study also suggested that upregulation of miR-183-5p enhanced M2 polarization and mediated a booster effect on cancer cells while downregulation of miR-183-5p reversed the M2 TAM-mediated tumor-promoting effects on CRC. miR-183-5p targets the thioesterase superfamily member 4 (THEM4) and initiated Akt and NF-kB pathways to exacerbate colon cancer formation. THEM4 is a C-terminal regulatory protein that can

inhibit phosphorylation of AKT and block downstream signaling. Western blotting determined the inhibition of p-Akt and p-NF-kB expression [260,272]. THEM4 can mediate phosphatidylinositol 3-kinase (PI3K)/Akt reversely and shows an anti-inflammatory and anti-tumor response.

**2.3.4 miRNAs-based therapeutic approach-** As previously discussed, various exosomal miRNAs are being transferred from one cell to another and promote tumor initiation, differentiation, progression and metastasis. Developing the exosomal miRNA-based therapy can open the possibility of a novel therapeutic approach in CRC which is now utilized as a new way to deal with cancer and clinical trials have begun where miRNA mimics or miRNA antagonists or tumor-suppressing miRNA delivered intra-tumor or systemically are being used for tumor therapy. miRNA-based therapies are broadly used in two ways: targeting oncogenic miRNAs or using tumor-suppressive miRNAs. Both approaches have been showing effective results [273]. Meanwhile, the use of exosomal-mediated miRNA delivery is more efficient than a free miRNA delivery system [274]. Exosomes act like natural nanoparticles which have several significant features including low immunogenicity and cytotoxicity, stability in circulation, easily recognized and taken up by the specific type of cell, as well as carrying stable functional molecules such as miRNAs, siRNA or drug [275]. For such a strategy, exosomes are required to be engineered to encapsulate miRNA with suitable properties which promote uptake by the target cell [276] such as modifying the exosome membrane to differentially promote uptake by the tumor cell.

**Table 2.3.2 Table of microRNA-based clinical studies in a different cancer type.**

| S.No. | Exosomal miRNA | Type | Function | References |
|---|---|---|---|---|
| **1** | **Anti-miR-221** | CRC | Enhance anti-tumor effects. | [277] |
| **2** | **Let-7a** | Breast cancer | Inhibits tumor growth. | [278] |

| | | | | |
|---|---|---|---|---|
| **3** | **miR-335** | hepatocellular carcinoma | Help in tumor shrinkage. | [279] |
| **4** | **miR-21-sponge** | Glioma | Prevent malignancy. | [280] |
| **5** | **miR-494** | melanoma | Inhibits tumor growth and metastasis. | [281] |
| **6** | **miR-126** | Acute myocardial ischemia | Reduce cell injury and inflammation. | [282] |
| **7** | **miR-92-a-3p** | Osteoarthritis | Suppress cartilage degeneration. | [283] |

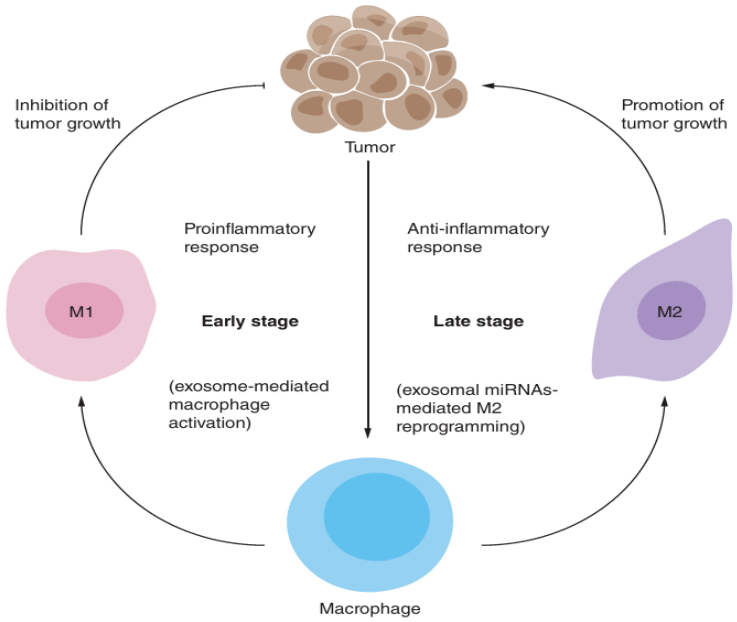



**Figure 2.3.2 Representation of exosome-mediated macrophage polarization into M1 phenotype and M2 phenotype**. In an early-stage colorectal cancer cell, secreted exosome promotes M1 polarization with a proinflammatory response, and in the later stage, the exosomal miRNA mediates reprogramming toward an M2 phenotype.

In the case of CRC, as far as we know, there is only one study that describes such a therapeutic approach. Mesenchymal stem cell (MSC) derived exosomes were used to transport an anti-miRNA oligonucleotide (AMO) to

the tumor cell. Anti-miRNA is the complementary sequence which binds and inhibits miRNA function [284]. Here, anti-miR-221 inhibits the function of the miR-221 which downregulates the expression of tumor suppressive genes including PTEN, p27kip1, TIMP3 and the Wnt signaling pathway [285]. The anti-miR-221 was incorporated into the MSCs-derived exosome through electroporation and the derived AMO-Exo showed an inhibitory effect on the NRP-1 receptor-positive tumor cell. The xenograft tumor model also confirmed that AMO-Exo targets the tumor cell and inhibits the growth. with associated decreased in expression of miR-221 [277]. Ohno and colleagues used EXO-miRNA in breast cancer and showed encapsulated miRNA Let-7a is transported to the epidermal growth factor receptor-expressing cancerous cells and effectively inhibits tumor growth as confirmed in a xenograft tumor model [278]. Schmittgen et al. used a similar approach for neuroblastoma wherein NK-cell-derived exosomes were used to deliver the tumor-suppressing miR-186 to restore its level, inhibit tumor progression and increase the survival. Similarly, the restoration of tumor-suppressive miR-335 enriched exosome led to cancer inhibition in hepatocellular carcinoma in a xenograft tumor model [279]. The exosomal miR-21 sponge construct was used to target elevated miR-21 in human glioma cells to restore the expression level of RECK and PDCD4 genes and prevent malignant property. A similar strategy can also be used in CRC as miR-21 has a major role in cancer progression and metastasis [280].

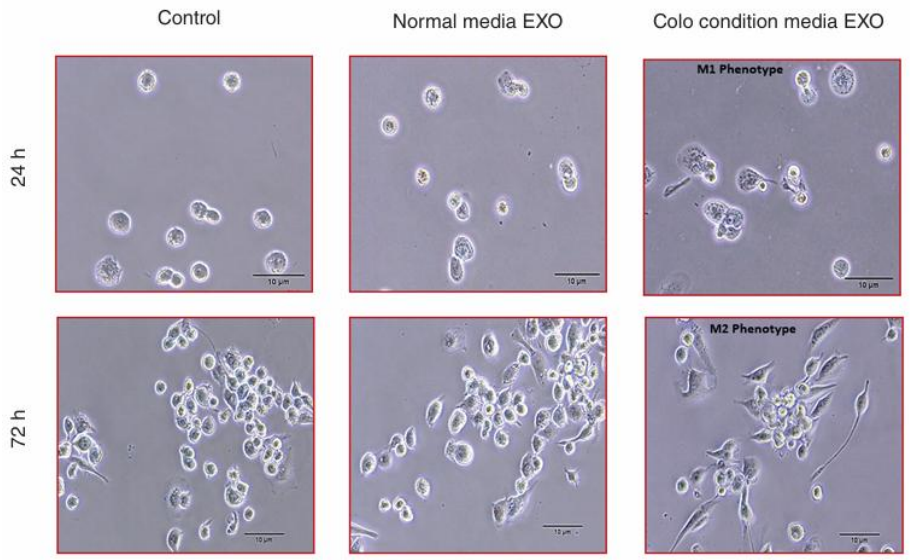



**Figure 2.3.3 Representation of THP-1 cell morphology in normal RPMI media and 48 h of Colo 205 CRC cells condition media isolated exosome and treated conditions after 24 and 72 h.** The THP-1 cells were treated with PMA (25 ng/ml) for 48 h before the experiment for their differentiation into monocytes. The images were taken under a bright-field microscope at 20× magnification. EXO: Exosomes; PMA: Phorbol 12-myristate 13-acetate.

Another way to deal with the exosomal miRNA is the inhibition of their release or uptake by the cell such cell-secreted oncogenic miRNAs are inhibited. Such a strategy was applied in melanoma where silencing of rab27a led to blockage of the Exo-miRNA cargo and regaining cellular levels of miR-494 which decreases tumor growth and metastasis [281]. This approach can also be used in the CRC to inhibit the release of exo-miRs from cancer cells so that the tumorigenic effect on the immune can be inhibited. miR-4689 has tumor suppression properties and is downregulated in the KRAS mutant colon cancer patients, so the incorporation of miR-4689 into the exosome can be used to negatively regulate the MAPK and PI3K/AKT pathways [286]. Similarly, miR-29a is also a tumor suppressive type and in the presence of its mimic shows a positive anti-tumor effect and decreases the protein expression of PI3K, AKT and GSK3-β and restricts the WNT/β-catenin signaling pathway in colon cancer. Thus, miR-29a

encapsulated into the exosome can make the delivery process more effective [287].

Finally, miRNA-based therapeutic approaches have been shown to advance not only in cancer but also in other diseases such as acute myocardial ischemia (AMI). miR-126-enriched exosomes derived from adipose stem cells were used to treat AMI and reduce cell injury and inflammatory factors [282]. miR-92-a-3p derived from MSCs exosomes has been shown to increase chondrogenesis and suppress cartilage degeneration in Osteoarthritis [283]. In the future, more results are expected that would provide evidence for the exosomal miRNA-based treatment in CRC.

In this section, we summarized the available literature on the CRC cell and macrophage-derived exosomal miRNAs which play a significant role in the onset, progression, metastasis, angiogenesis, invasion, and formation of pre-metastatic niche in CRC. Exosomes are small extracellular vesicles containing important cargos including mRNAs, miRNAs siRNAs, lncRNAs, and structural and functional tetraspanins and tetraspanin-associated proteins. Exosomes released from CRC cells and macrophages are the mediators of cross-talk between these cells in TME. These exosomes play several crucial functional roles in CRC-related mechanisms such as cancer growth, metastasis and drug resistance. Exosomes can influence macrophage polarization through RNAs or proteins, leading to tumorigenesis and the development of cancer. Here, we are proposing a disease model of CRC and introducing the new concept of early and late stages of response in macrophage polarization to CRCs see **Figure 2.3.2**. In early stages, exosome-mediated macrophage activation takes place and TAM recognize a cancer cell as foreign and initiate a pro-inflammatory response; in later-stage exosomal miRNAs from CRC cells modify the surrounding TME, resulting in reprogramming of macrophages towards an alternatively activated M2 phenotype. In support of our hypothesis, a preliminary experiment showed THP-1 macrophages' phenotypic changes

in response to COLO-205 cell-derived exosomes, where macrophages switch towards M2 type (elongated shape) at 72 hrs treatment see **Figure 2.3.3**. Greater comprehension of the function of exosome-derived miRNAs and TAM may reveal previously unknown mechanisms of cancer resistance to current therapeutic strategies as well as lead to the development of new prognostic tools and targets. Investigation of the exosome-mediated signaling pathway and its mechanisms during CRC is an exciting research area.

## 2.4 References


[1] J. Dai, Y. Su, S. Zhong, L. Cong, B. Liu, J. Yang, Y. Tao, Z. He, C. Chen, Y. Jiang, Exosomes: key players in cancer and potential therapeutic strategy, Sig Transduct Target Ther 5 (2020) 145. https://doi.org/10.1038/s41392-020-00261-0.

[2] M. Moradi-Chaleshtori, S.M. Hashemi, S. Soudi, M. Bandehpour, S. Mohammadi-Yeganeh, Tumor-derived exosomal microRNAs and proteins as modulators of macrophage function, Journal Cellular Physiology 234 (2019) 7970–7982. https://doi.org/10.1002/jcp.27552.

[3] Y. Lv, J. Qi, J.J. Babon, L. Cao, G. Fan, J. Lang, J. Zhang, P. Mi, B. Kobe, F. Wang, The JAK-STAT pathway: from structural biology to cytokine engineering, Sig Transduct Target Ther 9 (2024) 221. https://doi.org/10.1038/s41392-024-01934-w.

[4] J.E. Darnell, L.M. Kerr, G.R. Stark, Jak-STAT Pathways and Transcriptional Activation in Response to IFNs and Other Extracellular Signaling Proteins, Science 264 (1994) 1415–1421. https://doi.org/10.1126/science.8197455.

[5] J.P. Luyendyk, G.A. Schabbauer, M. Tencati, T. Holscher, R. Pawlinski, N. Mackman, Genetic Analysis of the Role of the PI3K-Akt Pathway in Lipopolysaccharide-Induced Cytokine and Tissue Factor Gene

Expression in Monocytes/Macrophages, The Journal of Immunology 180 (2008) 4218–4226. https://doi.org/10.4049/jimmunol.180.6.4218.

[6] Y. He, M.M. Sun, G.G. Zhang, J. Yang, K.S. Chen, W.W. Xu, B. Li, Targeting PI3K/Akt signal transduction for cancer therapy, Sig Transduct Target Ther 6 (2021) 425. https://doi.org/10.1038/s41392-021-00828-5.

[7] Y. Peng, Y. Wang, C. Zhou, W. Mei, C. Zeng, PI3K/Akt/mTOR Pathway and Its Role in Cancer Therapeutics: Are We Making Headway?, Front. Oncol. 12 (2022) 819128. https://doi.org/10.3389/fonc.2022.819128.

[8] S. Zhao, Y. Liu, L. He, Y. Li, K. Lin, Q. Kang, L. Liu, H. Zou, Gallbladder Cancer Cell-Derived Exosome-Mediated Transfer of Leptin Promotes Cell Invasion and Migration by Modulating STAT3-Mediated M2 Macrophage Polarization, Analytical Cellular Pathology 2022 (2022) 1–11. https://doi.org/10.1155/2022/9994906.

[9] H. Liu, T. Du, C. Li, G. Yang, STAT3 phosphorylation in central leptin resistance, Nutr Metab (Lond) 18 (2021) 39. https://doi.org/10.1186/s12986-021-00569-w.

[10] J. Li, Z. Yin, B. Huang, K. Xu, J. Su, Stat3 Signaling Pathway: A Future Therapeutic Target for Bone-Related Diseases, Front. Pharmacol. 13 (2022) 897539. https://doi.org/10.3389/fphar.2022.897539.

[11] A. Howes, L. Gabryšová, A. O'Garra, Role of IL-10 and the IL-10 Receptor in Immune Responses, in: Reference Module in Biomedical Sciences, Elsevier, 2014: p. B9780128012383000143. https://doi.org/10.1016/B978-0-12-801238-3.00014-3.

[12] H.M. Wilson, SOCS Proteins in Macrophage Polarization and Function, Front. Immunol. 5 (2014). https://doi.org/10.3389/fimmu.2014.00357.

[13] Y. Wang, J. Yi, X. Chen, Y. Zhang, M. Xu, Z. Yang, The regulation of cancer cell migration by lung cancer cell-derived exosomes through TGF-β and IL-10, Oncology Letters 11 (2016) 1527–1530. https://doi.org/10.3892/ol.2015.4044.

[14] L. Chen, Y. Shi, X. Zhu, W. Guo, M. Zhang, Y. Che, L. Tang, X. Yang, Q. You, Z. Liu, IL-10 secreted by cancer-associated macrophages regulates proliferation and invasion in gastric cancer cells via c-Met/STAT3 signaling, Oncol Rep (2019). https://doi.org/10.3892/or.2019.7206.

[15] T. Xia, M. Zhang, W. Lei, R. Yang, S. Fu, Z. Fan, Y. Yang, T. Zhang, Advances in the role of STAT3 in macrophage polarization, Front. Immunol. 14 (2023) 1160719. https://doi.org/10.3389/fimmu.2023.1160719.

[16] C. Casas, GRP78 at the Centre of the Stage in Cancer and Neuroprotection, Front. Neurosci. 11 (2017). https://doi.org/10.3389/fnins.2017.00177.

[17] S. Xia, W. Duan, W. Liu, X. Zhang, Q. Wang, GRP78 in lung cancer, J Transl Med 19 (2021) 118. https://doi.org/10.1186/s12967-021-02786-6.

[18] K. Iha, A. Sato, H.-Y. Tsai, H. Sonoda, S. Watabe, T. Yoshimura, M.-W. Lin, E. Ito, Gastric Cancer Cell-Derived Exosomal GRP78 Enhances Angiogenesis upon Stimulation of Vascular Endothelial Cells, CIMB 44 (2022) 6145–6157. https://doi.org/10.3390/cimb44120419.

[19] H. Zhang, S.-Q. Wang, L. Hang, C.-F. Zhang, L. Wang, C.-J. Duan, Y.-D. Cheng, D.-K. Wu, R. Chen, GRP78 facilitates M2 macrophage polarization and tumour progression, Cell. Mol. Life Sci. 78 (2021) 7709–7732. https://doi.org/10.1007/s00018-021-03997-2.

[20] M. Ahmadi, J. Rezaie, Tumor cells derived-exosomes as angiogenenic agents: possible therapeutic implications, J Transl Med 18 (2020) 249. https://doi.org/10.1186/s12967-020-02426-5.

[21] M.H. Kubala, V. Punj, V.R. Placencio-Hickok, H. Fang, G.E. Fernandez, R. Sposto, Y.A. DeClerck, Plasminogen Activator Inhibitor-1 Promotes the Recruitment and Polarization of Macrophages in Cancer, Cell Reports 25 (2018) 2177-2191.e7. https://doi.org/10.1016/j.celrep.2018.10.082.

[22] S. Li, X. Wei, J. He, X. Tian, S. Yuan, L. Sun, Plasminogen activator inhibitor-1 in cancer research, Biomedicine & Pharmacotherapy 105 (2018) 83–94. https://doi.org/10.1016/j.biopha.2018.05.119.

[23] C. Ryckman, K. Vandal, P. Rouleau, M. Talbot, P.A. Tessier, Proinflammatory Activities of S100: Proteins S100A8, S100A9, and S100A8/A9 Induce Neutrophil Chemotaxis and Adhesion, The Journal of Immunology 170 (2003) 3233–3242. https://doi.org/10.4049/jimmunol.170.6.3233.

[24] D. Prieto, N. Sotelo, N. Seija, S. Sernbo, C. Abreu, R. Durán, M. Gil, E. Sicco, V. Irigoin, C. Oliver, A.I. Landoni, R. Gabus, G. Dighiero, P. Oppezzo, S100-A9 protein in exosomes from chronic lymphocytic leukemia cells promotes NF-κB activity during disease progression, Blood 130 (2017) 777–788. https://doi.org/10.1182/blood-2017-02-769851.

[25] H.M. Koh, H.J. Lee, D.C. Kim, High expression of S100A8 and S100A9 is associated with poor disease-free survival in patients with cancer: a systematic review and meta-analysis, Transl Cancer Res TCR 10 (2021) 3225–3235. https://doi.org/10.21037/tcr-21-519.

[26] Z.P. Fan, M.L. Peng, Y.Y. Chen, Y.Z. Xia, C.Y. Liu, K. Zhao, H.P. Zhang, S100A9 Activates the Immunosuppressive Switch Through the PI3K/Akt Pathway to Maintain the Immune Suppression Function of

Testicular Macrophages, Front. Immunol. 12 (2021) 743354. https://doi.org/10.3389/fimmu.2021.743354.

[27] E. Vergadi, E. Ieronymaki, K. Lyroni, K. Vaporidi, C. Tsatsanis, Akt Signaling Pathway in Macrophage Activation and M1/M2 Polarization, The Journal of Immunology 198 (2017) 1006–1014. https://doi.org/10.4049/jimmunol.1601515.

[28] G. Chen, M. Wang, X. Liu, GDF15 promotes osteosarcoma cell migration and invasion by regulating the TGF-β signaling pathway, Mol Med Report (2019). https://doi.org/10.3892/mmr.2019.10664.

[29] X. Zheng, N. Ma, X. Wang, J. Hu, X. Ma, J. Wang, B. Cao, Exosomes derived from 5-fluorouracil-resistant colon cancer cells are enriched in GDF15 and can promote angiogenesis, J. Cancer 11 (2020) 7116–7126. https://doi.org/10.7150/jca.49224.

[30] L. Li, R. Zhang, H. Yang, D. Zhang, J. Liu, J. Li, B. Guo, GDF15 knockdown suppresses cervical cancer cell migration *in vitro* through the TGF-β/Smad2/3/Snail1 pathway, FEBS Open Bio 10 (2020) 2750–2760. https://doi.org/10.1002/2211-5463.13013.

[31] J. Wischhusen, I. Melero, W.H. Fridman, Growth/Differentiation Factor-15 (GDF-15): From Biomarker to Novel Targetable Immune Checkpoint, Front. Immunol. 11 (2020) 951. https://doi.org/10.3389/fimmu.2020.00951.

[32] G. Chen, M. Wang, X. Liu, GDF15 promotes osteosarcoma cell migration and invasion by regulating the TGF-β signaling pathway, Mol Med Report (2019). https://doi.org/10.3892/mmr.2019.10664.

[33] X. Zhang, S. Dong, Protective effect of growth differentiation factor 15 in sepsis by regulating macrophage polarization and its mechanism, Bioengineered 13 (2022) 9687–9707. https://doi.org/10.1080/21655979.2022.2059903.

[34] N. Nishikoba, K. Kumagai, S. Kanmura, Y. Nakamura, M. Ono, H. Eguchi, T. Kamibayashiyama, K. Oda, S. Mawatari, S. Tanoue, S. Hashimoto, H. Tsubouchi, A. Ido, HGF-MET Signaling Shifts M1 Macrophages Toward an M2-Like Phenotype Through PI3K-Mediated Induction of Arginase-1 Expression, Front. Immunol. 11 (2020) 2135. https://doi.org/10.3389/fimmu.2020.02135.

[35] P. Srivastava, Y.K. Dhuriya, V. Kumar, A. Srivastava, R. Gupta, R.K. Shukla, R.S. Yadav, H.N. Dwivedi, A.B. Pant, V.K. Khanna, PI3K/Akt/GSK3β induced CREB activation ameliorates arsenic mediated alterations in NMDA receptors and associated signaling in rat hippocampus: Neuroprotective role of curcumin, NeuroToxicology 67 (2018) 190–205. https://doi.org/10.1016/j.neuro.2018.04.018.

[36] Y.-C. Liu, X.-B. Zou, Y.-F. Chai, Y.-M. Yao, Macrophage Polarization in Inflammatory Diseases, Int. J. Biol. Sci. 10 (2014) 520–529. https://doi.org/10.7150/ijbs.8879.

[37] G.S.D. Purvis, E. Solito, C. Thiemermann, Annexin-A1: Therapeutic Potential in Microvascular Disease, Front. Immunol. 10 (2019) 938. https://doi.org/10.3389/fimmu.2019.00938.

[38] T.G. Araújo, S.T.S. Mota, H.S.V. Ferreira, M.A. Ribeiro, L.R. Goulart, L. Vecchi, Annexin A1 as a Regulator of Immune Response in Cancer, Cells 10 (2021) 2245. https://doi.org/10.3390/cells10092245.

[39] T. Wu, Y. Liu, N.M. Ali, B. Zhang, X. Cui, Effects of Exosomes on Tumor Bioregulation and Diagnosis, ACS Omega 8 (2023) 5157–5168. https://doi.org/10.1021/acsomega.2c06567.

[40] L.A. Moraes, S. Kar, S.L. Foo, T. Gu, Y.Q. Toh, P.B. Ampomah, K. Sachaphibulkij, G. Yap, O. Zharkova, H.M. Lukman, A.-M. Fairhurst, A.P. Kumar, L.H.K. Lim, Annexin-A1 enhances breast cancer growth and migration by promoting alternative macrophage polarization in the tumour

microenvironment, Sci Rep 7 (2017) 17925. https://doi.org/10.1038/s41598-017-17622-5.

[41] Q. Chen, Y. Li, W. Gao, L. Chen, W. Xu, X. Zhu, Exosome-Mediated Crosstalk Between Tumor and Tumor-Associated Macrophages, Front. Mol. Biosci. 8 (2021) 764222. https://doi.org/10.3389/fmolb.2021.764222.

[42] L. Kubiczkova, L. Sedlarikova, R. Hajek, S. Sevcikova, TGF-β – an excellent servant but a bad master, J Transl Med 10 (2012) 183. https://doi.org/10.1186/1479-5876-10-183.

[43] Y. Wang, J. Yi, X. Chen, Y. Zhang, M. Xu, Z. Yang, The regulation of cancer cell migration by lung cancer cell-derived exosomes through TGF-β and IL-10, Oncology Letters 11 (2016) 1527–1530. https://doi.org/10.3892/ol.2015.4044.

[44] S. Haque, J.C. Morris, Transforming growth factor-β: A therapeutic target for cancer, Human Vaccines & Immunotherapeutics 13 (2017) 1741–1750. https://doi.org/10.1080/21645515.2017.1327107.

[45] F. Zhang, H. Wang, X. Wang, G. Jiang, H. Liu, G. Zhang, H. Wang, R. Fang, X. Bu, S. Cai, J. Du, TGF-β induces M2-like macrophage polarization via SNAIL-mediated suppression of a pro-inflammatory phenotype, Oncotarget 7 (2016) 52294–52306. https://doi.org/10.18632/oncotarget.10561.

[46] L.-F. Hiew, C.-H. Poon, H.-Z. You, L.-W. Lim, TGF-β/Smad Signalling in Neurogenesis: Implications for Neuropsychiatric Diseases, Cells 10 (2021) 1382. https://doi.org/10.3390/cells10061382.

[47] Y.-H. Yeh, S.-W. Wang, Y.-C. Yeh, H.-F. Hsiao, T.-K. Li, Rhapontigenin inhibits TGF-β-mediated epithelial-mesenchymal transition via the PI3K/AKT/mTOR pathway and is not associated with HIF-1α

degradation, Oncology Reports 35 (2016) 2887–2895. https://doi.org/10.3892/or.2016.4664.

[48] F. Zhang, H. Wang, X. Wang, G. Jiang, H. Liu, G. Zhang, H. Wang, R. Fang, X. Bu, S. Cai, J. Du, TGF-β induces M2-like macrophage polarization via SNAIL-mediated suppression of a pro-inflammatory phenotype, Oncotarget 7 (2016) 52294–52306. https://doi.org/10.18632/oncotarget.10561.

[49] P.R. Kvietys, D.N. Granger, The Vascular Endothelium in Gastrointestinal Inflammation, in: Immunopharmacology of the Gastrointestinal System, Elsevier, 1993: pp. 69–94. https://doi.org/10.1016/B978-0-12-732860-7.50011-3.

[50] H.M. Lee, E.-J. Choi, J.H. Kim, T.D. Kim, Y.-K. Kim, C. Kang, Y.S. Gho, A membranous form of ICAM-1 on exosomes efficiently blocks leukocyte adhesion to activated endothelial cells, Biochemical and Biophysical Research Communications 397 (2010) 251–256. https://doi.org/10.1016/j.bbrc.2010.05.094.

[51] W. Zhang, W. Zhong, B. Wang, J. Yang, J. Yang, Z. Yu, Z. Qin, A. Shi, W. Xu, C. Zheng, L.M. Schuchter, G.C. Karakousis, T.C. Mitchell, R. Amaravadi, M. Herlyn, H. Dong, P.A. Gimotty, G. Daaboul, X. Xu, W. Guo, ICAM-1-mediated adhesion is a prerequisite for exosome-induced T cell suppression, Developmental Cell 57 (2022) 329-343.e7. https://doi.org/10.1016/j.devcel.2022.01.002.

[52] W. Gu, L. Yao, L. Li, J. Zhang, A.T. Place, R.D. Minshall, G. Liu, ICAM-1 regulates macrophage polarization by suppressing MCP-1 expression via miR-124 upregulation, Oncotarget 8 (2017) 111882–111901. https://doi.org/10.18632/oncotarget.22948.

[53] H. Sun, C. Wang, B. Hu, X. Gao, T. Zou, Q. Luo, M. Chen, Y. Fu, Y. Sheng, K. Zhang, Y. Zheng, X. Ren, S. Yan, Y. Geng, L. Yang, Q. Dong,

L. Qin, Exosomal S100A4 derived from highly metastatic hepatocellular carcinoma cells promotes metastasis by activating STAT3, Sig Transduct Target Ther 6 (2021) 187. https://doi.org/10.1038/s41392-021-00579-3.

[54] N. Chen, D. Sato, Y. Saiki, M. Sunamura, S. Fukushige, A. Horii, S100A4 is frequently overexpressed in lung cancer cells and promotes cell growth and cell motility, Biochemical and Biophysical Research Communications 447 (2014) 459–464. https://doi.org/10.1016/j.bbrc.2014.04.025.

[55] F. Fei, J. Qu, M. Zhang, Y. Li, S. Zhang, S100A4 in cancer progression and metastasis: A systematic review, Oncotarget 8 (2017) 73219–73239. https://doi.org/10.18632/oncotarget.18016.

[56] H. Sun, C. Wang, B. Hu, X. Gao, T. Zou, Q. Luo, M. Chen, Y. Fu, Y. Sheng, K. Zhang, Y. Zheng, X. Ren, S. Yan, Y. Geng, L. Yang, Q. Dong, L. Qin, Exosomal S100A4 derived from highly metastatic hepatocellular carcinoma cells promotes metastasis by activating STAT3, Sig Transduct Target Ther 6 (2021) 187. https://doi.org/10.1038/s41392-021-00579-3.

[57] S. Liu, H. Zhang, Y. Li, Y. Zhang, Y. Bian, Y. Zeng, X. Yao, J. Wan, X. Chen, J. Li, Z. Wang, Z. Qin, S100A4 enhances protumor macrophage polarization by control of PPAR-γ-dependent induction of fatty acid oxidation, J Immunother Cancer 9 (2021) e002548. https://doi.org/10.1136/jitc-2021-002548.

[58] G.Y. Chen, M. Liu, F. Wang, J. Bertin, G. Núñez, A Functional Role for Nlrp6 in Intestinal Inflammation and Tumorigenesis, The Journal of Immunology 186 (2011) 7187–7194. https://doi.org/10.4049/jimmunol.1100412.

[59] X. Rao, X. Zhou, G. Wang, X. Jie, B. Xing, Y. Xu, Y. Chen, J. Li, K. Zhu, Z. Wu, G. Wu, C. Wu, R. Zhou, NLRP6 is required for cancer-derived exosome-modified macrophage M2 polarization and promotes

metastasis in small cell lung cancer, Cell Death Dis 13 (2022) 891. https://doi.org/10.1038/s41419-022-05336-0.

[60] E. Brzozowska, S. Deshmukh, Integrin Alpha v Beta 6 (αvβ6) and Its Implications in Cancer Treatment, IJMS 23 (2022) 12346. https://doi.org/10.3390/ijms232012346.

[61] H. Lu, N. Bowler, L.A. Harshyne, D. Craig Hooper, S.R. Krishn, S. Kurtoglu, C. Fedele, Q. Liu, H.-Y. Tang, A.V. Kossenkov, W.K. Kelly, K. Wang, R.B. Kean, P.H. Weinreb, L. Yu, A. Dutta, P. Fortina, A. Ertel, M. Stanczak, F. Forsberg, D.I. Gabrilovich, D.W. Speicher, D.C. Altieri, L.R. Languino, Exosomal αvβ6 integrin is required for monocyte M2 polarization in prostate cancer, Matrix Biology 70 (2018) 20–35. https://doi.org/10.1016/j.matbio.2018.03.009.

[62] N. Sauer, N. Janicka, W. Szlasa, B. Skinderowicz, K. Kołodzińska, W. Dwernicka, M. Oślizło, J. Kulbacka, V. Novickij, K. Karłowicz-Bodalska, TIM-3 as a promising target for cancer immunotherapy in a wide range of tumors, Cancer Immunol Immunother 72 (2023) 3405–3425. https://doi.org/10.1007/s00262-023-03516-1.

[63] S. Qin, B. Dong, M. Yi, Q. Chu, K. Wu, Prognostic Values of TIM-3 Expression in Patients With Solid Tumors: A Meta-Analysis and Database Evaluation, Front. Oncol. 10 (2020) 1288. https://doi.org/10.3389/fonc.2020.01288.

[64] X. Li, Y. Liu, L. Yang, Y. Jiang, Q. Qian, TIM-3 shuttled by MV3 cells-secreted exosomes inhibits CD4+ T cell immune function and induces macrophage M2 polarization to promote the growth and metastasis of melanoma cells, Translational Oncology 18 (2022) 101334. https://doi.org/10.1016/j.tranon.2021.101334.

[65] X. Jiang, T. Zhou, Y. Xiao, J. Yu, S. Dou, G. Chen, R. Wang, H. Xiao, C. Hou, W. Wang, Q. Shi, J. Feng, Y. Ma, B. Shen, Y. Li, G. Han,

Tim-3 promotes tumor-promoting M2 macrophage polarization by binding to STAT1 and suppressing the STAT1-miR-155 signaling axis, OncoImmunology 5 (2016) e1211219. https://doi.org/10.1080/2162402X.2016.1211219.

[66] B. Lei, L.-X. Xie, S.-B. Zhang, B. Wan, L.-R. Zhong, X.-M. Zhou, X.-M. Mao, F.-P. Shu, Phosphoribosyl-pyrophosphate synthetase 2 (PRPS2) depletion regulates spermatogenic cell apoptosis and is correlated with hypospermatogenesis, Asian J Androl 22 (2020) 493. https://doi.org/10.4103/aja.aja_122_19.

[67] G. Liu, Y. Luo, P. Hou, *PRPS2* Enhances Resistance to Cisplatin via Facilitating Exosomes-mediated Macrophage M2 Polarization in Non-small Cell Lung Cancer, Immunological Investigations 51 (2022) 1423–1436. https://doi.org/10.1080/08820139.2021.1952217.

[68] R. Li, Y. Wang, X. Zhang, M. Feng, J. Ma, J. Li, X. Yang, F. Fang, Q. Xia, Z. Zhang, M. Shang, S. Jiang, Exosome-mediated secretion of LOXL4 promotes hepatocellular carcinoma cell invasion and metastasis, Mol Cancer 18 (2019) 18. https://doi.org/10.1186/s12943-019-0948-8.

[69] W. Wang, X. Wang, F. Yao, C. Huang, Lysyl Oxidase Family Proteins: Prospective Therapeutic Targets in Cancer, IJMS 23 (2022) 12270. https://doi.org/10.3390/ijms232012270.

[70] M. Yao, S. Liang, B. Cheng, Role of exosomes in hepatocellular carcinoma and the regulation of traditional Chinese medicine, Front. Pharmacol. 14 (2023) 1110922. https://doi.org/10.3389/fphar.2023.1110922.

[71] T. Görögh, J. Weise, C. Holtmeier, P. Rudolph, J. Hedderich, S. Gottschlich, M. Hoffmann, P. Ambrosch, K. Csiszar, Selective upregulation and amplification of the lysyl oxidase like-4 (LOXL4) gene in head and

neck squamous cell carcinoma, The Journal of Pathology 212 (2007) 74–82. https://doi.org/10.1002/path.2137.

[72] N.L.G.Y. Komalasari, N. Tomonobu, R. Kinoshita, Y. Chen, Y. Sakaguchi, Y. Gohara, F. Jiang, K. Yamamoto, H. Murata, I.M.W. Ruma, I.W. Sumardika, J. Zhou, A. Yamauchi, F. Kuribayashi, Y. Inoue, S. Toyooka, M. Sakaguchi, Lysyl oxidase-like 4 exerts an atypical role in breast cancer progression that is dependent on the enzymatic activity that targets the cell-surface annexin A2, Front. Oncol. 13 (2023) 1142907. https://doi.org/10.3389/fonc.2023.1142907.

[73] S.P. Papadakos, N. Machairas, I.E. Stergiou, K. Arvanitakis, G. Germanidis, A.E. Frampton, S. Theocharis, Unveiling the Yin-Yang Balance of M1 and M2 Macrophages in Hepatocellular Carcinoma: Role of Exosomes in Tumor Microenvironment and Immune Modulation, Cells 12 (2023) 2036. https://doi.org/10.3390/cells12162036.

[74] D. Cavallo-Medved, K. Moin, B. Sloane, Cathepsin B: Basis Sequence: Mouse, AFCS Nat Mol Pages 2011 (2011) A000508.

[75] D. Cavallo-Medved, B.F. Sloane, K. Moin, Cathepsin B, in: S. Choi (Ed.), Encyclopedia of Signaling Molecules, Springer New York, New York, NY, 2016: pp. 1–17. https://doi.org/10.1007/978-1-4614-6438-9_101523-1.

[76] D. Oelschlaegel, T. Weiss Sadan, S. Salpeter, S. Krug, G. Blum, W. Schmitz, A. Schulze, P. Michl, Cathepsin Inhibition Modulates Metabolism and Polarization of Tumor-Associated Macrophages, Cancers 12 (2020) 2579. https://doi.org/10.3390/cancers12092579.

[77] F. Cappuzzo, L. Toschi, G. Tallini, G.L. Ceresoli, I. Domenichini, S. Bartolini, G. Finocchiaro, E. Magrini, G. Metro, A. Cancellieri, R. Trisolini, L. Crino, P.A. Bunn, A. Santoro, W.A. Franklin, M. Varella-Garcia, F.R. Hirsch, Insulin-like growth factor receptor 1 (IGFR-1) is

significantly associated with longer survival in non-small-cell lung cancer patients treated with gefitinib, Annals of Oncology 17 (2006) 1120–1127. https://doi.org/10.1093/annonc/mdl077.

[78] S.-L. Liu, P. Sun, Y. Li, S.-S. Liu, Y. Lu, Exosomes as critical mediators of cell-to-cell communication in cancer pathogenesis and their potential clinical application, Transl. Cancer Res 8 (2019) 298–311. https://doi.org/10.21037/tcr.2019.01.03.

[79] Y. Sun, X. Sun, B. Shen, Molecular Imaging of IGF-1R in Cancer, Mol Imaging 16 (2017) 153601211773664. https://doi.org/10.1177/1536012117736648.

[80] O. Spadaro, C.D. Camell, L. Bosurgi, K.Y. Nguyen, Y.-H. Youm, C.V. Rothlin, V.D. Dixit, IGF1 Shapes Macrophage Activation in Response to Immunometabolic Challenge, Cell Reports 19 (2017) 225–234. https://doi.org/10.1016/j.celrep.2017.03.046.

[81] X. Guo, X. Bu, L. Yuan, L. Ji, Collagen type V alpha 2 promotes the development of gastric cancer via M2 macrophage polarization, Chin J Physiol 66 (2023) 93. https://doi.org/10.4103/cjop.CJOP-D-22-00078.

[82] J. Wang, Y.-H. Jiang, P.-Y. Yang, F. Liu, Increased Collagen Type V α2 (COL5A2) in Colorectal Cancer is Associated with Poor Prognosis and Tumor Progression, OTT Volume 14 (2021) 2991–3002. https://doi.org/10.2147/OTT.S288422.

[83] Y. Jin, X. Song, X. Sun, Y. Ding, Up-regulation of collagen type V alpha 2 ( *COL5A2* ) promotes malignant phenotypes in gastric cancer cell via inducing epithelial–mesenchymal transition (EMT), Open Medicine 18 (2023) 20220593. https://doi.org/10.1515/med-2022-0593.

[84] M. Ye, J. Wang, S. Pan, L. Zheng, Z.-W. Wang, X. Zhu, Nucleic acids and proteins carried by exosomes of different origins as potential

biomarkers for gynecologic cancers, Molecular Therapy - Oncolytics 24 (2022) 101–113. https://doi.org/10.1016/j.omto.2021.12.005.

[85] M.S. Ong, S. Deng, C.E. Halim, W. Cai, T.Z. Tan, R.Y.-J. Huang, G. Sethi, S.C. Hooi, A.P. Kumar, C.T. Yap, Cytoskeletal Proteins in Cancer and Intracellular Stress: A Therapeutic Perspective, Cancers 12 (2020) 238. https://doi.org/10.3390/cancers12010238.

[86] Z. Chen, L. Yang, Y. Cui, Y. Zhou, X. Yin, J. Guo, G. Zhang, T. Wang, Q.-Y. He, Cytoskeleton-centric protein transportation by exosomes transforms tumor-favorable macrophages, Oncotarget 7 (2016) 67387–67402. https://doi.org/10.18632/oncotarget.11794.

[87] N. Ferrara, H.-P. Gerber, J. LeCouter, The biology of VEGF and its receptors, Nat Med 9 (2003) 669–676. https://doi.org/10.1038/nm0603-669.

[88] S.Y. Ko, W. Lee, H.A. Kenny, L.H. Dang, L.M. Ellis, E. Jonasch, E. Lengyel, H. Naora, Cancer-derived small extracellular vesicles promote angiogenesis by heparin-bound, bevacizumab-insensitive VEGF, independent of vesicle uptake, Commun Biol 2 (2019) 386. https://doi.org/10.1038/s42003-019-0609-x.

[89] K.C. Wheeler, M.K. Jena, B.S. Pradhan, N. Nayak, S. Das, C.-D. Hsu, D.S. Wheeler, K. Chen, N.R. Nayak, VEGF may contribute to macrophage recruitment and M2 polarization in the decidua, PLoS ONE 13 (2018) e0191040. https://doi.org/10.1371/journal.pone.0191040.

[90] M. Perrot-Applanat, M. Di Benedetto, Autocrine functions of VEGF in breast tumor cells: Adhesion, survival, migration and invasion, Cell Adhesion & Migration 6 (2012) 547–553. https://doi.org/10.4161/cam.23332.

[91] C.P. Tanase, I. Ogrezeanu, C. Badiu, Angiogenesis, in: Molecular Pathology of Pituitary Adenomas, Elsevier, 2012: pp. 37–44. https://doi.org/10.1016/B978-0-12-415830-6.00004-4.

[92] B. Liu, L. Qu, S. Yan, Cyclooxygenase-2 promotes tumor growth and suppresses tumor immunity, Cancer Cell Int 15 (2015) 106. https://doi.org/10.1186/s12935-015-0260-7.

[93] M. Szweda, A. Rychlik, I. Babińska, A. Pomianowski, Significance of cyclooxygenase-2 in oncogenesis, Journal of Veterinary Research 63 (2019) 215–224. https://doi.org/10.2478/jvetres-2019-0030.

[94] J. Kim, S.-W. Hong, S. Kim, D. Kim, D. Hur, D.-H. Jin, B. Kim, Y. Kim, Cyclooxygenase-2 expression is induced by celecoxib treatment in lung cancer cells and is transferred to neighbor cells via exosomes, Int J Oncol (2017). https://doi.org/10.3892/ijo.2017.4227.

[95] H. Li, B. Yang, J. Huang, Y. Lin, T. Xiang, J. Wan, H. Li, S. Chouaib, G. Ren, Cyclooxygenase-2 in tumor-associated macrophages promotes breast cancer cell survival by triggering a positive-feedback loop between macrophages and cancer cells, Oncotarget 6 (2015) 29637–29650. https://doi.org/10.18632/oncotarget.4936.

[96] Y. Miki, M. Yashiro, T. Okuno, K. Kuroda, S. Togano, K. Hirakawa, M. Ohira, Clinico-pathological significance of exosome marker CD63 expression on cancer cells and stromal cells in gastric cancer, PLoS ONE 13 (2018) e0202956. https://doi.org/10.1371/journal.pone.0202956.

[97] Q. Chen, Y. Li, W. Gao, L. Chen, W. Xu, X. Zhu, Exosome-Mediated Crosstalk Between Tumor and Tumor-Associated Macrophages, Front. Mol. Biosci. 8 (2021) 764222. https://doi.org/10.3389/fmolb.2021.764222.

[98] Y.J. Piao, H.S. Kim, E.H. Hwang, J. Woo, M. Zhang, W.K. Moon, Breast cancer cell-derived exosomes and macrophage polarization are

associated with lymph node metastasis, Oncotarget 9 (2018) 7398–7410. https://doi.org/10.18632/oncotarget.23238.

[99] R. Hasan, G.-L. Zhou, The Cytoskeletal Protein Cyclase-Associated Protein 1 (CAP1) in Breast Cancer: Context-Dependent Roles in Both the Invasiveness and Proliferation of Cancer Cells and Underlying Cell Signals, IJMS 20 (2019) 2653. https://doi.org/10.3390/ijms20112653.

[100] M. Hua, S. Yan, Y. Deng, Q. Xi, R. Liu, S. Yang, J. Liu, C. Tang, Y. Wang, J. Zhong, CAP1 is overexpressed in human epithelial ovarian cancer and promotes cell proliferation, International Journal of Molecular Medicine 35 (2015) 941–949. https://doi.org/10.3892/ijmm.2015.2089.

[101] R. Sasaki, T. Kanda, O. Yokosuka, N. Kato, S. Matsuoka, M. Moriyama, Exosomes and Hepatocellular Carcinoma: From Bench to Bedside, IJMS 20 (2019) 1406. https://doi.org/10.3390/ijms20061406.

[102] S. Syeda, K. Rawat, A. Shrivastava, Exosome Load Increases Systemically and Mediates Pro-tumoral M2 Macrophage Polarization in Lymphoma, (2023). https://doi.org/10.20944/preprints202304.0062.v1.

[103] Y. Zhu, N. Wan, X. Shan, G. Deng, Q. Xu, H. Ye, Y. Sun, Celastrol targets adenylyl cyclase-associated protein 1 to reduce macrophages-mediated inflammation and ameliorates high fat diet-induced metabolic syndrome in mice, Acta Pharmaceutica Sinica B 11 (2021) 1200–1212. https://doi.org/10.1016/j.apsb.2020.12.008.

[104] F. Christian, E. Smith, R. Carmody, The Regulation of NF-κB Subunits by Phosphorylation, Cells 5 (2016) 12. https://doi.org/10.3390/cells5010012.

[105] K.T. Iacono, A.L. Brown, M.I. Greene, S.J. Saouaf, CD147 immunoglobulin superfamily receptor function and role in pathology, Experimental and Molecular Pathology 83 (2007) 283–295. https://doi.org/10.1016/j.yexmp.2007.08.014.

[106] D. Huang, D. Rao, Q. Jin, M. Lai, J. Zhang, Z. Lai, H. Shen, T. Zhong, Role of CD147 in the development and diagnosis of hepatocellular carcinoma, Front. Immunol. 14 (2023) 1149931. https://doi.org/10.3389/fimmu.2023.1149931.

[107] W. Olejarz, G. Kubiak-Tomaszewska, A. Chrzanowska, T. Lorenc, Exosomes in Angiogenesis and Anti-angiogenic Therapy in Cancers, IJMS 21 (2020) 5840. https://doi.org/10.3390/ijms21165840.

[108] J.-J. Lv, H. Wang, C. Zhang, T.-J. Zhang, H.-L. Wei, Z.-K. Liu, Y.-H. Ma, Z. Yang, Q. He, L.-J. Wang, L.-L. Duan, Z.-N. Chen, H. Bian, CD147 Sparks Atherosclerosis by Driving M1 Phenotype and Impairing Efferocytosis, Circulation Research 134 (2024) 165–185. https://doi.org/10.1161/CIRCRESAHA.123.323223.

[109] W.-T. Huang, I.-W. Chong, H.-L. Chen, C.-Y. Li, C.-C. Hsieh, H.-F. Kuo, C.-Y. Chang, Y.-H. Chen, Y.-P. Liu, C.-Y. Lu, Y.-R. Liu, P.-L. Liu, Pigment epithelium-derived factor inhibits lung cancer migration and invasion by upregulating exosomal thrombospondin 1, Cancer Letters 442 (2019) 287–298. https://doi.org/10.1016/j.canlet.2018.10.031.

[110] S. Syeda, K. Rawat, A. Shrivastava, Exosome Load Increases Systemically and Mediates Pro-tumoral M2 Macrophage Polarization in Lymphoma, (2023). https://doi.org/10.20944/preprints202304.0062.v1.

[111] M. Moradi-Chaleshtori, A. Koochaki, S. Shojaei, M. Paryan, M. Safarzadeh, S.M. Hashemi, S. Mohammadi-Yeganeh, Overexpression of pigment epithelium-derived factor in breast cancer cell-derived exosomes induces M1 polarization in macrophages, Immunology Letters 248 (2022) 31–36. https://doi.org/10.1016/j.imlet.2022.05.005.

[112] D. Martinez-Marin, C. Jarvis, T. Nelius, W. de Riese, O.V. Volpert, S. Filleur, PEDF increases the tumoricidal activity of macrophages towards

prostate cancer cells in vitro, PLoS ONE 12 (2017) e0174968. https://doi.org/10.1371/journal.pone.0174968.

[113] T. Nelius, C. Samathanam, D. Martinez-Marin, N. Gaines, J. Stevens, J. Hickson, W. de Riese, S. Filleur, Positive correlation between PEDF expression levels and macrophage density in the human prostate, The Prostate 73 (2013) 549–561. https://doi.org/10.1002/pros.22595.

[114] H. Dong, C. Xie, Y. Jiang, K. Li, Y. Lin, X. Pang, X. Xiong, J. Zheng, X. Ke, Y. Chen, Y. Li, H. Zhang, Tumor-Derived Exosomal Protein Tyrosine Phosphatase Receptor Type O Polarizes Macrophage to Suppress Breast Tumor Cell Invasion and Migration, Front. Cell Dev. Biol. 9 (2021) 703537. https://doi.org/10.3389/fcell.2021.703537.

[115] Z. Liu, J. Hou, L. Ren, J. He, B. Sun, L.-Z. Sun, S. Wang, Protein tyrosine phosphatase receptor type O expression in the tumor niche correlates with reduced tumor growth, angiogenesis, circulating tumor cells and metastasis of breast cancer, Oncology Reports 33 (2015) 1908–1914. https://doi.org/10.3892/or.2015.3772.

[116] W. Dai, W. Xiang, L. Han, Z. Yuan, R. Wang, Y. Ma, Y. Yang, S. Cai, Y. Xu, S. Mo, Q. Li, G. Cai, PTPRO represses colorectal cancer tumorigenesis and progression by reprogramming fatty acid metabolism, Cancer Communications 42 (2022) 848–867. https://doi.org/10.1002/cac2.12341.

[117] C.G. Evans, L. Chang, J.E. Gestwicki, Heat Shock Protein 70 (Hsp70) as an Emerging Drug Target, J. Med. Chem. 53 (2010) 4585–4602. https://doi.org/10.1021/jm100054f.

[118] G. Chanteloup, M. Cordonnier, N. Isambert, A. Bertaut, G. Marcion, C. Garrido, J. Gobbo, Membrane-bound exosomal HSP70 as a biomarker for detection and monitoring of malignant solid tumours: a pilot study, Pilot Feasibility Stud 6 (2020) 35. https://doi.org/10.1186/s40814-020-00577-2.

[119] J. Zhu, Y. Lou, P. Liu, L.X. Xu, Tumor-related HSP70 released after cryo-thermal therapy targeted innate immune initiation in the antitumor immune response, International Journal of Hyperthermia 37 (2020) 843–853. https://doi.org/10.1080/02656736.2020.1788173.

[120] T.M.S. Greiling, J.I. Clark, New Insights into the Mechanism of Lens Development Using Zebra Fish, in: International Review of Cell and Molecular Biology, Elsevier, 2012: pp. 1–61. https://doi.org/10.1016/B978-0-12-394307-1.00001-1.

[121] W. Xu, Y. Guo, Z. Huang, H. Zhao, M. Zhou, Y. Huang, D. Wen, J. Song, Z. Zhu, M. Sun, C.-Y. Liu, Y. Chen, L. Cui, X. Wang, Z. Liu, Y. Yang, P. Du, Small heat shock protein CRYAB inhibits intestinal mucosal inflammatory responses and protects barrier integrity through suppressing IKKβ activity, Mucosal Immunology 12 (2019) 1291–1303. https://doi.org/10.1038/s41385-019-0198-5.

[122] B. Rashidieh, A.L. Bain, S.M. Tria, S. Sharma, C.A. Stewart, J.L. Simmons, P.M. Apaja, P.H.G. Duijf, J. Finnie, K.K. Khanna, Alpha-B-Crystallin overexpression is sufficient to promote tumorigenesis and metastasis in mice, Exp Hematol Oncol 12 (2023) 4. https://doi.org/10.1186/s40164-022-00365-z.

[123] J. Zhang, J. Liu, J. Wu, W. Li, Z. Chen, L. Yang, Progression of the role of CRYAB in signaling pathways and cancers, OTT Volume 12 (2019) 4129–4139. https://doi.org/10.2147/OTT.S201799.

[124] R.A. Kore, E.C. Abraham, Phosphorylation negatively regulates exosome mediated secretion of cryAB in glioma cells, Biochimica et Biophysica Acta (BBA) - Molecular Cell Research 1863 (2016) 368–377. https://doi.org/10.1016/j.bbamcr.2015.11.027.

[125] E.-M.F. Lim, V. Hoghooghi, K.M. Hagen, K. Kapoor, A. Frederick, T.M. Finlay, S.S. Ousman, Presence and activation of pro-inflammatory

macrophages are associated with CRYAB expression in vitro and after peripheral nerve injury, J Neuroinflammation 18 (2021) 82. https://doi.org/10.1186/s12974-021-02108-z.

[126] Y. Han, D. Liu, L. Li, PD-1/PD-L1 pathway: current researches in cancer, Am J Cancer Res 10 (2020) 727–742.

[127] J. Yu, X. Wang, F. Teng, L. Kong, PD-L1 expression in human cancers and its association with clinical outcomes, OTT Volume 9 (2016) 5023–5039. https://doi.org/10.2147/OTT.S105862.

[128] V. Vautrot, H. Bentayeb, S. Causse, C. Garrido, J. Gobbo, Tumor-Derived Exosomes: Hidden Players in PD-1/PD-L1 Resistance, Cancers 13 (2021) 4537. https://doi.org/10.3390/cancers13184537.

[129] D.H. Kim, H. Kim, Y.J. Choi, S.Y. Kim, J.-E. Lee, K.J. Sung, Y.H. Sung, C.-G. Pack, M. Jung, B. Han, K. Kim, W.S. Kim, S.J. Nam, C.-M. Choi, M. Yun, J.C. Lee, J.K. Rho, Exosomal PD-L1 promotes tumor growth through immune escape in non-small cell lung cancer, Exp Mol Med 51 (2019) 1–13. https://doi.org/10.1038/s12276-019-0295-2.

[130] N. Liu, J. Zhang, M. Yin, H. Liu, X. Zhang, J. Li, B. Yan, Y. Guo, J. Zhou, J. Tao, S. Hu, X. Chen, C. Peng, Inhibition of xCT suppresses the efficacy of anti-PD-1/L1 melanoma treatment through exosomal PD-L1-induced macrophage M2 polarization, Molecular Therapy 29 (2021) 2321–2334. https://doi.org/10.1016/j.ymthe.2021.03.013.

[131] Z. Yang, J. Zhang, Y. Wang, J. Lu, Q. Sun, Caveolin-1 Deficiency Protects Mice Against Carbon Tetrachloride-Induced Acute Liver Injury Through Regulating Polarization of Hepatic Macrophages, Front. Immunol. 12 (2021) 713808. https://doi.org/10.3389/fimmu.2021.713808.

[132] X. Jiang, S. Wu, C. Hu, A narrative review of the role of exosomes and caveolin-1 in liver diseases and cancer, International

Immunopharmacology 120 (2023) 110284. https://doi.org/10.1016/j.intimp.2023.110284.

[133] S. Raja, S. Shah, A. Tariq, N. Bibi, K. Sughra, A. Yousuf, A. Khawaja, M. Nawaz, A. Mehmood, M. Khan, A. Hussain, Caveolin-1 and dynamin-2 overexpression is associated with the progression of bladder cancer, Oncol Lett (2019). https://doi.org/10.3892/ol.2019.10310.

[134] Z. Yang, J. Zhang, Y. Wang, J. Lu, Q. Sun, Caveolin-1 Deficiency Protects Mice Against Carbon Tetrachloride-Induced Acute Liver Injury Through Regulating Polarization of Hepatic Macrophages, Front. Immunol. 12 (2021) 713808. https://doi.org/10.3389/fimmu.2021.713808.

[135] P. Shivshankar, G.V. Halade, C. Calhoun, G.P. Escobar, A.J. Mehr, F. Jimenez, C. Martinez, H. Bhatnagar, C.H. Mjaatvedt, M.L. Lindsey, C.J. Le Saux, Caveolin-1 deletion exacerbates cardiac interstitial fibrosis by promoting M2 macrophage activation in mice after myocardial infarction, Journal of Molecular and Cellular Cardiology 76 (2014) 84–93. https://doi.org/10.1016/j.yjmcc.2014.07.020.

[136] K. Liu, H. Wang, J. Zhou, S. Zhu, M. Ma, H. Xiao, Y. Ding, HMGB1 in exosomes derived from gastric cancer cells induces M2-like macrophage polarization by inhibiting the NF-κB signaling pathway, Cell Biology International 48 (2024) 334–346. https://doi.org/10.1002/cbin.12110.

[137] H. Yang, H. Wang, U. Andersson, Targeting Inflammation Driven by HMGB1, Front. Immunol. 11 (2020) 484. https://doi.org/10.3389/fimmu.2020.00484.

[138] D. Tang, R. Kang, H.J. Zeh III, M.T. Lotze, High-mobility group box 1 and cancer, Biochimica et Biophysica Acta (BBA) - Gene Regulatory Mechanisms 1799 (2010) 131–140. https://doi.org/10.1016/j.bbagrm.2009.11.014.

[139] H. Fan, H.-B. Tang, Z. Chen, H.-Q. Wang, L. Zhang, Y. Jiang, T. Li, C.-F. Yang, X.-Y. Wang, X. Li, S.-X. Wu, G.-L. Zhang, Inhibiting HMGB1-RAGE axis prevents pro-inflammatory macrophages/microglia polarization and affords neuroprotection after spinal cord injury, J Neuroinflammation 17 (2020) 295. https://doi.org/10.1186/s12974-020-01973-4.

[140] Q. Yue, Y. Song, Z. Liu, L. Zhang, L. Yang, J. Li, Receptor for Advanced Glycation End Products (RAGE): A Pivotal Hub in Immune Diseases, Molecules 27 (2022) 4922. https://doi.org/10.3390/molecules27154922.

[141] S. Ahmad, M.Y. Khan, Z. Rafi, H. Khan, Z. Siddiqui, S. Rehman, U. Shahab, M.S. Khan, M. Saeed, S. Alouffi, M.S. Khan, Oxidation, glycation and glycoxidation—The vicious cycle and lung cancer, Seminars in Cancer Biology 49 (2018) 29–36. https://doi.org/10.1016/j.semcancer.2017.10.005.

[142] Q. Yue, Y. Song, Z. Liu, L. Zhang, L. Yang, J. Li, Receptor for Advanced Glycation End Products (RAGE): A Pivotal Hub in Immune Diseases, Molecules 27 (2022) 4922. https://doi.org/10.3390/molecules27154922.

[143] K. Liu, H. Wang, J. Zhou, S. Zhu, M. Ma, H. Xiao, Y. Ding, HMGB1 in exosomes derived from gastric cancer cells induces M2-like macrophage polarization by inhibiting the NF-κB signaling pathway, Cell Biology International 48 (2024) 334–346. https://doi.org/10.1002/cbin.12110.

[144] D.L. Galson, G.D. Roodman, Origins of Osteoclasts, in: Osteoimmunology, Elsevier, 2011: pp. 7–41. https://doi.org/10.1016/B978-0-12-375670-1.10002-0.

[145] K. Nakamura, K. Sawada, Y. Kinose, A. Yoshimura, A. Toda, E. Nakatsuka, K. Hashimoto, S. Mabuchi, K. Morishige, H. Kurachi, E. Lengyel, T. Kimura, Exosomes Promote Ovarian Cancer Cell Invasion through Transfer of CD44 to Peritoneal Mesothelial Cells, Molecular Cancer Research 15 (2017) 78–92. https://doi.org/10.1158/1541-7786.MCR-16-0191.

[146] R. Szatanek, M. Baj-Krzyworzeka, CD44 and Tumor-Derived Extracellular Vesicles (TEVs). Possible Gateway to Cancer Metastasis, IJMS 22 (2021) 1463. https://doi.org/10.3390/ijms22031463.

[147] X. Wang, K. Cheng, G. Zhang, Z. Jia, Y. Yu, J. Guo, Y. Hua, F. Guo, X. Li, W. Zou, H. Sun, J. Dong, Z. Yang, Enrichment of CD44 in Exosomes From Breast Cancer Cells Treated With Doxorubicin Promotes Chemoresistance, Front. Oncol. 10 (2020) 960. https://doi.org/10.3389/fonc.2020.00960.

[148] Y. He, C. Xue, Y. Yu, J. Chen, X. Chen, F. Ren, Z. Ren, G. Cui, R. Sun, CD44 is overexpressed and correlated with tumor progression in gallbladder cancer, CMAR Volume 10 (2018) 3857–3865. https://doi.org/10.2147/CMAR.S175681.

[149] Z. Pan, Y. Zhao, S. Zhou, J. Wang, F. Fan, CD44 Drives M1 Macrophage Polarization in Diabetic Retinopathy, Current Eye Research 48 (2023) 770–780. https://doi.org/10.1080/02713683.2023.2210273.

[150] Y. Xiao, K. Yang, Z. Wang, M. Zhao, Y. Deng, W. Ji, Y. Zou, C. Qian, Y. Liu, H. Xiao, H. Liu, CD44-Mediated Poor Prognosis in Glioma Is Associated With M2-Polarization of Tumor-Associated Macrophages and Immunosuppression, Front. Surg. 8 (2022) 775194. https://doi.org/10.3389/fsurg.2021.775194.

[151] T. Yan, K. Wang, J. Li, H. Hu, H. Yang, M. Cai, R. Liu, H. Li, N. Wang, Y. Shi, W. Hua, H. Liu, Suppression of the hyaluronic acid pathway

induces M1 macrophages polarization via STAT1 in glioblastoma, Cell Death Discov. 8 (2022) 193. https://doi.org/10.1038/s41420-022-00973-y.

[152] A.R. Soares, T. Martins-Marques, T. Ribeiro-Rodrigues, J.V. Ferreira, S. Catarino, M.J. Pinho, M. Zuzarte, S. Isabel Anjo, B. Manadas, J. P.G. Sluijter, P. Pereira, H. Girao, Gap junctional protein Cx43 is involved in the communication between extracellular vesicles and mammalian cells, Sci Rep 5 (2015) 13243. https://doi.org/10.1038/srep13243.

[153] P. He, M. Dai, Z. Li, X. Wang, H. Liu, Y. He, H. Jiang, Effect of connexin 43 in LPS/IL-4-induced macrophage M1/M2 polarization: An observational study, Medicine 103 (2024) e37811. https://doi.org/10.1097/MD.0000000000037811.

[154] Z. Wu, Y. Wu, M. Wang, D. Chen, J. Lv, J. Yan, D. Zhou, Y. Pang, H. Liang, D. Zhang, H. Li, Y. Wei, C. Xu, FAP-activated liposomes achieved specific macropinocytosis uptake by pancreatic stellate cells for efficient desmoplasia reversal, Chemical Engineering Journal 495 (2024) 153369. https://doi.org/10.1016/j.cej.2024.153369.

[155] J. Yan, M. Wang, S. Lv, D. Chen, Z. Wu, D. Zhou, S. Zhang, J. Lv, K. Xu, C. Xu, Y. Wei, SiATG5-loaded cancer cell membrane-fused liposomes induced increased uptake of albumin-bound chemotherapeutics by pancreatic cancer cells, Journal of Controlled Release 367 (2024) 620–636. https://doi.org/10.1016/j.jconrel.2024.01.055.

[156] K. Liu, L. Kong, H. Cui, L. Zhang, Q. Xin, Y. Zhuang, C. Guo, Y. Yao, J. Tao, X. Gu, C. Jiang, J. Wu, Thymosin α1 reverses oncolytic adenovirus-induced M2 polarization of macrophages to improve antitumor immunity and therapeutic efficacy, Cell Reports Medicine 5 (2024) 101751. https://doi.org/10.1016/j.xcrm.2024.101751.

[157] W.R. Francis, Z. Liu, S.E. Owens, X. Wang, H. Xue, A. Lord, V. Kanamarlapudi, Z. Xia, Role of hypoxia inducible factor 1α in cobalt nanoparticle induced cytotoxicity of human THP-1 macrophages, Biomater Transl 2 (2021) 143–150. https://doi.org/10.12336/biomatertransl.2021.02.004.

[158] K. Wadhonkar, S. Das, R. Subramanian, M.H. Sk, Y. Singh, M.S. Baig, The effect of cancer cell-derived exosomal proteins on macrophage polarization: An in-depth review, Experimental Cell Research 444 (2025) 114393. https://doi.org/10.1016/j.yexcr.2024.114393.

[159] T. Hirata, Y. Kizuka, N-Glycosylation, in: G. Lauc, I. Trbojević-Akmačić (Eds.), The Role of Glycosylation in Health and Disease, Springer International Publishing, Cham, 2021: pp. 3–24. https://doi.org/10.1007/978-3-030-70115-4_1.

[160] G. Bandini, A. Albuquerque-Wendt, J. Hegermann, J. Samuelson, F.H. Routier, Protein *O* - and *C* -Glycosylation pathways in *Toxoplasma gondii* and *Plasmodium falciparum*, Parasitology 146 (2019) 1755–1766. https://doi.org/10.1017/S0031182019000040.

[161] J. Eichler, Protein glycosylation, Current Biology 29 (2019) R229–R231. https://doi.org/10.1016/j.cub.2019.01.003.

[162] K.T. Schjoldager, Y. Narimatsu, H.J. Joshi, H. Clausen, Global view of human protein glycosylation pathways and functions, Nat Rev Mol Cell Biol 21 (2020) 729–749. https://doi.org/10.1038/s41580-020-00294-x.

[163] A. Pace, F. Scirocchi, C. Napoletano, I.G. Zizzari, L. D'Angelo, A. Santoro, M. Nuti, H. Rahimi, A. Rughetti, Glycan-Lectin Interactions as Novel Immunosuppression Drivers in Glioblastoma, IJMS 23 (2022) 6312. https://doi.org/10.3390/ijms23116312.

[164] S.A. Dusoswa, S.K. Horrevorts, M. Ambrosini, H. Kalay, N.J. Paauw, R. Nieuwland, M.D. Pegtel, T. Würdinger, Y. Van Kooyk, J.J.

Garcia-Vallejo, Glycan modification of glioblastoma-derived extracellular vesicles enhances receptor-mediated targeting of dendritic cells, J of Extracellular Vesicle 8 (2019) 1648995. https://doi.org/10.1080/20013078.2019.1648995.

[165] Á.M. Martins, C.C. Ramos, D. Freitas, C.A. Reis, Glycosylation of Cancer Extracellular Vesicles: Capture Strategies, Functional Roles and Potential Clinical Applications, Cells 10 (2021) 109. https://doi.org/10.3390/cells10010109.

[166] L. Wu, C. Gao, Comprehensive Overview the Role of Glycosylation of Extracellular Vesicles in Cancers, ACS Omega 8 (2023) 47380–47392. https://doi.org/10.1021/acsomega.3c07441.

[167] S. Lin, S. Zhou, T. Yuan, The "sugar-coated bullets" of cancer: Tumor-derived exosome surface glycosylation from basic knowledge to applications, Clin Transl Med 10 (2020) e204. https://doi.org/10.1002/ctm2.204.

[168] O. Moreno-Gonzalo, C. Villarroya-Beltri, F. Sánchez-Madrid, Post-translational modifications of exosomal proteins, Front Immunol 5 (2014) 383. https://doi.org/10.3389/fimmu.2014.00383.

[169] H. Wei, Q. Chen, L. Lin, C. Sha, T. Li, Y. Liu, X. Yin, Y. Xu, L. Chen, W. Gao, Y. Li, X. Zhu, Regulation of exosome production and cargo sorting, Int J Biol Sci 17 (2021) 163–177. https://doi.org/10.7150/ijbs.53671.

[170] Z. Andreu, M. Yáñez-Mó, Tetraspanins in extracellular vesicle formation and function, Front Immunol 5 (2014) 442. https://doi.org/10.3389/fimmu.2014.00442.

[171] S. Gordon, A. Plüddemann, S. Mukhopadhyay, Plasma membrane receptors of tissue macrophages: functions and role in pathology, The

Journal of Pathology 250 (2020) 656–666. https://doi.org/10.1002/path.5404.

[172] C. Reis e Sousa, S. Yamasaki, G.D. Brown, Myeloid C-type lectin receptors in innate immune recognition, Immunity 57 (2024) 700–717. https://doi.org/10.1016/j.immuni.2024.03.005.

[173] Y. Van Kooyk, G.A. Rabinovich, Protein-glycan interactions in the control of innate and adaptive immune responses, Nat Immunol 9 (2008) 593–601. https://doi.org/10.1038/ni.f.203.

[174] N.R. Mantuano, M.C. Oliveira-Nunes, F. Alisson-Silva, W.B. Dias, A.R. Todeschini, Emerging role of glycosylation in the polarization of tumor-associated macrophages, Pharmacological Research 146 (2019) 104285. https://doi.org/10.1016/j.phrs.2019.104285.

[175] A. Peixoto, M. Relvas-Santos, R. Azevedo, L.L. Santos, J.A. Ferreira, Protein Glycosylation and Tumor Microenvironment Alterations Driving Cancer Hallmarks, Front. Oncol. 9 (2019) 380. https://doi.org/10.3389/fonc.2019.00380.

[176] X. He, B. Wang, W. Deng, J. Cao, Z. Tan, X. Li, F. Guan, Impaired bisecting GlcNAc reprogrammed M1 polarization of macrophage, Cell Commun Signal 22 (2024) 73. https://doi.org/10.1186/s12964-023-01432-6.

[177] K. Wadhonkar, N. Singh, F.M. Heralde, S.P. Parihar, N. Hirani, M.S. Baig, Exosome-derived miRNAs regulate macrophage-colorectal cancer cell cross-talk during aggressive tumor development, Colorect. Cancer 12 (2023) CRC40. https://doi.org/10.2217/crc-2022-0012.

[178] T. Su, P. Zhang, F. Zhao, S. Zhang, Exosomal MicroRNAs Mediating Crosstalk Between Cancer Cells With Cancer-Associated Fibroblasts and Tumor-Associated Macrophages in the Tumor

Microenvironment, Front. Oncol. 11 (2021) 631703. https://doi.org/10.3389/fonc.2021.631703.

[179] M. Guo, H. Zhang, J. Zheng, Y. Liu, Glypican-3: A New Target for Diagnosis and Treatment of Hepatocellular Carcinoma, J. Cancer 11 (2020) 2008–2021. https://doi.org/10.7150/jca.39972.

[180] Y. Aydin, A.R. Koksal, P. Thevenot, S. Chava, Z. Heidari, D. Lin, T. Sandow, K. Moroz, M.A. Parsi, J. Scott, A. Cohen, S. Dash, Experimental Validation of Novel Glypican 3 Exosomes for the Detection of Hepatocellular Carcinoma in Liver Cirrhosis, JHC Volume 8 (2021) 1579–1596. https://doi.org/10.2147/JHC.S327339.

[181] T. Nishida, H. Kataoka, Glypican 3-Targeted Therapy in Hepatocellular Carcinoma, Cancers 11 (2019) 1339. https://doi.org/10.3390/cancers11091339.

[182] Z.-W. Zhu, Enhanced glypican-3 expression differentiates the majority of hepatocellular carcinomas from benign hepatic disorders, Gut 48 (2001) 558–564. https://doi.org/10.1136/gut.48.4.558.

[183] Q. Lin, L. Xiong, X. Pan, J. Gen, G. Bao, H. Sha, J. Feng, C. Ji, M. Chen, Expression of GPC3 protein and its significance in lung squamous cell carcinoma, Med Oncol 29 (2012) 663–669. https://doi.org/10.1007/s12032-011-9973-1.

[184] T. Ushiku, H. Uozaki, A. Shinozaki, S. Ota, K. Matsuzaka, S. Nomura, M. Kaminishi, H. Aburatani, T. Kodama, M. Fukayama, Glypican 3-expressing gastric carcinoma: Distinct subgroup unifying hepatoid, clear-cell, and α-fetoprotein-producing gastric carcinomas, Cancer Science 100 (2009) 626–632. https://doi.org/10.1111/j.1349-7006.2009.01108.x.

[185] D. Maeda, S. Ota, Y. Takazawa, H. Aburatani, S. Nakagawa, T. Yano, Y. Taketani, T. Kodama, M. Fukayama, Glypican-3 expression in

clear cell adenocarcinoma of the ovary, Modern Pathology 22 (2009) 824–832. https://doi.org/10.1038/modpathol.2009.40.

[186] T. Nakatsura, Y. Nishimura, Usefulness of the Novel Oncofetal Antigen Glypican-3 for Diagnosis of Hepatocellular Carcinoma and Melanoma:, BioDrugs 19 (2005) 71–77. https://doi.org/10.2165/00063030-200519020-00001.

[187] H. Takai, M. Ashihara, T. Ishiguro, H. Terashima, T. Watanabe, A. Kato, M. Suzuki, Involvement of glypican-3 in the recruitment of M2-polarized tumor-associated macrophages in hepatocellular carcinoma, Cancer Biology & Therapy 8 (2009) 2329–2338. https://doi.org/10.4161/cbt.8.24.9985.

[188] F. Takahashi-Yanaga, M. Kahn, Targeting Wnt Signaling: Can We Safely Eradicate Cancer Stem Cells?, Clinical Cancer Research 16 (2010) 3153–3162. https://doi.org/10.1158/1078-0432.CCR-09-2943.

[189] W. Gao, M. Ho, The role of glypican-3 in regulating Wnt in hepatocellular carcinomas, Cancer Rep 1 (2011) 14–19.

[190] P. Song, Z. Gao, Y. Bao, L. Chen, Y. Huang, Y. Liu, Q. Dong, X. Wei, Wnt/β-catenin signaling pathway in carcinogenesis and cancer therapy, J Hematol Oncol 17 (2024) 46. https://doi.org/10.1186/s13045-024-01563-4.

[191] M.E. Durkin, S. Chakravarti, B.B. Bartos, S.H. Liu, R.L. Friedman, A.E. Chung, Amino acid sequence and domain structure of entactin. Homology with epidermal growth factor precursor and low density lipoprotein receptor., The Journal of Cell Biology 107 (1988) 2749–2756. https://doi.org/10.1083/jcb.107.6.2749.

[192] X. Mao, S.K. Tey, C.L.S. Yeung, E.M.L. Kwong, Y.M.E. Fung, C.Y.S. Chung, L. Mak, D.K.H. Wong, M. Yuen, J.C.M. Ho, H. Pang, M.P. Wong, C.O. Leung, T.K.W. Lee, V. Ma, W.C. Cho, P. Cao, X. Xu, Y. Gao,

J.W.P. Yam, Nidogen 1-Enriched Extracellular Vesicles Facilitate Extrahepatic Metastasis of Liver Cancer by Activating Pulmonary Fibroblasts to Secrete Tumor Necrosis Factor Receptor 1, Advanced Science 7 (2020) 2002157. https://doi.org/10.1002/advs.202002157.

[193] S. Syeda, K. Rawat, A. Shrivastava, Exosome Load Increases Systemically and Mediates Pro-tumoral M2 Macrophage Polarization in Lymphoma, (2023). https://doi.org/10.20944/preprints202304.0062.v1.

[194] A. Zbinden, S.L. Layland, M. Urbanczyk, D.A. Carvajal Berrio, J. Marzi, M. Zauner, A. Hammerschmidt, E.M. Brauchle, K. Sudrow, S. Fink, M. Templin, S. Liebscher, G. Klein, A. Deb, G.P. Duffy, G.M. Crooks, J.A. Eble, H.K.A. Mikkola, A. Nsair, M. Seifert, K. Schenke-Layland, Nidogen-1 Mitigates Ischemia and Promotes Tissue Survival and Regeneration, Advanced Science 8 (2021) 2002500. https://doi.org/10.1002/advs.202002500.

[195] Y. Zhou, Y. Zhu, X. Fan, C. Zhang, Y. Wang, L. Zhang, H. Zhang, T. Wen, K. Zhang, X. Huo, X. Jiang, Y. Bu, Y. Zhang, NID1, a new regulator of EMT required for metastasis and chemoresistance of ovarian cancer cells, Oncotarget 8 (2017) 33110–33121. https://doi.org/10.18632/oncotarget.16145.

[196] Y. Guo, W. Pan, S. Liu, Z. Shen, Y. Xu, L. Hu, ERK/MAPK signalling pathway and tumorigenesis (Review), Exp Ther Med (2020). https://doi.org/10.3892/etm.2020.8454.

[197] J.A. Jazayeri, A. Upadhyay, A.B. Vernallis, G.J. Carroll, Targeting the Glycoprotein 130 Receptor Subunit to Control Pain and Inflammation, Journal of Interferon & Cytokine Research 30 (2010) 865–873. https://doi.org/10.1089/jir.2010.0035.

[198] S. Ham, L.G. Lima, E.P.Z. Chai, A. Muller, R.J. Lobb, S. Krumeich, S.W. Wen, A.P. Wiegmans, A. Möller, Breast Cancer-Derived Exosomes

Alter Macrophage Polarization via gp130/STAT3 Signaling, Front. Immunol. 9 (2018) 871. https://doi.org/10.3389/fimmu.2018.00871.

[199] P. Arnold, W. Lückstädt, W. Li, I. Boll, J. Lokau, C. Garbers, R. Lucius, S. Rose-John, C. Becker-Pauly, Joint Reconstituted Signaling of the IL-6 Receptor via Extracellular Vesicles, Cells 9 (2020) 1307. https://doi.org/10.3390/cells9051307.

[200] D.T. Martin, H. Shen, J.M. Steinbach-Rankins, X. Zhu, K.K. Johnson, J. Syed, W.M. Saltzman, R.M. Weiss, Glycoprotein-130 Expression Is Associated with Aggressive Bladder Cancer and Is a Potential Therapeutic Target, Molecular Cancer Therapeutics 18 (2019) 413–420. https://doi.org/10.1158/1535-7163.MCT-17-1079.

[201] I. Pozios, N.A. Hering, E. Guenzler, M. Arndt, S. Elezkurtaj, T. Knösel, C.J. Bruns, G.A. Margonis, K. Beyer, H. Seeliger, Gp130 is expressed in pancreatic cancer and can be targeted by the small inhibitor molecule SC144, J Cancer Res Clin Oncol 149 (2023) 271–280. https://doi.org/10.1007/s00432-022-04518-9.

[202] E. Chekol Abebe, Z. Tilahun Muche, A. Behaile T/Mariam, T. Mengie Ayele, M. Mekonnen Agidew, M. Teshome Azezew, E. Abebe Zewde, T. Asmamaw Dejenie, M. Asmamaw Mengstie, The structure, biosynthesis, and biological roles of fetuin-A: A review, Front. Cell Dev. Biol. 10 (2022) 945287. https://doi.org/10.3389/fcell.2022.945287.

[203] L. Stone, Fetuin-A—a marker for metastatic disease?, Nat Rev Urol 12 (2015) 178–178. https://doi.org/10.1038/nrurol.2015.34.

[204] P. Chatterjee, S. Seal, S. Mukherjee, R. Kundu, S. Mukherjee, S. Ray, S. Mukhopadhyay, S.S. Majumdar, S. Bhattacharya, Adipocyte Fetuin-A Contributes to Macrophage Migration into Adipose Tissue and Polarization of Macrophages, Journal of Biological Chemistry 288 (2013) 28324–28330. https://doi.org/10.1074/jbc.C113.495473.

[205] A.K. Hubbard, R. Rothlein, Intercellular adhesion molecule-1 (ICAM-1) expression and cell signaling cascades, Free Radical Biology and Medicine 28 (2000) 1379–1386. https://doi.org/10.1016/S0891-5849(00)00223-9.

[206] A. Benedicto, I. Romayor, B. Arteta, Role of liver ICAM-1 in metastasis, Oncology Letters 14 (2017) 3883–3892. https://doi.org/10.3892/ol.2017.6700.

[207] N. Allende-Vega, J. Marco Brualla, P. Falvo, C. Alexia, M. Constantinides, A.F. de Maudave, L. Coenon, D. Gitenay, G. Mitola, P. Massa, S. Orecchioni, F. Bertolini, I. Marzo, A. Anel, M. Villalba, Metformin sensitizes leukemic cells to cytotoxic lymphocytes by increasing expression of intercellular adhesion molecule-1 (ICAM-1), Sci Rep 12 (2022) 1341. https://doi.org/10.1038/s41598-022-05470-x.

[208] Q. Zhou, J. Xu, Y. Xu, S. Sun, J. Chen, Role of ICAM1 in tumor immunity and prognosis of triple-negative breast cancer, Front. Immunol. 14 (2023) 1176647. https://doi.org/10.3389/fimmu.2023.1176647.

[209] M. Yang, J. Liu, C. Piao, J. Shao, J. Du, ICAM-1 suppresses tumor metastasis by inhibiting macrophage M2 polarization through blockade of efferocytosis, Cell Death Dis 6 (2015) e1780–e1780. https://doi.org/10.1038/cddis.2015.144.

[210] A. Hamaï, F. Meslin, H. Benlalam, A. Jalil, M. Mehrpour, F. Faure, Y. Lecluse, P. Vielh, M.-F. Avril, C. Robert, S. Chouaib, ICAM-1 Has a Critical Role in the Regulation of Metastatic Melanoma Tumor Susceptibility to CTL Lysis by Interfering with PI3K/AKT Pathway, Cancer Research 68 (2008) 9854–9864. https://doi.org/10.1158/0008-5472.CAN-08-0719.

[211] T. Reed, J. Schorey, C. D'Souza-Schorey, Tumor-Derived Extracellular Vesicles: A Means of Co-opting Macrophage Polarization in

the Tumor Microenvironment, Front. Cell Dev. Biol. 9 (2021) 746432. https://doi.org/10.3389/fcell.2021.746432.

[212] S.S. Iyer, G. Cheng, Role of Interleukin 10 Transcriptional Regulation in Inflammation and Autoimmune Disease, Crit Rev Immunol 32 (2012) 23–63. https://doi.org/10.1615/CritRevImmunol.v32.i1.30.

[213] R. Kühn, J. Löhler, D. Rennick, K. Rajewsky, W. Müller, Interleukin-10-deficient mice develop chronic enterocolitis, Cell 75 (1993) 263–274. https://doi.org/10.1016/0092-8674(93)80068-P.

[214] M.T. Bejarano, M.G. Masucci, Interleukin-10 Abrogates the Inhibition of Epstein-Barr Virus–Induced B-Cell Transformation by Memory T-Cell Responses, Blood 92 (1998) 4256–4262. https://doi.org/10.1182/blood.V92.11.4256.

[215] J. Zhou, F. Ye, H. Chen, W. Lv, N. Gan, The Expression of Interleukin-10 in Patients with Primary Ovarian Epithelial Carcinoma and in Ovarian Carcinoma Cell Lines, J Int Med Res 35 (2007) 290–300. https://doi.org/10.1177/147323000703500302.

[216] S.I. Yoon, N.J. Logsdon, F. Sheikh, R.P. Donnelly, M.R. Walter, Conformational Changes Mediate Interleukin-10 Receptor 2 (IL-10R2) Binding to IL-10 and Assembly of the Signaling Complex, Journal of Biological Chemistry 281 (2006) 35088–35096. https://doi.org/10.1074/jbc.M606791200.

[217] K.C. El Kasmi, A.M. Smith, L. Williams, G. Neale, A. Panopolous, S.S. Watowich, H. Häcker, B.M.J. Foxwell, P.J. Murray, Cutting Edge: A Transcriptional Repressor and Corepressor Induced by the STAT3-Regulated Anti-Inflammatory Signaling Pathway, The Journal of Immunology 179 (2007) 7215–7219. https://doi.org/10.4049/jimmunol.179.11.7215.

[218] R. Azevedo, C. Gaiteiro, A. Peixoto, M. Relvas-Santos, L. Lima, L.L. Santos, J.A. Ferreira, CD44 glycoprotein in cancer: a molecular conundrum hampering clinical applications, Clin Proteom 15 (2018) 22. https://doi.org/10.1186/s12014-018-9198-9.

[219] M. Mishra, V. Chandavarkar, R. Sharma, D. Bhargava, Structure, function and role of CD44 in neoplasia, J Oral Maxillofac Pathol 23 (2019) 267. https://doi.org/10.4103/jomfp.JOMFP_246_18.

[220] W. Mu, Y. Xu, P. Gu, W. Wang, J. Li, Y. Ge, H. Wang, Exosomal CD44 Cooperates with Integrin α6β4 to Support Organotropic Metastasis via Regulating Tumor Cell Motility and Target Host Cell Activation, Engineering 7 (2021) 1413–1423. https://doi.org/10.1016/j.eng.2020.08.013.

[221] S. Liu, Z. Liu, A. Shang, J. Xun, Z. Lv, S. Zhou, C. Liu, Q. Zhang, Y. Yang, CD44 is a potential immunotherapeutic target and affects macrophage infiltration leading to poor prognosis, Sci Rep 13 (2023) 9657. https://doi.org/10.1038/s41598-023-33915-4.

[222] T. Yan, K. Wang, J. Li, H. Hu, H. Yang, M. Cai, R. Liu, H. Li, N. Wang, Y. Shi, W. Hua, H. Liu, Suppression of the hyaluronic acid pathway induces M1 macrophages polarization via STAT1 in glioblastoma, Cell Death Discov. 8 (2022) 193. https://doi.org/10.1038/s41420-022-00973-y.

[223] M.E.W. Logtenberg, F.A. Scheeren, T.N. Schumacher, The CD47-SIRPα Immune Checkpoint, Immunity 52 (2020) 742–752. https://doi.org/10.1016/j.immuni.2020.04.011.

[224] T. Muramatsu, Basigin (CD147), a multifunctional transmembrane glycoprotein with various binding partners, J Biochem 159 (2016) 481–490. https://doi.org/10.1093/jb/mvv127.

[225] C. Gu, A. Shang, G. Liu, J. Zhu, W. Zhang, L. Jin, Z. Sun, D. Li, Identification of CD147-positive extracellular vesicles as novel non-

invasive biomarkers for the diagnosis and prognosis of colorectal cancer, Clinica Chimica Acta 548 (2023) 117510. https://doi.org/10.1016/j.cca.2023.117510.

[226] A. Landras, C. Reger de Moura, F. Jouenne, C. Lebbe, S. Menashi, S. Mourah, CD147 Is a Promising Target of Tumor Progression and a Prognostic Biomarker, Cancers 11 (2019) 1803. https://doi.org/10.3390/cancers11111803.

[227] J.-J. Lv, H. Wang, C. Zhang, T.-J. Zhang, H.-L. Wei, Z.-K. Liu, Y.-H. Ma, Z. Yang, Q. He, L.-J. Wang, L.-L. Duan, Z.-N. Chen, H. Bian, CD147 Sparks Atherosclerosis by Driving M1 Phenotype and Impairing Efferocytosis, Circulation Research 134 (2024) 165–185. https://doi.org/10.1161/CIRCRESAHA.123.323223.

[228] J.-Y. Kim, W.-J. Kim, H. Kim, K. Suk, W.-H. Lee, The Stimulation of CD147 Induces MMP-9 Expression through ERK and NF-κB in Macrophages: Implication for Atherosclerosis, Immune Netw 9 (2009) 90. https://doi.org/10.4110/in.2009.9.3.90.

[229] F. Li, J. Wang, Y. Yan, C. Bai, J. Guo, CD147 promotes breast cancer migration and invasion by inducing epithelial-mesenchymal transition via the MAPK/ERK signaling pathway, BMC Cancer 23 (2023) 1214. https://doi.org/10.1186/s12885-023-11724-2.

[230] N. Tominaga, K. Hagiwara, N. Kosaka, K. Honma, H. Nakagama, T. Ochiya, RPN2-mediated glycosylation of tetraspanin CD63 regulates breast cancer cell malignancy, Mol Cancer 13 (2014) 134. https://doi.org/10.1186/1476-4598-13-134.

[231] Tetraspanin CD63 independently predicts poor prognosis in colorectal cancer, Histol Histopathol 35 (2020) 887–892. https://doi.org/10.14670/HH-18-209.

[232] Y. Miki, M. Yashiro, T. Okuno, K. Kuroda, S. Togano, K. Hirakawa, M. Ohira, Clinico-pathological significance of exosome marker CD63 expression on cancer cells and stromal cells in gastric cancer, PLoS ONE 13 (2018) e0202956. https://doi.org/10.1371/journal.pone.0202956.

[233] P. Lewitowicz, J. Matykiewicz, D. Koziel, M. Chrapek, A. Horecka-Lewitowicz, S. Gluszek, CD63 and GLUT-1 Overexpression Could Predict a Poor Clinical Outcome in GIST: A Study of 54 Cases with Follow-Up, Gastroenterology Research and Practice 2016 (2016) 1–8. https://doi.org/10.1155/2016/6478374.

[234] J.S. Isenberg, D.D. Roberts, THBS1 (thrombospondin-1), Atlas of Genetics and Cytogenetics in Oncology and Haematology (2020). https://doi.org/10.4267/2042/70774.

[235] S. Kaur, D.D. Roberts, Emerging functions of thrombospondin-1 in immunity, Seminars in Cell & Developmental Biology 155 (2024) 22–31. https://doi.org/10.1016/j.semcdb.2023.05.008.

[236] M. Xiao, J. Zhang, W. Chen, W. Chen, M1-like tumor-associated macrophages activated by exosome-transferred THBS1 promote malignant migration in oral squamous cell carcinoma, J Exp Clin Cancer Res 37 (2018) 143. https://doi.org/10.1186/s13046-018-0815-2.

[237] X. Wang, L. Tian, J. Lu, I.O.-L. Ng, Exosomes and cancer - Diagnostic and prognostic biomarkers and therapeutic vehicle, Oncogenesis 11 (2022) 54. https://doi.org/10.1038/s41389-022-00431-5.

[238] K. Matsusaka, Y. Fujiwara, C. Pan, S. Esumi, Y. Saito, J. Bi, Y. Nakamura, A. Mukunoki, T. Takeo, N. Nakagata, D. Yoshii, R. Fukuda, T. Nagasaki, R. Tanaka, H. Komori, H. Maeda, H. Watanabe, K. Tamada, Y. Komohara, T. Maruyama, α1-Acid Glycoprotein Enhances the Immunosuppressive and Protumor Functions of Tumor-Associated

Macrophages, Cancer Research 81 (2021) 4545–4559. https://doi.org/10.1158/0008-5472.CAN-20-3471.

[239] S. Xu, C. Wang, L. Yang, J. Wu, M. Li, P. Xiao, Z. Xu, Y. Xu, K. Wang, Targeting immune checkpoints on tumor-associated macrophages in tumor immunotherapy, Front. Immunol. 14 (2023) 1199631. https://doi.org/10.3389/fimmu.2023.1199631.

[240] E. Sonkoly, A. Pivarcsi, microRNAs in Inflammation, International Reviews of Immunology 28 (2009) 535–561. https://doi.org/10.3109/08830180903208303.

[241] G. Mahesh, R. Biswas, MicroRNA-155: A Master Regulator of Inflammation, Journal of Interferon & Cytokine Research 39 (2019) 321–330. https://doi.org/10.1089/jir.2018.0155.

[242] A. Tahamtan, M. Teymoori-Rad, B. Nakstad, V. Salimi, Anti-Inflammatory MicroRNAs and Their Potential for Inflammatory Diseases Treatment, Front. Immunol. 9 (2018) 1377. https://doi.org/10.3389/fimmu.2018.01377.

[243] J. Van Scheppingen, J.D. Mills, T.S. Zimmer, D.W.M. Broekaart, V. Iori, A. Bongaarts, J.J. Anink, A.M. Iyer, A. Korotkov, F.E. Jansen, W. Van Hecke, W.G. Spliet, P.C. Van Rijen, J.C. Baayen, A. Vezzani, E.A. Van Vliet, E. Aronica, mi R 147b: A novel key regulator of interleukin 1 beta-mediated inflammation in human astrocytes, Glia 66 (2018) 1082–1097. https://doi.org/10.1002/glia.23302.

[244] C.E. Arnold, C.S. Whyte, P. Gordon, R.N. Barker, A.J. Rees, H.M. Wilson, A critical role for suppressor of cytokine signalling 3 in promoting M 1 macrophage activation and function *in vitro* and *in vivo*, Immunology 141 (2014) 96–110. https://doi.org/10.1111/imm.12173.

[245] A. Villagra, F. Cheng, H.-W. Wang, I. Suarez, M. Glozak, M. Maurin, D. Nguyen, K.L. Wright, P.W. Atadja, K. Bhalla, J. Pinilla-Ibarz,

E. Seto, E.M. Sotomayor, The histone deacetylase HDAC11 regulates the expression of interleukin 10 and immune tolerance, Nat Immunol 10 (2009) 92–100. https://doi.org/10.1038/ni.1673.

[246] L. Lin, J. Hou, F. Ma, P. Wang, X. Liu, N. Li, J. Wang, Q. Wang, X. Cao, Type I IFN Inhibits Innate IL-10 Production in Macrophages through Histone Deacetylase 11 by Downregulating MicroRNA-145, The Journal of Immunology 191 (2013) 3896–3904. https://doi.org/10.4049/jimmunol.1203450.

[247] D. Wang, X. Wang, M. Si, J. Yang, S. Sun, H. Wu, S. Cui, X. Qu, X. Yu, Exosome-encapsulated miRNAs contribute to CXCL12/CXCR4-induced liver metastasis of colorectal cancer by enhancing M2 polarization of macrophages, Cancer Letters 474 (2020) 36–52. https://doi.org/10.1016/j.canlet.2020.01.005.

[248] Y. Takano, T. Masuda, H. Iinuma, R. Yamaguchi, K. Sato, T. Tobo, H. Hirata, Y. Kuroda, S. Nambara, N. Hayashi, T. Iguchi, S. Ito, H. Eguchi, T. Ochiya, K. Yanaga, S. Miyano, K. Mimori, Circulating exosomal microRNA-203 is associated with metastasis possibly via inducing tumor-associated macrophages in colorectal cancer, Oncotarget 8 (2017) 78598–78613. https://doi.org/10.18632/oncotarget.20009.

[249] H. Shinohara, Y. Kuranaga, M. Kumazaki, N. Sugito, Y. Yoshikawa, T. Takai, K. Taniguchi, Y. Ito, Y. Akao, Regulated Polarization of Tumor-Associated Macrophages by miR-145 via Colorectal Cancer–Derived Extracellular Vesicles, The Journal of Immunology 199 (2017) 1505–1515. https://doi.org/10.4049/jimmunol.1700167.

[250] S. Zhao, Y. Mi, B. Guan, B. Zheng, P. Wei, Y. Gu, Z. Zhang, S. Cai, Y. Xu, X. Li, X. He, X. Zhong, G. Li, Z. Chen, D. Li, Tumor-derived exosomal miR-934 induces macrophage M2 polarization to promote liver metastasis of colorectal cancer, J Hematol Oncol 13 (2020) 156. https://doi.org/10.1186/s13045-020-00991-2.

[251] T. Cooks, I.S. Pateras, L.M. Jenkins, K.M. Patel, A.I. Robles, J. Morris, T. Forshew, E. Appella, V.G. Gorgoulis, C.C. Harris, Mutant p53 cancers reprogram macrophages to tumor supporting macrophages via exosomal miR-1246, Nat Commun 9 (2018) 771. https://doi.org/10.1038/s41467-018-03224-w.

[252] M. Qian, S. Wang, X. Guo, J. Wang, Z. Zhang, W. Qiu, X. Gao, Z. Chen, J. Xu, R. Zhao, H. Xue, G. Li, Hypoxic glioma-derived exosomes deliver microRNA-1246 to induce M2 macrophage polarization by targeting TERF2IP via the STAT3 and NF-κB pathways, Oncogene 39 (2020) 428–442. https://doi.org/10.1038/s41388-019-0996-y.

[253] W.-X. Xu, D.-D. Wang, Z.-Q. Zhao, H.-D. Zhang, S.-J. Yang, Q. Zhang, L. Li, J. Zhang, Exosomal microRNAs shuttling between tumor cells and macrophages: cellular interactions and novel therapeutic strategies, Cancer Cell Int 22 (2022) 190. https://doi.org/10.1186/s12935-022-02594-y.

[254] Y. Shao, T. Chen, X. Zheng, S. Yang, K. Xu, X. Chen, F. Xu, L. Wang, Y. Shen, T. Wang, M. Zhang, W. Hu, C. Ye, X. Yu, J. Shao, S. Zheng, Colorectal cancer-derived small extracellular vesicles establish an inflammatory premetastatic niche in liver metastasis, Carcinogenesis 39 (2018) 1368–1379. https://doi.org/10.1093/carcin/bgy115.

[255] S.A.A. Patel, N.J. Gooderham, IL6 Mediates Immune and Colorectal Cancer Cell Cross-talk *via* miR-21 and miR-29b, Molecular Cancer Research 13 (2015) 1502–1508. https://doi.org/10.1158/1541-7786.MCR-15-0147.

[256] Y. Yin, B. Liu, Y. Cao, S. Yao, Y. Liu, G. Jin, Y. Qin, Y. Chen, K. Cui, L. Zhou, Z. Bian, B. Fei, S. Huang, Z. Huang, Colorectal Cancer-Derived Small Extracellular Vesicles Promote Tumor Immune Evasion by Upregulating PD-L1 Expression in Tumor-Associated Macrophages,

Advanced Science 9 (2022) 2102620. https://doi.org/10.1002/advs.202102620.

[257] G.T. Noh, J. Kwon, J. Kim, M. Park, D.-W. Choi, K.-A. Cho, S.-Y. Woo, B.-Y. Oh, K.Y. Lee, R.-A. Lee, Verification of the role of exosomal microRNA in colorectal tumorigenesis using human colorectal cancer cell lines, PLoS ONE 15 (2020) e0242057. https://doi.org/10.1371/journal.pone.0242057.

[258] Y.-S. Ma, T.-M. Wu, C.-C. Ling, F. Yu, J. Zhang, P.-S. Cao, L.-P. Gu, H.-M. Wang, H. Xu, L. Li, Z.-J. Wu, G.-R. Wang, W. Li, Q.-L. Lin, J.-B. Liu, D. Fu, M2 macrophage-derived exosomal microRNA-155-5p promotes the immune escape of colon cancer by downregulating ZC3H12B, Molecular Therapy Oncolytics 20 (2021) 484–498. https://doi.org/10.1016/j.omto.2021.02.005.

[259] J. Lan, L. Sun, F. Xu, L. Liu, F. Hu, D. Song, Z. Hou, W. Wu, X. Luo, J. Wang, X. Yuan, J. Hu, G. Wang, M2 Macrophage-Derived Exosomes Promote Cell Migration and Invasion in Colon Cancer, Cancer Research 79 (2019) 146–158. https://doi.org/10.1158/0008-5472.CAN-18-0014.

[260] S. Zhang, D. Li, M. Zhao, F. Yang, C. Sang, C. Yan, Z. Wang, Y. Li, Exosomal miR-183-5p Shuttled by M2 Polarized Tumor-Associated Macrophage Promotes the Development of Colon Cancer via Targeting THEM4 Mediated PI3K/AKT and NF-κB Pathways, Front. Oncol. 11 (2021) 672684. https://doi.org/10.3389/fonc.2021.672684.

[261] C. Nejad, H.J. Stunden, M.P. Gantier, A guide to miRNAs in inflammation and innate immune responses, The FEBS Journal 285 (2018) 3695–3716. https://doi.org/10.1111/febs.14482.

[262] C. Villarroya-Beltri, C. Gutiérrez-Vázquez, F. Sánchez-Cabo, D. Pérez-Hernández, J. Vázquez, N. Martin-Cofreces, D.J. Martinez-Herrera,

A. Pascual-Montano, M. Mittelbrunn, F. Sánchez-Madrid, Sumoylated hnRNPA2B1 controls the sorting of miRNAs into exosomes through binding to specific motifs, Nat Commun 4 (2013) 2980. https://doi.org/10.1038/ncomms3980.

[263] R.A. Franklin, W. Liao, A. Sarkar, M.V. Kim, M.R. Bivona, K. Liu, E.G. Pamer, M.O. Li, The cellular and molecular origin of tumor-associated macrophages, Science 344 (2014) 921–925. https://doi.org/10.1126/science.1252510.

[264] A.Q. Ohandjo, Z. Liu, E.B. Dammer, C.D. Dill, T.L. Griffen, K.M. Carey, D.E. Hinton, R. Meller, J.W. Lillard, Transcriptome Network Analysis Identifies CXCL13-CXCR5 Signaling Modules in the Prostate Tumor Immune Microenvironment, Sci Rep 9 (2019) 14963. https://doi.org/10.1038/s41598-019-46491-3.

[265] W. Liu, L. Ma, J. Zhang, MicroRNA-934 promotes colorectal cancer cell proliferation by directly targeting Dickkopf-related protein 2, Exp Ther Med 22 (2021) 1041. https://doi.org/10.3892/etm.2021.10473.

[266] S. Ghafouri-Fard, T. Khoshbakht, B.M. Hussen, M. Taheri, M. Samadian, A Review on the Role of miR-1246 in the Pathoetiology of Different Cancers, Front. Mol. Biosci. 8 (2022) 771835. https://doi.org/10.3389/fmolb.2021.771835.

[267] Y.-J. Huang, T.-H. Huang, V.K. Yadav, M.R. Sumitra, D.T. Tzeng, P.-L. Wei, J.-W. Shih, A.T. Wu, Preclinical investigation of ovatodiolide as a potential inhibitor of colon cancer stem cells via downregulating sphere-derived exosomal β-catenin/STAT3/miR-1246 cargoes, Am J Cancer Res 10 (2020) 2337–2354.

[268] N. Yamada, N. Tsujimura, M. Kumazaki, H. Shinohara, K. Taniguchi, Y. Nakagawa, T. Naoe, Y. Akao, Colorectal cancer cell-derived microvesicles containing microRNA-1246 promote angiogenesis by

activating Smad 1/5/8 signaling elicited by PML down-regulation in endothelial cells, Biochimica et Biophysica Acta (BBA) - Gene Regulatory Mechanisms 1839 (2014) 1256–1272. https://doi.org/10.1016/j.bbagrm.2014.09.002.

[269] C. Han, C. Zhang, H. Wang, L. Zhao, Exosome-mediated communication between tumor cells and tumor-associated macrophages: implications for tumor microenvironment, OncoImmunology 10 (2021) 1887552. https://doi.org/10.1080/2162402X.2021.1887552.

[270] D. Löffler, K. Brocke-Heidrich, G. Pfeifer, C. Stocsits, J. Hackermüller, A.K. Kretzschmar, R. Burger, M. Gramatzki, C. Blumert, K. Bauer, H. Cvijic, A.K. Ullmann, P.F. Stadler, F. Horn, Interleukin-6–dependent survival of multiple myeloma cells involves the Stat3-mediated induction of microRNA-21 through a highly conserved enhancer, Blood 110 (2007) 1330–1333. https://doi.org/10.1182/blood-2007-03-081133.

[271] D.C. Chonov, M.M.K. Ignatova, J.R. Ananiev, M.V. Gulubova, IL-6 Activities in the Tumour Microenvironment. Part 1, Open Access Maced J Med Sci 7 (2019) 2391–2398. https://doi.org/10.3889/oamjms.2019.589.

[272] J. Wang, C.M.E. Fry, C.L. Walker, Carboxyl-terminal modulator protein regulates Akt signaling during skeletal muscle atrophy in vitro and a mouse model of amyotrophic lateral sclerosis, Sci Rep 9 (2019) 3920. https://doi.org/10.1038/s41598-019-40553-2.

[273] R. Takahashi, M. Prieto-Vila, I. Kohama, T. Ochiya, Development of mi RNA -based therapeutic approaches for cancer patients, Cancer Science 110 (2019) 1140–1147. https://doi.org/10.1111/cas.13965.

[274] J.D. Arroyo, J.R. Chevillet, E.M. Kroh, I.K. Ruf, C.C. Pritchard, D.F. Gibson, P.S. Mitchell, C.F. Bennett, E.L. Pogosova-Agadjanyan, D.L. Stirewalt, J.F. Tait, M. Tewari, Argonaute2 complexes carry a population of circulating microRNAs independent of vesicles in human plasma, Proc.

Natl. Acad. Sci. U.S.A. 108 (2011) 5003–5008. https://doi.org/10.1073/pnas.1019055108.

[275] S. Lakhal, M.J.A. Wood, Exosome nanotechnology: An emerging paradigm shift in drug delivery: Exploitation of exosome nanovesicles for systemic in vivo delivery of RNAi heralds new horizons for drug delivery across biological barriers, BioEssays 33 (2011) 737–741. https://doi.org/10.1002/bies.201100076.

[276] F. Ingenito, G. Roscigno, A. Affinito, S. Nuzzo, I. Scognamiglio, C. Quintavalle, G. Condorelli, The Role of Exo-miRNAs in Cancer: A Focus on Therapeutic and Diagnostic Applications, IJMS 20 (2019) 4687. https://doi.org/10.3390/ijms20194687.

[277] S. Han, G. Li, M. Jia, Y. Zhao, C. He, M. Huang, L. Jiang, M. Wu, J. Yang, X. Ji, X. Liu, C. Chen, X. Chu, Delivery of Anti-miRNA-221 for Colorectal Carcinoma Therapy Using Modified Cord Blood Mesenchymal Stem Cells-Derived Exosomes, Front. Mol. Biosci. 8 (2021) 743013. https://doi.org/10.3389/fmolb.2021.743013.

[278] S. Ohno, M. Takanashi, K. Sudo, S. Ueda, A. Ishikawa, N. Matsuyama, K. Fujita, T. Mizutani, T. Ohgi, T. Ochiya, N. Gotoh, M. Kuroda, Systemically Injected Exosomes Targeted to EGFR Deliver Antitumor MicroRNA to Breast Cancer Cells, Molecular Therapy 21 (2013) 185–191. https://doi.org/10.1038/mt.2012.180.

[279] F. Wang, L. Li, K. Piontek, M. Sakaguchi, F.M. Selaru, Exosome miR-335 as a novel therapeutic strategy in hepatocellular carcinoma, Hepatology 67 (2018) 940–954. https://doi.org/10.1002/hep.29586.

[280] H. Monfared, Y. Jahangard, M. Nikkhah, J. Mirnajafi-Zadeh, S.J. Mowla, Potential Therapeutic Effects of Exosomes Packed With a miR-21-Sponge Construct in a Rat Model of Glioblastoma, Front. Oncol. 9 (2019) 782. https://doi.org/10.3389/fonc.2019.00782.

[281] J. Li, J. Chen, S. Wang, P. Li, C. Zheng, X. Zhou, Y. Tao, X. Chen, L. Sun, A. Wang, K. Cao, S. Tang, J. Zhou, Blockage of transferred exosome-shuttled miR-494 inhibits melanoma growth and metastasis, Journal Cellular Physiology 234 (2019) 15763–15774. https://doi.org/10.1002/jcp.28234.

[282] Q. Luo, D. Guo, G. Liu, G. Chen, M. Hang, M. Jin, Exosomes from MiR-126-Overexpressing Adscs Are Therapeutic in Relieving Acute Myocardial Ischaemic Injury, Cell Physiol Biochem 44 (2017) 2105–2116. https://doi.org/10.1159/000485949.

[283] G. Mao, Z. Zhang, S. Hu, Z. Zhang, Z. Chang, Z. Huang, W. Liao, Y. Kang, Exosomes derived from miR-92a-3p-overexpressing human mesenchymal stem cells enhance chondrogenesis and suppress cartilage degradation via targeting WNT5A, Stem Cell Res Ther 9 (2018) 247. https://doi.org/10.1186/s13287-018-1004-0.

[284] R. Rupaimoole, F.J. Slack, MicroRNA therapeutics: towards a new era for the management of cancer and other diseases, Nat Rev Drug Discov 16 (2017) 203–222. https://doi.org/10.1038/nrd.2016.246.

[285] F. Fornari, L. Gramantieri, M. Ferracin, A. Veronese, S. Sabbioni, G.A. Calin, G.L. Grazi, C. Giovannini, C.M. Croce, L. Bolondi, M. Negrini, MiR-221 controls CDKN1C/p57 and CDKN1B/p27 expression in human hepatocellular carcinoma, Oncogene 27 (2008) 5651–5661. https://doi.org/10.1038/onc.2008.178.

[286] M. Hiraki, J. Nishimura, H. Takahashi, X. Wu, Y. Takahashi, M. Miyo, N. Nishida, M. Uemura, T. Hata, I. Takemasa, T. Mizushima, J.-W. Soh, Y. Doki, M. Mori, H. Yamamoto, Concurrent Targeting of KRAS and AKT by MiR-4689 Is a Novel Treatment Against Mutant KRAS Colorectal Cancer, Molecular Therapy - Nucleic Acids 4 (2015) e231. https://doi.org/10.1038/mtna.2015.5.

[287] X. Han, J. Zheng, Y. Wang, Z. Gao, miRNA-29a inhibits colon cancer growth by regulation of the PTEN/Akt/GSK3β and Wnt/β-catenin signaling pathways, Oncol Lett (2018). https://doi.org/10.3892/ol.2018.8905.

# Chapter 3

## Role of Colorectal Cancer-Derived Exosomes in Modulating Macrophage Phenotypes During Tumor Development

## Chapter 3: Role of Colorectal Cancer-Derived Exosomes in Modulating Macrophage Phenotypes During Tumor Development

### 3.1 Graphical Abstract

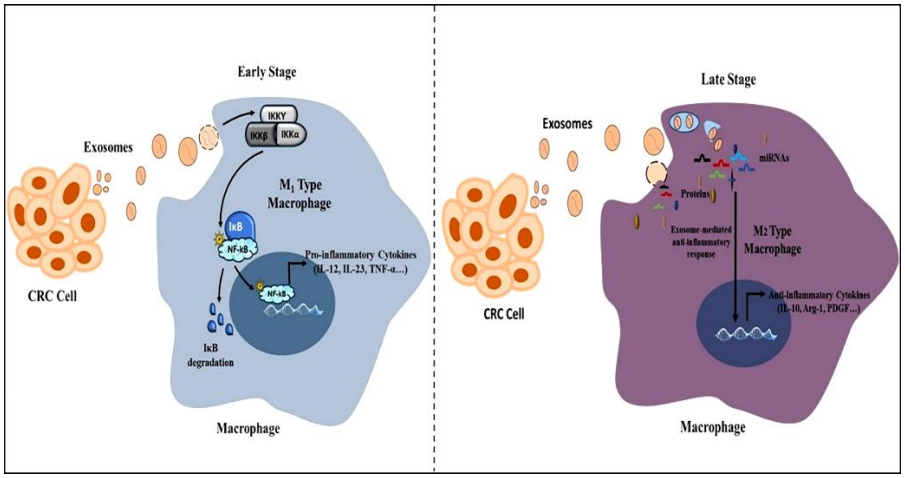



**Figure 3.1: Interplay between CRC cells and macrophages gene expression in Colorectal cancer microenvironment**: Exosome-mediated early-stage M1-like macrophage activation and Exosomal miRNAs mediated late-stage M2-like tumor supportive reprogramming of macrophages in TME.

### 3.2 Overview:

Colorectal cancer (CRC) is one of the deadliest cancer types and is characterized by a complex tumor microenvironment (TME), which includes cancer and immune cells engaging in intricate signaling crosstalk. TME is dependent on the CRC stage and contributes to cancer aggressiveness and therapy resistance. It has been established that tumor-associated immune cells can support cancer progression. However, the underlying mechanisms are not fully elucidated. Here, we provide evidence that communication between CRC and immune cells, particularly tumor-associated macrophages (TAMs), occurs through the release of soluble factors and extracellular vesicles (EVs), such as exosomes. Our study reveals that TAMs initially recognize exosomes as foreign entities, triggering a pro-inflammatory response. Over time, however, the contents

of these phagocytosed exosomes reprogram the TAMs into an anti-inflammatory, tumor-supportive phenotype. Our data indicate that such a phenotypic transition in CRC TAMs is primarily triggered by the activation of the NF-kB transcription factor, and that inhibiting NF-kB signaling may significantly decrease the tumor-supportive functions of TAMs in CRC. Thus, pharmacologically slowing the transition of CRC TAMs from pro-inflammatory to tumor-supportive states may be a promising strategy to reduce cancer aggressiveness.

### 3.3 Introduction

Colorectal cancer (CRC) is the 3$^{rd}$ most common cancer type, affecting both males and females, and is the second leading cause of cancer-related deaths [1]. The American Cancer Society estimated that there were 152,810 new cases of CRC in the United States in 2024. Several risk factors have been identified that may promote CRC progression. These include increasing age, lifestyle, family history, as well as chronic inflammatory diseases [2]. Additionally, epigenetic factors may influence CRC development. Recently, the tumor microenvironment (TME) has been shown to play an important role in CRC pathophysiology. The crosstalk between CRC cells and the immune system is critical for regulating the progression and development of CRC and includes the modulation of TME [3]. This study investigated the role of the microenvironment in CRC development to identify new therapeutic approaches for slowing down CRC progression.

Tumor-associated macrophages (TAM) are among the most abundant immune cells in the CRC microenvironment, and the presence of TAM can either promote or inhibit tumor growth, depending on the context [4]. In TME, macrophages exist either in the classically activated M1-like state, which is often associated with antitumor function, such as proinflammatory response, antigen presentation, and increased phagocytosis or in the alternatively activated M2-like state, which is associated with suppressing

immune responses and supports tumor growth by promoting angiogenesis, via releasing growth factors [5]. The interplay between CRC cells and macrophages within TME resembles the one between allies and adversaries, and determines the course of cancer cell behavior [6]. In part, the intercommunication between CRC cells and macrophages involves paracrine signaling in which CRC cells secrete some soluble factors as well as extracellular vesicles (EVs) in the surrounding TME, which can then reprogram TAM towards a tumor-supportive state [7]. Classically, EVs are subdivided based on size into exosomes, microvesicles, and apoptotic bodies [8]. The exosomes are a commonly studied subset of EVs in cancer research. It is well-established that exosomes are involved in transporting bioactive molecules from donor cells to recipient cells [9].

Exosomes are lipid bilayer membrane-coated vesicles with a diameter ranging from 40 to 150 nanometers (nm) and are secreted by nearly all types of cells, including cancer cells, in the extracellular microenvironment [7,10]. Exosomes act as carriers for the cargo of bioactive material that is destined to be transferred from donor cells to recipient cells via three different mechanisms: i) The exosomal membrane coating proteins may directly interact with the proteins present on the recipient cell membrane and initiate intracellular signaling; ii) The exosomes' membrane may directly fuse with the membrane of the recipient cell membrane and releases its content; and iii) Recipient cells directly phagocytose exosomes to engulf and intracellularly release the cargo into the cancer cell cytosol [11]. The exosomes containing bioactive materials are composed of functional proteins, DNA, mRNAs, miRNAs, and lipids, which may modulate crucial cancer-related mechanisms involved in metastasis, drug resistance, and influence macrophage polarization during tumorigenesis [12]. Exosomes have emerged as crucial mediators in the communication between cancer cells as well as immune cells and have attracted considerable interest in cancer research. Here, we hypothesized that CRC-derived exosomes initially activate macrophages through NF-κB signaling, inducing a

transient pro-inflammatory phenotype, but prolonged exposure reprograms macrophages toward a tumor-supportive M2-like state. To validate our hypothesis, we isolated the CRC cell-derived exosomes and used them to treat macrophages to determine how such treatment affects macrophage function. To monitor the kinetics of macrophage gene expression rate changes in the CRC microenvironment, we cultured macrophages and treated them with exosomes derived from CRC cells to study their effects on macrophage behavior. To our knowledge, this is the first report describing the early and late time points of gene expression in macrophages treated with CRC cell-derived exosomes.

### 3.4 Method

**3.4.1 Cell lines and culture-** The Colo 205 human colon cancer cell line and the THP-1 human monocyte cell line were procured from the NCCS, Pune, India. COLO205 (May 2023) and THP-1 (Feb 2022) cells were STR-authenticated, confirmed mycoplasma-free, and cultured under recommended conditions. These cells were cultured in RPMI 1640 medium (Gibco), supplemented with 10% heat-inactivated fetal bovine serum (Gibco), and a mixture of 100 U/ml penicillin and 100 µg/ml streptomycin (Invitrogen). The cultures were incubated at 37°C in a 5% CO2 concentration. The cells were differentiated into macrophages by exposing them to 25 ng/ml phorbol 12-myristate 13-acetate (PMA; Sigma-Aldrich) in the culture medium for a duration of 24 hours. Afterward, the PMA-containing medium was replaced with fresh RPMI complete medium before the cells were treated with exosomes.

**3.4.2 Exosome extraction and characterization-**Colo 205 cells grew to reach a 70-80% confluency, and then the culture medium was replaced with an FBS-free medium. After 48 hours of culture, the cell supernatant was harvested, cleared by centrifugation first at 300×g for 5 minutes and then at 2000×g for 30 minutes, filtered via a 0.22 µm PVDF filter, and the

exosomes were isolated using ultra-centrifugation at 1,00,000×g for 2 hours. After exosome isolation, the obtained pellets were resuspended in phosphate-buffered saline (PBS) and kept frozen at -80°C for later use. To characterize exosomes, we used various techniques listed below.

**3.4.2.1 Nanoparticle tracking analysis-** We used the nanoparticle tracking analysis (NTA) to detect the particle size (~30-1000 nm) and to determine the relative concentration of exosomes in liquid samples. The NTA analysis was performed with Nanosight. The exosome samples were diluted 1000 times (5 µl/5 mL) in Milli-Q water before analysis. NTA version 3.4 (Build 3.4.003, Nanosight) was used to capture and analyze the data.

**3.4.2.2 Scanning electron microscopy (SEM)**- Scanning electron microscopy was utilized to confirm the size and morphology of the exosomes. 5 µL of the exosome suspension was diluted in PBS and then fixed with glutaraldehyde for 15 minutes. The sample was then rinsed with PBS, dehydrated using ethanol, and air-dried at room temperature for 24 hours. Finally, a coating of gold-palladium was applied to the samples, and imaging was conducted using a scanning electron microscope.

**3.4.2.3 Western blot analysis of exosome markers-** Protein lysates were prepared by boiling exosomes for 5 minutes at 95°C in an equal volume of radioimmunoprecipitation assay (RIPA) buffer, supplemented with protease and phosphatase inhibitors. Proteins were resolved on a 12% sodium dodecyl sulfate polyacrylamide gel (SDS-PAGE) and then transferred to nitrocellulose membranes (Bio-Rad). The nitrocellulose membranes were blocked with 5% BSA (Himedia) in Tris-buffered saline solution supplemented with Tween 20 (TBST) and probed with the following primary antibodies: anti-CD63 (Sigma-Aldrich) and anti-TSG101 (Sigma-Aldrich) 1-1000 in TBST overnight at 4 °C. Finally, the membranes were incubated with the secondary antibodies conjugated with Horseradish peroxidase (HRP), and the chemiluminescence signal was

detected using a gel documentation system Image Quant LAS 4000 (GE Healthcare).

**3.4.3 Exosomes labelling and uptake analysis-** Exosomes were labelled with PKH67 fluorescent membrane dye (Sigma-Aldrich) following the manufacturer's protocol. Briefly, exosomes were incubated with PKH67 dye solution for 5 minutes at room temperature in the dark, and excess dye was quenched by adding 1% BSA (Himedia) in PBS. Labelled exosomes were washed twice by ultracentrifugation at 100,000 × g for 90 minutes to eliminate any residual free dye, followed by resuspension in PBS. THP-1 cells were then incubated with the labelled exosomes at 37 °C in a $CO_2$ incubator for 30 minutes, 4, 12, and 24 hours to assess time-dependent uptake. After incubation, the cells were washed twice with PBS (pH 7.4) at room temperature to remove unbound exosomes and subsequently fixed in freshly prepared 4% paraformaldehyde in PBS for 15 minutes. THP-1 cells were washed twice with PBS, mounted in DAPI-containing mounting medium, and examined under a laser scanning confocal microscope (Olympus, Tokyo, Japan) at 100X magnification to confirm the uptake of PKH67-labelled exosomes.

**3.4.4 RNA isolation and quantitative real-time PCR (qRT-PCR)-** The cells were collected and washed with PBS following the treatment of macrophages under various conditions. Total mRNA was extracted from macrophages using the RNAiso Plus reagent (Takara Bio Inc., Shiga, Japan), according to the manufacturer's instructions. The concentration and purity of the isolated RNA were assessed using a Nanodrop spectrophotometer. For cDNA preparation, 1000 ng of total RNA was reverse-transcribed using the cDNA Synthesis Kit (Takara), following the manufacturer's instructions. Real-time quantitative PCR (qPCR) was performed using SYBR Green Master Mix (Applied Biosystems, MA, USA) Quant Studio 3 Real-Time PCR System (Applied Biosystems). The experiments were conducted with at least three independent repeats to

assess the gene expression of GAPDH, TNF-α, IL-12, IL-23, ARG-1, TGF-β, and PDGF. The primer sequences are provided in **Supplementary Table 1**. The cycle threshold values were analyzed using the 2-ΔΔCt method to determine relative cytokine expression, with GAPDH serving as the reference gene to standardize the expression levels of the cytokine genes.

**3.4.5 Western Blotting of THP-1 cell lysates-** THP-1 cells were lysed in RIPA lysis buffer supplemented with protease and phosphatase inhibitors. The Bradford assay was performed to determine the protein concentration. The proteins (50 μg/well) were resolved on a 10% SDS-PAGE and then transferred to the nitrocellulose membranes (Bio-Rad). The membranes were blocked with 5% BSA (Himedia) in TBST and probed with the primary antibodies (anti-phosphoNF-κB/p65 (Abcam), anti-NF-κB/p65 (Santa Cruz Biotechnology), IKB (Invitrogen), or β-Actin (Invitrogen) diluted 1-1000 in TBST) overnight at 4 °C. Finally, the membranes were incubated with the secondary antibodies conjugated to Horseradish peroxidase (HRP), and the chemiluminescence signal was detected using a gel documentation system (Fusion Solo 6X, Vilber).

**3.4.6 Immunofluorescence-** THP-1 cells were cultured on glass coverslips until they reached 70–75% confluency, after which they were differentiated into macrophages by treating them with 25 ng/ml PMA for 24 hours. Following differentiation, the media was replaced with fresh complete RPMI medium, and THP-1 cells were incubated with exosomes at 37°C for 30 minutes, 4, 12, 24, and 72 hours in a $CO_2$ incubator. Cells were washed twice with PBS (pH 7.4) at room temperature (RT), fixed in freshly prepared 4% paraformaldehyde in PBS for 15 minutes, permeabilized with 0.01% Triton-X solution in PBS for 10 minutes at RT, and washed 2x with PBS. The fixed cells were blocked with 5% BSA (Himedia) for 1 hours on a shaker and then incubated with the primary antibodies against IκB (Invitrogen) or NF-κB/p65 (Santa Cruz Biotechnology) at a 1:200 dilution in TBST overnight at 4°C. Subsequently, cells were washed 2 times with

TBST and were incubated with Alexa Fluor 488-conjugated secondary antibodies for 1 hour. Cells were washed 2x with TBST and then counterstained with DAPI (Sigma) for nuclear visualization. The cells were then examined using a confocal laser scanning microscope (Olympus, Tokyo, Japan) at 100X magnification.

**3.4.7 Measurement of macrophage phagocytic capacity-** To assess the phagocytic function of macrophages, *E-coli* were labelled with Fluorescein Isothiocyanate (FITC, 1mg/ml in DMSO). The FITC-labelled bacteria were washed three times with PBS to remove unbound dye and resuspended in RPMI medium to obtain $10x10^5$ FITC-labelled E. coli/well in 12-well plate. Macrophages were co-cultured with FITC-stained *E-coli* for 1 hour at 37 °C at a 1:10 ratio. Cells were washed to eliminate any non-internalized bacteria and fixed in freshly prepared 4% paraformaldehyde (pH 7.2) in PBS for 15 minutes at RT. The images were taken under a confocal laser scanning microscope (Olympus, Tokyo, Japan) at 100X magnification.

**3.4.8 In vivo tumor development and immunohistochemical analysis in Swiss albino mice-** To validate our in vitro finding, an in vivo allogenic murine model was established. CT-26 cells were mixed with RAW-264.7 macrophages pretreated with CT26-derived exosomes for 72 hours. The mixture of CT-26 ($1\times10^6$) and RAW-264.7 ($2\times10^5$) cells in PBS was injected into the right flanks of 6-week-old male Swiss albino mice to establish a subcutaneous tumor model. Tumor progression was monitored throughout the study. At the end of 4 weeks, mice were sacrificed, and tumor tissue was collected for histological and molecular characterization. Hematoxylin and eosin (H&E) staining was performed to assess tumor morphology and tissue architecture. Furthermore, immunohistochemical analysis was performed to check the expression of cell adhesion and angiogenic tumor-associated markers, including I-CAM and VE-cadherin, within the tumor.

**3.4.9 Statistical analysis-** Statistical analysis was performed using GraphPad Prism (version 8.0.1 (244), CA, US). Data were presented as mean ± standard deviation (SD). P-values were determined using the one-way ANOVA test when three data sets were compared or the Student's t-test when two data sets were analyzed. The data sets were considered significantly different if P values were 0.05 or less.

## 3.5 Results

**3.5.1 Molecular and phenotypic alterations in macrophages induced by CRC cell-conditioned media-**We first set out to assess the ability of CRC cell-derived conditioned media to induce macrophage polarization. It was reported that the polarization of macrophages affects their morphology, with the pro-inflammatory macrophages exhibiting mostly irregular shape and the anti-inflammatory macrophages having an elongated, spindle-like morphology [13]. In our experiments, we treated THP-1 macrophages with the conditioned media collected from COLO-205 colorectal cancer cell cultures and then analyzed the resulting phenotypic changes in the treated THP-1 cells. We found that the conditioned medium-treated THP-1 macrophages exhibited a markedly altered morphology, displaying both proinflammatory M1-like and anti-inflammatory M2-like phenotypes, specifically after longer incubation times, see **Figure 3.2A**. The morphology of untreated THP-1 macrophages was mostly round, with some fibroblast-like cells. In contrast, the morphology of conditioned medium-treated THP-1 macrophages was both oval and irregular, consistent with the morphology of pro-inflammatory macrophages, or elongated and spindle-like, consistent with the anti-inflammatory macrophage morphology, see **Figure 3.2A**. Taken together, these results indicate that conditioned media collected from COLO-205 cell cultures induce significant phenotypic changes in THP-1 macrophages. After noticing the pronounced effects of conditioned media on macrophage morphology, we next aimed at identifying the specific components responsible for driving macrophage

phenotypic transition. It was reported [7,14] that cultured CRC cells are prone to release large amounts of small extracellular vesicles, such as exosomes, capable of carrying various biologically active factors. Therefore, we continued our study by investigating the role of conditioned medium-derived exosomes inducing macrophage polarization.

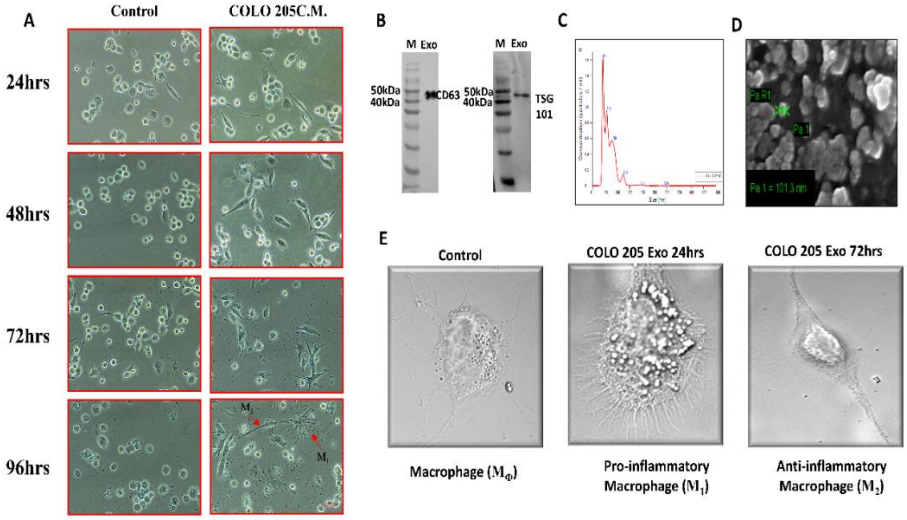



**Figure 3.2 Morphology of THP-1 cells treated with Colo205 conditioned media and exosomes**. (a) Morphological changes in THP-1 cells incubated with Colo205 cell culture-derived conditioned media for 24, 48, 72, and 96 hours. Images captured using a 20× magnification (scale bar = 20 μm). (b) Western blot analysis for the detection of exosome-specific markers. (c) Nanoparticle tracking analysis (NTA) to determine the concentration and average size of the exosomes. (d) Scanning electron microscopy (SEM) images showing the morphology and size of the exosomes. (e) Time-dependent macrophage polarization induced by CRC-cell-derived exosomes. Images captured using a confocal microscope at 100× magnification (scale bar = 30 μm).

**3.5.2 CRC cell-derived exosome isolation and characterization-** We used ultracentrifugation to isolate exosomes from the conditioned media derived from colorectal cancer cells. The isolated exosomes were validated by assessing the expression of CD63 and TSG101, well-established biomarkers of exosomes [15], using Western blot analysis, see **Figure 3.2**.

We also performed Nanoparticle Tracking Analysis (NTA), which is used to establish the size distribution and concentration of exosomes. We found that the sizes of our purified exosomes predominantly ranged from 40 to 150 nm, whereas the concentration amounted to $1.6 \times 10^7$ particles/ml after dilution, see **Figure 3.2C**. Scanning electron microscopy (SEM) was then performed to further confirm the average size of exosomes in our preparations. We found that the typical size of exosomes in our preparations was approximately 100 nm see **Figure 3.2D**, which is consistent with the published literature [15].

**3.5.3 Fluorescent labelling and confocal analysis reveal efficient uptake of PKH67-labelled CRC cell-derived exosomes by macrophages-** Following the characterization of the isolated exosomes, their internalization by macrophages was evaluated. THP-1 cells were exposed to PKH67-labelled exosomes to assess time-dependent internalization and incubated for 30 minutes, 4, 12, and 24 hours. The microscopic observation revealed a sequential increase in PKH67 fluorescence in THP-1 cells incubated with labelled exosomes, see **Figure 3.3.** The nuclei were counterstained with DAPI (blue), while PKH67-labelled exosomes appeared as distinct green fluorescent puncta. Minimal green fluorescence was detected at the 30-minute and 4-hour time points, confirming the absence of nonspecific dye signals. A pronounced accumulation of PKH67 fluorescence was observed in the cytoplasmic region of THP-1 cells at 12 hours, indicating active uptake of exosomes. However, the fluorescence intensity began to decline at 24 hours, suggesting possible degradation or exosome processing within the cells. The merged images displayed discrete green puncta within the cytoplasm (indicated by red arrows), confirming internalization rather than surface adherence. Collectively, these findings demonstrate efficient, time-dependent uptake of cancer cell-derived exosomes by macrophage-like THP-1 cells.

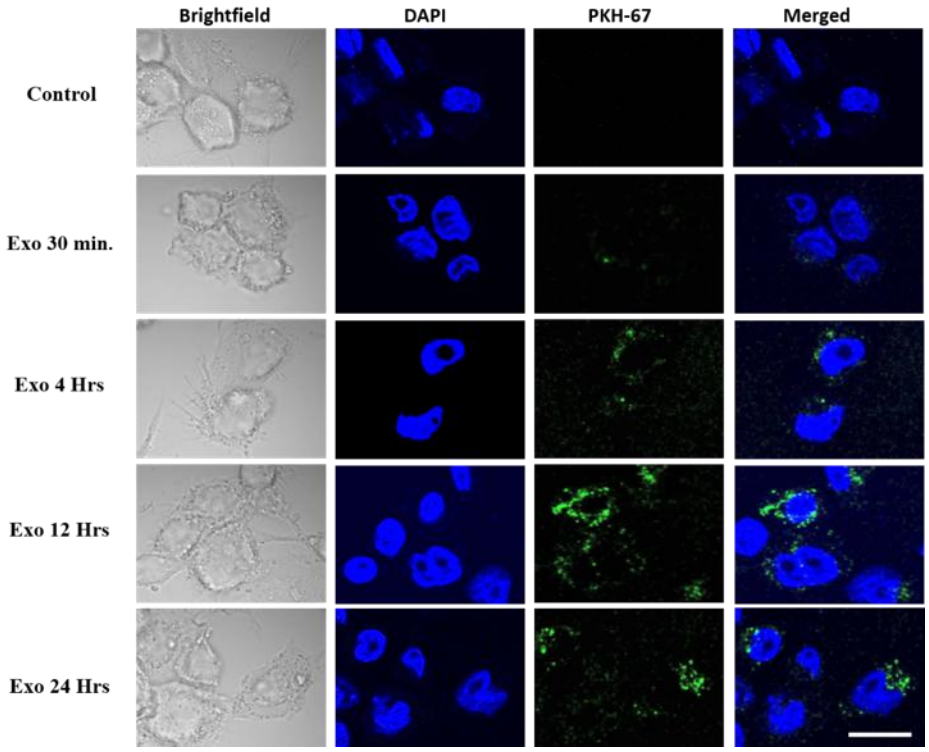



**Figure 3.3: Uptake of PKH67-labeled exosomes by macrophages**. THP-1 cells were co-cultured with PKH67-labeled exosomes (green) derived from CRC (Colo-205) cells and subsequently fixed for Confocal microscopy. Cells were incubated with PKH67-labeled exosomes for 30 minutes, 4, 12, and 24 hours. Cell nuclei were counterstained with DAPI (blue). Red arrows denote exosomes internalized by THP-1 macrophage cells, magnification 100× (scale bar = 20μm).

**3.5.4 CRC cell-derived exosome treatment altered phenotype and cytokine production in macrophages-** Once the uptake of exosomes was confirmed, our next step was to investigate their effects on macrophage phenotype. We treated THP-1 macrophages with the purified exosomes for 24, 48, 72, and 96 hours at a final dose of $8 \times 10^8$ particles/ml, as calculated from the NTA-determined concentration ($1.6 \times 10^7$particles/ml). The treatment conditions were **Control, Normal Medium (N.M. exo) -** normal media isolated exosome (media+FBS), **Colo exo-** Colo 205 cell-conditioned media isolated exosome, see **Figure 3.4A**. Following treatment with Colo 205 cell-derived exosomes, macrophages showed a pro-inflammatory morphology at 24 hours, while at 72 and 96 hours, their

morphology shifted to resemble the anti-inflammatory phenotype. Next, we determined the effect of exosomes in macrophages at the molecular level. To investigate cytokine expression in THP-1 cells treated with COLO-205-derived exosomes for 24, 72, and 96 hours, we performed real-time RT-PCR to measure changes in mRNA levels of cytokines. The mRNA levels of pro-inflammatory molecules IL-23, IL-12, and TNF-α were significantly increased in THP-1 cells treated with exosomes for 24 hours, while at 72 and 96 hours, their expression significantly declined. On the other hand, the exosome treatment boosted the production of M2-type marker IL-10, ARG-1, and PDGF mRNA levels at 72 and 96 hours in these experiments see **Figure 3.5**.

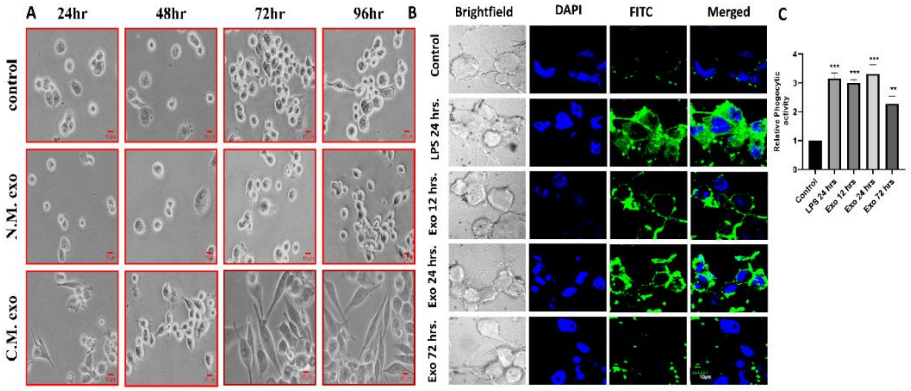



**Figure 3.4: Morphological changes and phagocytic activity of THP-1 macrophages treated with Colo205-derived exosomes.** (a) Morphology of THP-1 cells treated with Colo205-derived exosomes. PMA-treated THP-1 cells were grouped as follows: Control, N.M. exo (exosomes isolated from normal complete media with FBS), and Colo exo (exosomes isolated from Colo205 cell-conditioned media). Cells were incubated for 24, 48, 72, and 96 hours. Images were taken at 20× magnification (scale bar = 20 µm). (b) Phagocytic activity of THP-1 macrophages treated with Colo205-derived exosomes for 12, 24, and 72 hours. Phagocytosis was assessed using FITC-labeled *E. coli*. (c) Bar graph showing the relative fluorescence intensity of FITC-labeled *E. coli* uptake, quantified from the images in (B), and **Supplementary Figure S3.1** documents the phagocytic activity of THP-1 macrophages treated with CRC cell-derived exosomes, assessed

by Oil Red O staining. Images were acquired using a confocal microscope at 100× (scale bar = 20 μm). *$P < 0.05$, **$P < 0.005$, ***$P < 0.0005$, ****$P < 0.00005$.

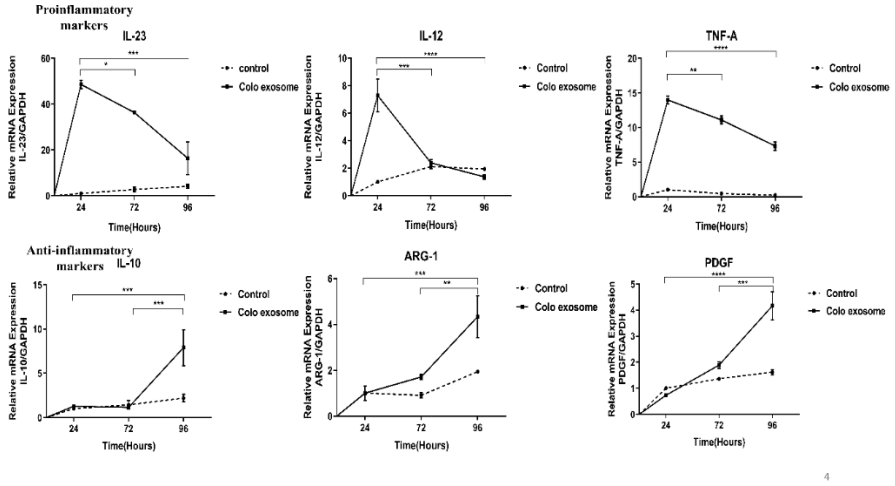



**Figure 3.5: Time-dependent cytokine and immunomodulatory factor expression in macrophages treated with CRC cell-derived exosomes.** THP-1 macrophages were treated with exosomes isolated from CRC cells, and the expression levels of pro-inflammatory (IL-23, IL-12, TNF-α) and anti-inflammatory (IL-10, ARG-1) cytokines, along with PDGF, were analysed at 24, 72, and 96 hours. Gene expression was measured using RT-qPCR. *$P < 0.05$, **$P < 0.005$, ***$P < 0.0005$, ****$P < 0.00005$.

**3.5.5 Exposure to CRC-derived exosomes initially increased the rate of phagocytosis in THP-1-derived macrophages but then decreased macrophage phagocytic function over time-** Next, we evaluated the phagocytic activity of THP-1-derived macrophages following exosome treatment. Macrophages were treated with COLO-205-derived exosomes for 12, 24, or 72 hours and stimulated with LPS (1000 ng) for 24 hours as a control. Following the treatments, macrophages were incubated with FITC-stained *E. coli* as described in the methods. The phagocytic activity of macrophages showed a significant increase at the early points of 12 and 24 hours of exosome treatments and LPS-stimulated macrophages, but decreased at the 72-hour time point compared to the 12 and 24-hour time points, see **Figure 3.4B**. Additionally, we determined the ability of CRC-

exosome-treated macrophages to phagocytose the oxidized LDL (low-density lipoprotein) particles and obtained similar results, see **Supplementary Figure S3.1**. Oil Red O staining was used in the oxidized LDL experiments to assess the phagocytic activity of CRC-exosome-treated macrophages.

**3.5.6 CRC-exosome treatment activates the NF-κB signaling and promotes the expression of M1-like markers in macrophages-** We then investigated the molecular mechanisms by which CRC cell-derived exosomes influence macrophage polarization. Differentiated THP-1 cells were cultured and treated with COLO-205-derived exosomes for 30 minutes, 4, 12, 24, and 72 hours to evaluate the protein expression of IKK, IκB, and NF-κB. The NF-κB signaling plays a pivotal role in inflammation and cancer progression [16]. The results of the Western blot analysis revealed that the protein levels of phosphorylated NF-κB (p-NF-κB) increased at 30 minutes, but then gradually decreased over 4, 12, 24, and 72 hours, respectively, see **Figure 3.6 A and B**. Meanwhile, the total NF-κB protein levels remained unchanged in THP-1 cells treated with exosomes derived from Colo 205 cells. To further investigate, confocal microscopy was performed to assess the translocation of p65 from the cytoplasm to the nucleus. Initially, at the 30-minute time point, a majority of the p65 proteins were observed within the nucleus in CRC-exosome-treated macrophages. However, under control, 4, 12, 24, and 72 hours conditions, p65 was predominantly localized in the cytoplasm, see **Figure 3.6 C and D**. Together, the results from both experiments indicate a decrease in p65 phosphorylation and its nuclear translocation in response to prolonged exosome treatment.

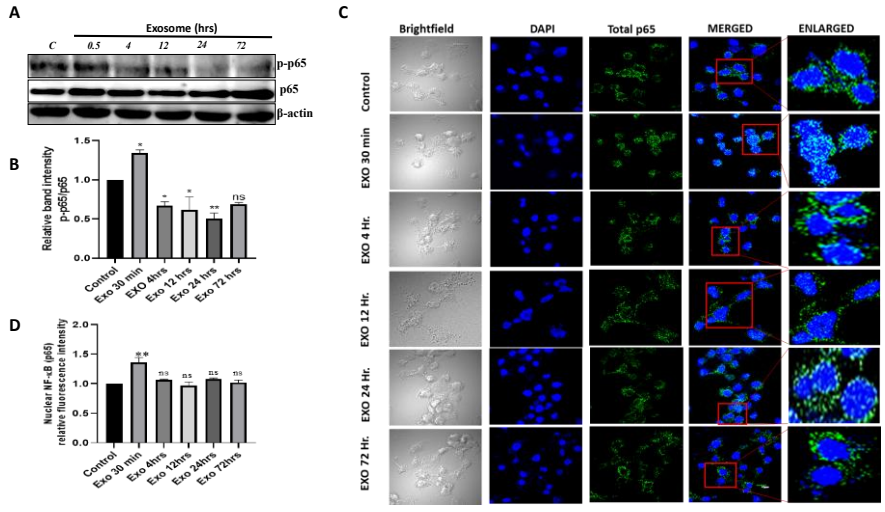



**Figure 3.6: p65 Expression in THP-1 Cells Treated with COLO-205-Derived Exosomes** (A-B) Immunoblot analysis of NF-κB (p65) and its quantification demonstrates a significant downregulation of p65 phosphorylation in THP-1 macrophage cells following treatment with COLO-205-derived exosomes. THP-1 cells were incubated with exosomes for 30 min, 4, 12, 24, and 72 hrs. Western blot analysis revealed an initial increase in phosphorylated NF-κB (p-NF-κB) levels at 30 minutes, followed by a gradual decline at subsequent time points (4, 12, 24, and 72 hours). (C-D) The nuclear translocation of NF-κB (p65) was assessed using confocal microscopy. The accompanying graph represents the quantitative analysis of protein levels. Statistical significance is indicated as follows: $*P < 0.05$, $**P < 0.005$, $***P < 0.0005$, $****P < 0.00005$ compared to the control group. Scale bar=10μm.

We also determined the protein expression of IκB, an upstream molecule of NF-κB, using immunocytochemistry and Western blotting, see **Figure 3.7 A-D**. The results revealed that IκB levels in THP-1 macrophages dropped sharply within 30 minutes after treatment with CRC-derived exosomes, but remained stable at the later time points of 4, 12, 24, and 72 hours. To better understand why IκB was degraded early and then restored at 4 hours, we performed additional experiments at 10, 20, 30, 40, 50, 60 minutes, as well as at 2, 3, and 4 hours timepoints. Interestingly, IκB degradation was first detectable after 20 minutes, peaked around 30–60 minutes, and the protein

began to reappear at 2 hours, see **Figure 3.7 E-F**, which highlights the fact that IκB degradation primarily takes place during the early response of macrophages to exosomes derived from cancer cells.

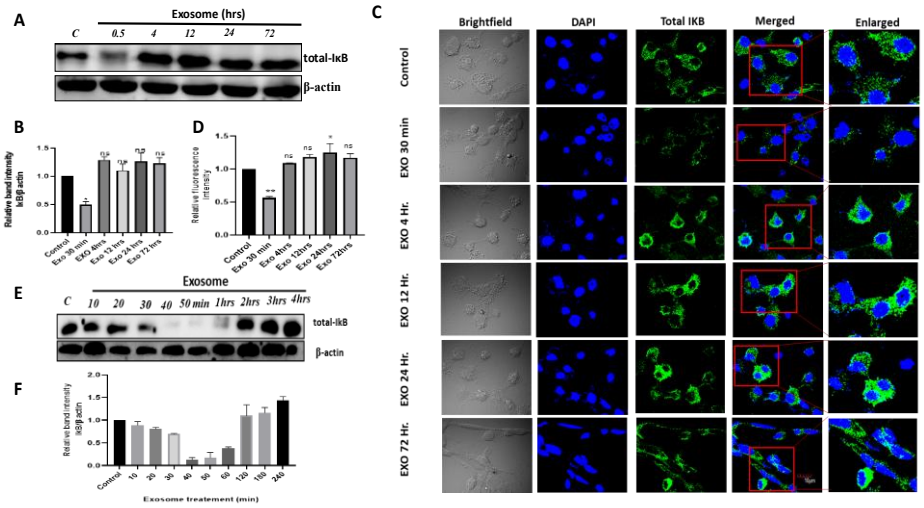



**Figure 3.7: IκB degradation in macrophage cells treated with CRC cell-derived exosomes:** (A and B) Immunoblot analysis and quantification show that CRC-derived exosomes modulate total IκB level in macrophages. Cand D) Immunofluorescence analysis confirms change in IκB expression (E and F) confirms the kinetics of IκB degradation at 10, 20 30,40, 50,60 min, 2, 3, 4 hours. Significance: $*P < 0.05$, $**P < 0.005$, $***P < 0.0005$, $****P < 0.00005$ vs. control, Scale bar=10μm.

Next, we aimed to determine whether IKK phosphorylation was affected. To assess this, we examined the levels of Phospho-IKK using immunoblotting, see **Figure 3.8 A-D** and confocal microscopy. We found that the phosphorylated IKK protein increased at 30 minutes time point but later began to gradually decrease at 4, 12, 24, and 72 hours. Collectively, these data suggest that treatment with CRC cell-derived exosomes initially activates NF-κB signaling and promotes the expression of M1-type markers in macrophages. However, over time, the exosomal cargo may shift macrophages toward an anti-inflammatory phenotype.

**3.5.7 IKK inhibitor treatment attenuated NF-κB signaling activation induced by CRC exosomes in macrophages-** To investigate whether blocking IKK activity could suppress NF-κB signaling in response to CRC cell-derived exosomes, THP-1-derived macrophages were pre-treated with TPCA-1, a selective IKK inhibitor, before CRC exosome exposure. Western blot analysis revealed that TPCA-1 treatment significantly reduced the phosphorylation of IKK, which is a critical step for NF-κB activation. Similarly, we assessed the degradation of IκB in the presence and absence of TPCA-1, see **Figure 3.8 E**. Western blot results showed that IκB levels dropped noticeably at 30 minutes in CRC-exosome-treated macrophages. However, when the cells were pre-treated with TPCA-1, IκB levels remained stable, suggesting that TPCA-1 helps protect against this early protein degradation by blocking IKK activity. further supporting the role of IKK in mediating exosome-induced NF-κB activation.

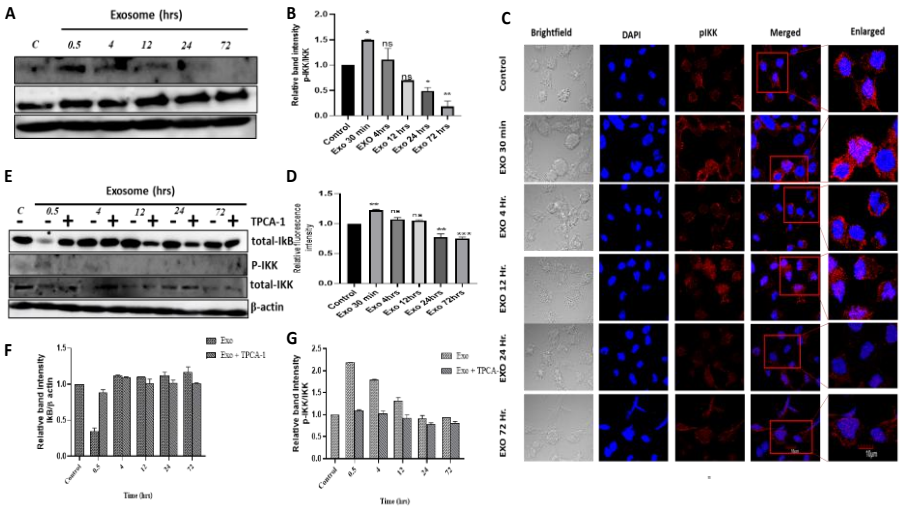



**Figure 3.8: IKK inhibitor treatment attenuated NF-κB signaling induced by CRC exosomes in macrophages:** (A-B) Immunoblot analysis and quantification indicate that CRC exosomes modulate the p-IKK phosphorylation in macrophages, with an initial increase at 30 minutes followed by a gradual decrease at 4-72 hours. (C-D) Immunofluorescence analysis further confirms p-IKK expression in macrophages. (E-G) Treatment with the IKK inhibitor TPCA-1 attenuates exosome-induced changes in p-IKK and IκB expression level compared to control

conditions. Significance: *$P <$ 0.05, **$P <$ 0.005, ***$P <$ 0.0005, ****$P <$ 0.00005 vs. control, Scale bar=10μm.

**3.5.8 CRC-derived exosome-treated macrophages upregulate the EMT marker and PD-L1 expression in CRC cells-** We next set out to determine how CRC-exosome-treated THP-1 cells affect the CRC cell growth, migration, and immune evasion. To assess cell migration, COLO-205 cells were grown in 6-well plates until they reached about 50% confluency, and a straight scratch was made across the cell monolayer using a sterile pipette tip to create a wound. The loosely attached cells were gently washed away with PBS. The cells were then treated with conditioned media collected from different macrophage groups: untreated (MΦ CM), LPS-stimulated (LPS CM), IL-4-stimulated (IL-4 CM), and exosome-treated macrophages for 24 and 72 hours (Exo 24 hours CM and Exo 72 hours CM). LPS and IL-4 CM treatment served as pro- and anti-inflammatory controls, respectively. The highest migratory response was observed with Exo 72 hours CM, which indicates that exosome-mediated macrophage reprogramming supports CRC cell migration over time, see **Figure 3.9 A**. To investigate the expression of epithelial-mesenchymal transition (EMT) and immune checkpoint in CRC cells, we treated cancer cells with the conditioned medium obtained from THP-1 macrophages exposed to CRC exosomes for 24 and 48 hours and then performed real-time RT-PCR to detect the mRNA levels of snail, fibronectin, AKR1B1, and PD-L1 in Colo-205 cells. We found that the mRNA levels of snail, fibronectin, AKR1B, and PD-L1 were significantly increased in Colo-205 cells treated with conditioned medium obtained from CRC-exosome-treated THP-1 cells, see **Figure 3.9 B**. Overall, the data suggest that CRC exosomes can activate THP-1-derived macrophages, which, in turn, may facilitate the growth, migration, and immune evasion of CRC cells themselves.

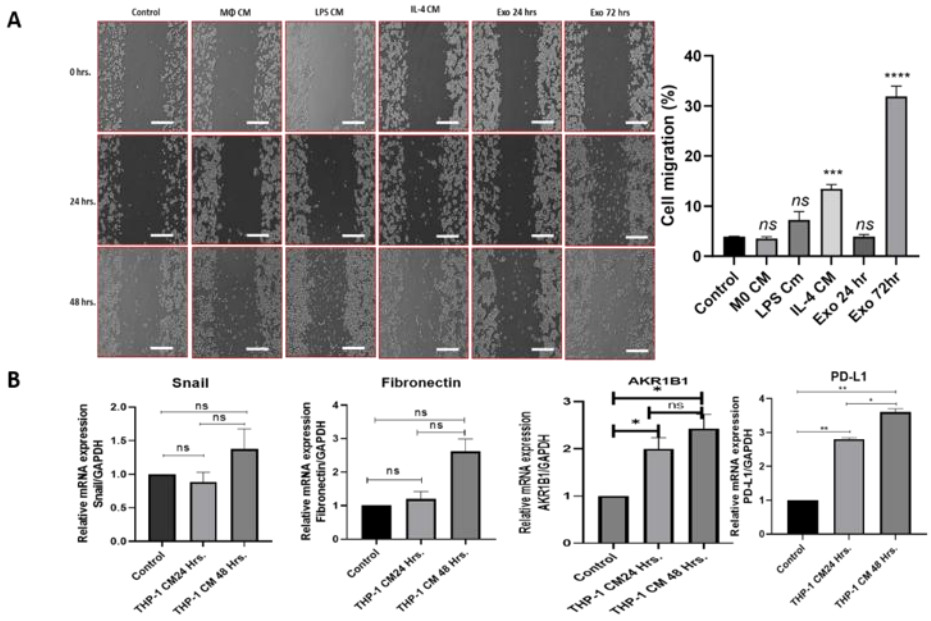



**Figure 3.9: CRC-derived exosomes-treated macrophages promote EMT, PD-L1 expression, and migration in colorectal cancer cells:** (a) Assessment of cell migration in Colo-205 colorectal cancer cells using the scratch assay and quantification; COLO-205 cells were seeded in 6-well plates and cultured to ~50% confluence. A straight-line scratch was created using a sterile pipette tip, and detached cells were removed by gentle washing with PBS. Cells were exposed to conditioned media from untreated macrophages (MΦ CM), LPS-stimulated macrophages (LPS CM), IL-4-stimulated macrophages (IL-4 CM), and exosome-stimulated macrophages for 24 and 72 hours (Exo 24 hours CM, Exo 72 hours CM). Images were captured at 0, 24, and 48 hours post-scratch using a phase-contrast microscope, magnification: 10× (scale bar = 200 μm). (b) Macrophages exposed to CRC-derived exosomes exhibited an enhanced expression of snail, fibronectin, AKR1B1, and PD-L1 in CRC cells, as confirmed through qRT-PCR. *$P < 0.05$, **$P < 0.005$, ***$P < 0.0005$, ****$P < 0.00005$.

**3.5.9 CT-26 exosome-treated macrophages promote tumor progression with increased adhesion and angiogenic markers.** Following the in vitro observations, to determine whether exosome-mediated macrophage reprogramming contributes to tumor progression in vivo, we established an allogeneic mouse model. Injection of CT-26 cells and exosome-treated RAW264.7 macrophages 72-hour treatment groups significantly promote

tumor growth in the mouse model compared with the control group injected with CT-26 cells alone. Histopathological examination via H&E staining also depicts increased cell number, angiogenesis, as well as high nuclear to cytoplasmic (N/C) ratio within tumor tissue compared to the control group, See in **Figure 3.10A**.

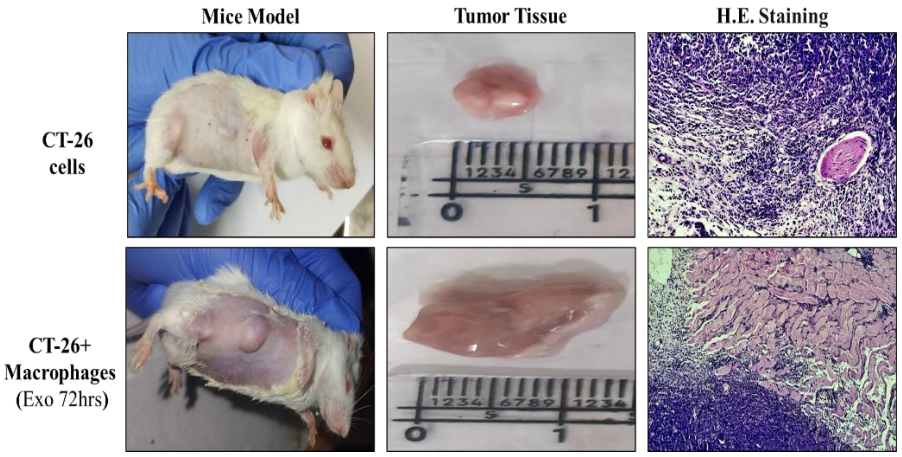



**Figure 3.10A: Subcutaneous tumor development and histopathological characterization in a murine allograft model of CRC.** Representative images showing subcutaneous tumor development, excised tumor morphology, and H&E-stained tumor sections from different treatment groups.

In addition, immunohistochemical analysis suggested elevated expression of I-CAM and VE-cadherin in tumor sections derived from mice injected with exosome-treated macrophages. Enhanced I-CAM expression was observed in injection with CT-26 cells, and exosome-treated RAW264.7 macrophages 72-hours treatments groups. A similar kind of expression, VE-cadherin level also observed under confocal microscopy, as shown in **Figure 3.10B**.

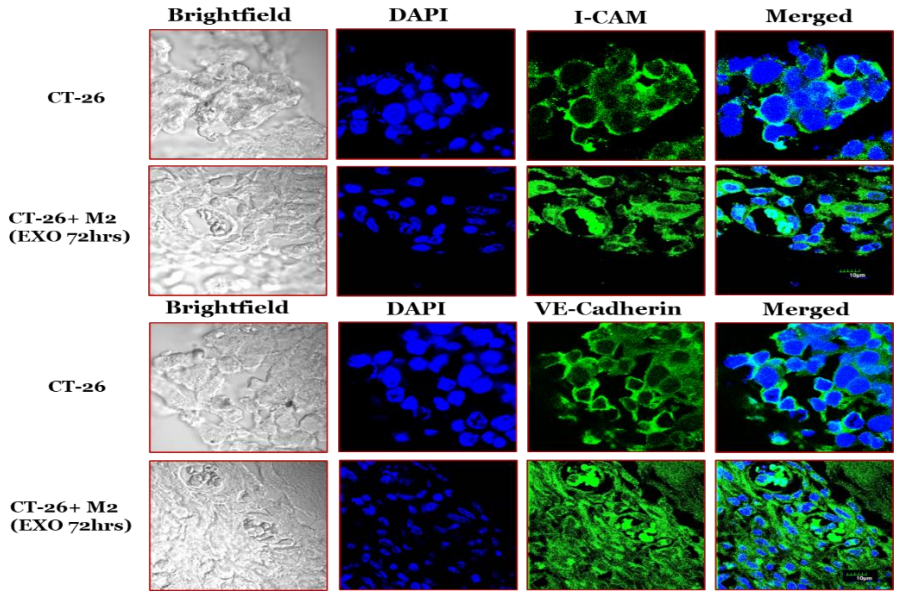



**Figure 3.10B: Enhanced expression of cell adhesion and angiogenic factor during CRC progression.** Immunohistochemical staining shows evaluated expression of ICAM-1 and VE-cadherin in tumor tissues from mice co-injected with CT-26 cells and exosome-treated macrophages for a 72-hour treatment condition, compared to the control group. Images taken under a 100X confocal microscope.

### 3.6 Discussion

In the tumor microenvironment, TAMs are the most abundant cells, and higher levels of TAMs have been linked to poor prognosis in multiple cancers [17,18]. The cancer cell and macrophage communication through exosomes plays an important role in aggressive tumor proliferation and metastasis. Exosomes are nanosized (40-150 nm) vesicles made up from a lipid bilayer, which act as carriers for bioactive material (proteins and nucleic acids) during cell-to-cell communication [7]. **Figure 3.11** illustrates temporal changes in macrophage-associated gene expression under CRC conditions, highlighting the dynamic interplay between CRC cells and macrophage signaling pathways identified in this study. We found that in TME, cancer cells communicate with TAMs by releasing soluble factors as well as EVs and reprogram macrophages towards an anti-inflammatory

tumor-supportive type. These new findings are consistent with earlier findings that have established the role of exosomes in supporting tumor progression in various cancer models [19–23], including CRC cell proliferation and metastasis [24,25]. In the present study, we highlight the fact that exposure to CRC exosomes initially elicits a pro-inflammatory response in macrophages, which is later followed by a shift towards an anti-inflammatory phenotype in the exosome-treated macrophages.

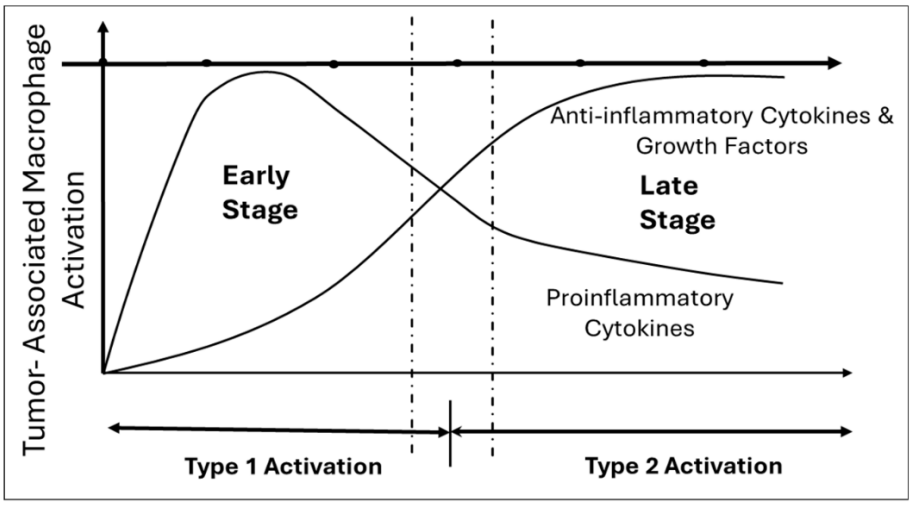



**Figure 3.11:** Kinetics study of macrophage gene expression during early and late stages of CRC-derived exosome treatment. The figure illustrates temporal changes in the expression of macrophage-associated genes, highlighting their dynamic regulation during tumor progression.

We initially performed experiments to determine how CRC cells in the TME influenced the behavior of macrophages. THP-1 macrophages were treated with conditioned media collected from COLO-205 cells, and phenotypic changes in these macrophages were subsequently analyzed. These macrophages exhibited a proinflammatory M1-like and anti-inflammatory M2-like phenotype, as shown in **Figure 3.2A**. This observation prompted us to investigate whether exosomes present within the conditioned media influenced the shift in macrophage polarization towards the M1-like or M2-like tumor supportive phenotype. In TME, cancer cell-conditioned media drives a mixed population of M1 and

M2-like macrophages [26]. We aimed to identify the specific components within the conditioned media responsible for driving macrophage polarization. The proinflammatory response may come through soluble factors such as proteins present in conditioned media [27]. Existing literature supported that exosomes were primarily responsible for promoting the polarization of macrophages toward the M2-like tumor supportive phenotype [4,21,28–30].

Consequently, we explored the role of exosomes in our study. We isolated exosomes using ultracentrifugation techniques and subsequently characterized them through Western blot analysis, NTA, and SEM to validate our exosome quality. Using Western blots, we confirmed that our isolated particles do express CD63 and TSG101, the markers of exosomes [31]. We also perform SEM and NTA to determine the particle size as well as the relative concentration of exosomes in our samples. Our data were consistent with the published literature on exosomes [32,33]. Following the characterization and uptake of the exosomes, we proceeded to examine their impact on macrophage polarization. We treated THP-1 macrophages with exosomes isolated from COLO-205 cells and then observed molecular and phenotypic changes in these macrophages. Short-term CRC exosome-treated macrophages exhibited a strong pro-inflammatory response, characterized by markedly increased mRNA levels of pro-inflammatory cytokines, such as IL-23, IL-12, and TNF-α at 24 hours post-treatment. However, at later times, 72 and 96 hours after initiating exosome treatments, the expression of pro-inflammatory cytokines significantly subsided. Conversely, long-term CRC exosome-treated macrophages exhibited an anti-inflammatory phenotype with increased expression of M2-specific markers, including IL-10, ARG-1, and PDGF at 72 and 96 hours post-treatment, see **Figure 3.5**. These results suggest that short-term treatment with CRC exosomes skewed macrophages towards the M1 phenotype, which may be due to recognition of exosomes as foreign entities. On the other hand, at a later time point, exosomal contents phagocytosed by

macrophages promoted the reprogramming of macrophages into an anti-inflammatory, tumor-supportive phenotype. To further validate our results, we performed an additional experiment to determine whether exosomes are responsible for macrophage polarization toward the M2-like phenotype. This was achieved by evaluating the phagocytic activity of the macrophages. Interestingly, it was reported that M1-like macrophages exhibit a significantly higher phagocytic activity compared to M2-like macrophages [34]. Similarly, it was reported that M1-like macrophages demonstrate enhanced phagocytosis of bacterial pathogens through increased complement secretion and upregulation of surface receptors [35]. Our findings align with the previous research, revealing that COLO-205 exosome-treated THP-1 macrophages exhibited increased phagocytic activity against FITC-labelled *E. coli* at 12, 24, and LPS-24 hours; however, this activity declined significantly at 72 hours, see **Figure 3.4B**. Here, LPS was used as a positive control to induce the M1-like phenotype. These findings suggest that early exposure to exosomes may induce a proinflammatory response in macrophages. To further elucidate this mechanism, our focus then shifted to identifying the specific signaling pathways that drive M1-like activation of macrophages.

An earlier study reported that exosomes derived from body fluids can engage TLRs and activate NF-κB signaling in macrophages [36]. Therefore, we mainly focused on NF-κB signaling to investigate how exosomes mediate macrophage activation. THP-1 cells were cultured and treated with COLO-205-derived exosomes to evaluate the expression of IκB and NF-κB. Western blot analysis showed that phosphorylated NF-κB levels increased at 30 minutes, then gradually decreased at 4, 12, 24, and 72 hours, while total NF-κB protein levels remained unchanged in THP-1 cells treated with Colo 205-derived exosomes. The same set of experiments was performed to determine the p65 translocation to the nucleus by using an immunofluorescence approach. The data showed that after 30 minutes, most p65 molecules were in the nucleus. However, in control samples at 4, 12,

24, and 72 hours, p65 was mainly found in the cytoplasm, see **Figure 3.6E**. Overall, the results from both experiments suggest a reduction in p65 phosphorylation and its subsequent translocation to the nucleus following exosome treatment. Initially, NF-κB activation is strongly associated with the early pro-inflammatory response observed following exosome exposure. We further confirmed the expression pattern of IκB, an upstream inhibitor of NF-κB, using confocal microscopy and western blotting. The results demonstrated a significant IκB degradation at the 30-minute time point compared to the control, as well as at 4, 12, 24, and 72 hours, see **Figure 3.7A**. To further support our hypothesis, we determined the expression of the upstream molecule, IKK, and found that IκB degradation occurs primarily during the early stages of macrophage activation. To validate this, we conducted experiments to assess IKK phosphorylation and its impact on IκB degradation in response to exosomes through immunoblot and confocal microscopy during macrophage activation. Our results showed increased IKK phosphorylation at the 30-minute time point compared to other conditions, indicating its key role in the early stages of macrophage activation. Our study confirms that IKK phosphorylation induces IκB degradation, promoting NF-κB translocation into the nucleus and activating proinflammatory gene expression, which aligns with previous findings in other disease models [37].

It would be interesting to investigate whether other transcription factors, beyond NF-κB, contribute to the pro-inflammatory response of macrophages. In our study, we observed elevated expression of the cytokines IL-23 and IL-12, which are primarily transcribed through the AP-1 signaling pathway [38]. Fujioka et al., study also revealed that inhibition of constitutive NF-κB activation led to a significant suppression of AP-1 transcriptional activity, accompanied by a marked downregulation of *c-Fos* expression levels, suggesting a regulatory interplay between NF-κB and AP-1 signaling pathways [39]. This opens new directions to study the exosome-mediated early response of macrophages and explore the interplay

between NF-κB and AP-1 signaling. This could offer valuable insights into macrophage activation and cytokine regulation. So far, we have investigated the molecular mechanisms involved in the early response of macrophages. However, it is also crucial to further investigate the signaling molecules that drive the activation of tumor-supportive macrophages during the later response of macrophages in cancer progression.

We also provided evidence that macrophages may make cancer cells more aggressive if they are cultured with CRC exosomes. Such a co-culture promotes CRC cancer cell migration and epithelial-mesenchymal transition. We treated COLO-205 cells with conditioned medium isolated from exosome-treated THP-1 cells and examined the EMT marker and immune checkpoint expression in cancer cells. Treatment of COLO-205 cells with conditioned medium from exosome-treated THP-1 cells resulted in a significant increase in the mRNA expression of Snail, fibronectin, AKR1B1, and PD-L1. Thus, it appears that the exosomes from CRC cells may "educate" macrophages to produce more PD-L1 [4]. It was reported that upregulation of AKR1B1 expression is associated with poor prognosis in CRC [40]. In addition to this, our preliminary in vivo finding suggested CRC-derived exosomes promote tumor growth and increase the expression of ICAM and VE-cadherin within TME. The increased expression of I-CAM is associated with tumor progression, metastasis, and EMT, while VE-cadherin expression points out enhanced angiogenesis as well as vascular remodeling at the tumor site. These findings suggest that exosomes from CRC cells can induce a tumor-supportive phenotype in macrophages, thereby contributing to the growth, migration, and immune evasion of CRC cells. Our findings are consistent with the prior research, which showed that exosomes derived from cancer cells can promote the proliferation, migration, and invasion of gastric cancer cells through the activation of the NF-κB pathway in macrophages [41].

## 3.7 Conclusions

In conclusion, our findings highlight that exposure to CRC-derived exosomes initially elicits a pro-inflammatory response in macrophages, which subsequently shifts towards an anti-inflammatory tumor supportive phenotype. This switching may contribute to cancer aggressiveness by promoting the secretion of anti-inflammatory cytokines, growth factors, and enhancing the metastatic potential of cancer cells, as evidenced by increased expression of epithelial-to-mesenchymal transition (EMT) markers. Collectively, these findings identify a temporal NF-κB-dependent macrophage response to CRC-derived exosomes and suggest that preventing macrophage reprogramming may represent a therapeutic strategy to restrain CRC progression.

## 3.8 References

[1] J. Xiang, S. Liu, Z. Chang, J. Li, Y. Liu, H. Wang, H. Zhang, C. Wang, L. Yu, Q. Tang, G. Wang, Integrating transcriptomics and machine learning for immunotherapy assessment in colorectal cancer, Cell Death Discov. 10 (2024) 162. https://doi.org/10.1038/s41420-024-01934-3.

[2] E. Theodoratou, M. Timofeeva, X. Li, X. Meng, J.P.A. Ioannidis, Nature, Nurture, and Cancer Risks: Genetic and Nutritional Contributions to Cancer, Annu. Rev. Nutr. 37 (2017) 293–320. https://doi.org/10.1146/annurev-nutr-071715-051004.

[3] D. Lin, T. Zheng, S. Huang, R. Liu, S. Guan, Z. Zhang, Identification of a novel macrophage-related prognostic signature in colorectal cancer, Sci Rep 14 (2024) 2767. https://doi.org/10.1038/s41598-024-53207-9.

[4] Y. Yin, B. Liu, Y. Cao, S. Yao, Y. Liu, G. Jin, Y. Qin, Y. Chen, K. Cui, L. Zhou, Z. Bian, B. Fei, S. Huang, Z. Huang, Colorectal Cancer-Derived Small Extracellular Vesicles Promote Tumor Immune Evasion by Upregulating PD-L1 Expression in Tumor-Associated Macrophages, Advanced Science 9 (2022) 2102620. https://doi.org/10.1002/advs.202102620.

[5] H. Shinohara, Y. Kuranaga, M. Kumazaki, N. Sugito, Y. Yoshikawa, T. Takai, K. Taniguchi, Y. Ito, Y. Akao, Regulated Polarization of Tumor-Associated Macrophages by miR-145 via Colorectal Cancer–Derived Extracellular Vesicles, The Journal of Immunology 199 (2017) 1505–1515. https://doi.org/10.4049/jimmunol.1700167.

[6] Y. Zhang, Y. Zhao, Q. Li, Y. Wang, Macrophages, as a Promising Strategy to Targeted Treatment for Colorectal Cancer Metastasis in Tumor Immune Microenvironment, Front. Immunol. 12 (2021) 685978. https://doi.org/10.3389/fimmu.2021.685978.

[7] K. Wadhonkar, N. Singh, F.M. Heralde, S.P. Parihar, N. Hirani, M.S. Baig, Exosome-derived miRNAs regulate macrophage-colorectal cancer cell cross-talk during aggressive tumor development, Colorect. Cancer 12 (2023) CRC40. https://doi.org/10.2217/crc-2022-0012.

[8] M. Sheta, E.A. Taha, Y. Lu, T. Eguchi, Extracellular Vesicles: New Classification and Tumor Immunosuppression, Biology 12 (2023) 110. https://doi.org/10.3390/biology12010110.

[9] E. Yang, X. Wang, Z. Gong, M. Yu, H. Wu, D. Zhang, Exosome-mediated metabolic reprogramming: the emerging role in tumor microenvironment remodeling and its influence on cancer progression, Sig Transduct Target Ther 5 (2020) 242. https://doi.org/10.1038/s41392-020-00359-5.

[10] L. Milane, A. Singh, G. Mattheolabakis, M. Suresh, M.M. Amiji, Exosome mediated communication within the tumor microenvironment, Journal of Controlled Release 219 (2015) 278–294. https://doi.org/10.1016/j.jconrel.2015.06.029.

[11] F.M. Barros, F. Carneiro, J.C. Machado, S.A. Melo, Exosomes and Immune Response in Cancer: Friends or Foes?, Front. Immunol. 9 (2018) 730. https://doi.org/10.3389/fimmu.2018.00730.

[12] Exosomes, Nat Biotechnol 38 (2020) 1150–1150. https://doi.org/10.1038/s41587-020-0696-8.

[13] F.Y. McWhorter, T. Wang, P. Nguyen, T. Chung, W.F. Liu, Modulation of macrophage phenotype by cell shape, Proc. Natl. Acad. Sci. U.S.A. 110 (2013) 17253–17258. https://doi.org/10.1073/pnas.1308887110.

[14] W. Zhang, L. Chen, K. Ma, Y. Zhao, X. Liu, Y. Wang, M. Liu, S. Liang, H. Zhu, N. Xu, Polarization of macrophages in the tumor microenvironment is influenced by EGFR signaling within colon cancer

cells, Oncotarget 7 (2016) 75366–75378. https://doi.org/10.18632/oncotarget.12207.

[15] J. Dai, Y. Su, S. Zhong, L. Cong, B. Liu, J. Yang, Y. Tao, Z. He, C. Chen, Y. Jiang, Exosomes: key players in cancer and potential therapeutic strategy, Sig Transduct Target Ther 5 (2020) 145. https://doi.org/10.1038/s41392-020-00261-0.

[16] B. Hoesel, J.A. Schmid, The complexity of NF-κB signaling in inflammation and cancer, Mol Cancer 12 (2013) 86. https://doi.org/10.1186/1476-4598-12-86.

[17] M. De Palma, C.E. Lewis, Macrophage Regulation of Tumor Responses to Anticancer Therapies, Cancer Cell 23 (2013) 277–286. https://doi.org/10.1016/j.ccr.2013.02.013.

[18] W. Zhou, S.Q. Ke, Z. Huang, W. Flavahan, X. Fang, J. Paul, L. Wu, A.E. Sloan, R.E. McLendon, X. Li, J.N. Rich, S. Bao, Periostin secreted by glioblastoma stem cells recruits M2 tumour-associated macrophages and promotes malignant growth, Nat Cell Biol 17 (2015) 170–182. https://doi.org/10.1038/ncb3090.

[19] G.T. Bardi, M.A. Smith, J.L. Hood, Melanoma exosomes promote mixed M1 and M2 macrophage polarization, Cytokine 105 (2018) 63–72. https://doi.org/10.1016/j.cyto.2018.02.002.

[20] Z. Pan, R. Zhao, B. Li, Y. Qi, W. Qiu, Q. Guo, S. Zhang, S. Zhao, H. Xu, M. Li, Z. Gao, Y. Fan, J. Xu, H. Wang, S. Wang, J. Qiu, Q. Wang, X. Guo, L. Deng, P. Zhang, H. Xue, G. Li, EWSR1-induced circNEIL3 promotes glioma progression and exosome-mediated macrophage immunosuppressive polarization via stabilizing IGF2BP3, Mol Cancer 21 (2022) 16. https://doi.org/10.1186/s12943-021-01485-6.

[21] C. Deng, M. Huo, H. Chu, X. Zhuang, G. Deng, W. Li, H. Wei, L. Zeng, Y. He, H. Liu, J. Li, C. Zhang, H. Chen, Exosome circATP8A1

induces macrophage M2 polarization by regulating the miR-1-3p/STAT6 axis to promote gastric cancer progression, Mol Cancer 23 (2024) 49. https://doi.org/10.1186/s12943-024-01966-4.

[22] A. Shang, C. Gu, W. Wang, X. Wang, J. Sun, B. Zeng, C. Chen, W. Chang, Y. Ping, P. Ji, J. Wu, W. Quan, Y. Yao, Y. Zhou, Z. Sun, D. Li, Exosomal circPACRGL promotes progression of colorectal cancer via the miR-142-3p/miR-506-3p- TGF-β1 axis, Mol Cancer 19 (2020) 117. https://doi.org/10.1186/s12943-020-01235-0.

[23] B. Chen, Y. Sang, X. Song, D. Zhang, L. Wang, W. Zhao, Y. Liang, N. Zhang, Q. Yang, Exosomal miR-500a-5p derived from cancer-associated fibroblasts promotes breast cancer cell proliferation and metastasis through targeting USP28, Theranostics 11 (2021) 3932–3947. https://doi.org/10.7150/thno.53412.

[24] D. Wang, X. Wang, M. Si, J. Yang, S. Sun, H. Wu, S. Cui, X. Qu, X. Yu, Exosome-encapsulated miRNAs contribute to CXCL12/CXCR4-induced liver metastasis of colorectal cancer by enhancing M2 polarization of macrophages, Cancer Letters 474 (2020) 36–52. https://doi.org/10.1016/j.canlet.2020.01.005.

[25] Z. Liang, H. Liu, F. Wang, L. Xiong, C. Zhou, T. Hu, X. He, X. Wu, D. Xie, X. Wu, P. Lan, LncRNA RPPH1 promotes colorectal cancer metastasis by interacting with TUBB3 and by promoting exosomes-mediated macrophage M2 polarization, Cell Death Dis 10 (2019) 829. https://doi.org/10.1038/s41419-019-2077-0.

[26] K.C.S. Pe, R. Saetung, V. Yodsurang, C. Chaotham, K. Suppipat, P. Chanvorachote, S. Tawinwung, Triple-negative breast cancer influences a mixed M1/M2 macrophage phenotype associated with tumor aggressiveness, PLoS ONE 17 (2022) e0273044. https://doi.org/10.1371/journal.pone.0273044.

[27] S. Gunalp, D.G. Helvaci, A. Oner, A. Bursalı, A. Conforte, H. Güner, G. Karakülah, E. Szegezdi, D. Sag, TRAIL promotes the polarization of human macrophages toward a proinflammatory M1 phenotype and is associated with increased survival in cancer patients with high tumor macrophage content, Front. Immunol. 14 (2023) 1209249. https://doi.org/10.3389/fimmu.2023.1209249.

[28] A. Pritchard, S. Tousif, Y. Wang, K. Hough, S. Khan, J. Strenkowski, B.K. Chacko, V.M. Darley-Usmar, J.S. Deshane, Lung Tumor Cell-Derived Exosomes Promote M2 Macrophage Polarization, Cells 9 (2020) 1303. https://doi.org/10.3390/cells9051303.

[29] J. Xu, J. Zhang, Z. Zhang, Z. Gao, Y. Qi, W. Qiu, Z. Pan, Q. Guo, B. Li, S. Zhao, X. Guo, M. Qian, Z. Chen, S. Wang, X. Gao, S. Zhang, H. Wang, X. Guo, P. Zhang, R. Zhao, H. Xue, G. Li, Hypoxic glioma-derived exosomes promote M2-like macrophage polarization by enhancing autophagy induction, Cell Death Dis 12 (2021) 373. https://doi.org/10.1038/s41419-021-03664-1.

[30] M. Li, H. Xu, Y. Qi, Z. Pan, B. Li, Z. Gao, R. Zhao, H. Xue, G. Li, Tumor-derived exosomes deliver the tumor suppressor miR-3591-3p to induce M2 macrophage polarization and promote glioma progression, Oncogene 41 (2022) 4618–4632. https://doi.org/10.1038/s41388-022-02457-w.

[31] B.H. Sung, A. Von Lersner, J. Guerrero, E.S. Krystofiak, D. Inman, R. Pelletier, A. Zijlstra, S.M. Ponik, A.M. Weaver, A live cell reporter of exosome secretion and uptake reveals pathfinding behavior of migrating cells, Nat Commun 11 (2020) 2092. https://doi.org/10.1038/s41467-020-15747-2.

[32] S.M. Davidson, C.M. Boulanger, E. Aikawa, L. Badimon, L. Barile, C.J. Binder, A. Brisson, E. Buzas, C. Emanueli, F. Jansen, M. Katsur, R. Lacroix, S.K. Lim, N. Mackman, M. Mayr, P. Menasché, R. Nieuwland, S.

Sahoo, K. Takov, T. Thum, P. Vader, M.H.M. Wauben, K. Witwer, J.P.G. Sluijter, Methods for the identification and characterization of extracellular vesicles in cardiovascular studies: from exosomes to microvesicles, Cardiovascular Research 119 (2023) 45–63. https://doi.org/10.1093/cvr/cvac031.

[33] M. Wu, Y. Ouyang, Z. Wang, R. Zhang, P.-H. Huang, C. Chen, H. Li, P. Li, D. Quinn, M. Dao, S. Suresh, Y. Sadovsky, T.J. Huang, Isolation of exosomes from whole blood by integrating acoustics and microfluidics, Proc. Natl. Acad. Sci. U.S.A. 114 (2017) 10584–10589. https://doi.org/10.1073/pnas.1709210114.

[34] Y. Qie, H. Yuan, C.A. Von Roemeling, Y. Chen, X. Liu, K.D. Shih, J.A. Knight, H.W. Tun, R.E. Wharen, W. Jiang, B.Y.S. Kim, Surface modification of nanoparticles enables selective evasion of phagocytic clearance by distinct macrophage phenotypes, Sci Rep 6 (2016) 26269. https://doi.org/10.1038/srep26269.

[35] R.C. Strunk, F.S. Cole, D.H. Perlmutter, H.R. Colten, gamma-Interferon increases expression of class III complement genes C2 and factor B in human monocytes and in murine fibroblasts transfected with human C2 and factor B genes, J Biol Chem 260 (1985) 15280–15285.

[36] N.P. Bretz, J. Ridinger, A.-K. Rupp, K. Rimbach, S. Keller, C. Rupp, F. Marmé, L. Umansky, V. Umansky, T. Eigenbrod, M. Sammar, P. Altevogt, Body Fluid Exosomes Promote Secretion of Inflammatory Cytokines in Monocytic Cells via Toll-like Receptor Signaling, Journal of Biological Chemistry 288 (2013) 36691–36702. https://doi.org/10.1074/jbc.M113.512806.

[37] M.S. Baig, A. Roy, U. Saqib, S. Rajpoot, M. Srivastava, A. Naim, D. Liu, R. Saluja, S.M. Faisal, Q. Pan, K. Turkowski, G.N. Darwhekar, R. Savai, Repurposing Thioridazine (TDZ) as an anti-inflammatory agent, Sci Rep 8 (2018) 12471. https://doi.org/10.1038/s41598-018-30763-5.

[38] M. Srivastava, U. Saqib, S. Banerjee, K. Wary, B. Kizil, K. Muthu, M.S. Baig, Inhibition of the TIRAP-c-Jun interaction as a therapeutic strategy for AP1-mediated inflammatory responses, International Immunopharmacology 71 (2019) 188–197. https://doi.org/10.1016/j.intimp.2019.03.031.

[39] S. Fujioka, J. Niu, C. Schmidt, G.M. Sclabas, B. Peng, T. Uwagawa, Z. Li, D.B. Evans, J.L. Abbruzzese, P.J. Chiao, NF-κB and AP-1 Connection: Mechanism of NF-κB-Dependent Regulation of AP-1 Activity, Molecular and Cellular Biology 24 (2004) 7806–7819. https://doi.org/10.1128/mcb.24.17.7806-7819.2004.

[40] N.P. Syamprasad, B. Rajdev, S. Jain, S.R. Panda, E.R. Puppala, P. Chaudhari, J.R. Vaidya, G.J. Kumar, V.G.M. Naidu, Pivotal role of AKR1B1 in pathogenesis of colitis associated colorectal carcinogenesis, International Immunopharmacology 119 (2023) 110145. https://doi.org/10.1016/j.intimp.2023.110145.

[41] L. Wu, X. Zhang, B. Zhang, H. Shi, X. Yuan, Y. Sun, Z. Pan, H. Qian, W. Xu, Exosomes derived from gastric cancer cells activate NF-κB pathway in macrophages to promote cancer progression, Tumor Biol. 37 (2016) 12169–12180. https://doi.org/10.1007/s13277-016-5071-5.

# Chapter 4

## Identification of small-molecule inhibitors targeting the PD-1/PD-L1 interaction in colorectal cancer: insights from docking and molecular dynamics simulations

**Identification of small-molecule inhibitors targeting the PD-1/PD-L1 interaction in colorectal cancer: insights from docking and molecular dynamics simulations**

## 4.1 Graphical Abstract

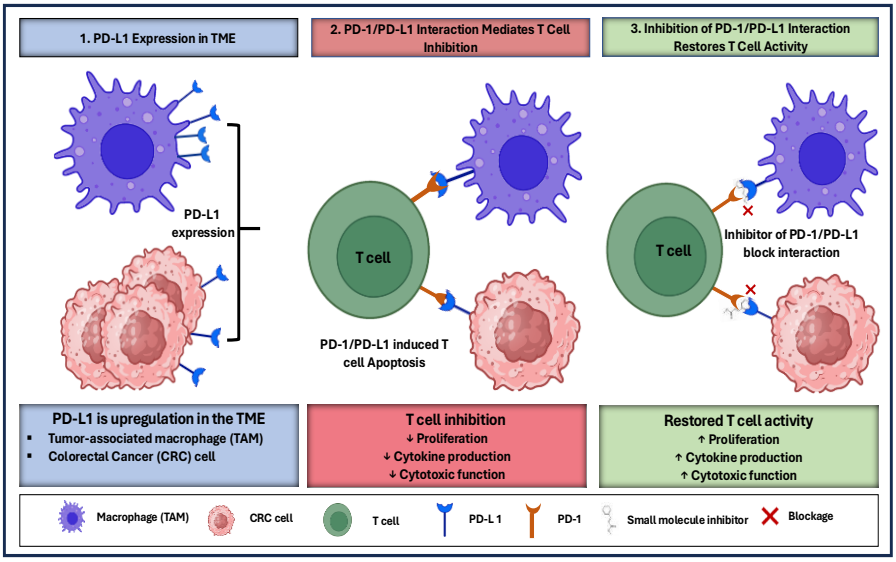



**Figure 4.1: Graphical Abstract: Mechanism of Blocking PD-1/PD-L1 Axis in Tumor Immunity.** Figure illustrates PD-1 expression on cytotoxic T cells interacting with PD-L1 on cancer cells and tumor-associated macrophages, suppressing T-cell activity. Blocking this interaction with small-molecule inhibitors can restore and enhance anti-tumor T-cell-mediated immunity.

## 4.2 Overview

The PD-1/PD-L1 checkpoint plays a crucial role in tumor immune evasion and is widely recognized as an important therapeutic target in cancer immunotherapy. Although monoclonal antibodies that inhibit PD-1/PD-L1 interactions have achieved clinical success, but face some drawbacks, including high cost, immune-related adverse effects, and limited tumor penetration. Consequently, identifying small-molecule inhibitors capable of disrupting this interaction is gaining significant attention as a promising alternative to overcome these limitations. In the present study, the marine natural product database was screened to identify potential inhibitors of the PD-1/PD-L1 interactions using in silico approaches, such as molecular docking, pharmacokinetics prediction, and molecular dynamics simulations. The top-ranked screened compounds exhibited strong binding affinity towards PD-L1 and formed stable interactions with key residues at the PD-1/PD-L1 binding interface. Among these, CMNPD3605 exhibited the strongest inhibitory potential in our in-silico predictions and showed greater promise than currently reported small-molecule inhibitors in clinical studies. Molecular dynamics simulations further confirmed the structural stability of the protein-ligand complexes, supported by stable RMSD, RMSF profiles, and favorable binding free energy values. Overall, these findings suggest that marine-derived natural compounds may serve as promising small-molecule inhibitors targeting the PD-1/PD-L1 immune checkpoint pathway and provide a basis for future experimental validation in CRC therapy.

## 4.3 Introduction

Colorectal cancer (CRC) is one of the most frequently diagnosed cancers worldwide and a major cause of cancer-related mortality [1]. Despite advances in detection and treatment, CRC continues to be the second leading cause of cancer-related deaths only in the United States, with ~153,000 cases and ~52,000 deaths expected in 2025 [2]. The development and progression of CRC are governed not only by genetic and epigenetic alterations but also profoundly influenced by the tumor microenvironment (TME) [3]. The crosstalk between cancer cells and immune cells plays a crucial role in shaping disease progression and therapeutic response [4,5]. In addition to soluble cytokines, growth factors, and extracellular vesicles (EVs) are important mediators of intercellular communication in cancer, facilitating tumor progression and immune evasion [6,7]. The immune evasion is primarily mediated through the immune checkpoint by the immune checkpoint pathways, including PD-1/PD-L1 signaling [8]. Cancer cells expressed PD-L1 (Programmed Death-Ligand 1), which interacts with PD-1 (Programmed Death-1) receptors expressed by T cytotoxic cells and initiates programmed cell death in T cytotoxic cells, resulting in decreased anticancer activity [9]. The PD-L1 is primarily expressed by cancer cells, neutrophils, natural killer (NK) cells, and macrophage-lineage cells, and is absent from all other normal human tissues [9,10]. In addition, Yin et al reported that CRC cells-derived EVs carrying microRNAs induce M2 macrophage polarization and increase PD-L1 expression via PTEN/AKT and SOCS1/STAT1 signaling [10]. The PD-L1 upregulation in cancer is associated with immune evasion and tumor progression, making it a promising target for therapeutic intervention [11]. Therefore, targeting the interaction between PD-L1/PD-1 represents a promising therapeutic strategy.

PD-1/PD-L1 checkpoint blockade immunotherapy for tumors showed promising results in patients with tumors, including lung cancer [12], breast cancer [13], and gastric cancer [14]. Currently PD-1/PD-L1-directed

monoclonal antibodies (mAbs) are useful in clinical trials [15,16]. Although some cancer patients respond well to monoclonal antibody therapy, several limitations remain associated with this treatment. These antibodies often exhibit poor oral bioavailability, restricted tumor penetrations, immune-related side effects, and high treatment costs [17]. In order to enhance tumor immunotherapy, the substitution of monoclonal antibodies (mAbs) with small molecule inhibitors is necessary, which will allow for the elimination of the constraints which are associated with the former. Therefore, exploring alternative therapeutic strategies, particularly small molecules and natural compounds, is essential to block the PD-1/PD-L1 interaction. In this context, the present study aims to identify potential small-molecule inhibitors from marine natural product databases that can disrupt the PD-1/PD-L1 interaction using in silico approaches, including molecular docking and molecular dynamics simulations, to explore novel therapeutic candidates for CRC treatment. We analysed the inhibitor binding and complex dynamics by using molecular docking and MD simulations. Initially, molecules were subjected to a structured screening workflow to evaluate their binding affinity and interaction profiles at the PDL1 interface. The Top candidates from screening exhibited high affinity and stable interactions in the PD-L1 binding site. They were evaluated for their ADMET properties and interactions with PD-L1, following which Molecular dynamics simulations of PD-L1 and its inhibitor-bound complexes were carried out for a duration of 200 nanoseconds. These simulations provided detailed insights into conformational dynamics, complex stability, and intermolecular interaction patterns at the PD-L1 interface. In the context of cancer treatment, the findings collectively lend support to the use of small-molecule inhibitors of PD-L1 as potential therapeutic interventions.

## 4.4 Materials and methods

**4.4.1Cell lines and culture:** The Colo 205 human colorectal carcinoma cell line and the THP-1 human monocytic cell line were obtained from the National Centre for Cell Science (NCCS), Pune, India. Both cell lines were maintained in RPMI-1640 medium (Gibco) supplemented with 10% heat-inactivated fetal bovine serum (FBS; Gibco) and antibiotics (100 U/mL penicillin and 100 µg/mL streptomycin; Invitrogen). Cultures were incubated at 37°C in a humidified atmosphere containing 5% $CO_2$. Differentiation of THP-1 monocytes into macrophages was induced by treatment with 25 ng/mL phorbol 12-myristate 13-acetate (PMA; Sigma-Aldrich) for 24 hours. Following differentiation, the PMA-containing medium was replaced with fresh complete RPMI medium before exposure to exosomes.

**4.4.2 Exosome isolation and characterization:** Colo-205 cultures were allowed to grow to 70–80% confluence, and the culture medium was replaced with serum-free media. The conditioned media were collected after 48 hours and centrifuged at 300×g for 5 minutes and 2,000×g for 30 minutes to remove cell debris. Centrifuged supernatant was passed through a 0.22 µm PVDF filter, and then proceeded to ultracentrifugation at 100000×g for 2 h to isolate exosomes. Subsequently, isolated exosomes were characterized through NTA and SEM.

**4.4.2.1 Nanoparticle tracking analysis:** To characterize the exosomes, nanoparticle tracking analysis (NTA) used to detect size as well as concentrations of the sample. The NTA analysis was performed with Nanosight (NTA Version: NTA 3.4 Build 3.4.003). The exosome samples were diluted 1000 times in Milli-Q water before analysis

**4.4.2.2 Scanning electron microscopy (SEM):** To confirm the size and morphology of exosomes, a scanning electron microscope was utilized. 10 µL of the exosome suspension was diluted in PBS and then fixed with

glutaraldehyde for 15 minutes. The sample was then rinsed with PBS, dehydrated using ethanol, and air-dried at room temperature for 24 hours. Finally, a coating of gold-palladium was applied to the samples, and imaging was conducted using a scanning electron microscope.

**4.4.3 RNA isolation and quantitative real-time PCR (qRT-PCR):** THP-1 and Colo-205 cells were collected and washed with PBS after respective treatments. Total RNA was extracted using RNAiso Plus reagent (Takara Bio Inc., Japan) following the manufacturer's protocol. RNA concentration and purity were determined using a Nanodrop spectrophotometer. For cDNA synthesis, 1000 ng of RNA was reverse-transcribed using the Takara cDNA Synthesis Kit. qRT-PCR was performed with SYBR Green Master Mix on a QuantStudio 3 Real-Time PCR System (Applied Biosystems). Gene expression of **GAPDH** and **PD-L1** was quantified using the 2^–ΔΔCt method, with **GAPDH** as the internal reference. Primer sequences are listed in **Supplementary Table S3.1.**

**4.4.4 Target structure preparation:** The PD-L1–PD-1 complex structure (PDB ID: 4ZQK; Resolution: 2.45 Å) [18] was initially inspected to define the protein–protein interaction interface. 4ZQK was selected because it provides the best resolution among available PD-1/PD-L1 complexes and represents a human-derived crystal structure with a clear depiction of the native PD-1/PD-L1 binding interface, making it an appropriate and reliable template for screening studies. Using UCSF Chimera [19], residues at the PD-L1 interface located within 3 Å proximity to PD-1 were identified and catalogued through detailed inspection of the protein–protein complex. For all subsequent simulations, the PD-L1 protein was isolated by removing the PD-1 chain and any non-protein entities. The resulting PD-L1 structure was then prepared using the protein preparation wizard module [20] of Schrödinger, which performed all necessary corrections, including assignment of bond orders, addition of hydrogens, optimization of hydrogen-bonding networks, and assignment of protonation states at pH

7.0. The prepared PD-L1 receptor, focused on its functional interface (F19, Y56, Q66, R113, A121, D122, Y123, K124, R125) [21], was then used for grid generation for molecular docking studies using the receptor grid generation module [22].

**4.4.5 Ligand library processing:** The ligand library was assembled from the Comprehensive Marine Natural Products Database (CMNPD) [23], a manually curated, open-access resource that catalogues over 31,000 marine natural products with associated 2D/3D structures, physicochemical and predicted ADMET properties, standardized bioactivity annotations, source-organism taxonomy and geographic metadata, and literature citations. CMNPD supports structure-based discovery workflows through downloadable bulk datasets and a web interface that enables structure, substructure and property queries, visualisation and network exploration, and provides compound-level report pages containing computed descriptors, bioactivity records and bibliographic links. For reproducibility, the CMNPD dataset (31,561 entries) was downloaded and a standardized LigPrep [24] workflow was applied, which involved desalting, generating possible tautomers, correcting protonation at physiological pH (7.0 ± 2.0), and generating all relevant stereoisomers and low-energy 3D conformers. Ligands were minimized using the OPLS3e [25] force field and stored in Maestro format for downstream virtual screening.

**4.4.6 Virtual screening and ADMET predictions:** A tiered virtual screening workflow was applied to the full CMNPD library against the PD-L1 interface grid using Glide [26] HTVS, SP, and XP precision in sequence. High-throughput virtual screening (HTVS) was performed for initial filtering, then standard precision (SP) docking for pose refinement, and lastly, extra precision (XP) docking for final ranking. The docking grid was centred on the mapped PD-L1 interface residues, and van der Waals scaling was set at 0.8 for nonpolar atoms with a partial charge cutoff of 0.15 for diverse chemical sampling. Top hits from XP docking were ranked by

GlideScore and manually inspected to ensure meaningful engagement with interface residues. Lead compounds: CMNPD16477, CMNPD21979 and CMNPD3605 were prioritized for further study alongside the benchmark inhibitor INCB086550 [27]. Subsequently, three prioritized leads and the control were evaluated computationally for ADMET properties using pkCSM [28]. Predicted endpoints included Caco-2 permeability, blood–brain barrier penetration, CYP2D6 inhibition, AMES mutagenicity, hepatotoxicity, and skin sensitization. All three leads passed the predefined ADMET filters and were advanced, along with the control, to molecular dynamics simulations.

**4.4.7 Protein–protein docking:** The PD-1 and PD-L1 structures from the crystal complex (PDB ID: 4ZQK) were taken forward for Protein-protein docking. The interacting interface was defined based on residues within 3 Å proximity at the PD-1/PD-L1 binding surface. Protein–protein docking was performed using the HADDOCK web server [29], with the defined interface residues specified as active sites to guide the docking process. To validate the docking protocol, the docked PD-1/PD-L1 complex was superimposed with the original crystal structure using the Chimera MatchMaker tool. The resulting overlap showed close agreement with the experimental structure, confirming the accuracy of the workflow. This validated protocol was then applied to assess the impact of ligand binding on the PD-1/PD-L1 interaction by docking ligand-bound PD-L1 against PD-1 under identical parameters.

**4.4.8 Molecular dynamics simulations:** Molecular dynamics (MD) simulations were employed to assess the stability and dynamic behavior of the docked PD-L1–ligand complexes under explicit solvent conditions. The top-ranking complexes from virtual screening and ADMET analyses were prepared for simulation using the LEaP module of AmberTools19 [30]. Counterions were added as needed to neutralize each system, which was then solvated in a periodic octahedral box of TIP3P water molecules,

providing a 10.0 Å buffer in all directions [31]. Parameterization was achieved by assigning the Amber ff14SB [32] force field to the protein, and the Antechamber-derived AM1-BCC [33] atomic charge, along with the GAFF2 [34] force field to ligand molecules. All simulations were conducted using the pmemd.cuda module of AMBER18 [30,35–37]. Long-range electrostatic interactions were treated using the particle-mesh Ewald (PME) [38] method, and all covalent bonds involving hydrogen atoms were constrained using the SHAKE [39] algorithm. A 10 Å non-bonded cutoff was applied. Each simulation used a 2.0 fs time step. Energy minimization and multi-step heating to 300 K followed by equilibration were first performed, after which the systems were subjected to 200 ns of unrestrained MD in the NPT ensemble at 1 atm and 300 K. Pressure and Temperature during the simulations were controlled using the Berendsen barostat [40] and Langevin thermostat [41,42], respectively. All trajectory post-processing and quantitative analyses, including RMSD, RMSF, hydrogen bonds, radius of gyration, and solvent-accessible surface area, were performed using the CPPTRAJ [43] module in AMBER18.

**4.4.9 Trajectory analysis:** Protein stability was evaluated by calculating the backbone root-mean-square deviation (RMSD) and root-mean-square fluctuation (RMSF), focusing on both global protein behavior and specifically on the PD-L1 interface region. Ligand stability was monitored by calculating the ligand RMSD relative to its initial docked conformation. To assess protein compactness and folding, the radius of gyration (Rg) was computed over the molecular dynamics trajectories, while solvent-accessible surface area (SASA) calculations provided insights into changes in surface exposure. Hydrogen bond analysis between the protein and the ligands was carried out with the CPPTRAJ module in AmberTools18. Standard geometric definitions were used, considering donor-acceptor distances within 3.5Å and bond angles above 120º.

**4.4.10 Binding free energy calculations and data visualization:** Binding free energies ($\Delta G_{bind}$) were estimated using the Molecular Mechanics Poisson–Boltzmann Surface Area (MM/PBSA) method [44,45]. It was computed as:

$\Delta G_{bind} = (G_{complex}) - (G_{protein}) - (G_{ligand})$

where each $G_x$ represents the average free energies of the respective species i.e., complex, protein, or ligand, obtained from equilibrated molecular dynamics snapshots. These total free energy values were further split into contributions from molecular mechanics and solvation energies:

$G = E_{MM} + G_{solv}$

Where

$E_{MM} = E_{bonded} + \Delta E_{vdW} + \Delta E_{elec}$

and

$G_{solv} = \Delta G_{pol} + \Delta G_{np}$

Here, $\Delta E_{vdW}$ and $\Delta E_{elec}$ are the van der Waals and electrostatic interaction energies, $\Delta G_{pol}$ is the polar solvation free energy estimated using the Poisson–Boltzmann equation, and $\Delta G_{np}$ is the non-polar solvation free energy calculated from solvent-accessible surface area (SASA) models.

The entropic term ($-T\Delta S$) was excluded from the MM/PBSA calculations due to its high computational demand and statistical variability. Previous studies have noted that entropy is often omitted in MM/PBSA protocols because of approximations in statistical mechanical treatments, limitations of entropy estimation methods, and challenges in achieving statistically converged sampling [46]. This omission represents a methodological limitation, as ligands with differing conformational flexibility may not be ranked with complete accuracy. Neglecting entropic contributions could bias comparisons against more rigid ligands. This caveat is explicitly considered when interpreting the predicted affinity rankings.

To assess how individual residues contribute to binding affinity, MM/PBSA energy components were decomposed on a per-residue basis. Snapshots

were taken every 100 ps during the production run, and the resulting profiles were averaged to pinpoint residues that play a central role in ligand binding and stabilisation of the PD-L1 interface. This approach offers a clear quantitative view of the thermodynamic forces driving the interaction. Data analysis and visualisation were carried out in Python (v3.13.5), using NumPy for array handling and numerical routines, and Matplotlib for generating publication-quality figures that highlight the key energetic trends across the dataset.

## 4.5 Results

**4.5.1 Exosome-mediated upregulation of PD-L1 in macrophages and CRC cells:** Consistent with the literature and our previous study, we observed that CRC-derived exosomes upregulate PD-L1 expression in macrophages. Now we want to investigate whether CRC-exosome-treated macrophages further enhance PD-L1 expression in CRC cells or not. To validate this, we Colo-205 cells–derived exosomes were successfully isolated by ultracentrifugation and subsequently characterized by nanoparticle tracking analysis (NTA), see in **Figure 4.2 A,** and scanning electron microscopy (SEM), see in **Figure 4.2 B,** and used to treat cells. The Size and morphology of the exosome are consistent with what was mentioned earlier in the research. To quantify the expression of PD-L1, RT-PCR was performed, and the results showed that exosomes derived from Colo 205 cells upregulate PD-L1 expression in macrophages. To extend these findings, colo-205 cells were treated with conditioned medium obtained from exosome-treated macrophages for 48 hours, which resulted in a further elevation of PD-L1 expression relative to control cells, see in **Figure 4.2 C**. Collectively, in TME, cancer cells increase PD-L1 expression on themselves and stimulate its upregulation in macrophages, resulting in a dual immunosuppressive mechanism that induces T-cell apoptosis and promotes tumor immune evasion. Based on these observations, we turned to an in-silico approach for the identification of potential PD-L1 inhibitors,

aiming to design small molecules with favourable binding and therapeutic properties.

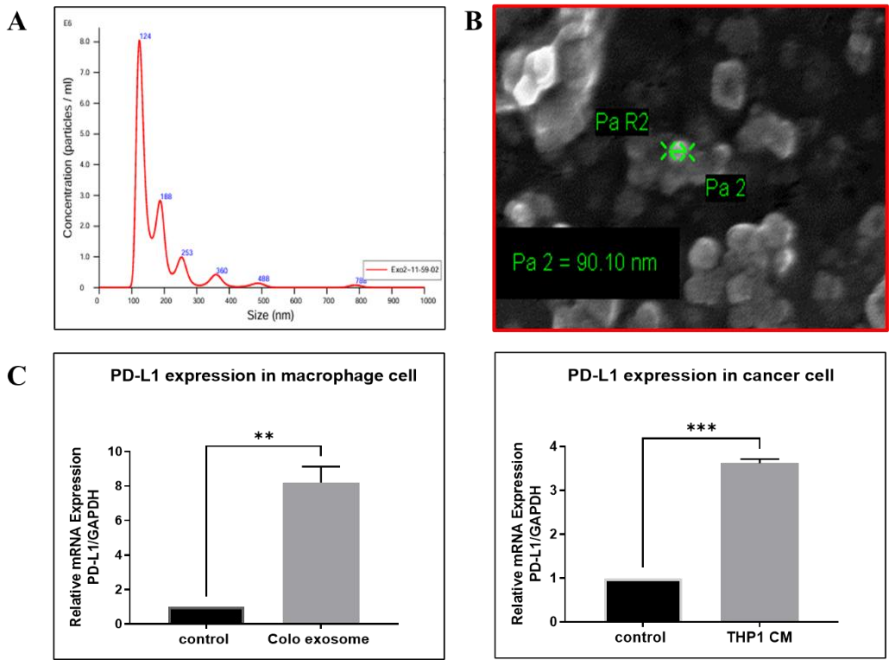
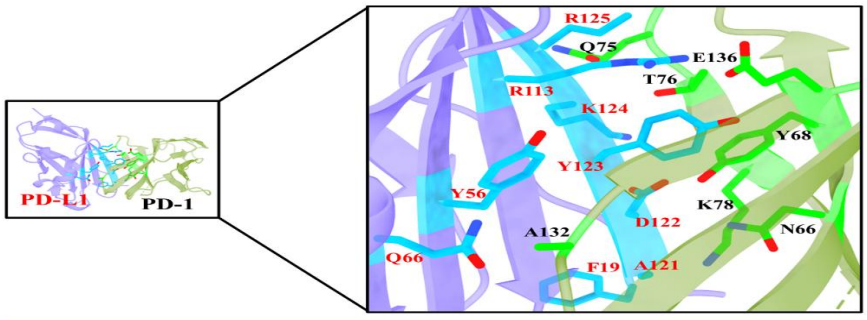



**Figure 4.2 Exosome characterization and PD-L1 expression analysis.** Colo-205–derived exosomes were isolated by ultracentrifugation and characterized by (A) nanoparticle tracking analysis (NTA) and (B) scanning electron microscopy (SEM).(C) CRC cells-derived exosomes induced PD-L1 expression in macrophages and conditioned media (CM) obtained from exosome-stimulated macrophages subsequently elevated PD-L1 expression in CRC cells was quantified by RT-PCR *$*p<0.05$, **$p<0.005$, ***$p<0.0005$, ****$p<0.00005$ .

**4.5.2 Site-directed docking reveals high-affinity marine natural products engaging the PD-L1- PD-1 interface:** The PD-L1 receptor model used for in silico studies was derived from the crystal structure of the PD-1–PD-L1 complex (PDB ID: 4ZQK). Structural analysis performed in UCSF Chimera identified a prominent PD-1 binding interface on PD-L1, defined by nine key residues: F19, Y56, Q66, R113, A121, D122, Y123, K124, and R125 (**Figure 4.3**). These residues were used to generate a focused Glide docking grid for all subsequent ligand screening steps. Upon

screening the CMNPD ligand library, comprising 31,561 marine-derived compounds, via a hierarchical virtual screening workflow using the Glide module targeting the PD-L1 interface grid, three marine-derived compounds i.e. CMNPD16477, CMNPD21979, and CMNPD3605, were prioritized for further investigation based on docking scores, pose quality, and residue-level interactions, see **Figure 4.4**. INCB086550, a previously reported small-molecule PD-L1 inhibitor, was included as a control throughout the workflow to benchmark docking performance, dynamic behaviour, and energetic metrics. Prior to molecular dynamics simulations, all prioritized compounds and the control inhibitor were evaluated using pkCSM for in silico ADMET profiling (**Supplementary information Table S4.1**). CMNPD16477, CMNPD21979, and CMNPD3605 met the predefined thresholds for absorption, distribution, metabolism, and toxicity, and were subsequently evaluated for their ability to disrupt the PD-1/PD-L1 protein–protein interaction in silico.




| Crystal Structure | Interacting Residues and its position in PD-L1 and PD-1 complex | | No of Residue |
|---|---|---|---|
| PD-1 PD-L1 Complex (4ZQK) | PD-L1 | F19,Y56,Q66,R113,A121, D122,Y123,K124,R125 | 9 |
| | PD-1 | N66,Y68,Q75,T76,K78, A132,E136 | 7 |

**Figure 4.3:** Structural visualization and residue-level analysis of the PD-1/PD-L1 complex (PDB: 4ZQK), highlighting interface residues within 3Å proximity. Identified contact residues were used to define the PD-L1 binding grid for virtual screening.

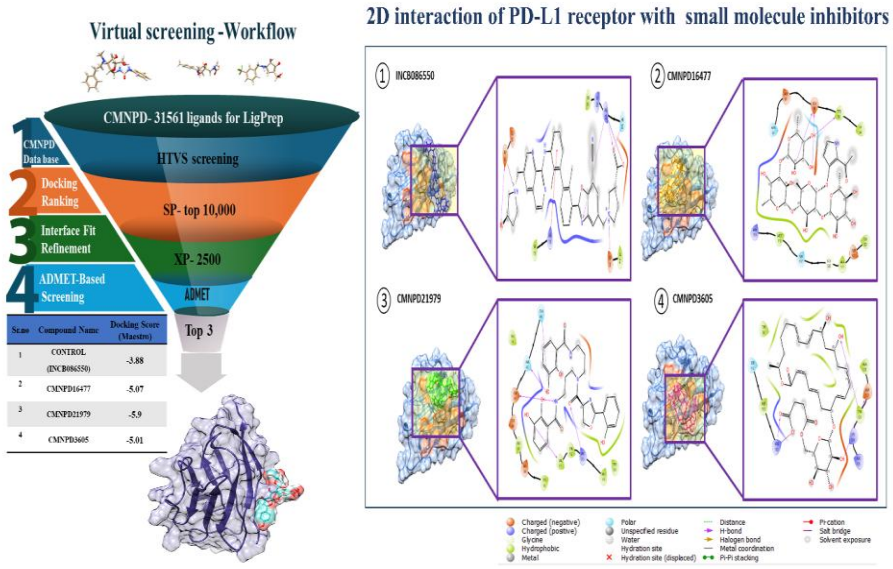
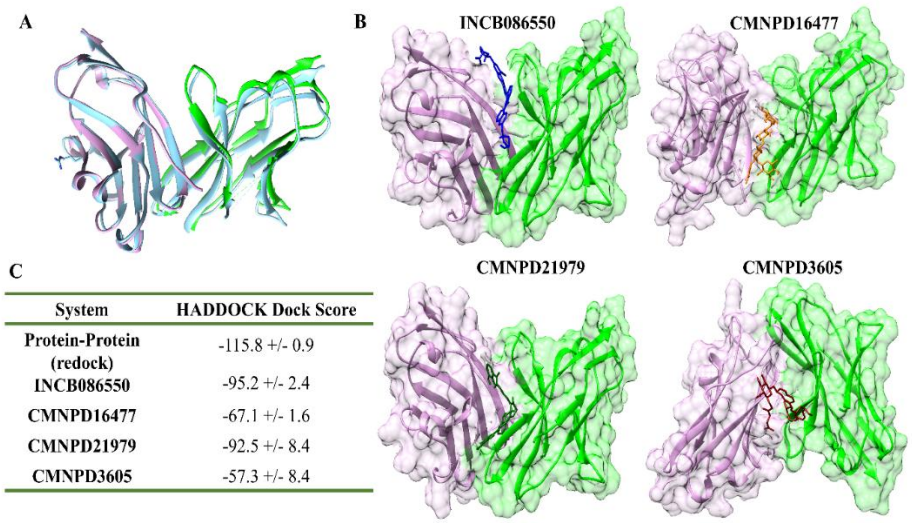



**Figure 4.4: Virtual screening workflow and molecular interaction of small-molecule inhibitors with PD-L1.** (A) Schematic representation of the virtual screening workflow used to identify potential PD-L1 inhibitors, including ligand selection, docking, and pharmacokinetic evaluation steps. (B) Two-dimensional interaction diagrams illustrating the binding modes of selected small-molecule inhibitors within the PD-L1 binding pocket, highlighting key residues involved in hydrogen bonding and hydrophobic interactions. The virtual screening and molecular docking analyses were performed using the Schrödinger Maestro suite, and the final figure was assembled using Microsoft PowerPoint.

**4.5.3 Protein–protein docking suggests inhibitor-mediated modulation of PD-1/PD-L1 binding:** Protein–protein docking of the PD-1/PD-L1 complex (PDB ID: 4ZQK) validated the native interface through redocking (−115.8 ± 0.9), see in **Figure 4.5A**. When ligands were introduced at the PD-L1 interface, the complexes showed altered docking scores and conformations, suggesting that the ligands may potentially modulate the interaction and reduce the ability of PD-1 and PD-L1 to associate in their native orientation. Among the tested compounds, CMNPD3605 was predicted to have the most favorable effect, with a docking score of −57.3 ± 8.4, compared to the control inhibitor INCB086550 (−95.2 ± 2.4). CMNPD21979 (−92.5 ± 8.4) and CMNPD16477 (−67.1 ± 1.6) also showed

potential to influence the complex, see in **Figure 4.5B & C**. These findings indicate that the prioritized ligands are predicted to interfere with PD-1/PD-L1 binding and may potentially modulate the stability of the complex relative to the control. All the complexes were subsequently advanced to explicit solvent molecular dynamics simulations. All four ligand–PD-L1 complexes were subjected to 200 ns all-atom explicit solvent molecular dynamics simulations under identical conditions. Trajectories were inspected to assess equilibration and production sampling. Each complex reached equilibrium within the initial 10 to 30 ns, and the remaining trajectory was treated as the production phase. Analysis of the trajectory mainly focused on overall structural stability, compactness, flexibility, and interaction profiles. Summary statistics for key structural and interaction parameters derived from the 200 ns production trajectories have been summarized in **Supplementary Information Table S4.2**.




| System | HADDOCK Dock Score |
|---|---|
| Protein-Protein (redock) | -115.8 +/- 0.9 |
| INCB086550 | -95.2 +/- 2.4 |
| CMNPD16477 | -67.1 +/- 1.6 |
| CMNPD21979 | -92.5 +/- 8.4 |
| CMNPD3605 | -57.3 +/- 8.4 |

**Figure 4.5. Molecular docking of PD-1/PD-L1 complex with control and top ligands.** (A) Structural alignment of the PD-1/PD-L1 protein–protein complex (PDB ID: 4ZQK) is shown, with the redocking of the native interface (PPI) serving as reference. B) Docking scores (mean ± SD) are summarized in the accompanying table, indicating relative protein-protein binding affinities compared to the native redock and control ligand. C) The control ligand INCB086550 is depicted in blue,

while three candidate ligands are shown bound at the interface: CMNPD16477 (orange), CMNPD21979 (green), and CMNPD3605 (pink).

### 4.5.4 Marine database-derived ligands enhance PD-L1 structural stability and binding persistence:

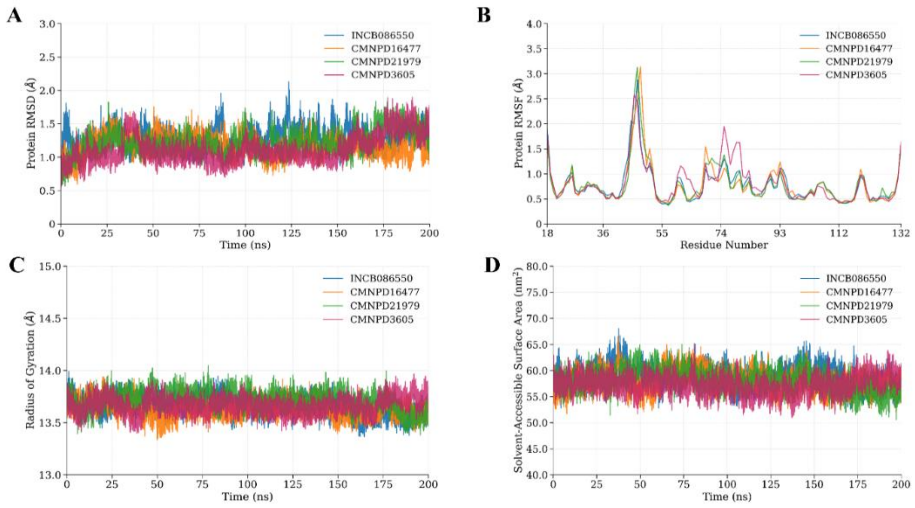



**Figure 4.6. Molecular dynamics trajectory analysis.** (A) RMSD showing overall structural stability during the simulation. (B) RMSF depicting residue-wise flexibility. (C) The radius of gyration (Rg) indicates protein compactness. (D) Solvent-accessible surface area (SASA) reflects changes in solvent exposure over time.

To check how each ligand influences PD-L1's structural behaviour, Root Mean Square Deviation (RMSD) analysis was done across the 200 ns simulation trajectory, see **Figure 4.6 A; Supplementary information Table S4.2**. RMSD evaluation showed that all protein-ligand complexes reached stability rapidly and remained in equilibrium throughout the simulation. Backbone deviations averaged between 1.13 and 1.31 Å, with only brief, minor fluctuations that stayed below 1.5 Å. Compared to the control complex ($1.31 \pm 0.15$ Å), all CMNPD ligand-bound systems exhibited lower or comparable RMSD values: CMNPD16477 showed the

lowest mean RMSD (1.13 ± 0.13 Å), suggesting enhanced conformational rigidity, while CMNPD21979 (1.28 ± 0.18 Å) and CMNPD3605 (1.19 ± 0.21 Å) also maintained stable profiles. The RMSD profiles show that the CMNPD ligands stabilize the PD-L1 structure as well as, or better than, the reference compound. All ligand-bound complexes quickly reached equilibrium and remained stable throughout the simulation. Subtle variations in the RMSD traces highlight how each ligand uniquely influences the protein's conformational stability and flexibility.

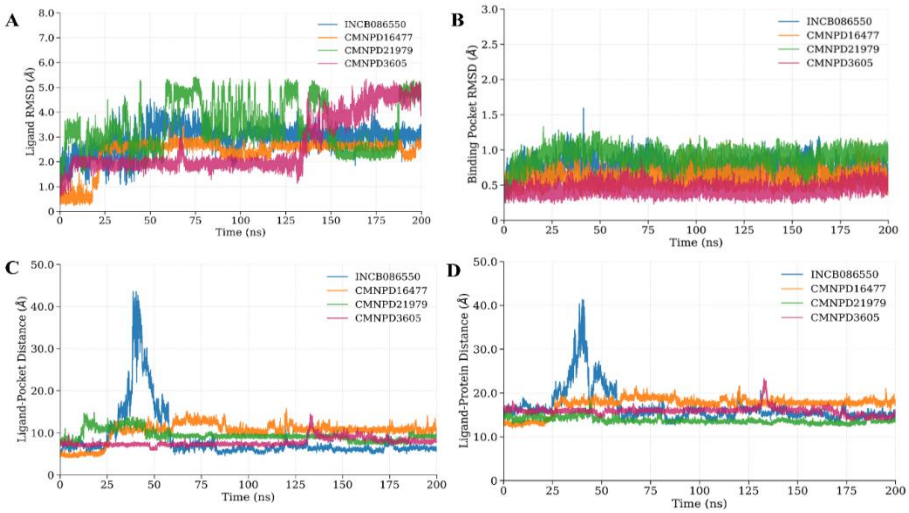



**Figure 4.7. Molecular dynamics analysis of PD-L1 complexes with INCB086550, CMNPD16477, CMNPD21979, and CMNPD3605. (A)** Ligand RMSD **(B)** Binding pocket RMSD **(C)** Ligand–pocket distance and **(D)** Ligand–protein distance plotted as a function of simulation time. These traces illustrate the degree of ligand stability, pocket rigidity, and spatial fluctuations for each system, allowing for direct comparison of binding persistence and conformational dynamics.

Using INCB086550 as a reference, the RMSD and distance profiles tracked over the 200 ns production runs highlighted unique interaction behaviours for each test compound, See **Figure 4.7; Supplementary information Table S4.2**. Compared to the control's moderate ligand mobility (ligand RMSD 3.09 ± 0.22 Å) and shortest pocket separation (6.34 ± 0.67 Å),

CMNPD16477 maintained the most conserved ligand pose (ligand RMSD $2.57 \pm 0.17$ Å) and a more stable pocket (pocket RMSD $0.61 \pm 0.11$ Å), despite sampling the largest ligand–pocket and ligand–protein separations ($10.82 \pm 0.67$ Å and $17.86 \pm 0.88$ Å), indicating a stable but more external binding geometry. CMNPD21979 exhibited a broader ensemble of ligand conformations (ligand RMSD $3.50 \pm 1.05$ Å) and induced the greatest pocket flexibility (pocket RMSD $0.90 \pm 0.09$ Å), with intermediate ligand–pocket distance ($8.75 \pm 0.67$ Å) and the shortest ligand–protein separation ($13.39 \pm 0.37$ Å), reflecting a compact yet dynamically flexible placement. CMNPD3605 showed similar ligand heterogeneity (ligand RMSD $3.37 \pm 1.19$ Å), but achieved the greatest rigidity in the local pocket (pocket RMSD $0.45 \pm 0.08$ Å), with ligand–pocket and ligand–protein distances ($8.30 \pm 1.06$ Å and $15.87 \pm 0.98$ Å) falling between the other ligands. Across the simulation, the binding pocket interaction with CMNPD3605 remained consistently stable, even with ligand movement. All the selected compounds maintained steady ligand–protein and ligand–pocket distances which indicate sustained binding with no signs of transient dissociation. However, the control ligand experienced a brief dissociation near the 50 ns time point. This consistent behaviour highlights robust interactions between the ligands and the PD-L1 binding site. To gain deeper insight how these interactions influence PD-L1's structural dynamics, the next step involved analysing residue-level flexibility.

**4.5.5 Root-mean-square fluctuation analysis reveals PD-L1 stabilization by marine database-derived ligands:** Upon analysing the RMSF values of PD-L1 residues 18-132, two regions were found to show relatively increased fluctuation; one peak was around the residues 47-49, and another lay approximately at residues 63-83. It is to be noted that both these regions are located away from the key interacting surface consisting of residues F19, Y56, Q66, R113, A121, D122, Y123, K124, and R125, and thus represent flexible loop regions that are positioned far from the ligand-binding interface. Apart from the fluctuations seen in those two regions, all

three molecules showed reduced mobility at the interface and interacted with the nine key residues, which reflects a stable binding surface; see Figure **4.6B; Supplementary information Table S4.2**. Minimum compound-specific fluctuations were observed, but they stayed confined to limited regions. CMNPD3605 showed a slight increase in flexibility at residue 66 (~0.8 Å compared to ~0.5 Å for the others), while CMNPD21979 exhibited a modest rise at residues 124–125 (~0.7 Å versus ~0.5–0.6 Å). Minor fluctuations did not compromise the stability of the interface. Overall, the findings indicate that all three ligands reinforce the PD-1 binding surface. To validate this effect further, global structural parameters were examined to evaluate protein integrity and solvent exposure.

**4.5.6 Protein compactness and solvent exposure validate structural integrity of ligand-bound PD-L1 complexes:** To evaluate how PD-L1 behaves when bound to the three ligands, the radius of gyration (Rg) was assessed throughout the 200 ns production runs. The results provide a view of the protein's overall folding and show that it consistently retained a compact, stable conformation in all ligand-bound states, see Figure **4.6C; Supplementary information Table S4.2**. All ligand-bound PD-L1 systems remained structurally compact and well-folded throughout the simulation, with average radius of gyration (Rg) values showing minimal variation: INCB086550 ($13.62 \pm 0.08$ Å), CMNPD16477 ($13.60 \pm 0.07$ Å), CMNPD21979 ($13.69 \pm 0.09$ Å), and CMNPD3605 ($13.67 \pm 0.08$ Å). The close similarity in Rg values indicates that each ligand helps PD-L1 retain its native compact fold, with no evidence of loosening or unfolding. Among the tested compounds, CMNPD16477 showed the lowest average Rg, suggesting a modest increase in protein compaction compared with both the reference and the other ligand-bound systems. In all cases, the Rg stabilised early and remained steady throughout the trajectory, in line with the low RMSD values and the strong interface stability observed for these ligands. Taken together, these results confirm that all three compounds support the structural integrity of PD-L1 during extended simulations.

Consistent with this, Solvent-accessible surface area (SASA) analysis over the 200 ns trajectories revealed that all ligand-bound PD-L1 complexes maintained consistently low and tightly grouped SASA values. This demonstrates that none of the compounds induced significant unfolding or increased exposure of the protein surface, see **Figure 4.6D; Supplementary information Table S4.2**. CMNPD16477 and CMNPD21979 exhibited nearly identical SASA profiles, averaging $57.44 \pm 1.58$ and $57.27 \pm 1.89$ nm², respectively. CMNPD3605 displayed the lowest mean SASA ($57.03 \pm 1.94$ nm²), suggesting slightly reduced solvent exposure at the binding interface. By contrast, the control compound INCB086550 recorded the highest average SASA ($58.24 \pm 1.96$ nm²), reflecting a modest increase in surface accessibility. The small differences in fluctuations across all systems indicate that structural adjustments did not disturb the overall fold of PD-L1. These results align with the compactness observed in the ligand-bound states and support the conclusion that each compound potentially contributes to maintaining PD-L1's structural integrity. To further understand the molecular basis of this stability, hydrogen-bonding analysis was carried out to evaluate how consistently and selectively each ligand engages the PD-L1 interface.

**4.5.7 Hydrogen bonding patterns indicate stable and selective ligand anchoring at the PD-L1 interface:** The hydrogen bonding pattern of the ligands at the PD-L1 interface played a central role in defining their stability and selectivity, see **Figure 4.8; Supplementary information Table S4.3**. CMNPD16477 consistently engaged Gln66 (16.45% occupancy) and Ser117 (19.45%), supporting a stable binding pose that may support its inhibitory effect and target specificity. In contrast, CMNPD21979 adopted a more flexible binding mode, with no hydrogen bond occupancy exceeding 10%. For most of the trajectory, its hydrogen bond count was close to zero, reflecting a tendency to assume multiple conformations and a less persistent inhibitory profile. Among the compounds tested, CMNPD3605 showed the

most robust interaction pattern. It formed durable hydrogen bonds with key interface residues, Arg113 and Arg125, with Arg113 reaching 50.87% occupancy. Over the course of the simulation, CMNPD3605 maintained an average of 4–6 hydrogen bonds and occasionally reached as many as 11, highlighting its strong anchoring and resistance to dissociation. By comparison, the control compound INCB086550 exhibited moderate hydrogen bond occupancy with several polar and charged residues, resulting in intermediate bond numbers and a more diffuse interaction profile. Overall, CMNPD3605 emerged as the most effective ligand in terms of hydrogen bonding, surpassing the control compound by establishing a focused and long-lasting interaction network. This strong and persistent binding suggests its potential to act as a putative inhibitor of PD-L1 interactions, as summarized in **Supplementary information Table S4.3**. To further investigate the energetic basis of these interactions, binding free energy calculations were performed.

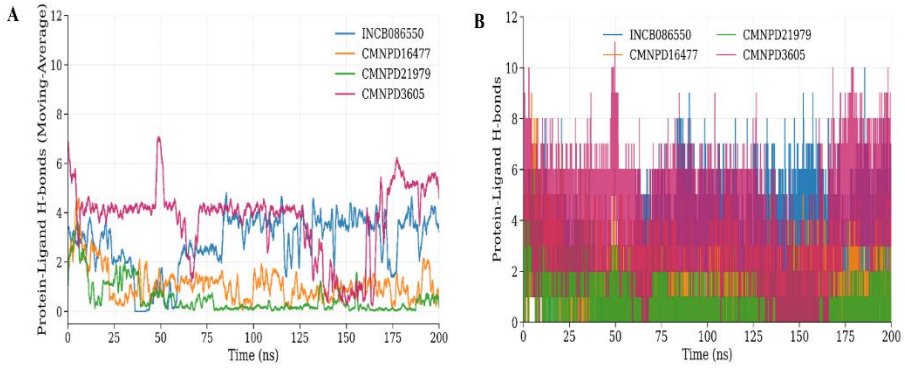
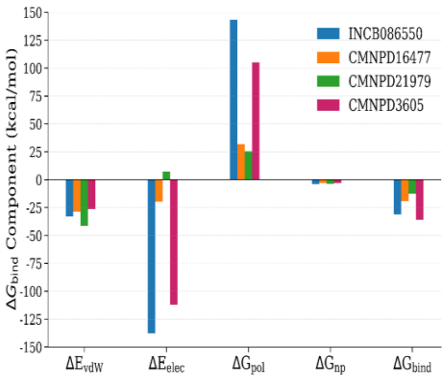



**Figure 4.8: Protein–ligand hydrogen bond formation during 200 ns molecular dynamics simulations for PD-L1 complexes with INCB086550, CMNPD16477, CMNPD21979, and CMNPD3605.** (A) Moving-average number of hydrogen bonds quantifies persistence and fluctuation of polar contacts, and (B) total hydrogen bonds at each timestep reveal the overall temporal pattern and differences in anchoring strategy among ligands.

**4.5.8 End-state free energy decomposition identifies CMNPD3605 as the most thermodynamically favourable PD-L1 binder:** To evaluate the binding strength of each compound with PD-L1, MM/PBSA calculations were performed. This well-established method [47–49] breaks down the total binding free energy into its individual components, as illustrated in **Figure 4.9**. The accompanying bar chart and table present the mean values and standard deviations for each term, together with the overall $\Delta G_{bind}$ for every complex. This analysis aimed to clarify the energetic contributions that either support or oppose stable ligand–protein interactions. Among the compounds tested, CMNPD16477 exhibited the weakest binding affinity. CMNPD21979 contributed a strong van der Waals component ($\Delta E_{vdW}$ = −41.49 ± 0.10 kcal/mol) and achieved moderate overall binding strength. On the other hand, CMNPD3605 emerged as the top-performing ligand, with the most favourable total binding free energy (ΔGbind = −35.95 ± 0.16 kcal/mol), outperforming even the reference compound INCB086550 (ΔGbind = −31.28 ± 0.23 kcal/mol). This result positions CMNPD3605 as the most promising predicted candidate among the marine database-derived ligands, with a stronger thermodynamic profile than the control. In all systems, van der Waals and electrostatic interactions were the primary contributors to binding, and solvation energies were important in shaping the net affinity. Complex formation was always favored by nonpolar solvation ($\Delta G_{np}$) and inhibited by polar solvation ($\Delta G_{pol}$) because of their positive terms. Interestingly, CMNPD21979 exhibited very favourable interactions between van der Waals, but the binding energy of the entire system was not optimum, which highlights the significance of balancing between solvation and electrostatic potential. Taken together, these results highlight CMNPD3605 as the most potent PD-L1 binder in the series and a promising candidate to be developed as a PD-L1/PD-1 interaction inhibitor. In order to identify the residues that are most important in this binding profile, a residue-level energy decomposition was performed subsequently. It should be noted that the entropic contribution (−TΔS) was

not included in these MM/PBSA calculations. While this omission may influence comparisons between ligands of differing conformational flexibility, particularly CMNPD21979, the consistently favourable van der Waals and electrostatic interactions observed for CMNPD3605 provide strong support for its binding stability. Thus, even within this methodological limitation, CMNPD3605 is predicted to exhibit a robust thermodynamic profile relative to the control inhibitor.

A




B

| SYSTEM | $\Delta E_{vdW}$ | $\Delta E_{elec}$ | $\Delta G_{pol}$ | $\Delta G_{np}$ | $\Delta G_{bind}$ |
|---|---|---|---|---|---|
| CONTROL | -33.16 | -137.51 | 143.32 | -3.93 | -31.28 |
| (INCB086550) | (0.17) | (1.24) | (1.12) | (0.01) | (0.23) |
| CMNPD16477 | -28.50 | -19.44 | 31.88 | -3.19 | -19.26 |
| | (0.09) | (0.21) | (0.17) | (0.01) | (0.11) |
| CMNPD21979 | -41.49 | 7.13 | 25.39 | -3.76 | -12.74 |
| | (0.10) | (0.15) | (0.18) | (0.008) | (0.13) |
| CMNPD3605 | -26.11 | -111.87 | 105.23 | -3.20 | -35.95 |
| | (0.10) | (0.45) | (0.43) | (0.01) | (0.16) |

**Figure 4.9:** MM/PBSA binding free energy decomposition for PD-L1 complexes with INCB086550, CMNPD16477, CMNPD21979, and CMNPD3605. Bars depict the contributions (kcal/mol) of van der Waals (ΔE_vdW), electrostatic (ΔE_elec), polar solvation (ΔG_pol), and nonpolar (ΔG_np) terms, as well as total binding free energy (ΔG_bind), highlighting differences in the thermodynamic drivers of binding across ligand systems.

**4.5.9 Residue-level MM/PBSA analysis pinpoints key anchoring residues and confirms CMNPD3605 as the most stabilizing ligand:** To gain a more detailed insight into the role of individual residues in the stability of these complexes, a residue-wise MM/PBSA decomposition was conducted on each of the ligand-PD-L1 complexes (**Supplementary information Table S4.4**). When comparing overall ligand contributions, the control compound INCB086550 showed the strongest stabilizing effect (−22.65 kcal/mol), followed by CMNPD3605 (−15.63 kcal/mol),

CMNPD21979 (−8.10 kcal/mol), and CMNPD16477 (−7.48 kcal/mol). CMNPD3605 was the most striking ligand of marine origin since its stabilization profile was closest to the control, and it was much stronger than either of the others. In all systems, arginine residues proved to be important anchoring points. In the case of CMNPD3605, Arg113 and Arg125 were useful for complex stability, with $\Delta G_{total}$ values of −8.49 and −7.89 kcal/mol, respectively. Arg113 interacted with CMNPD21979 with less strength (−2.43 kcal/mol). Tyr56 consistently provided favourable van der Waals interactions, contributing modest stabilization (−1.54 kcal/mol for CMNPD16477 and −3.07 kcal/mol for CMNPD21979). Additional support came from residues like Ala121, Tyr123, and Met115, which helped reinforce packing around the main anchors. For example, Tyr123 contributed −1.98 kcal/mol for CMNPD3605, while Met115 showed stabilizing effects across all ligands, ranging from −0.96 to −2.83 kcal/mol. Some polar residues, including Asp122 and Lys124, introduced desolvation penalties when not fully compensated by new electrostatic contacts. For instance, Asp122 contributed +0.97 kcal/mol in the CMNPD3605 complex, and Lys124 showed a G_total value of +1.56 kcal/mol in the control, consistent with unfavourable polar solvation terms.

Overall, CMNPD3605 attains superior per-residue stabilization by engaging both R113 and R125 and by recruiting supportive van der Waals contacts (Met115, Tyr123), which together explain its more favourable ligand-level $\Delta G_{total}$ relative to the other screened compounds. In short, CMNPD16477 contributes to structural stabilization and compactness, CMNPD21979 offers a flexible binding mode suited to dynamic targets, and CMNPD3605 excels in forming persistent, high-occupancy interactions with critical interface residues. CMNPD3605 demonstrated the most favorable thermodynamic profile among the novel ligands, closely aligning with the control compound and emerging as the strongest candidate for further development. All three ligands preserved PD-L1's

global fold and compactness during the simulations, showing consistent binding and energetics that support their potential as effective modulators. Taken together, the combination of robust thermodynamic performance, specific binding interactions, and sustained structural stability highlights CMNPD3605 as a potential lead candidate for future therapeutic exploration.

### 4.6 Discussion and conclusion

CRC-derived exosomes upregulated PD-L1 expression in macrophages, which supports an immunosuppressive phenotype. Furthermore, this exosome-educated macrophage-derived factor enhances PD-L1 expression in CRC cells, revealing previously unrecognized bidirectional communication between CRC cells and macrophages. This observation demonstrates for the first time that CRC-derived exosome not only directly modulates macrophage function but also reprogram macrophages to further reinforce immune checkpoint signaling in cancer cells. This positive feedback mechanism promotes suppression of T cells mediated anti-tumor immune response. Given the central role of PD-L1 in exosome-mediated immune suppressive mechanisms, we further explored therapeutic strategies to disrupt PD-1/PD-L1 signaling.

Three candidate pharmaceuticals were identified using in-silico docking as stable binders of the PD-L1 pocket, capable of inhibiting PD-1/PD-L1 interactions and preserving T cell-mediated antitumor efficacy. The PD-1/PD-L1 axis is crucial in the majority of malignancies, and its inhibition is challenging due to its flat and hydrophobic surface. Even so, seven FDA-approved antibodies available since 2006 have shown notable anticancer effects [50]. Despite this progress, the adaptive nature and molecular heterogeneity of tumor lead to a few patients failing to respond to these highly specific therapies [51]. The development of small-molecule inhibitors is essential to overcome the challenges associated with antibodies. Small-molecule inhibitors offer distinct advantages over

antibody-based therapies, including suitability for oral administration, minimal immunogenicity and a relatively short half-life, which allows rapid management of any adverse reactions. Although PD-L1 is a challenging target due to its predominantly flat and hydrophobic interface, our screened compound achieves stronger predicted binding and stability than inhibitors currently available in clinical trials.

This study employed a comprehensive pipeline that included hierarchical virtual screening, ADMET evaluation, and molecular dynamics simulation. Similar methodological frameworks have been reported in earlier work, such as Li et al. 2025, who combined interface-guided docking with long-timescale MD simulations to evaluate small-molecule modulators of protein–protein interactions [52]. In line with such precedents, our study applied a validated docking protocol and extended explicit solvent MD simulations to assess the stability and interaction profiles of marine-derived ligands at the PD-1/PD-L1 interface. Through this integrated approach, marine natural product–derived ligands were identified as promising new compounds with PD-L1 inhibitory potential. The analysis has shown that all the shortlisted CMNPD compounds had some properties that were useful in stabilizing the PD-L1 structure and interacting with critical binding residues. The study focused on defining and targeting the important PD-L1 interface site and comparing the best binders with a recognized small-molecule inhibitor. All selected compounds maintained the structural integrity and compactness of PD-L1 throughout the 200 ns molecular dynamics simulations. The stability of their binding was further supported by van der Waals and electrostatic interactions, as confirmed by per-residue MM/PBSA decomposition. The prominent interactions with Arg113 and Arg125 indicated that these residue sites are critical for effective inhibition. Identification of hotspot residues (Y56, Y123, K124, M115) from previous studies [52] aligns with our observation that Arg113 and Arg125, together with adjacent interface residues, contribute to ligand stabilization. This

convergence indicates that our results are consistent with established computational insights, while extending them to marine-derived scaffolds.

The marine compounds were found to form more persistent and multivalent hydrogen interactions with the interface residues in comparison with INCB086550, and thereby increase more of the stabilization of the PD-L1 structure. Their unique chemical scaffolds and binding characteristics suggest that they may offer potential benefits over existing PD-L1 inhibitors. CMNPD16477 consistently reduced interface flexibility, promoted a more compact protein structure, and formed stable polar contacts, together supporting a persistent binding mode and the potential for prolonged inhibition. However, it had the lowest binding affinity compared to the compounds that were analysed. CMNPD21979 did not affect the overall compactness or interface integrity of the protein, but exhibited less hydrogen bond occupancy and more ligand RMSD. CMNPD3605 was the best ligand among the three test compounds in this study, as it demonstrated stable hydrogen bonding and high binding free energy, indicative of high anchoring and increased affinity, especially at the core residues of PD-L1. It showed long-lasting high-affinity binding with important interface residues with the most favourable thermodynamic profile among the marine database-derived compounds. CMNPD3605 was able to sustain a steady protein conformation with time and provided similar or even better results than the benchmark inhibitor INCB086550. Based on these in silico results, CMNPD3605 represents a promising candidate for further preclinical and clinical development as a PD-L1 inhibitor for PD-L1–associated conditions. Definitely, in the future, we will plan experimental validation of lead compounds.

To conclude, marine-derived ligands explored in this study show potential for further development as small-molecule immune checkpoint inhibitors. The in-silico analyses provided detailed insights into their binding mechanisms and stabilizing effects on the PD-L1 interface, offering a

foundation for future experimental validation. CMNPD3605 is the most promising candidate for prompt preclinical and clinical assessment. Nonetheless, the remaining two ligands, CMNPD16477 and CMNPD21979, demonstrated encouraging molecular dynamics outcomes and could significantly benefit from focused optimization and modification to enhance their therapeutic efficacy.

## 4.7 References


[1] K. Mani, D. Deng, C. Lin, M. Wang, M.L. Hsu, N.G. Zaorsky, Causes of death among people living with metastatic cancer, Nat Commun 15 (2024) 1519. https://doi.org/10.1038/s41467-024-45307-x.

[2] R.L. Siegel, N.S. Wagle, J. Star, T.B. Kratzer, R.A. Smith, A. Jemal, Colorectal cancer statistics, 2026, CA A Cancer J Clinicians 76 (2026) e70067. https://doi.org/10.3322/caac.70067.

[3] K. Wadhonkar, D. Das, R. Kant Chittela, A.G. Obukhov, M.S. Baig, Role of colorectal cancer-derived exosomes in modulating macrophage phenotype during tumor development, Carcinogenesis 47 (2025) bgag003. https://doi.org/10.1093/carcin/bgag003.

[4] K. Wadhonkar, Y. Singh, A. Rughetti, S. Das, R. Yangdol, M.H. Sk, M.S. Baig, Role of cancer cell-derived exosomal glycoproteins in macrophage polarization, Mol Biol Rep 52 (2025) 451. https://doi.org/10.1007/s11033-025-10535-x.

[5] K.E. de Visser, J.A. Joyce, The evolving tumor microenvironment: From cancer initiation to metastatic outgrowth, Cancer Cell 41 (2023) 374–403. https://doi.org/10.1016/j.ccell.2023.02.016.

[6] K. Wadhonkar, N. Singh, F.M. Heralde, S.P. Parihar, N. Hirani, M.S. Baig, Exosome-derived miRNAs regulate macrophage-colorectal

cancer cell cross-talk during aggressive tumor development, Colorect. Cancer 12 (2023) CRC40. https://doi.org/10.2217/crc-2022-0012.

[7] K. Wadhonkar, S. Das, R. Subramanian, M.H. Sk, Y. Singh, M.S. Baig, The effect of cancer cell-derived exosomal proteins on macrophage polarization: An in-depth review, Experimental Cell Research 444 (2025) 114393. https://doi.org/10.1016/j.yexcr.2024.114393.

[8] J.-W. Cui, Y. Li, Y. Yang, H.-K. Yang, J.-M. Dong, Z.-H. Xiao, X. He, J.-H. Guo, R.-Q. Wang, B. Dai, Z.-L. Zhou, Tumor immunotherapy resistance: Revealing the mechanism of PD-1 / PD-L1-mediated tumor immune escape, Biomedicine & Pharmacotherapy 171 (2024) 116203. https://doi.org/10.1016/j.biopha.2024.116203.

[9] H. Dong, S.E. Strome, D.R. Salomao, H. Tamura, F. Hirano, D.B. Flies, P.C. Roche, J. Lu, G. Zhu, K. Tamada, V.A. Lennon, E. Celis, L. Chen, Tumor-associated B7-H1 promotes T-cell apoptosis: A potential mechanism of immune evasion, Nat Med 8 (2002) 793–800. https://doi.org/10.1038/nm730.

[10] Y. Yin, B. Liu, Y. Cao, S. Yao, Y. Liu, G. Jin, Y. Qin, Y. Chen, K. Cui, L. Zhou, Z. Bian, B. Fei, S. Huang, Z. Huang, Colorectal Cancer-Derived Small Extracellular Vesicles Promote Tumor Immune Evasion by Upregulating PD-L1 Expression in Tumor-Associated Macrophages, Advanced Science 9 (2022) 2102620. https://doi.org/10.1002/advs.202102620.

[11] R.I. Alsantali, A.M. Almohyawi, M.A. Rather, J.M. Mir, N.A. Dangroo, F.A. Almalki, T. Ben Hadda, R.S. Jassas, S.I. Alkubaysi, S.A. Ahmed, From silico to benchtop: cosmosiin as a PD-1/PDL-1 immune checkpoint inhibitor revealed through DFT, network pharmacology analysis, and molecular docking integrated experimental verification, RSC Adv. 15 (2025) 22285–22310. https://doi.org/10.1039/D5RA03831F.

[12] L. Xia, Y. Liu, Y. Wang, PD-1/PD-L1 Blockade Therapy in Advanced Non-Small-Cell Lung Cancer: Current Status and Future Directions, The Oncologist 24 (2019) S31–S41. https://doi.org/10.1634/theoncologist.2019-IO-S1-s05.

[13] L.A. Emens, Breast Cancer Immunotherapy: Facts and Hopes, Clinical Cancer Research 24 (2018) 511–520. https://doi.org/10.1158/1078-0432.CCR-16-3001.

[14] X. Liu, M.G. Choi, K. Kim, K.-M. Kim, S.T. Kim, S.H. Park, R. Cristescu, S. Peter, J. Lee, High PD-L1 expression in gastric cancer (GC) patients and correlation with molecular features, Pathology - Research and Practice 216 (2020) 152881. https://doi.org/10.1016/j.prp.2020.152881.

[15] M.-M. Zhan, X.-Q. Hu, X.-X. Liu, B.-F. Ruan, J. Xu, C. Liao, From monoclonal antibodies to small molecules: the development of inhibitors targeting the PD-1/PD-L1 pathway, Drug Discovery Today 21 (2016) 1027–1036. https://doi.org/10.1016/j.drudis.2016.04.011.

[16] S. Tan, C.W.-H. Zhang, G.F. Gao, Seeing is believing: anti-PD-1/PD-L1 monoclonal antibodies in action for checkpoint blockade tumor immunotherapy, Sig Transduct Target Ther 1 (2016) 16029. https://doi.org/10.1038/sigtrans.2016.29.

[17] M.A. Rather, S. Rasool, A. Khursheed, S.S.S.J. Ahmed, F. Bashir, A.H. Shalla, B.N. Dar, J.M. Mir, N.A. Dangroo, Decoding the Therapeutic Potential of Apigenin as a Nonpeptide *PD-1/PD-L1* Immune Checkpoint Inhibitor in Breast Cancer: An Integrated, Multimethod Study Using Network Pharmacology, Bioinformatics, Molecular Docking, and Dynamics Simulations, Journal of Chemistry 2025 (2025) 5133015. https://doi.org/10.1155/joch/5133015.

[18] K.M. Zak, G. Dubin, T.A. Holak, Structure of the complex of human programmed death-1 (PD-1) and its ligand PD-L1.: 4zqk, (2015). https://doi.org/10.2210/pdb4zqk/pdb.

[19] E.F. Pettersen, T.D. Goddard, C.C. Huang, G.S. Couch, D.M. Greenblatt, E.C. Meng, T.E. Ferrin, UCSF Chimera—A visualization system for exploratory research and analysis, J Comput Chem 25 (2004) 1605–1612. https://doi.org/10.1002/jcc.20084.

[20] G. Madhavi Sastry, M. Adzhigirey, T. Day, R. Annabhimoju, W. Sherman, Protein and ligand preparation: parameters, protocols, and influence on virtual screening enrichments, J Comput Aided Mol Des 27 (2013) 221–234. https://doi.org/10.1007/s10822-013-9644-8.

[21] M. Bojko, K. Węgrzyn, E. Sikorska, M. Kocikowski, M. Parys, C. Battin, P. Steinberger, M.M. Kogut, M. Winnicki, A.K. Sieradzan, M. Spodzieja, S. Rodziewicz-Motowidło, Design, synthesis and biological evaluation of PD-1 derived peptides as inhibitors of PD-1/PD-L1 complex formation for cancer therapy, Bioorganic Chemistry 128 (2022) 106047. https://doi.org/10.1016/j.bioorg.2022.106047.

[22] Schrödinger Release 2025-3: Glide, Schrödinger, LLC, New York, NY, 2025.), (n.d.).

[23] C. Lyu, T. Chen, B. Qiang, N. Liu, H. Wang, L. Zhang, Z. Liu, CMNPD: a comprehensive marine natural products database towards facilitating drug discovery from the ocean, Nucleic Acids Research 49 (2021) D509–D515. https://doi.org/10.1093/nar/gkaa763.

[24] Schrödinger Release 2025-3: LigPrep, Schrödinger, LLC, New York, NY, 2025., (n.d.).

[25] K. Roos, C. Wu, W. Damm, M. Reboul, J.M. Stevenson, C. Lu, M.K. Dahlgren, S. Mondal, W. Chen, L. Wang, R. Abel, R.A. Friesner, E.D. Harder, OPLS3e: Extending Force Field Coverage for Drug-Like Small

Molecules, J. Chem. Theory Comput. 15 (2019) 1863–1874. https://doi.org/10.1021/acs.jctc.8b01026.

[26] Y. Yang, K. Yao, M.P. Repasky, K. Leswing, R. Abel, B.K. Shoichet, S.V. Jerome, Efficient Exploration of Chemical Space with Docking and Deep Learning, J. Chem. Theory Comput. 17 (2021) 7106–7119. https://doi.org/10.1021/acs.jctc.1c00810.

[27] H.K. Koblish, L. Wu, L.-C.S. Wang, P.C.C. Liu, R. Wynn, J. Rios-Doria, S. Spitz, H. Liu, A. Volgina, N. Zolotarjova, K. Kapilashrami, E. Behshad, M. Covington, Y. Yang, J. Li, S. Diamond, M. Soloviev, K. O'Hayer, S. Rubin, C. Kanellopoulou, G. Yang, M. Rupar, D. DiMatteo, L. Lin, C. Stevens, Y. Zhang, P. Thekkat, R. Geschwindt, C. Marando, S. Yeleswaram, J. Jackson, P. Scherle, R. Huber, W. Yao, G. Hollis, Characterization of INCB086550: A Potent and Novel Small-Molecule PD-L1 Inhibitor, Cancer Discovery 12 (2022) 1482–1499. https://doi.org/10.1158/2159-8290.CD-21-1156.

[28] D.E.V. Pires, T.L. Blundell, D.B. Ascher, pkCSM: Predicting Small-Molecule Pharmacokinetic and Toxicity Properties Using Graph-Based Signatures, J. Med. Chem. 58 (2015) 4066–4072. https://doi.org/10.1021/acs.jmedchem.5b00104.

[29] C. Dominguez, R. Boelens, A.M.J.J. Bonvin, HADDOCK: A Protein−Protein Docking Approach Based on Biochemical or Biophysical Information, J. Am. Chem. Soc. 125 (2003) 1731–1737. https://doi.org/10.1021/ja026939x.

[30] D.A. Case, T.E. Cheatham, T. Darden, H. Gohlke, R. Luo, K.M. Merz, A. Onufriev, C. Simmerling, B. Wang, R.J. Woods, The Amber biomolecular simulation programs, J Comput Chem 26 (2005) 1668–1688. https://doi.org/10.1002/jcc.20290.

[31] D.J. Price, C.L. Brooks, A modified TIP3P water potential for simulation with Ewald summation, The Journal of Chemical Physics 121 (2004) 10096–10103. https://doi.org/10.1063/1.1808117.

[32] J.A. Maier, C. Martinez, K. Kasavajhala, L. Wickstrom, K.E. Hauser, C. Simmerling, ff14SB: Improving the Accuracy of Protein Side Chain and Backbone Parameters from ff99SB, J. Chem. Theory Comput. 11 (2015) 3696–3713. https://doi.org/10.1021/acs.jctc.5b00255.

[33] A. Jakalian, D.B. Jack, C.I. Bayly, Fast, efficient generation of high-quality atomic charges. AM1-BCC model: II. Parameterization and validation, J Comput Chem 23 (2002) 1623–1641. https://doi.org/10.1002/jcc.10128.

[34] J. Wang, R.M. Wolf, J.W. Caldwell, P.A. Kollman, D.A. Case, Development and testing of a general amber force field, J Comput Chem 25 (2004) 1157–1174. https://doi.org/10.1002/jcc.20035.

[35] A.W. Götz, M.J. Williamson, D. Xu, D. Poole, S. Le Grand, R.C. Walker, Routine Microsecond Molecular Dynamics Simulations with AMBER on GPUs. 1. Generalized Born, J. Chem. Theory Comput. 8 (2012) 1542–1555. https://doi.org/10.1021/ct200909j.

[36] T.-S. Lee, D.S. Cerutti, D. Mermelstein, C. Lin, S. LeGrand, T.J. Giese, A. Roitberg, D.A. Case, R.C. Walker, D.M. York, GPU-Accelerated Molecular Dynamics and Free Energy Methods in Amber18: Performance Enhancements and New Features, J. Chem. Inf. Model. 58 (2018) 2043–2050. https://doi.org/10.1021/acs.jcim.8b00462.

[37] R. Salomon-Ferrer, A.W. Götz, D. Poole, S. Le Grand, R.C. Walker, Routine Microsecond Molecular Dynamics Simulations with AMBER on GPUs. 2. Explicit Solvent Particle Mesh Ewald, J. Chem. Theory Comput. 9 (2013) 3878–3888. https://doi.org/10.1021/ct400314y.

[38] T. Darden, D. York, L. Pedersen, Particle mesh Ewald: An $N \cdot \log(N)$ method for Ewald sums in large systems, The Journal of Chemical Physics 98 (1993) 10089–10092. https://doi.org/10.1063/1.464397.

[39] V. Kr□utler, W.F. Van Gunsteren, P.H. H□nenberger, A fast SHAKE algorithm to solve distance constraint equations for small molecules in molecular dynamics simulations, J. Comput. Chem. 22 (2001) 501–508. https://doi.org/10.1002/1096-987X(20010415)22:5%3C501::AID-JCC1021%3E3.0.CO;2-V.

[40] H.J.C. Berendsen, J.P.M. Postma, W.F. Van Gunsteren, A. DiNola, J.R. Haak, Molecular dynamics with coupling to an external bath, The Journal of Chemical Physics 81 (1984) 3684–3690. https://doi.org/10.1063/1.448118.

[41] R.J. Loncharich, B.R. Brooks, R.W. Pastor, Langevin dynamics of peptides: The frictional dependence of isomerization rates of $N$-acetylalanyl-$N'$-methylamide, Biopolymers 32 (1992) 523–535. https://doi.org/10.1002/bip.360320508.

[42] R.W. Pastor, B.R. Brooks, A. Szabo, An analysis of the accuracy of Langevin and molecular dynamics algorithms, Molecular Physics 65 (1988) 1409–1419. https://doi.org/10.1080/00268978800101881.

[43] D.R. Roe, T.E. Cheatham, PTRAJ and CPPTRAJ: Software for Processing and Analysis of Molecular Dynamics Trajectory Data, J. Chem. Theory Comput. 9 (2013) 3084–3095. https://doi.org/10.1021/ct400341p.

[44] P.A. Kollman, I. Massova, C. Reyes, B. Kuhn, S. Huo, L. Chong, M. Lee, T. Lee, Y. Duan, W. Wang, O. Donini, P. Cieplak, J. Srinivasan, D.A. Case, T.E. Cheatham, Calculating Structures and Free Energies of Complex Molecules: Combining Molecular Mechanics and Continuum Models, Acc. Chem. Res. 33 (2000) 889–897. https://doi.org/10.1021/ar000033j.

[45] B.R. Miller, T.D. McGee, J.M. Swails, N. Homeyer, H. Gohlke, A.E. Roitberg, *MMPBSA.py* : An Efficient Program for End-State Free Energy Calculations, J. Chem. Theory Comput. 8 (2012) 3314–3321. https://doi.org/10.1021/ct300418h.

[46] S.K. Panday, E. Alexov, Protein–Protein Binding Free Energy Predictions with the MM/PBSA Approach Complemented with the Gaussian-Based Method for Entropy Estimation, ACS Omega 7 (2022) 11057–11067. https://doi.org/10.1021/acsomega.1c07037.

[47] Y. Başar, İ. Demirtaş, S. Yenigün, Y. İpek, T. Özen, L. Behçet, Molecular docking, molecular dynamics, MM/PBSA approaches and bioactivity studies of nepetanudoside B isolated from endemic *Nepeta aristata*, Journal of Biomolecular Structure and Dynamics 43 (2025) 5486–5499. https://doi.org/10.1080/07391102.2024.2309641.

[48] S. El Rhabori, M. Alaqarbeh, L. Naanaai, Y. El Allouche, A. El Aissouq, M. Bouachrine, H. Zaitan, S. Chtita, F. Khalil, Integrative computational strategy for anticancer drug discovery: QSAR-ANN modeling, molecular docking, ADMET prediction, molecular dynamics and MM-PBSA simulations, and retrosynthetic analysis, New J. Chem. 49 (2025) 14748–14768. https://doi.org/10.1039/D5NJ02417J.

[49] A. Hajipasha, N.G. Cherati, M. Darzi, S.S. Nateghi, S.A.S. Mohsenian, M. Noorzaei, F.K. Dinaki, M. Halimi, Structure-based identification of novel FAK1 inhibitors using pharmacophore modeling, molecular dynamics, and MM/PBSA calculations, Sci Rep 15 (2025) 39506. https://doi.org/10.1038/s41598-025-23203-8.

[50] S. Upadhaya, S.T. Neftelinov, J. Hodge, J. Campbell, Challenges and opportunities in the PD1/PDL1 inhibitor clinical trial landscape, Nat Rev Drug Discov 21 (2022) 482–483. https://doi.org/10.1038/d41573-022-00030-4.

[51] G.R. Sartori, A.D.O. Albuquerque, A.H. Santos-Costa, L.M. Andrade, D.D.S. Almeida, E.M. Gaieta, J.V. Sampaio, V.T.D.M.L. Albuquerque, J.H. Martins Da Silva, In silico mapping of the dynamic interactions and structure-activity relationship of flavonoid compounds against the immune checkpoint programmed-cell death 1 pathway, Front. Drug. Discov. 2 (2022) 1032587. https://doi.org/10.3389/fddsv.2022.1032587.

[52] S. Li, D. Xiong, V.V. Klochkov, I.A. Khodov, X. He, Molecular dynamics reveals novel small-molecule inhibitors block PD-1/PD-L1 by promoting PD-L1 dimer stability, Phys. Chem. Chem. Phys. 27 (2025) 24932–24947. https://doi.org/10.1039/D5CP03584H.

# Chapter 5

## Structure-Based Prioritization of Marine Natural Products as Candidate FUT8 Binders

## Structure-based discovery of novel FUT8 inhibitors to modulate CEA function in colorectal cancer

### 5.1 Graphical Abstract

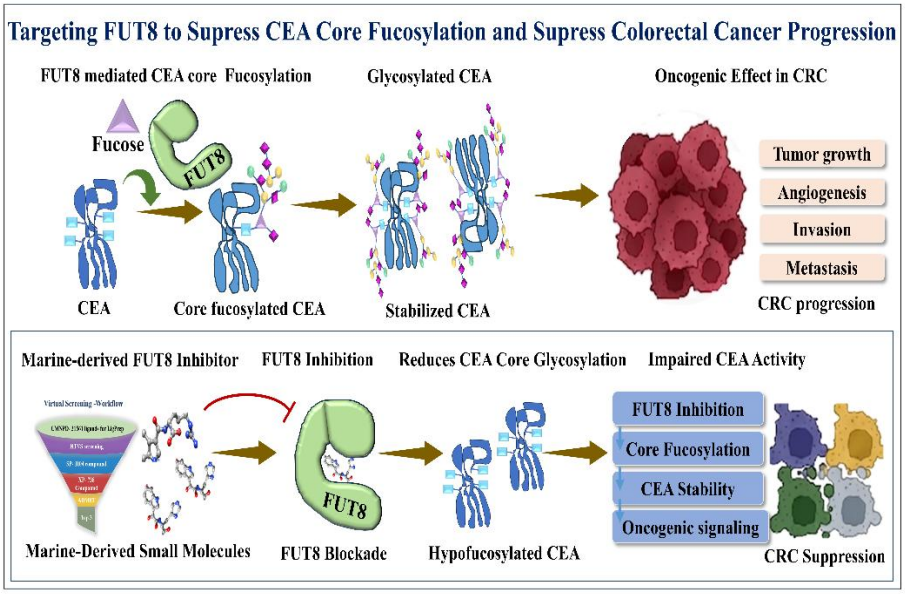



**Figure 5.1: Graphical abstract:** proposed mechanism illustrating FUT8-mediated core fucosylation of CEA and identification of marine-derived FUT8 inhibitor through an in-silico approach to suppress colorectal cancer progression.

### 5.2 Overview

The glycosylation of proteins is one of the most common post-translational modifications, helping to maintain their structural and functional roles. The unusual glycosylation changes the structural profile of glycoproteins within colorectal cancer (CRC), leading to survival, invasion, and metastasis of tumor cells. The carcinoembryonic antigen (CEA) is a highly glycosylated, well-established CRC biomarker, difficult to target directly due to its structural complexity, and promotes tumor cell proliferation. Thus, targeting glycosylation machinery, which is involved in the regulation of CEA function, may offer a more feasible therapeutic approach. Fucosyltransferase8 (FUT8) is a solo enzyme that actively performs core fucosylation of CEA and facilitates oncogenic functions. Hence, targeting

FUT8 is an alternative strategy to disrupt the CEA-mediated response. To identify a therapeutic inhibitor, the marine natural product library was screened to target FUT8 using an in-silico approach. Structure-based virtual screening, molecular docking, pharmacokinetics and toxicity (ADMET) analyses, molecular dynamics simulation, and binding free energy (MM/PBSA) calculation were performed to evaluate the candidate compound. The top-ranked compound showed strong and stable interactions with key catalytic residues at the FUT8 interface. Notably, CMNPD23066 predicted the highest inhibitory potential, with a more favorable structural stability and binding free energy than the currently reported FUT8 inhibitor. In addition, molecular dynamics simulation confirmed the stability of the protein-ligand complexes, supported by favorable RMSD, RMSF, and binding free energy values. Collectively, this study highlights FUT8 as a promising therapeutic target in CRC and provides computational evidence that marine-derived small molecules can inhibit FUT8 to destabilize CEA tumor-promoting function.

**5.3 Introduction:**

Glycosylation of proteins is a highly conserved post-translational modification that profoundly influences protein structure, stability, and function, and regulates key cellular processes, including cell growth, differentiation, signal transduction, and immune evasion of tumor cells [1,2]. Aberrant glycosylation of proteins is one of the hallmarks of cancer and is increasingly recognized as a critical driver of cancer development and progression [3]. The alternation in glycoprotein synthesis is commonly linked with CRC progression and metastasis [4]. Despite substantial advances having been made in our understanding of cancer-associated glycosylation, the underlying molecular mechanisms responsible for these changes and their role in tumor biology are still not fully elucidated. Recently, it has been well known that glycoproteins play a crucial role in shaping the tumor microenvironment (TME) by regulating interactions

between cancer cells and surrounding immune cells, including macrophages [5]. These glycoproteins mediated communication, contribute to immune suppression, and support aggressive tumor development [6]. Among the glycoproteins affected by these modifications, carcinoembryonic antigen (CEA) has attracted considerable attention due to its extensive glycosylation, overexpression in CRC, and well-established role in tumor progression and metastasis.

The Carcinoembryonic antigen (CEA or CEACAM5) glycoprotein is abundantly expressed on the surface of CRC cells and routinely used for disease diagnosis, prognosis, and therapeutic monitoring [7]. In addition to its diagnostic significance, it is involved in tumor promotion through cell adhesion, invasion, metastasis, and immune evasion [8]. The enhanced expression pattern of CEA is generally associated with advanced disease stage, high risk of metastasis, and poor patient outcome [9]. CEA facilitates tumor progression and metastasis via multiple mechanisms, including N-domain dimerization of CEA, which forms bridges and disrupts epithelial polarity, promoting metastasis. Similarly, it supports tumor growth by activating the FAK/ERK and PI3K/AKT signalling and enhances cell survival, proliferation [8]. CEA proteins also affect with TGF-β/SMAD3-mediated signaling and increase the survival of CRC cells [10]. Furthermore, CEA not only boosts tumor cell survival and metastasis but also educates tumor-associated M0 macrophages to acquire a pro-tumorigenic M2-like phenotype [11]. Collectively, these functions highlight CEA as a key regulator of TME, promoting tumor progression and thus making it an attractive target for therapeutic intervention in CRC.

Although CEA represents an attractive therapeutic target, its structural characteristics pose significant challenges for direct inhibition. Currently, CEA-targeted therapeutic approaches are mainly based on antibodies, which often face challenges, including limited penetration, high production cost, and immune-related side effects [8]. As a result, no FDA-approved

CEA-targeted therapeutic antibody is currently available for clinical use. Given these limitations, an alternative approach that includes small molecules offers several pharmacological advantages, including lower production cost and superior tissue penetration [12]. However, developing small molecules that directly target CEA remains challenging because CEA is a large, highly glycosylated cell-surface protein, which may limit access to the potential ligand binding pocket and complicate targeting [13,14]. Therefore, targeting the upstream regulator that governs CEA biosynthesis and function may represent a more effective therapeutic strategy. In this context, fucosyltransferase 8 (FUT8) is the sole enzyme responsible for core fucosylation, regulating structural and biological activity of glycoproteins, including CEA [15,16]. In our recent review, we summarized the role of cancer-derived exosomes containing glycoproteins reprogram macrophages towards tumor-promoting M2-like macrophage polarization, creating immunosuppressive the FUT8 active site and promoting tumor growth [6]. These findings suggest that aberrant glycosylation influences the functional properties of tumor-associated glycoproteins but also educates immune cells. Given its important role in glycoprotein maturation, targeting FUT8 may represent a promising strategy to disrupt glycoprotein-driven oncogenic signalling and immune modulation in CRC.

Recently, a few studies have demonstrated that targeting FUT8 using small-molecule inhibitors can effectively suppress tumor growth and metastasis in both in vitro and in vivo models [17,18]. However, despite these encouraging findings, no FUT8-targeted therapy has yet advanced to clinical application. Therefore, the identification of a more potent FUT8 inhibitor is still needed to identify one with improved efficacy and therapeutic potential. In the current study, we used a structure-based in silico approach to identify novel FUT8 inhibitors from the marine natural products database. To validate the screening results, FDW028, which has demonstrated significant tumor-suppressive activity in preclinical models, was used as a positive control [18]. To identify a better potential FUT8

inhibitor, we performed molecular docking, molecular dynamics simulations, and pharmacokinetic analyses. The findings from our study provide a foundation for future studies aimed at evaluating FUT8-directed therapeutic strategies in CRC.

## Materials and Methods

### Expression Analysis of CEACAM5 and FUT8 in Colorectal Cancer

The expression patterns of CEACAM5 and FUT8 were analysed using publicly available datasets from Human Protein Atlas (HPA) [19] and GEPIA2 [20]. The HPA was used to obtain protein and RNA expression profiles across human cancers. GEPIA2, a web server based on the RNA sequencing data of The Cancer Genome Atlas (TCGA) and the Genotype-Tissue Expression (GTEx) project, was used to assess the transcript expression levels in colon adenocarcinoma (COAD) and rectum adenocarcinoma (READ). Expression analyses were performed to investigate the expression of CEACAM5 and FUT8 in CRC tissues and to assist in target selection for further computational studies.

### Target Preparation

The crystal structure of human α-1,6-fucosyltransferase (FUT8) complexed with GDP and NM5M2-Asn (PDB ID: 6X5U) [21] was obtained from the Protein Data Bank[22]. The structure was solved using X-ray crystallography at 3.20 Å resolution. The model was chosen because of its good resolution and because it represents the human FUT8 enzyme in a ligand-bound conformation and contains key residues involved in catalysis which makes it well suited for structure-based inhibitor screening and molecular dynamics investigations. Prior to virtual screening, the FUT8 crystal structure was prepared by removal of nonessential chains, water molecules and other heteroatoms using UCSF Chimera [23]. The cleaned structure was then imported into Schrödinger Maestro and processed with the Protein Preparation Wizard. Hydrogen atoms were added during

preparation, missing side-chain atoms were modelled and metal coordination states were assigned wherever appropriate. Four disulfide bonds were identified and preserved between Cys943-Cys917, Cys1012-Cys874, Cys1308-Cys815, and Cys2984-Cys2932. Residue protonation states were assigned at a physiological pH (7.0–7.4) using PROPKA, and hetero groups were ionized and tautomerized with Epik [24], Finally, the structure was restrained energy minimized with the OPLS4 force field to optimize hydrogen-bonding interactions and to relieve unfavourable steric clashes while preserving the overall crystallographic geometry [24].The docking site was defined according to residues previously reported as important for the binding of the FUT8 ligand. Specifically, Arg365, Lys369, Tyr250, Ser469, Gln470, Gly221, Tyr220, and Asp453 were used to identify and centre the binding pocket [18]. The Glide Receptor Grid Generation module in Schrödinger was then used to generate a receptor grid, with the grid centred on the selected active-site region [25]. The prepared protein structure and corresponding receptor grid were subsequently employed for virtual screening of the CMNPD library.

**Ligand Library Preparation**

The screening library was obtained from the Comprehensive Marine Natural Products Database (CMNPD), a curated and publicly accessible repository of marine-derived compounds that integrates chemical structures with associated biological, physicochemical, taxonomic, and literature information [26]. The database contains structurally diverse natural products isolated from a wide range of marine organisms and has been widely used as a resource for natural product-based drug discovery.

Prior to virtual screening, the CMNPD library was prepared using the LigPrep module in Schrödinger. Ligand preparation included removal of salts, generation of relevant tautomeric and ionization states, assignment of protonation states at physiological pH ($7.0 \pm 2.0$), and generation of possible stereoisomers where applicable. Three-dimensional conformations were

subsequently generated and energy-minimized using the OPLS3e [27] force field to obtain low-energy structures suitable for molecular docking. The prepared ligands were then exported in Maestro format and used for subsequent virtual screening against the FUT8 active site.

**Virtual Screening**

The CMNPD library was screened against the FUT8 active site using a hierarchical Glide docking methodology. In order to effectively rank compounds while preserving docking accuracy, the screening methodology proceeded through high-throughput virtual screening (HTVS), standard precision (SP), and extra precision (XP) docking sequentially. The chemical library was first filtered using HTVS, and then ligand poses were refined and false positives were removed using SP docking. The top-ranked compounds were then screened via XP docking for a thorough evaluation and final ranking. The receptor grid created around the FUT8 catalytic pocket, defined by the essential binding residues Arg365, Lys369, Tyr250, Ser469, Gln470, Gly221, Tyr220, and Asp453, was used for docking calculations. The van der Waals scaling factor for nonpolar ligand atoms was set to 0.8 with a partial charge cutoff of 0.15 in order to improve sampling of chemically varied ligands. The highest scoring hits were visually examined to confirm favourable binding orientations and interactions with catalytically significant residues inside the FUT8 active site after compounds were sorted based on their GlideScore values.

**ADMET Analysis**

The pharmacokinetic and toxicity profiles of the top-ranked compounds identified from virtual screening were evaluated using the pkCSM web server [28]. Canonical SMILES of the selected compounds were submitted individually for prediction of absorption, distribution, metabolism, excretion, and toxicity (ADMET) properties. Key parameters assessed included aqueous solubility, Caco-2 permeability, intestinal absorption, P-

glycoprotein substrate and inhibitor status, blood-brain barrier (BBB) permeability, central nervous system (CNS) permeability, cytochrome P450 (CYP450) substrate and inhibition profiles, total clearance, AMES mutagenicity, hERG channel inhibition, hepatotoxicity, and skin sensitization. Compounds exhibiting favorable pharmacokinetic characteristics and the absence of major toxicity liabilities were prioritized for molecular dynamics simulations and further binding free-energy analyses.

**Molecular Dynamics Simulations**

Molecular dynamics (MD) simulations were performed to evaluate the stability and dynamic behavior of the top FUT8-ligand complexes identified from virtual screening and ADMET filtering. Complexes were prepared with the LEaP module of AmberTools19 [29]; counter ions were added to neutralize each system, and structures were solvated in a periodic octahedral box of TIP3P water molecules with a 10.0 Å buffer on all sides . The protein was assigned the Amber ff14SB [30] force field , while ligands were parameterized using Antechamber-derived AM1-BCC atomic charges and the GAFF2 force field . All simulations were executed with the pmemd.cuda module of AMBER18. Long-range electrostatics were treated with particle-mesh Ewald (PME) , covalent bonds involving hydrogen were constrained using SHAKE, and a 10 Å non-bonded cutoff was applied. A 2.0 fs time step was used throughout.

Each system underwent energy minimization followed by multi-step heating to 300 K and equilibration. Production runs consisted of 200 ns of unrestrained MD in the NPT ensemble at 1 atm and 300 K. Temperature and pressure were controlled using the Langevin thermostat and Berendsen barostat , respectively. Trajectory post-processing and quantitative analyses including RMSD, RMSF, hydrogen bonds, radius of gyration (Rg), and solvent-accessible surface area (SASA), were performed with CPPTRAJ [31] in AMBER18.

**Trajectory Analysis**

Protein stability was assessed by computing backbone root-mean-square deviation (RMSD) and root-mean-square fluctuation (RMSF), examining both global protein behavior and the specific FUT8 binding-pocket region. Ligand stability was monitored by calculating ligand RMSD relative to its initial docked pose. Protein compactness and folding were evaluated via radius of gyration (Rg), while SASA provided insights into changes in surface exposure. Protein-ligand hydrogen bonds were analyzed using CPPTRAJ, and interactions with an occupancy greater than 10% were considered.

**Binding Free Energy Calculations and Data Visualization**

Binding free energies ($\Delta G_{bind}$) were estimated using the Molecular Mechanics Poisson-Boltzmann Surface Area (MM/PBSA) method, computed as:

$$\Delta G_{bind} = G_{complex} - G_{protein} - G_{ligand}$$

where each $G_x$ represents the average free energy of the respective species (complex, protein, or ligand) obtained from equilibrated MD snapshots. Total free energies were decomposed into molecular mechanics and solvation contributions:

$$G = E_{MM} + G_{solv}$$

with

$$E_{MM} = E_{bonded} + \Delta E_{vdW} + \Delta E_{elec}$$ and

$$G_{solv} = \Delta G_{pol} + \Delta G_{np}$$

Here, $\Delta E_{vdW}$ and $\Delta E_{elec}$ are the van der Waals and electrostatic interaction energies; $\Delta G_{pol}$ is the polar solvation free energy estimated via the Poisson-Boltzmann equation; and $\Delta G_{np}$ is the non-polar solvation free

energy calculated from SASA-based models. The entropic term (−TΔS) was omitted from MM/PBSA calculations due to high computational cost and statistical variability. Previous studies note that entropy is often excluded in MM/PBSA protocols because of approximations in statistical mechanical treatments, limitations of entropy estimation methods, and challenges in achieving statistically converged sampling [32]. This omission is a methodological limitation since ligands having different conformational flexibility may not be ranked with full accuracy and neglecting the entropic contributions may bias the comparisons against more rigid ligands. This caveat was explicitly considered in the interpretation of the predicted affinity rankings. The contribution of individual residues to binding affinity was evaluated by decomposing the MM/PBSA energy components for each residue. Snapshots were collected at 100 ps intervals throughout the production run and the resulting profiles were averaged to pinpoint residues that were central to ligand binding and stabilization of the FUT8 pocket. This method gives a quantitative measurement of the thermodynamic forces driving the interaction. Data analysis and visualization were performed in Python (v3.13.5) using NumPy for arrays and numerical routines and Matplotlib for creating publication-quality figures that highlight important energetic trends across the dataset.

## 5.5 Results

**5.5.1 Expression Analysis Highlights CEACAM5 and FUT8 as Targets in CRC:** We explored the expression profiles of CEACAM5 and FUT8 based on data from the Human Protein Atlas (HPA) and GEPIA2 **(Figure 5.2)**. HPA protein expression data revealed detectable expression of both CEACAM5 and FUT8 in several human malignancies, including CRC **(Figure 5.2 A,D)**. In addition, RNA expression profiles of HPA showed CEACAM5 and FUT8 transcripts in CRC tissues **(Figure 5.2 B,E)**. To further assess their expression in CRC, transcript levels were analysed in colon adenocarcinoma (COAD) and rectum adenocarcinoma (READ) using

GEPIA2. Expression of CEACAM5 was significantly increased in tumour tissues compared to the corresponding normal tissues in both COAD and READ **(Figure 5.2C)**. Consistent with this observation, FUT8 expression was also higher in CRC tissues than in normal controls **(Figure 5.2F)**. This analysis confirms the expression of both CEACAM5 and FUT8 in CRC and their relevance to tumour biology. The high expression of FUT8 in CRC tumours was the rationale for selecting it as the target for subsequent structure-based screening studies.

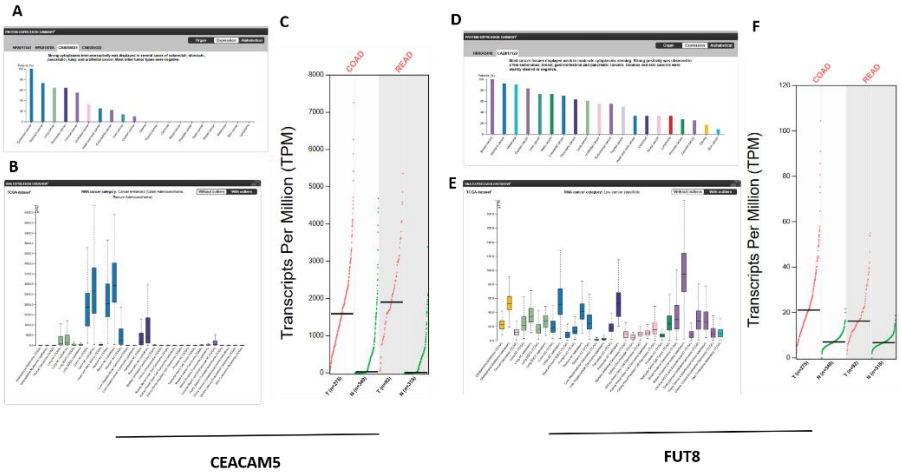



**Figure 5.2. Expression analysis of CEACAM5 and FUT8 in colorectal cancer.** (A) HPA protein expression profile of CEACAM5 across human cancers. (B) HPA RNA expression profile of CEACAM5. (C) GEPIA2 comparison of CEACAM5 transcript levels between tumor (T) and normal (N) tissues in colon adenocarcinoma (COAD) and rectum adenocarcinoma (READ). (D) HPA protein expression profile of FUT8 across human cancers. (E) HPA RNA expression profile of FUT8. CEACAM5 and FUT8 were both expressed in colorectal cancer tissues, with higher transcript levels observed in tumor samples than in corresponding normal tissues. (F) GEPIA2 comparison of FUT8 transcript levels between tumor and normal tissues in COAD and READ.

**5.5.2 Structure-based virtual screening identifies potential FUT8 inhibitors:** The 31,561 compounds retrieved from the CMNPD database were prepared using LigPrep to generate 63,576 conformations of ligands

for virtual screening. The prepared library was screened against the FUT8 catalytic pocket by a hierarchical Glide docking workflow with HTVS, SP and XP docking. The ligand used as reference is FDW028 (PubChem CID: 53208107) had an XP GlideScore of −6.547 kcal/mol and was used as a benchmark for hit selection. Compounds were passed on to the next level of screening only if their score was higher than that of the reference ligand at each level of the screening workflow. Thus, 1,104 HTVS compounds were subjected to SP docking, which resulted in 738 compounds that progressed to XP docking. Final XP screening retrieved 149 compounds with docking scores better than the control ligand **Figure 5.3 A**. The top ranked compounds were further evaluated based on docking score, interacting residues with the active pocket residues, and predicted pharmacokinetic properties. Among these, CMNPD23062, CMNPD23066 and CMNPD8620 were the most promising candidates with XP GlideScore of −11.529, −11.452 and −10.496 kcal/mol respectively. Docking pose analysis showed that all three compounds occupied the FUT8 catalytic pocket and interacted with some residues of the binding site such as Arg365, Lys369, Ser469, Gln470 and Tyr220 **(Figure 5.3 B)**.

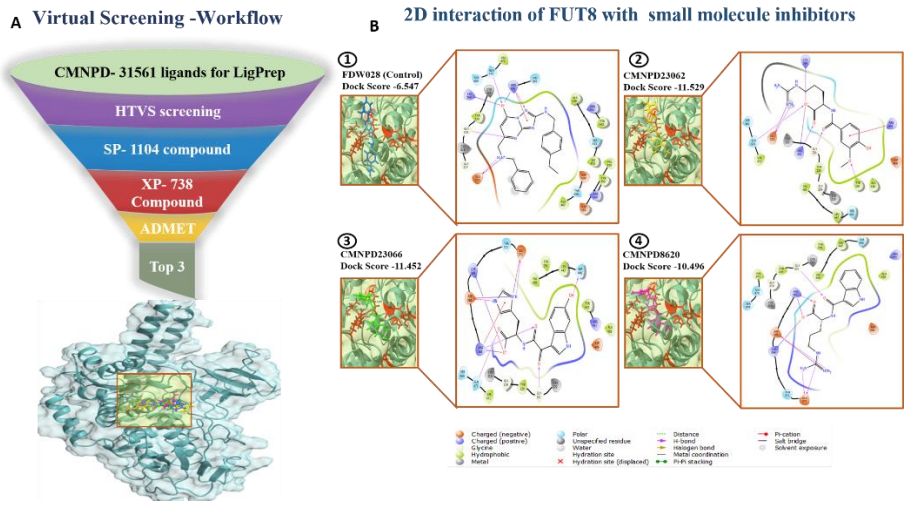



**Figure 5.3.** Virtual Screening Workflow and 2D interactions of FUT8 with small molecule inhibitors

**5.5.3 Selected FUT8 Inhibitors Show Favourable ADMET Profiles:** The pkCSM predicted the pharmacokinetic and toxicity properties of CMNPD23062, CMNPD23066, and CMNPD8620 **(Table 5.1)**. All three compounds exhibited promising ADMET properties such as moderate aqueous solubility and intestinal absorption within the acceptable range (31.60-39.26%). None were predicted to inhibit P-glycoprotein or major CYP450 isoforms, suggesting low potential for transporter or CYP mediated drug interactions. Distribution analysis showed low blood–brain barrier penetration (logBB = −1.43 to −1.07) and low CNS permeability (logPS = −4.20 to −3.53), indicating low predicted central nervous system exposure. Moreover, all compounds showed predicted moderate clearance values and were not identified as substrates of CYP2D6 or CYP3A4. Crucially, CMNPD23062, CMNPD23066 and CMNPD8620 were predicted as non-mutagenic (AMES negative), non-hepatotoxic and non-inhibitors of hERG I and hERG II. Additionally, none of the compounds were predicted to induce skin sensitization. These findings show that the selected compounds are suitable for subsequent molecular dynamics simulations and binding free-energy analyses. Average structural stability parameters calculated from the 200 ns molecular dynamics production trajectories have been summarised in **supplementary table S5.1.**

**Table 5.1.** Predicted ADMET profiles of CMNPD23062, CMNPD23066, and CMNPD8620 were generated using pkCSM.

| ADMET Properties | CMNPD23062 | CMNPD23066 | CMNPD8620 |
|---|---|---|---|
| **Water solubility (log mol/L)** | -2.892 | -2.892 | -2.892 |
| **Caco-2 permeability (log Papp)** | -0.608 | -0.18 | -0.337 |
| **Intestinal absorption (%)** | 31.6 | 39.26 | 34.12 |
| **P-glycoprotein substrate** | Yes | Yes | Yes |
| **P-glycoprotein I inhibitor** | No | No | No |
| **P-glycoprotein II inhibitor** | No | No | No |
| **BBB permeability (logBB)** | -1.43 | -1.072 | -1.165 |
| **CNS permeability (logPS)** | -3.823 | -4.195 | -3.527 |
| **CYP2D6 substrate** | No | No | No |
| **CYP3A4 substrate** | No | No | No |
| **CYP inhibition (1A2, 2C19, 2C9, 2D6, 3A4)** | No | No | No |
| **Total clearance (log mL/min/kg)** | 0.487 | 0.756 | 0.452 |
| **AMES toxicity** | No | No | No |
| **hERG I inhibitor** | No | No | No |
| **hERG II inhibitor** | No | No | No |
| **Hepatotoxicity** | No | No | No |
| **Skin sensitisation** | No | No | No |

**5.5.4 RMSD analysis indicates stable binding of marine-derived compounds to FUT8:** The structural stability of FUT8 in complex with the top-ranked marine natural compounds was examined by observing the root mean square deviation (RMSD) of the protein backbone, active-site binding pocket, and ligand during the 200 ns molecular dynamics simulations. Backbone RMSD profiles indicated that all FUT8-ligand complexes were structurally stable during the whole period of the simulation without any large-scale conformational drift **(Figure 5.4A)**. Following an initial

equilibration phase during the first 20-40 ns, the systems reached relatively stable trajectories and fluctuated within a narrow range. The FUT8-CMNPD8620 complex exhibited the lowest average protein RMSD (3.10 ± 0.36 Å), closely followed by FUT8-CMNPD23062 (3.18 ± 0.41 Å), suggesting enhanced stabilization of the protein structure relative to the control system (3.64 ± 0.30 Å). FUT8-CMNPD23066 displayed a slightly higher average backbone RMSD (3.88 ± 0.29 Å); however, the fluctuations remained moderate and indicative of a stable complex throughout the simulation.

To further assess ligand-induced effects on the catalytic region, the RMSD of binding-pocket residues was analyzed (**Supplementary figure S5.1 A**). All complexes maintained low pocket RMSD values (<1.6 Å), indicating preservation of the active-site architecture during the simulation. Among the screened compounds, CMNPD23066 exhibited the lowest binding-pocket RMSD (0.88 ± 0.12 Å), suggesting enhanced local stability of the catalytic site. CMNPD23062 also maintained a stable binding pocket with an average RMSD of 1.11 ± 0.15 Å, comparable to the control system (1.16 ± 0.19 Å). Although CMNPD8620 showed the highest pocket RMSD (1.50 ± 0.22 Å), the values remained low overall and did not indicate any disruption of binding-site integrity.

The stability of ligand binding was further examined using ligand RMSD analysis (**supplementary figure S5.1 B**). All screened compounds exhibited lower ligand RMSD values than the control ligand, indicating that they remained stably bound within the FUT8 active site throughout the simulation. CMNPD23066 showed the lowest average ligand RMSD (1.10 ± 0.09 Å), followed by CMNPD23062 (1.40 ± 0.11 Å) and CMNPD8620 (1.62 ± 0.31 Å), whereas the control ligand displayed the highest deviation (2.17 ± 0.30 Å). The ligand RMSD trajectories remained relatively stable over the 200 ns simulation, suggesting that the compounds maintained consistent binding orientations with minimal positional movement within

the catalytic pocket. Overall, all three FUT8-ligand complexes remained stable throughout the 200 ns simulation, as demonstrated by the consistent protein, binding-pocket, and ligand RMSD profiles. No major structural changes were observed, indicating that binding of the screened compounds did not destabilize FUT8 and was accommodated within the active site. Having established the overall stability of the complexes, residue-level flexibility was subsequently investigated using RMSF analysis.

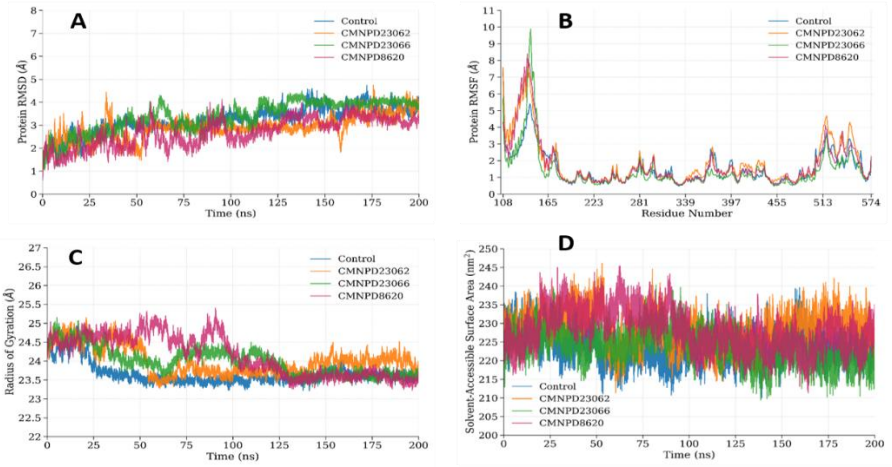



**Figure 5.4. Molecular dynamics analysis of FUT8 complexes with the control ligand and selected marine-derived compounds.** (A) Protein backbone RMSD, (B) residue-wise RMSF, (C) radius of gyration (Rg), and (D) solvent-accessible surface area (SASA) over 200 ns simulations.

**5.5.5 Residue flexibility analysis indicates active-site stability:** The root mean square fluctuation (RMSF) of the FUT8 residues was calculated over the 200 ns simulation to investigate residue-level flexibility and identify regions affected by ligand binding **(Figure 5.4 B)**. All systems showed similar fluctuation profiles indicating that ligand binding does not induce many changes in the dynamic behavior of the protein. The largest fluctuations were seen in terminal and loop regions particularly in the vicinity of residues 120-160 and 500-540. Most residues showed RMSF values below 2 Å suggesting a generally stable protein structure. Importantly, the residues forming the active site of FUT8 were relatively

stable through the course of the simulations. The catalytic region comprising Arg365 and Lys369 showed less fluctuations in CMNPD23066-bound complex than the control and other ligand-bound systems, suggesting the increased stabilization of this functionally important region. Similarly, residues Ser469 and Gln470 showed the lowest RMSF values in the presence of CMNPD23066 indicating restricted local motion in the vicinity of the binding pocket. The active-site residue Asp453 also remained stable in all the systems, though slightly higher fluctuations were observed in the CMNPD23062 complex. Contrarily, Tyr220, Gly221 and Tyr250 showed only minor differences among the complexes and were kept at low RMSF values during the simulation, indicating the preservation of the active-site geometry. The analysis of RMSF suggests that the binding of screened compounds does not increase the flexibility of the FUT8 catalytic pocket. Key active-site residues remained stable and CMNPD23066 showed a tendency to reduce the local fluctuations near several catalytic residues. After determining the structural stability and residue-level dynamics of the complexes, the compactness and overall conformational behavior of FUT8 were further analyzed using radius of gyration (Rg) and solvent-accessible surface area (SASA) analyses.

**5.5.6: Ligand binding preserves FUT8 compactness and solvent accessibility:** In order to further see how ligand binding affects the overall structural integrity of FUT8, the radius of gyration (Rg) and solvent-accessible surface area (SASA) were analysed throughout the 200 ns simulations. The Rg profiles remained relatively stable for all systems, showing retention of protein compactness during the simulation **(Figure 5.4C)**. Following an initial equilibration period, all complexes converged and fluctuated within a narrow range. The control system exhibited an average Rg of 23.59 ± 0.11 Å, while the ligand-bound complexes showed comparable values of 23.89 ± 0.19 Å, 23.74 ± 0.22 Å, and 23.66 ± 0.20 Å for CMNPD23062, CMNPD23066, and CMNPD8620, respectively. Although CMNPD23062 displayed a slightly higher average Rg, the

differences among the systems were small, suggesting that ligand binding did not induce significant expansion or compaction of the FUT8 structure.

Consistent with the Rg analysis, the SASA trajectories showed only moderate fluctuations throughout the simulations, indicating stable solvent exposure of the protein surface **(Figure 5.4D)**. The average SASA values were 223.87 ± 3.61 nm² for the control, 227.79 ± 4.18 nm² for CMNPD23062, 221.52 ± 3.62 nm² for CMNPD23066, and 224.87 ± 3.46 nm² for CMNPD8620. Among the complexes, CMNPD23066 exhibited the lowest average SASA, suggesting slightly reduced solvent exposure and a more compact surface arrangement, whereas CMNPD23062 showed marginally higher solvent accessibility. However, the overall similarity of the SASA profiles indicates that ligand binding did not substantially alter the solvent-accessible surface of FUT8. The Rg and SASA analyses together show that all three compounds maintained the compactness and structural integrity of FUT8 throughout the simulation. No major changes in protein packing or solvent exposure further support the formation of stable FUT8-ligand complexes.

**5.5.7 Persistent hydrogen bonding stabilizes FUT8-ligand interactions:** Hydrogen bond analysis was performed in order to evaluate the overall stability and strength of ligand binding to the FUT8 active site throughout the 200 ns simulations **(Figure 5.5)**. Consistent with the RMSD and RMSF analyses, all ligand-bound systems maintained persistent hydrogen-bonding interactions with key catalytic residues, showing stable occupancy of the binding pocket. The moving-average hydrogen bond profiles showed that CMNPD23066 maintained the highest number of protein-ligand hydrogen bonds throughout the simulation, with an average of approximately 5-7 interactions. CMNPD8620 also exhibited stable hydrogen bonding, having an average of 4-6 interactions, whereas CMNPD23062 maintained a smaller but persistent network of approximately 3-4 hydrogen bonds. These findings were corroborated by the hydrogen bond analysis conducted during

the simulation, which revealed that whereas CMNPD8620 and CMNPD23062 often maintained lower but constant contacts, CMNPD23066 regularly maintained 8–12 hydrogen bonds during the trajectory. The control complex, on the other hand, showed fewer and more dispersed hydrogen bonding. CMNPD23066 produced the most lasting connections with active-site residues, according to a thorough occupancy analysis **(supplementary table S5.2)** Significantly, Arg365 hydrogen bonds displayed remarkably high occupancies of 95.63% and 67.11%, suggesting that this residue is a key anchoring point for ligand binding. Together with highly occupied contacts involving Asp368 (71.89%) and Glu373 (55.04%), further stable interactions were noted with Lys369, Gln470, and Asp453. With occupancies of 48.64 and 55.52%, CMNPD23062 mostly formed a stable hydrogen bonding network through Ser469 and Gln470, with additional contributions from Arg365. Likewise, CMNPD8620 continued to interact with Gln470, Ser469, Arg365, and Lys369; here, Asp368 had the most contribution to the hydrogen bond (50.89% occupancy). Together, these findings show that all three drugs maintain stable binding within the FUT8 active site via sustained hydrogen-bond interactions with important catalytic residues, such as Asp453, Arg365, Lys369, Ser469, and Gln470. In line with the active-site stability seen in the RMSF analysis, CMNPD23066 showed the largest and longest-lasting hydrogen-bonding network among the screened compounds.

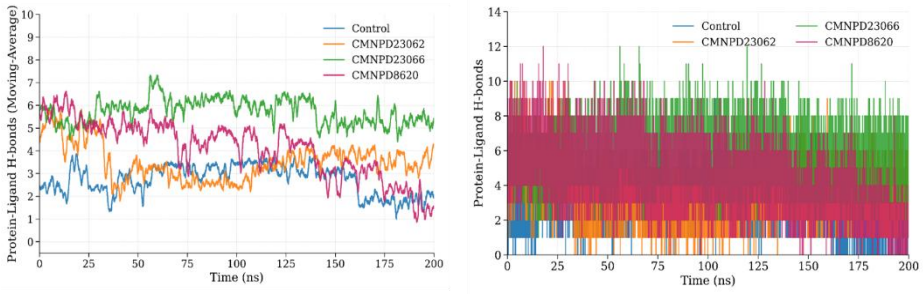
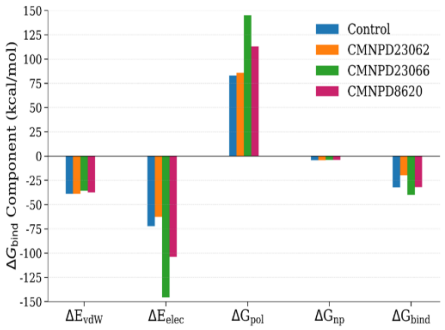



**Figure 5.5. Hydrogen-bond analysis of FUT8 complexes during 200 ns molecular dynamics simulations.** (A) Moving average of protein–ligand

hydrogen bonds and (B) distribution of hydrogen bonds over time for the control ligand and selected marine-derived compounds.

**5.5.8 MM/PBSA analysis reveals favourable binding energies for the selected compounds:** To assess ligand binding in greater detail, MM/PBSA calculations were carried out on trajectories from the 200-ns molecular dynamics simulations **(Figure 5.6)**. All complexes yielded negative binding free energies (ΔG_bind), consistent with thermodynamically favourable interactions with FUT8.Among the tested molecules, CMNPD23066 displayed the strongest affinity, with a binding free energy of −40.07 ± 0.19 kcal/mol. This value was lower than that of the reference inhibitor FDW028 (−32.19 ± 0.14 kcal/mol) and all other screened compounds. CMNPD8620 also showed a favourable profile (−31.96 ± 0.25 kcal/mol), comparable to the reference, whereas CMNPD23062 had the weakest binding (−19.88 ± 0.15 kcal/mol).




| System | $\Delta E_{vdW}$ | $\Delta E_{elec}$ | $\Delta G_{pol}$ | $\Delta G_{np}$ | $\Delta G_{bind}$ |
|---|---|---|---|---|---|
| Control (FDW028) | -38.81 (0.10) | -72.32 (0.37) | 83.00 (0.29) | -4.06 (0.01) | -32.19 (0.14) |
| CMNPD23062 | -38.76 (0.10) | -62.65 (0.57) | 85.78 (0.49) | -4.25 (0.004) | -19.88 (0.15) |
| CMNPD23066 | -35.59 (0.12) | -145.59 (0.33) | 145.16 (0.24) | -4.05 (0.002) | -40.07 (0.19) |
| CMNPD8620 | -37.50 (0.10) | -103.71 (0.72) | 113.17 (0.54) | -3.92 (0.003) | -31.97 (0.25) |

**Figure 5.6: MM/PBSA binding free energy decomposition of FUT8–ligand complexes.** Average van der Waals (ΔE_vdW), electrostatic (ΔE_elec), polar solvation (ΔG_pol), nonpolar solvation (ΔG_np), and total binding free energies (ΔG_bind) calculated from MD trajectories for the control ligand and selected compounds. Negative values indicate favorable contributions to binding.

The binding energies were primarily driven by van der Waals and electrostatic contributions, while polar solvation opposed complex formation to varying extents. Notably, CMNPD23066 exhibited the largest electrostatic component, in line with the extensive hydrogen-bonding

interactions observed during simulation. To pinpoint the residues contributing most to these favourable contacts, residue-level free energy decomposition was subsequently performed.

**5.5.9 Residue decomposition analysis highlights key binding determinants:** To pinpoint the residues that stabilize ligand binding within the FUT8 active site, we carried out residue-level free energy decomposition **(Supplementary Table S5.3)**. The analysis showed that several amino acids positioned in or near the catalytic pocket contributed significantly to ligand affinity, in agreement with the hydrogen-bonding and RMSF observations. For the reference complex, the strongest stabilizing effects were attributed to Arg441 (−3.81 kcal/mol) and Glu373 (−3.71 kcal/mol), with smaller inputs from Tyr442 and Leu438. In contrast, the screened compounds displayed interaction profiles focused on catalytically important residues, most notably Arg365, Lys369, Ser469, and Gln470. In the CMNPD23062 complex, Ser469 was the dominant contributor to binding, exhibiting a total interaction energy of −5.63 kcal/mol. Additional favourable contributions were observed from Val471 (−2.73 kcal/mol), Gln470 (−2.25 kcal/mol), and Val450 (−1.74 kcal/mol). Residue-level decomposition highlighted the role of Ser469 and Gln470, two active-site residues that anchor CMNPD23062 within this region of the pocket. This stabilization aligns with the persistent hydrogen bonds observed between the ligand and these residues throughout the MD trajectory.

For CMNPD23066, the dominant energetic contributions came from Lys369 (−7.99 kcal/mol) and Arg365 (−7.88 kcal/mol). Both residues are part of the catalytic site and consistently formed hydrogen bonds with the ligand, while also showing reduced flexibility in RMSF analysis. Additional stabilization was contributed by Asp368 (−2.36 kcal/mol), Gln470 (−2.30 kcal/mol), Val450 (−2.52 kcal/mol), and Glu373 (−1.85 kcal/mol). The involvement of Arg365, Lys369, and Gln470 indicates that CMNPD23066 is stabilized through an interaction network spanning multiple regions of

the FUT8 active site. This anchoring effect reflects the compound's ability to engage several catalytic residues simultaneously.In a similar manner, CMNPD8620 formed strong contacts with multiple residues within the active site, reinforcing its stable binding profile. Lys369 (−5.45 kcal/mol) and Asp368 (−5.11 kcal/mol) were the primary contributors, followed by Arg365 (−2.64 kcal/mol), Gln470 (−2.29 kcal/mol), and Ser469 (−2.27 kcal/mol). The combined participation of the Arg365–Lys369 and Ser469–Gln470 regions indicates that CMNPD8620 engages a broad interaction network across the FUT8 catalytic pocket.

Importantly, Arg365, Lys369, Ser469, and Gln470 consistently appeared as major contributors among the screened compounds, underscoring their central role in ligand recognition and stabilization. These residues also correspond to sites that maintained persistent hydrogen-bond occupancy and exhibited limited structural fluctuations throughout the simulations. Overall, the residue-level energy decomposition highlights that the screened compounds are stabilized through distinct yet overlapping interaction networks within the catalytic pocket, supporting the favourable binding behaviour observed in the MD trajectories.

### 5.6 Discussion and conclusion

Colorectal cancer is currently a major cause of cancer related death and there is a need for new therapeutic strategies [33]. Among CRC-related biomarkers, carcinoembryonic antigen (CEA/CEACAM5) is widely recognized for its functions in tumor progression [34]. While CEA is a well-characterized tumor-associated antigen, its large extracellular architecture, extensive glycosylation, and the difficulties associated with efficient tumor penetration make direct therapeutic targeting problematic [8]. An alternative approach is to target upstream regulators that affect CEA maturation and function. FUT8 is the sole enzyme responsible for core fucosylation in mammals and has been implicated in the regulation of multiple glycoproteins involved in cancer biology [35]. Because CEA is

highly glycosylated, modulation of FUT8 activity may affect CEA associated functions and other glycoprotein mediated processes in CRC [36]. Recent investigations showed FUT8 was highly expressed in CRC cells. It is the only member of the Fucosyltransferase family that catalyses the core fucosylation of glycoproteins [37,38]. This unique enzymatic activity of FUT8 plays a pivotal role in the promotion of CRC cells invasion, metastasis, and tumor progression [39]. An analysis of publicly available datasets further indicated elevated FUT8 expression in CRC tissues, which supported its investigation as a potential therapeutic target.

To identify potential FUT8 targeting compounds, we conducted a structure-based virtual screening with the Comprehensive Marine Natural Products Database (CMNPD). Marine natural products are a rich source of structurally diverse bioactive scaffolds and have provided numerous leads in drug discovery. Following hierarchical docking and ADMET-based prioritization, three compounds, namely CMNPD23062, CMNPD23066 and CMNPD8620 were selected for detailed computational evaluation. In comparison to the reference ligand FDW028, all three compounds exhibited significantly better docking score and binding stability within the FUT8 catalytic pocket during 200 ns molecular dynamics simulations. The combined analysis of RMSD, RMSF, Rg and SASA revealed that the ligand binding did not induce significant structural perturbations and the active-site architecture remained stable throughout the simulations. Continuous hydrogen bond interactions with essential catalytic residues namely Arg365, Lys369, Ser469 and Gln470 also favoured stable ligand occupancy.

MM/PBSA calculations predicted favourable binding for all three compounds, with CMNPD23066 having the most favourable binding free energy. The increased binding was accompanied by increased electrostatic interactions and an expanded network of hydrogen bonding, suggesting more efficient interactions with the FUT8 catalytic pocket. Residue-wise

energy decomposition consistently identified Arg365, Lys369, Ser469 and Gln470 as major contributors to ligand stabilization, highlighting their importance in FUT8 ligand recognition. Moreover, all the selected compounds showed acceptable predicted pharmacokinetic and safety properties, including the lack of significant predicted toxicity parameters. But there are caveats to consider. The present work is purely computational and needs experimental validation to confirm the predicted binding modes and biological activity of the identified compounds. Additionally, the MM/PBSA calculations did not include the entropic contribution, which could affect the absolute ranking of the ligand affinities. Although FUT8 expression was upregulated in CRC datasets, the effects of FUT8 modulation on CEA function, core fucosylation and tumour-associated phenotypes were not directly examined and warrant future investigation.

By integrating virtual screening, molecular dynamics simulations, and binding free-energy analyses, we identified CMNPD23062, CMNPD23066, and CMNPD8620 as marine-derived compounds capable of forming stable interactions within the FUT8 catalytic pocket. Of these, CMNPD23066 consistently showed the strongest computational profile, with higher binding affinity, stable interactions during simulations, and the most favourable MM/PBSA binding free energy. CMNPD23062 and CMNPD8620 also demonstrated stable binding and acceptable ADMET properties, making them promising scaffolds for further optimization. Taken together, these results provide a basis for future biochemical and cellular studies to evaluate the potential of these compounds as modulators of FUT8 activity in colorectal cancer.

## 5.7 References

[1] M. Wang, J. Zhu, D.M. Lubman, C. Gao, Aberrant glycosylation and cancer biomarker discovery: a promising and thorny journey, Clinical Chemistry and Laboratory Medicine (CCLM) 57 (2019) 407–416. https://doi.org/10.1515/cclm-2018-0379.

[2] K. Ohtsubo, J.D. Marth, Glycosylation in Cellular Mechanisms of Health and Disease, Cell 126 (2006) 855–867. https://doi.org/10.1016/j.cell.2006.08.019.

[3] J. Munkley, D.J. Elliott, Hallmarks of glycosylation in cancer, Oncotarget 7 (2016) 35478–35489. https://doi.org/10.18632/oncotarget.8155.

[4] S. Venkitachalam, K. Guda, Altered glycosyltransferases in colorectal cancer, Expert Review of Gastroenterology & Hepatology 11 (2017) 5–7. https://doi.org/10.1080/17474124.2017.1253474.

[5] E.F. Giurini, S.G. Pappas, K.H. Gupta, Sweet Surprises: Decoding Tumor-Associated Glycosylation in Cancer Progression and Therapeutic Potential, Cells 15 (2026) 233. https://doi.org/10.3390/cells15030233.

[6] K. Wadhonkar, Y. Singh, A. Rughetti, S. Das, R. Yangdol, M.H. Sk, M.S. Baig, Role of cancer cell-derived exosomal glycoproteins in macrophage polarization, Mol Biol Rep 52 (2025) 451. https://doi.org/10.1007/s11033-025-10535-x.

[7] Q. Han, Y. Zhu, F. Xing, Y. Xia, Current opinions on CEA in the diagnosis and prognosis of colorectal cancer, Translational Oncology 70 (2026) 102835. https://doi.org/10.1016/j.tranon.2026.102835.

[8] L. Sun, G. Zhao, J. Zhou, Z. Sun, H. Ji, S. Wang, N. Li, Advances and perspectives in CEA-targeted therapies: From classic biomarker toward actionable therapeutic target, Med 7 (2026) 100986. https://doi.org/10.1016/j.medj.2025.100986.

[9] O.N. Dilek, D.İ. Arslan Kahraman, G. Kahraman, Carcinoembryonic antigen in the diagnosis, treatment, and follow-up of focal liver lesions, World J Gastrointest Surg 16 (2024) 999–1007. https://doi.org/10.4240/wjgs.v16.i4.999.

[10] Y. Li, H. Cao, Z. Jiao, S.B. Pakala, D.N.R. Sirigiri, W. Li, R. Kumar, L. Mishra, Carcinoembryonic Antigen Interacts with TGF-β Receptor and Inhibits TGF-β Signaling in Colorectal Cancers, Cancer Research 70 (2010) 8159–8168. https://doi.org/10.1158/0008-5472.CAN-10-1073.

[11] E.-Y. Huang, J.-C. Chang, H.-H. Chen, C.-Y. Hsu, H.-C. Hsu, K.-L. Wu, Carcinoembryonic antigen as a marker of radioresistance in colorectal cancer: a potential role of macrophages, BMC Cancer 18 (2018) 321. https://doi.org/10.1186/s12885-018-4254-4.

[12] K. Wadhonkar, F. Siddiqui, M.S. Baig, Identification of small-molecule inhibitors targeting the PD-1/PD-L1 interaction in colorectal cancer: insights from docking and molecular dynamics simulations, (2026). https://doi.org/10.21203/rs.3.rs-8751886/v1.

[13] L. Pont, V. Kuzyk, F. Benavente, V. Sanz-Nebot, O.A. Mayboroda, M. Wuhrer, G.S.M. Lageveen-Kammeijer, Site-Specific *N* -Linked Glycosylation Analysis of Human Carcinoembryonic Antigen by Sheathless Capillary Electrophoresis–Tandem Mass Spectrometry, J. Proteome Res. 20 (2021) 1666–1675. https://doi.org/10.1021/acs.jproteome.0c00875.

[14] A. Kumar, F. Duffieux, M. Gagnaire, C. Rapisarda, T. Bertrand, A. Rak, Structural insights into epitope-paratope interactions of a monoclonal antibody targeting CEACAM5-expressing tumors, Nat Commun 15 (2024) 9377. https://doi.org/10.1038/s41467-024-53746-9.

[15] M. Shi, X.-R. Nan, B.-Q. Liu, The Multifaceted Role of FUT8 in Tumorigenesis: From Pathways to Potential Clinical Applications, IJMS 25 (2024) 1068. https://doi.org/10.3390/ijms25021068.

[16] M. Ghirardello, I. Yruela, P. Merino, R. Sackstein, I. Sanz-Martínez, R. Hurtado-Guerrero, Structure, function, and implications of

fucosyltransferases in health and disease, Nat Commun 16 (2025) 11279. https://doi.org/10.1038/s41467-025-66871-w.

[17] Y. Zhou, T. Fukuda, Q. Hang, S. Hou, T. Isaji, A. Kameyama, J. Gu, Inhibition of fucosylation by 2-fluorofucose suppresses human liver cancer HepG2 cell proliferation and migration as well as tumor formation, Sci Rep 7 (2017) 11563. https://doi.org/10.1038/s41598-017-11911-9.

[18] M. Wang, Z. Zhang, M. Chen, Y. Lv, S. Tian, F. Meng, Y. Zhang, X. Guo, Y. Chen, M. Yang, J. Li, T. Qiu, F. Xu, Z. Li, Q. Zhang, J. Yang, J. Sun, H. Zhang, H. Zhang, H. Li, W. Wang, FDW028, a novel FUT8 inhibitor, impels lysosomal proteolysis of B7-H3 via chaperone-mediated autophagy pathway and exhibits potent efficacy against metastatic colorectal cancer, Cell Death Dis 14 (2023) 495. https://doi.org/10.1038/s41419-023-06027-0.

[19] M. Uhlén, L. Fagerberg, B.M. Hallström, C. Lindskog, P. Oksvold, A. Mardinoglu, Å. Sivertsson, C. Kampf, E. Sjöstedt, A. Asplund, I. Olsson, K. Edlund, E. Lundberg, S. Navani, C.A.-K. Szigyarto, J. Odeberg, D. Djureinovic, J.O. Takanen, S. Hober, T. Alm, P.-H. Edqvist, H. Berling, H. Tegel, J. Mulder, J. Rockberg, P. Nilsson, J.M. Schwenk, M. Hamsten, K. Von Feilitzen, M. Forsberg, L. Persson, F. Johansson, M. Zwahlen, G. Von Heijne, J. Nielsen, F. Pontén, Tissue-based map of the human proteome, Science 347 (2015) 1260419. https://doi.org/10.1126/science.1260419.

[20] Z. Tang, B. Kang, C. Li, T. Chen, Z. Zhang, GEPIA2: an enhanced web server for large-scale expression profiling and interactive analysis, Nucleic Acids Research 47 (2019) W556–W560. https://doi.org/10.1093/nar/gkz430.

[21] R. Kadirvelraj, Z.A. Wood, Human Alpha-1,6-fucosyltransferase (FUT8) bound to GDP and NM5M2-Asn: 6x5u, (2020). https://doi.org/10.2210/pdb6x5u/pdb.

[22] H.M. Berman, The Protein Data Bank, Nucleic Acids Research 28 (2000) 235–242. https://doi.org/10.1093/nar/28.1.235.

[23] E.F. Pettersen, T.D. Goddard, C.C. Huang, G.S. Couch, D.M. Greenblatt, E.C. Meng, T.E. Ferrin, UCSF Chimera—A visualization system for exploratory research and analysis, J Comput Chem 25 (2004) 1605–1612. https://doi.org/10.1002/jcc.20084.

[24] R.C. Johnston, K. Yao, Z. Kaplan, M. Chelliah, K. Leswing, S. Seekins, S. Watts, D. Calkins, J. Chief Elk, S.V. Jerome, M.P. Repasky, J.C. Shelley, Epik: p $K_a$ and Protonation State Prediction through Machine Learning, J. Chem. Theory Comput. 19 (2023) 2380–2388. https://doi.org/10.1021/acs.jctc.3c00044.

[25] Y. Yang, K. Yao, M.P. Repasky, K. Leswing, R. Abel, B.K. Shoichet, S.V. Jerome, Efficient Exploration of Chemical Space with Docking and Deep Learning, J. Chem. Theory Comput. 17 (2021) 7106–7119. https://doi.org/10.1021/acs.jctc.1c00810.

[26] C. Lyu, T. Chen, B. Qiang, N. Liu, H. Wang, L. Zhang, Z. Liu, CMNPD: a comprehensive marine natural products database towards facilitating drug discovery from the ocean, Nucleic Acids Research 49 (2021) D509–D515. https://doi.org/10.1093/nar/gkaa763.

[27] K. Roos, C. Wu, W. Damm, M. Reboul, J.M. Stevenson, C. Lu, M.K. Dahlgren, S. Mondal, W. Chen, L. Wang, R. Abel, R.A. Friesner, E.D. Harder, OPLS3e: Extending Force Field Coverage for Drug-Like Small Molecules, J. Chem. Theory Comput. 15 (2019) 1863–1874. https://doi.org/10.1021/acs.jctc.8b01026.

[28] D.E.V. Pires, T.L. Blundell, D.B. Ascher, pkCSM: Predicting Small-Molecule Pharmacokinetic and Toxicity Properties Using Graph-Based Signatures, J. Med. Chem. 58 (2015) 4066–4072. https://doi.org/10.1021/acs.jmedchem.5b00104.

[29] D.A. Case, H.M. Aktulga, K. Belfon, D.S. Cerutti, G.A. Cisneros, V.W.D. Cruzeiro, N. Forouzesh, T.J. Giese, A.W. Götz, H. Gohlke, S. Izadi, K. Kasavajhala, M.C. Kaymak, E. King, T. Kurtzman, T.-S. Lee, P. Li, J. Liu, T. Luchko, R. Luo, M. Manathunga, M.R. Machado, H.M. Nguyen, K.A. O'Hearn, A.V. Onufriev, F. Pan, S. Pantano, R. Qi, A. Rahnamoun, A. Risheh, S. Schott-Verdugo, A. Shajan, J. Swails, J. Wang, H. Wei, X. Wu, Y. Wu, S. Zhang, S. Zhao, Q. Zhu, T.E. Cheatham, D.R. Roe, A. Roitberg, C. Simmerling, D.M. York, M.C. Nagan, K.M. Merz, AmberTools, J. Chem. Inf. Model. 63 (2023) 6183–6191. https://doi.org/10.1021/acs.jcim.3c01153.

[30] J.A. Maier, C. Martinez, K. Kasavajhala, L. Wickstrom, K.E. Hauser, C. Simmerling, ff14SB: Improving the Accuracy of Protein Side Chain and Backbone Parameters from ff99SB, J. Chem. Theory Comput. 11 (2015) 3696–3713. https://doi.org/10.1021/acs.jctc.5b00255.

[31] D.R. Roe, T.E. Cheatham, PTRAJ and CPPTRAJ: Software for Processing and Analysis of Molecular Dynamics Trajectory Data, J. Chem. Theory Comput. 9 (2013) 3084–3095. https://doi.org/10.1021/ct400341p.

[32] S.K. Panday, E. Alexov, Protein–Protein Binding Free Energy Predictions with the MM/PBSA Approach Complemented with the Gaussian-Based Method for Entropy Estimation, ACS Omega 7 (2022) 11057–11067. https://doi.org/10.1021/acsomega.1c07037.

[33] S.H. Shaham, P. Vij, M.K. Tripathi, Advances in Targeted and Chemotherapeutic Strategies for Colorectal Cancer: Current Insights and Future Directions, Biomedicines 13 (2025) 642. https://doi.org/10.3390/biomedicines13030642.

[34] F. Liang, Y. Xu, H. Zheng, W. Tang, Establishing a carcinoembryonic antigen-associated competitive endogenous RNA network and forecasting an important regulatory axis in colon

adenocarcinoma patients, J Gastrointest Oncol 15 (2024) 220–236. https://doi.org/10.21037/jgo-24-43.

[35] Q. Yang, L.-X. Wang, Mammalian α-1,6-Fucosyltransferase (FUT8) Is the Sole Enzyme Responsible for the N-Acetylglucosaminyltransferase I-independent Core Fucosylation of High-mannose N-Glycans, Journal of Biological Chemistry 291 (2016) 11064–11071. https://doi.org/10.1074/jbc.M116.720789.

[36] J. Chen, L. Yang, C. Li, L. Zhang, W. Gao, R. Xu, R. Tian, Chemical Proteomic Approach for In-Depth Glycosylation Profiling of Plasma Carcinoembryonic Antigen in Cancer Patients, Molecular & Cellular Proteomics 22 (2023) 100662. https://doi.org/10.1016/j.mcpro.2023.100662.

[37] C.-Y. Chen, Y.-H. Jan, Y.-H. Juan, C.-J. Yang, M.-S. Huang, C.-J. Yu, P.-C. Yang, M. Hsiao, T.-L. Hsu, C.-H. Wong, Fucosyltransferase 8 as a functional regulator of nonsmall cell lung cancer, Proc. Natl. Acad. Sci. U.S.A. 110 (2013) 630–635. https://doi.org/10.1073/pnas.1220425110.

[38] L. Muinelo-Romay, C. Vázquez-Martín, S. Villar-Portela, E. Cuevas, E. Gil-Martín, A. Fernández-Briera, Expression and enzyme activity of α(1,6)fucosyltransferase in human colorectal cancer, Intl Journal of Cancer 123 (2008) 641–646. https://doi.org/10.1002/ijc.23521.

[39] Y. Lv, Z. Zhang, M. Wang, Y. Wang, M. Chen, J. Jia, Y. Guo, K. Wang, Z. Li, W. Wang, H. Li, Discovery of novel FUT8 inhibitors with promising affinity and in vivo efficacy for colorectal cancer therapy, Bioorganic Chemistry 149 (2024) 107492. https://doi.org/10.1016/j.bioorg.2024.107492.

# Chapter 6

## Summary

## Chapter 6: Summary

Colorectal cancer (CRC) is one of the most frequently diagnosed cancers worldwide and continues to be a major cause of cancer-related mortality. CRC progression was earlier thought to be driven by genetic mutations within epithelial cells; however, growing evidences clear that tumor progression is not determined only by the genetic alterations within cancer cells. Importantly, the surrounding tumor microenvironment (TME) plays a crucial role in shaping disease progression and therapeutic response. The TME contains a complex network of stromal cells and immune cells that continuously interact with tumor cells through the release of soluble factors as well as extracellular vesicles. Among the immune cells present within the TME, macrophages are particularly abundant and functionally diverse and can adopt different activation states depending on the signals they receive from their surroundings. The signalling molecule includes soluble cytokines, growth factors, and extracellular vesicles as important mediators of intercellular communication during cancer progression. Among these vesicles, exosomes have received particular attention due to their ability to transfer biologically active molecules from donor to recipient cells and emerge as a key regulator of tumor progression and immunomodulation. The current study was designed to understand the mechanistic role of CRC-derived exosomes in the regulation of macrophage polarization, with a specific focus on NF-κB signalling pathways. In addition, we also explore the therapeutic potential of targeting the immune checkpoint PD-1/PD-L1 axis.

The Main objectives of this work were to understand how CRC-derived exosomes influence macrophage reprogramming within TME. Macrophages exhibit considerable plasticity and can adopt a classically activated antitumor M1-like TAMs state or alternatively

activated tumor supportive M2-like TAMs state. The finding from our study demonstrates that CRC-derived exosomes are a crucial mediator of the switching of macrophages towards a tumor-supportive phenotype. The exposure of macrophages to CRC cell-derived exosomes resulted in a significant change in morphology, gene expression, and functional response, indicating a phenotypic change towards a tumor-supportive type.

Mechanistically, our study provides strong evidence of the involvement of NF-κB signalling in exosome-mediated macrophage polarization. The NF-κB transcription factor is the master regulator that controls the expression of genes involved in inflammation and immune response, cell survival, and tumor progression. The result from our experiments reveals that the exposure of macrophages to CRC cells-derived exosomes leads to a time-dependent activation of NF-κB signalling, as evidenced by increased phosphorylation of IKK and degradation of IκB and subsequently translocation of NF-κB into the nucleus. The early phage activation occurs within minutes to hours after the exosome treatment, but over time, exosomal cargo rapidly triggers intracellular signalling and reprograms macrophages towards tumor supportive types, which reflects an adaptive cellular response. These molecular changes contribute to the establishment of a pro-tumorigenic microenvironment, which helps in aggressive tumor growth, angiogenesis, and immune evasion.

Further, we want to confirm the role of NF-κB signalling, so we treat cells with IKK inhibitor TPCA-1. This inhibition of IKK effectively reduced exosome-induced NF-κB activation, as evidenced by decreased IKK phosphorylation and stabilization of IκB levels. The IKK inhibition in macrophages resulted in a significant decrease in the downstream signalling cascade, confirming the critical role of

IKK/NFκB pathways in response to the CRC-derived exosomes. These results highlight the potential role in the initial activation of tumor-promoting inflammation in macrophages, while over time, exosomal cargo comes into play and initiates activation of other signalling pathways that switch macrophages towards an anti-inflammatory phenotype.

Additionally, in our study, we observed that exosomes derived from CRC cells upregulated PD-L1 expression in macrophages. Furthermore, conditioned medium from these exosome-treated macrophages was collected and applied to CRC cells, revealing that macrophage-derived factors further enhanced PD-L1 expression in tumor cells compared to untreated controls. The upregulated expression within both the cells synergistically suppresses T cell function through apoptosis and promotes tumor immune escape. Although monoclonal antibodies that inhibit PD-1/PD-L1 interactions have achieved clinical success, but face some drawbacks, including high cost, immune-related adverse effects, and limited tumor penetration. Consequently, identifying small-molecule inhibitors capable of disrupting this interaction is gaining significant attention as a promising alternative to overcome these limitations.

Based on these observations, we turned towards an in-silico approach for the identification of potential PD-L1 inhibitors, aiming to design small molecules with favourable binding and therapeutic properties. A marine natural product database was used as source of structurally different and biologically active compounds. The molecular docking and MD simulations was performed to identify binding energy and interaction patterns of these compounds with PD-L1. The analysis identified few lead compounds with promising binding characteristics indicates their potential to disrupt the PD-

1/PD-L1 interaction. In our in-silico study, the lead compound CMNPD3605 displays better performance compared to positive control compound which is already under clinical investigations. The inhibition of the PD-1/PD-L1 signalling is expected to restore T cells functions and inhibits tumor growth.

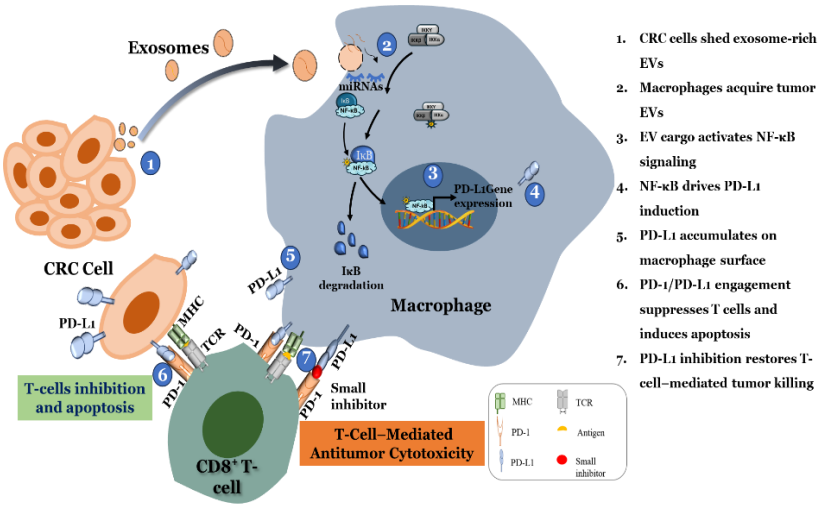



**Figure 6.1**. Cancer cells and secreted exosomes upregulate PD-L1 in macrophages, targeting PD-1/PD-L1 interaction and restoring T-Cell-mediated response in CRC

Similarly, immune check point PD-1/PD-L1 targeting, we also explored the functional role of glycoproteins in CRC progression. In the literature survey and the Human Protein Atlas (HPA) data analysis, significantly upregulated expression of carcinoembryonic antigen (CEA) glycoprotein was observed in patient samples and experimental models. This upregulated CEA molecule enhances CRC cell proliferation, metastasis, and promotes macrophage polarization towards a tumor-promoting phenotype. Due to the structural complexity and highly glycosylated nature of CEA, direct targeting using small molecules was considered challenging. Therefore, we explored the glycosylation machinery regulating CEA function, and we identified that FUT8 is a solo enzyme

involved in core fucosylation of CEA proteins. Core fucosylation is necessary to maintain the structural integrity and oncogenic function of CEA proteins. Therefore, targeting FUT8-mediated core fucosylation of CEA to destabilize its structure is an important and promising strategy. To target FUT8, a marine-derived compound was evaluated using computational approaches. In the screening result, we identified promising compounds with favorable binding, stability, and pharmacokinetic properties. The overall approach includes targeting the glycosylation of CEA to limit its function and suppress CRC progression. The findings from these studies provide a foundation for further experimental validation of screened compounds and highlight their potential in cancer immunotherapy.

Collectively, the present study provides a comprehensive understanding of cross-talk between CRC cells derived exosomes, macrophage phenotypic change, inflammatory signaling, and immune checkpoint regulation. Our study highlights the role of exosomes within TME and identifies that NF-κB signaling is one of the major pathways driving macrophage phenotypic change. Furthermore, it also underscores targeting PD-1/PD-L1 and glycoprotein-mediated signaling using marine database-derived small molecule will be new potential therapeutic interventions. Overall, the integration of experimental and computational approaches in this study enhances our understanding and opens new avenues for the development of CRC treatment.

At last, regardless of findings still, there remain certain open hangs in the current work which could be definitely addressed in the future. This study primarily relies on in-vitro and in silico data; further validation is needed in an in vivo model or a clinical sample to establish translational relevance. Additionally, the specific exosome containing cargo responsible for macrophage polarization

remains to be fully characterized. Further study should focus on detailed profiling of key components, including miRNAs, proteins or glycoproteins, and lipids, to identify key mediators of macrophage reprogramming.

# Chapter 7

## Future Prospects

## Chapter 7: Future Prospects

The findings of the present study provide important insight into the function of CRC cells-derived exosomes in the regulation of macrophage polarization and temporal gene expression kinetics during both the early and late phases of macrophage reprogramming. Additionally, it also highlights that CRC cell-derived exosomes activate NF-κB signaling, which further upregulates PD-L1 expression in macrophages. The blockade of PD-1/PD-L1 immune checkpoint using a small molecule may represent a potential therapeutic strategy for CRC treatment. Furthermore, we also explored targeting glycoproteins specially CEA, which is a well-established marker significantly overexpressed in CRC and contributes significantly to CRC cells invasion, metastasis, and tumor progression. Targeting CEA with small molecules is not feasible due to its extensive glycosylation and complex structure; therefore, we targeted its biosynthesis using the FUT8 inhibitor. This formed the base for future endless possibilities to be explored in the direction of both therapeutics as well as elucidating the signaling mechanisms in CRC.

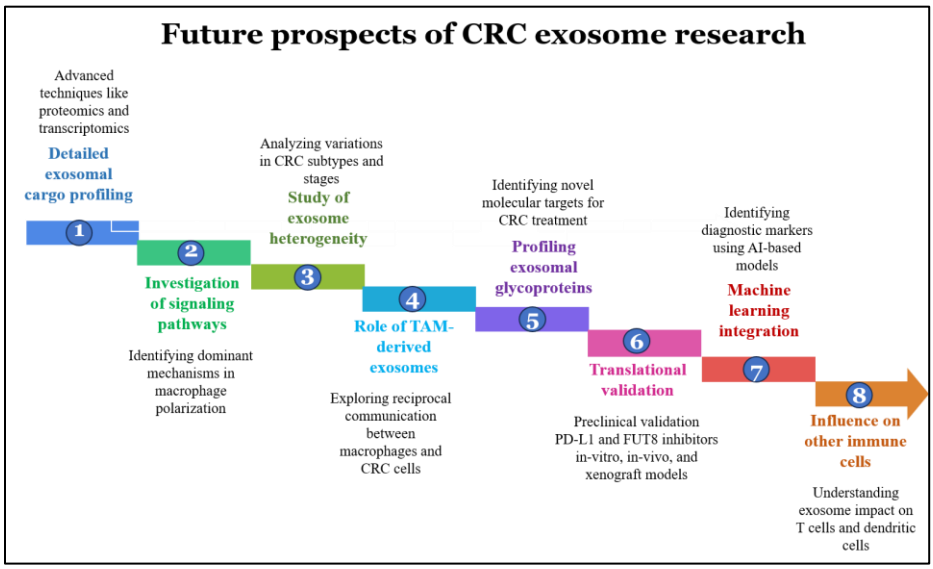



**Figure 7.1 Potential future directions from the current research work.**

- One of the key directions that warrants further exploration is detailed profiling of exosomal cargo responsible for macrophage reprogramming. However, this study establishes the functional role of CRC-derived exosomes, but the precise molecular component involvement remains unclear. Advanced techniques, including Proteomics, transcriptomics, and RNA sequencing, can be used for profiling of exosomes. Particularly can be focus on miRNAs and glycoproteins, which are majorly responsible for macrophage polarization and CRC progression.
- Additionally, quantitative cell counting and flow cytometric analysis using specific M1/M2 markers would provide more robust quantitative validation of macrophage polarization. In current study, prominent NF-κB activation was observed during the early time point following CRC-derived exosome treatment; but over the time response was diminished. This suggest that alternative signaling pathways may become dominant during the later timepoint of macrophage polarization. Therefore, further investigation is required to identify which signaling mechanism is dominant at later timepoint during exosome-mediated macrophage reprogramming and tumor progression.
- Another important direction involves the investigation of heterogeneity of exosomes derived from CRC subtypes and stages. Since CRC is a highly heterogeneous disease, exosomes released from early and late-stage tumors may contain different biological signals. Understanding these variations could help to identify novel exosome-based biomarkers for CRC diagnosis and therapeutic response.
- One more promising future direction would be to investigate the role of the other side, i.e., exosomes released from tumor-associated macrophages (TAMs) in CRC cells. While the present study focuses on CRC-derived exosomes and their effect on macrophages. It is

also equally important to understand reciprocal communication from macrophages to tumor cells. It will be interesting to see how TAMs-secreted exosomes support CRC cells proliferation, metastasis, immune evasion, and therapy resistance. This may provide deeper insight into bidirectional exosome mediated communication within TME.

- In addition, the detailed profiling of exosomal glycoproteins to identify novel molecular targets involved in CRC progression. To understand glycoprotein-mediated signaling and their role in macrophage polarization during CRC progression. Furthermore, targeting this glycoproteins synthesis in CRC cells or inhibiting their downstream activity in macrophages will be novel therapeutic approach to suppress tumor progression and restore anti-tumor immune response.
- From a translational perspective, currently, both of our therapeutic approaches in this thesis are based on comprehensive in silico analysis. Although the computational findings provide a strong rationale for the identified lead compounds, their biological efficacy and safety remain to be experimentally validated. Future studies will focus on validating these candidates through in vitro assay using CRC cell lines, followed by in vivo validation in an appropriate animal model, and then preclinical evaluation. If these studies are successful, the identified compound could be further optimized and advanced towards a clinical trial. These studies will provide deeper insight about response in TME and help to improve clinical translation.
- In the future, machine learning approaches can be integrated into this project to identify novel diagnostic markers using data sets. Combining transcriptomic profiling with an artificial intelligence-based predictive model may help uncover key molecular signatures associated with macrophage polarization and cancer development.

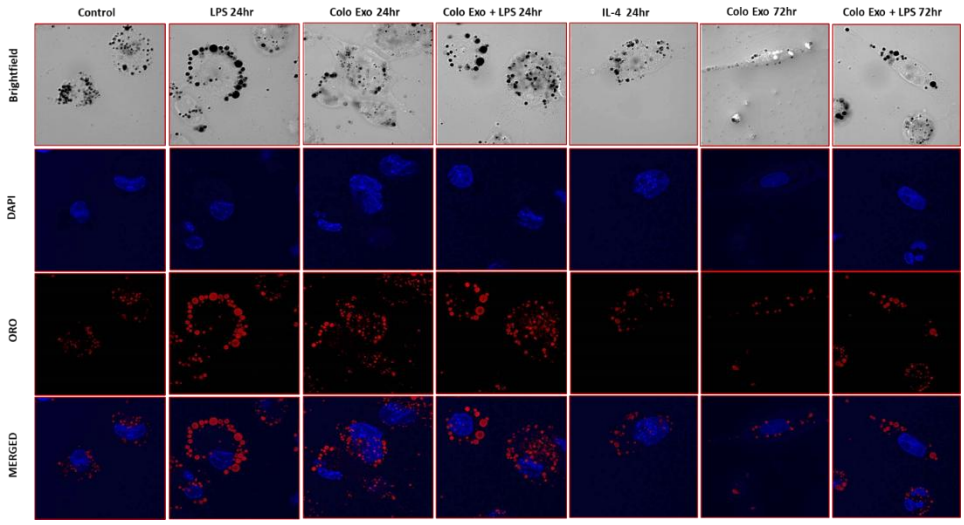
- Finally, future studies should also explore how CRC-derived exosomes influence other immune cells, including T cells and dendritic cells. Understanding this broader tumor immune crosstalk may provide a more comprehensive view of exosome-dependent immune regulation in CRC progression.

In conclusion, our findings lay the strong foundation for future research focused on exosome mediated communication between CRC cells and tumor-associated macrophages. Further exploration using advanced molecular approaches and clinically relevant models may help for identification of novel molecular mechanisms involved in tumor progression and immune regulation.

# APPENDIX-A

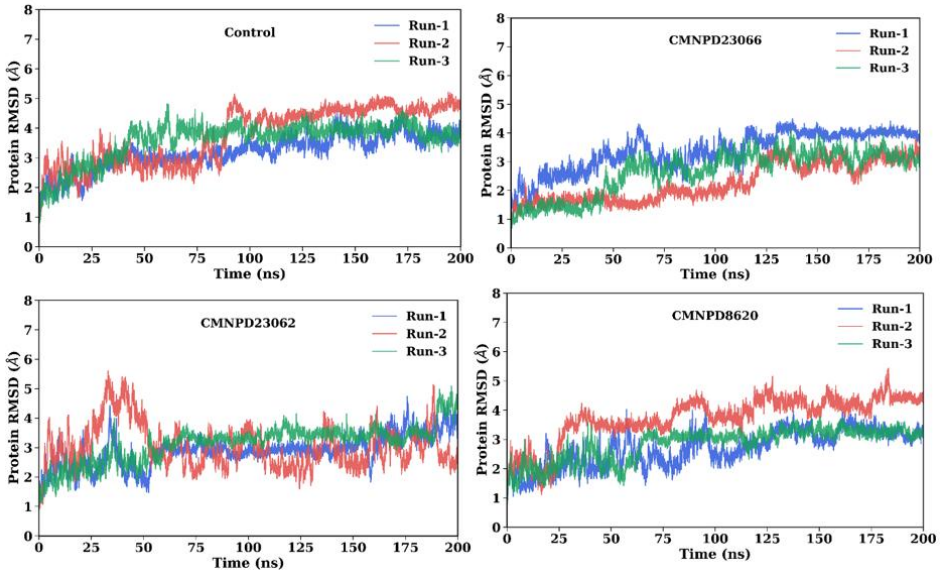
## Appendix A: Supplementary Figure

## Supplementary Figures from Chapter 3:

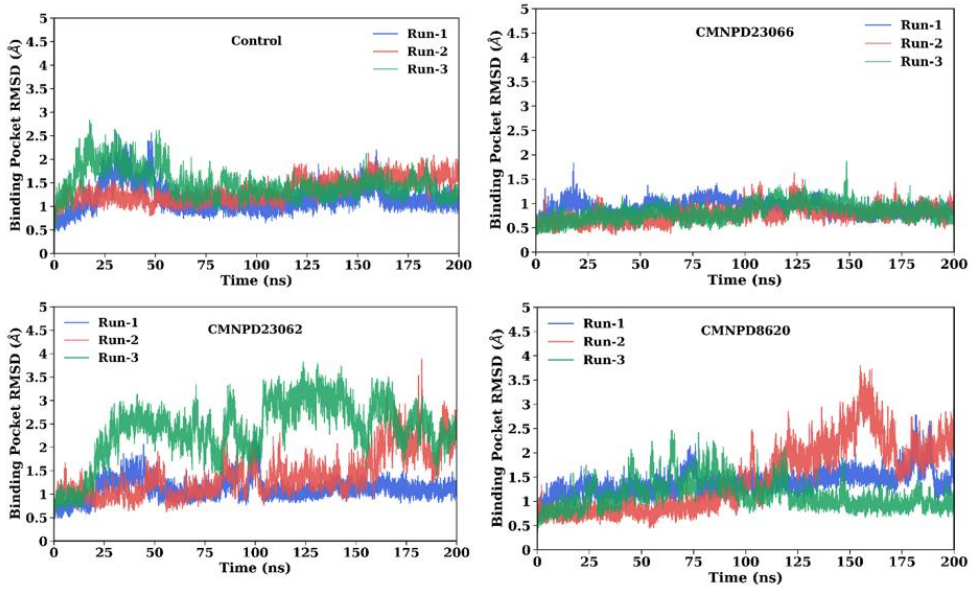



**Supplementary Figure S3.1: Phagocytic activity of THP-1 macrophages treated with CRC cell-derived exosomes assessed by Oil Red O staining.** THP-1-derived macrophages were treated with colorectal cancer (CRC) cell-derived exosomes under various conditions for 24 and 72 hrs. Cells were then incubated with oxidized LDL and stained with Oil Red O (ORO) to evaluate phagocytic activity. ORO staining (red) indicates phagocytosed material. Notably, macrophages treated with LPS and/or exosomes for 24 hours exhibited enhanced phagocytic activity, characteristic of a pro-inflammatory (M1-like) phenotype. In contrast, reduced phagocytic activity was observed in macrophages treated with IL-4 or exosomes for 72 hrs and morphology matching with of an anti-inflammatory (M2-like) phenotype. supplementaryImages were acquired using a confocal microscope at 100× (scale bar = 20 μm).

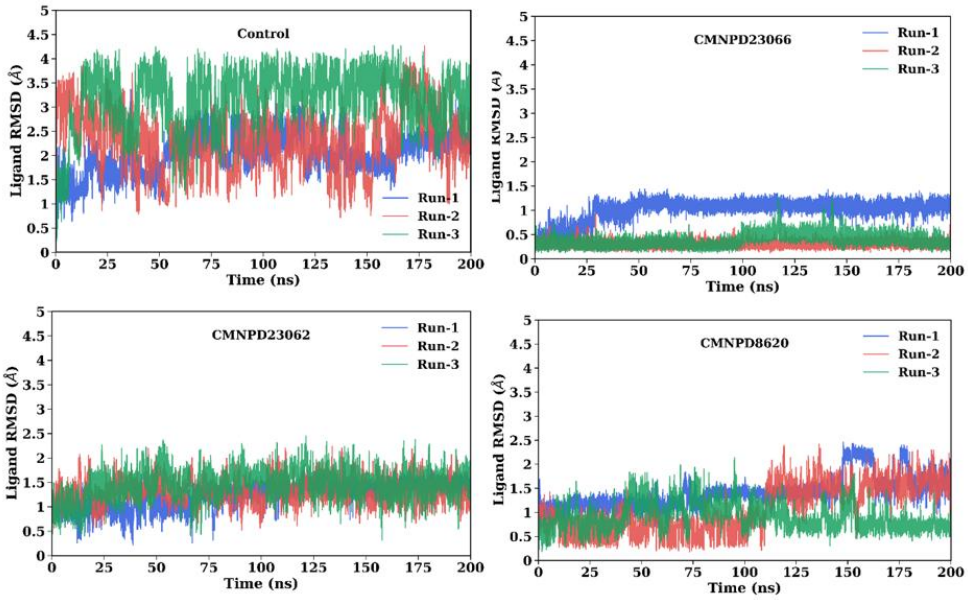
**Supplementary Figure from Chapter 5:**



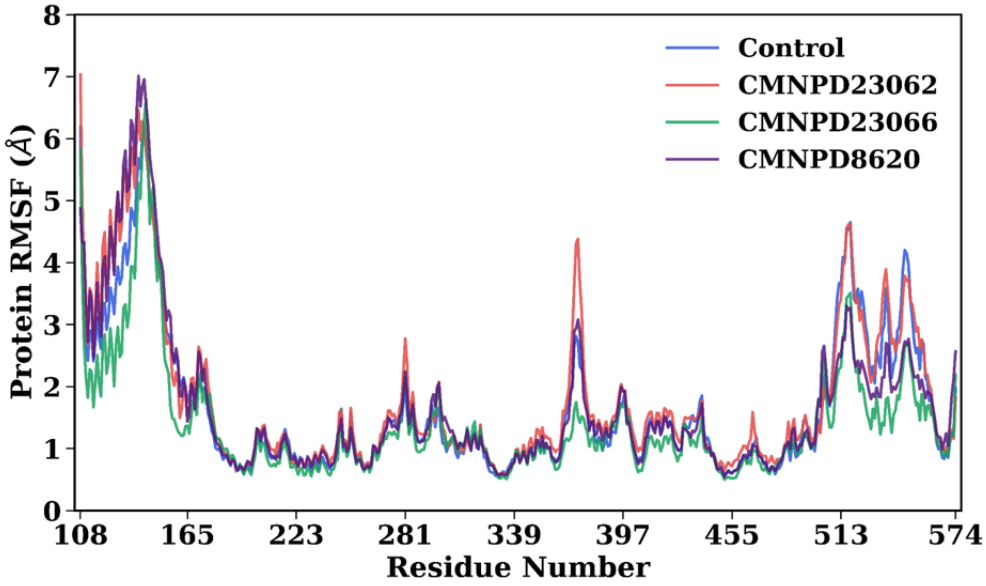

**Supplementary Figure S5.1:** Protein backbone RMSD profiles of FUT8 complexes with the control ligand, CMNPD23066, CMNPD23062, and CMNPD8620 across three independent 200-ns molecular dynamics simulations.



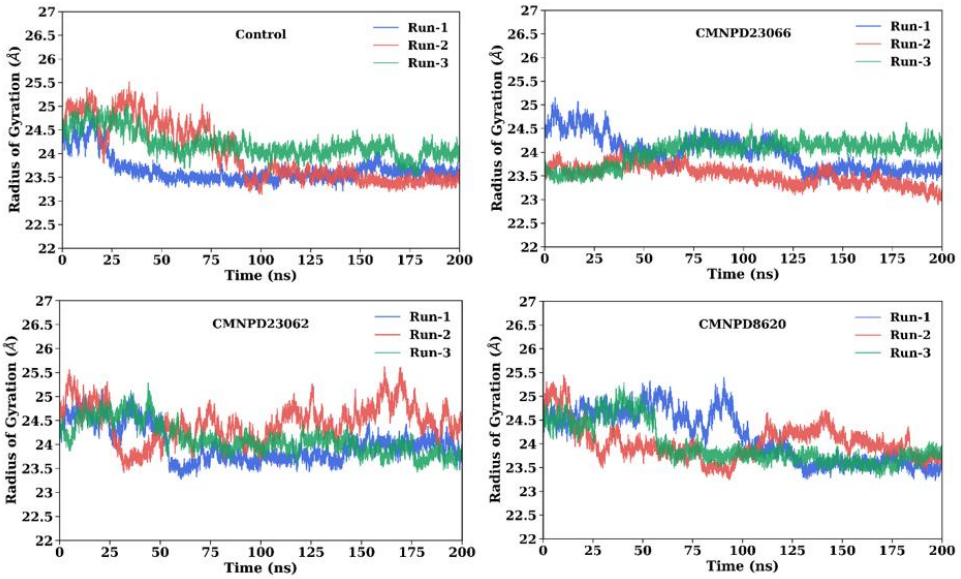

**Supplementary Figure S5.2**: Binding-pocket RMSD profiles of FUT8 complexes with the control ligand, CMNPD23066, CMNPD23062, and CMNPD8620 across three independent 200-ns molecular dynamics simulations.



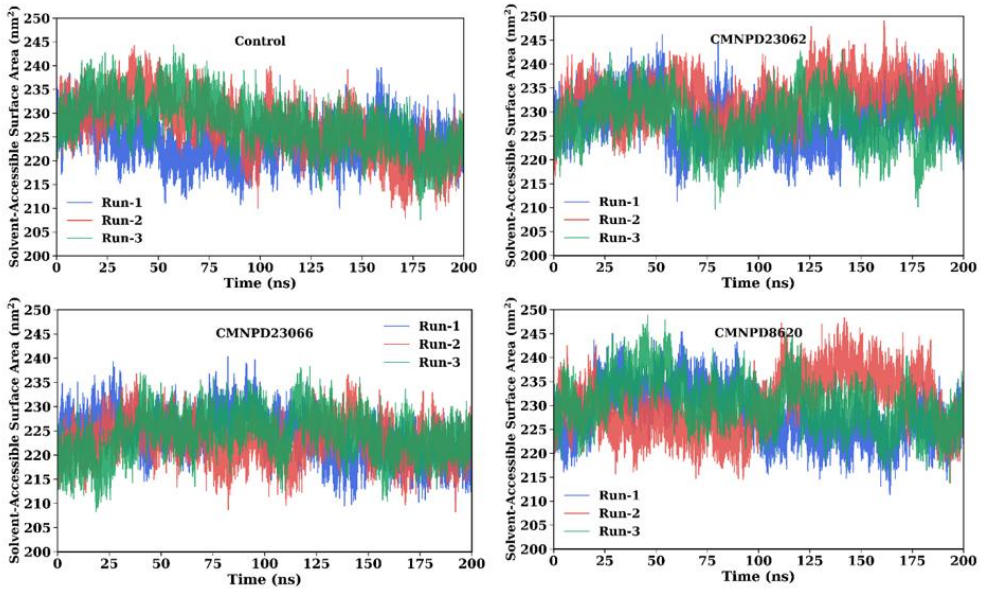

**Supplementary Figure S5.3:** Ligand RMSD profiles of the control ligand, CMNPD23066, CMNPD23062, and CMNPD8620 across three independent 200-ns molecular dynamics simulations.



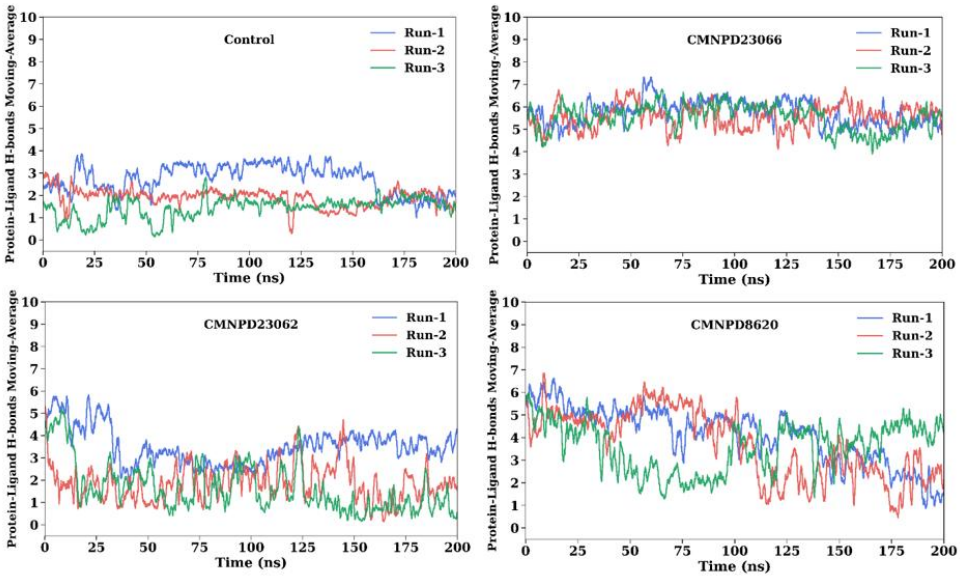

**Supplementary Figure S5.4**: Residue-wise RMSF profiles of FUT8 in complex with the control ligand, CMNPD23062, CMNPD23066, and CMNPD8620 across the molecular dynamics simulations.



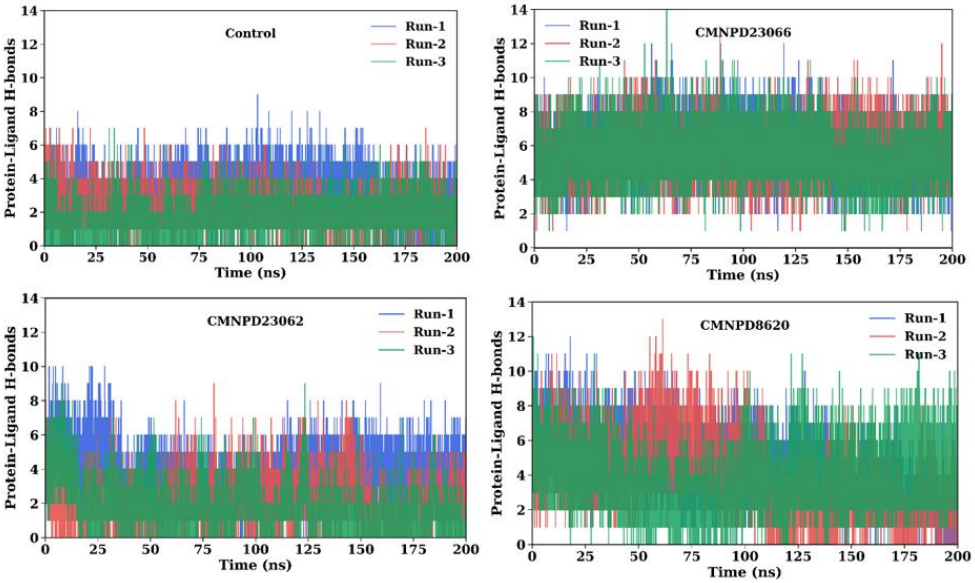

**Supplementary Figure S5.5:** Radius of gyration (Rg) profiles of FUT8 complexes with the control ligand, CMNPD23066, CMNPD23062, and CMNPD8620 across three independent 200-ns molecular dynamics simulations.




**Supplementary Figure S5.6:** Solvent-accessible surface area (SASA) profiles of FUT8 complexes with the control ligand, CMNPD23062, CMNPD23066, and CMNPD8620 across three independent 200-ns molecular dynamics simulations.




**Supplementary Figure S5.7:** Moving-average protein–ligand hydrogen-bond profiles of FUT8 complexes with the control ligand, CMNPD23066, CMNPD23062, and CMNPD8620 across three independent 200-ns molecular dynamics simulations.




**Supplementary Figure S5.8:** Protein–ligand hydrogen-bond counts of FUT8 complexes with the control ligand, CMNPD23066, CMNPD23062, and CMNPD8620 across three independent 200-ns molecular dynamics simulations.

## Appendix B: Supplementary Tables

### Supplementary Table S3.1 Primer sequences from Chapter 3.

| Sr. No. | Gene | Sequence |
|---|---|---|
| **1** | h-GAPDH-F | 5'-AATCCCATCACCATCTTCCA-3' |
| | h-GAPDH-R | 5'-TGGACTCCACGACGTACTCA-3' |
| **2** | h-FIBRONECTIN-F | 5'-CTGACAGCTCATCCGTGGTT-3' |
| | h-FIBRONECTIN-R | 5'-TTGGTGGGCTGACATTCTCC-3' |
| **3** | h-SNAIL 1-F | 5'-ACCCCAATCGGAAGCCTAAC-3' |
| | h-SNAIL 1-R | 5'-TCCCAGATGAGCATTGGCAG-3' |
| **4** | h-TNF-a-F | 5'-CCCGAGTGACAAGCCTGTAG-3' |
| | h-TNF-a-R | 5'-GATGGCAGAGAGGAGGTTGAC-3' |
| **5** | h-PDGF-A-F | 5'-ATAAAGGCCGGAACAGCTGAAA-3' |
| | h-PDGF-A-R | 5'-GCGCGCAAAGTATCTCTATCTA-3' |
| **6** | h-IL-10-F | 5'-TGCCTTCAGCAGAGTGAAGA-3' |
| | h-IL-10-R | 5'-GTCTTGGTTCTCAGCTTGGG-3' |
| **7** | h-IL 12 B -F | 5'-AGGGACATCATCAAACCTGACC-3' |
| | h-IL 12 B -R | 5'-GCTGAGGTCTTGTCCGTGAA-3' |
| **8** | h-IL 23A-F | 5'-GGGACAACAGTCAGTTCTGCTT-3' |
| | h-IL 23A-R | 5'-TGGGACTGAGGCTTGGAATC-3' |
| **9** | h-ARG-1-F | 5'-ACTTAAAGAACAAGAGTGTGATGTG-3' |
| | h-ARG-1-R | 5'-CACCAGGCTGATTCTTCCGT-3' |
| **10** | h-PD-L1-F | 5′-ATGGTGGTGCCGACTACAAG-3' |
| | h-PD-L1-R | 5'-GGAATTGGTGGTGGTGGTCT-3' |
| **11** | h-AKR1B1-F | 5'-AAGCCGTCTCCTGCTCA-3' |
| | h-AKR1B1-R | 5'-TTGCTGACGATGAAGAGC-3' |

**Supplementary Table S4.1, From Chapter 4:**

Predicted ADMET Properties for Selected PD-L1 Inhibitors. In silico ADMET profiles of the control inhibitor (INCB086550) and three leading CMNPD-derived ligands. Parameters include molecular weight (Mol wt), Caco-2 permeability (log Papp in 10^-6 cm/s), predicted blood–brain barrier (BBB) permeability (log BB), CYP2D6 substrate status, AMES test for mutagenicity, hepatotoxicity, and skin sensitization. All compounds exhibit favorable drug-likeness with no predicted CYP2D6 liability, mutagenicity, hepatotoxicity, or skin sensitization risk.

| Compound ID | INCB086550 CONTROL | CMNPD16477 | CMNPD21979 | CMNPD3605 |
|---|---|---|---|---|
| **Mol Wt (Da)** | **694.816** | **709.695** | **592.605** | **663.737** |
| **Caco2 permeability: Numeric (log Papp in $10^{-6}$ cm/s)** | **-0.118** | **-0.316** | **0.14** | **-0.118** |
| **BBB permeability Numeric (log BB)** | **-1.098** | **-1.815** | **-2.044** | **-1.098** |
| **CYP2D6 substrate** | **No** | **No** | **No** | **No** |
| **AMES toxicity** | **No** | **No** | **No** | **No** |
| **Hepatotoxicity** | **No** | **No** | **No** | **No** |
| **Skin Sensitisation** | **No** | **No** | **No** | **No** |

**Supplementary Table S4.2, From Chapter 4:**

Average metrics calculated using the 200 ns of production run trajectories, with standard deviations in parentheses.

| Metric | Control | CMNPD16477 | CMNPD21979 | CMNPD3605 |
|---|---|---|---|---|
| **Protein RMSD (Å)** | 1.31 (0.15) | 1.13 (0.13) | 1.28 (0.18) | 1.19 (0.21) |
| **Ligand RMSD (Å)** | 3.09 (0.22) | 2.57 (0.17) | 3.50 (1.05) | 3.37 (1.19) |
| **Binding Pocket RMSD (Å)** | 0.73 (0.11) | 0.61 (0.11) | 0.90 (0.09) | 0.45 (0.08) |
| **Ligand-Pocket Distance (Å)** | 6.34 (0.67) | 10.82 (0.73) | 8.75 (0.67) | 8.30 (1.06) |
| **Ligand-Protein Distance (Å)** | 15.29 (0.90) | 17.86 (0.58) | 13.39 (0.37) | 15.87 (1.20) |
| **Radius of Gyration (Å)** | 13.62 (0.08) | 13.63 (0.07) | 13.69 (0.09) | 13.67 (0.08) |
| **Solvent-Accessible Surface Area ($nm^2$)** | 58.24 (1.96) | 57.44 (1.58) | 57.27 (1.89) | 57.03 (1.94) |

**Supplementary Table S4.3, From Chapter 4:**

Analysis of hydrogen bond formation through the molecular dynamics simulations. Only hydrogen bonds with an occupancy greater than 10% are shown.

| Compound ID | Acceptor | Donor | Dist. | Angle | Occupancy (%) |
|---|---|---|---|---|---|
| **INCB086550 CONTROL** | Lig@N4 | Arg125@NH1 | 2.90 | 154.41 | 20.07 |
| | DAsp61@OD1 | Lig@N5 | 2.78 | 157.68 | 39.61 |
| | Asp26@OD2 | Lig@N1 | 2.74 | 157.64 | 35.20 |
| | Asp26@OD1 | Lig@N1 | 2.74 | 158.14 | 34.21 |
| | Asp61@OD2 | Lig@N5 | 2.78 | 157.12 | 34.03 |
| | Asp61@OD2 | Lig@O3 | 2.69 | 164.68 | 31.96 |
| | Asp61@OD1 | Lig@O3 | 2.68 | 164.18 | 21.47 |
| **CMNPD16477** | Lig@O14 | Ser117@OG | 2.79 | 162.48 | 19.45 |
| | Gln66@OE1 | Lig@O6 | 2.73 | 161.45 | 16.45 |
| **CMNPD21979** | - | - | - | - | - |
| **CMNPD3605** | Lig@O13 | Arg113@NH2 | 2.80 | 159.95 | 50.87 |
| | Lig@O13 | Arg125@NH2 | 2.81 | 160.22 | 49.35 |
| | Lig@O12 | Arg125@NE | 2.84 | 160.24 | 47.33 |
| | Lig@O3 | Tyr123@OH | 2.82 | 157.44 | 38.46 |
| | Lig@O12 | Arg113@NE | 2.84 | 160.89 | 34.49 |
| | Lig@O12 | Arg125@NH2 | 2.82 | 154.87 | 25.45 |
| | Lig@O12 | Arg113@NH2 | 2.82 | 154.73 | 20.74 |
| | Lig@O13 | Arg113@NE | 2.84 | 154.40 | 13.16 |
| | Lig@O13 | Arg125@NE | 2.86 | 157.50 | 12.26 |
| | Glu58@OE2 | Lig@O9 | 2.70 | 159.37 | 11.63 |
| | Glu58@OE1 | Lig@O8 | 2.71 | 160.99 | 10.63 |

**Supplementary Table S4.4, From Chapter 4:**

Residue-wise binding free energy (kcal/mol) decomposition of the crucial contributing residues.

| Compound | Residue | $E_{vdW}$ (kcal/mol) | $E_{elec}$ (kcal/mol) | $G_{pol}$ (kcal/mol) | $G_{np}$ (kcal/mol) | $G_{total}$ (kcal/mol) |
|---|---|---|---|---|---|---|
| **INCB086550 CONTROL** | Lig | -16.58 | -68.75 | 62.68 | 0 | -22.65 |
| | Asp26 | -2.14 | -29.99 | 30.52 | 0 | -1.61 |
| | Asp61 | -1.08 | -47.28 | 47.33 | 0 | -1.03 |
| | Lys124 | -1.44 | 14.87 | -11.86 | 0 | 1.56 |
| **CMNPD16477** | Lig | -14.25 | -9.72 | 16.49 | 0 | -7.48 |
| | Tyr56 | -1.99 | -0.57 | 1.02 | 0 | -1.54 |
| | Ala121 | -1.60 | 0.66 | -0.44 | 0 | -1.38 |
| | Met115 | -1.57 | -0.56 | 0.98 | 0 | -1.15 |
| | Ile54 | -1.06 | 0.003 | -0.06 | 0 | -1.11 |
| | Gly120 | -1.76 | -1.49 | 2.21 | 0 | -1.03 |
| | Gly119 | -1.61 | -2.07 | 2.76 | 0 | -0.92 |
| **CMNPD21979** | Lig | -20.74 | 3.56 | 9.08 | 0 | -8.10 |
| | Tyr56 | -3.91 | -0.71 | 1.55 | 0 | -3.07 |
| | Met115 | -4.14 | -0.77 | 2.08 | 0 | -2.83 |
| | Arg113 | -1.18 | -2.63 | 1.38 | 0 | -2.43 |
| | Tyr123 | -2.25 | -0.15 | 1.26 | 0 | -1.14 |
| | Asp61 | -0.33 | 2.66 | -0.88 | 0 | 1.45 |
| | Glu58 | -1.02 | 5.68 | 6.55 | 0 | 11.21 |
| **CMNPD3605** | Lig | -13.06 | -55.94 | 53.36 | 0 | -15.63 |
| | Arg113 | -1.82 | -48.32 | 41.65 | 0 | -8.49 |
| | Arg125 | -0.19 | -49.57 | 41.85 | 0 | -7.89 |
| | Tyr123 | -5.39 | -2.81 | 6.22 | 0 | -1.98 |
| | Met115 | -1.24 | -0.32 | 0.60 | 0 | -0.96 |
| | Asp122 | -0.32 | 14.26 | -12.98 | 0 | 0.97 |
| | Glu58 | -0.96 | 19.57 | -15.96 | 0 | 2.65 |

**Supplementary Table from Chapter 5:**

**Supplementary Table S5.1:** Ensemble XP docking scores of FDW028 and prioritized marine-derived compounds across multiple FUT8 receptor conformations. Docking scores were obtained using the Glide XP docking protocol. More negative values indicate more favorable predicted docking. XP Docking score among CMNPD8620, CMNPD23062 and CMNPD23066 for each receptor model have been noted. FDW028 was used as the reference compound. Chain A of 6X5U was used for the original virtual-screening workflow, whereas the remaining receptor models were evaluated as part of the ensemble-docking analysis.

| FUT8 receptor model | FDW028 | CMNPD8620 | CMNPD23062 | CMNPD23066 |
|---|---|---|---|---|
| **6X5U chain A** | −6.547 | −10.496 | −11.529 | −11.452 |
| **6X5U chain B** | −6.389 | −10.839 | −11.529 | −11.452 |
| **6X5U chain C** | −4.134 | −10.588 | −10.847 | −10.429 |
| **6X5U chain D** | −7.911 | −10.601 | −11.192 | −8.686 |
| **6X5U chain E** | −4.909 | −10.725 | −11.227 | −7.962 |
| **6VLE chain A** | −3.396 | −4.409 | −5.189 | −4.322 |
| **9L65 chain A** | −2.207 | −5.278 | −5.428 | −4.576 |
| **6X5H chain A** | −3.484 | −10.055 | −11.049 | −11.478 |
| **9L64 chain A** | −3.590 | −4.547 | −5.469 | −3.660 |
| **6TKV chain A** | −7.186 | −10.125 | −9.167 | −11.049 |
| **2DE0 chain A** | −2.535 | −7.917 | −7.039 | −7.722 |

**Supplementary Table S5.2:** Average structural stability paramrters calculated using the 200 ns of production run trajectories, with standard deviations in parentheses.

| Metric | Control | CMNPD23062 | CMNPD23066 | CMNPD8620 |
|---|---|---|---|---|
| **Protein RMSD (Å)** | 3.64 (±0.30) | 3.18 (±0.41) | 3.88 (±0.29) | 3.10 (±0.36) |
| **Ligand RMSD (Å)** | 2.17 (±0.30) | 1.40 (±0.11) | 1.10 (±0.09) | 1.62 (±0.31) |
| **Binding Pocket RMSD (Å)** | 1.16 (±0.19) | 1.11 (±0.15) | 0.88 (±0.12) | 1.50 (±0.22) |
| **Radius of Gyration (Å)** | 23.59 (±0.11) | 23.89 (±0.19) | 23.74 (±0.22) | 23.66 (±0.20) |
| **Solvent-Accessible Surface Area ($nm^2$)** | 223.87 (±3.61) | 227.79 (±4.18) | 221.52 (±3.62) | 224.87 (±3.46) |

**Supplementary table S5.3:** Analysis of hydrogen bond formation through the molecular dynamics simulations. Only hydrogen bonds with an occupancy greater than 10% are shown.

| Acceptor | Donor | Dist. | Angle | Occupancy (%) |
|---|---|---|---|---|
| | | **Control** | | |
| **Lig@N6** | Lys369@NZ@HZ2 | 2.87 | 159.55 | 15.90 |
| **Lig@N6** | Lys369@NZ@HZ1 | 2.87 | 160.04 | 12.45 |
| **Lig@N6** | Lys369@NZ@HZ3 | 2.87 | 159.55 | 10.61 |
| **Asp368@O** | Lig@N4 | 2.75 | 157.02 | 65.67 |
| **Glu373@OE1** | Lig@N4 | 2.75 | 153.45 | 40.25 |
| **Glu373@OE2** | Lig@N4 | 2.76 | 154.51 | 39.73 |
| **Glu373@OE1** | Lig@N4 | 2.73 | 160.66 | 11.03 |
| **Glu373@OE2** | Lig@N4 | 2.74 | 160.68 | 10.38 |
| | | **CMNPD23062** | | |
| **Lig@O4** | Gln470@N | 2.82 | 162.42 | 55.52 |
| **Lig@O5** | Ser469@OG | 2.70 | 163.58 | 48.64 |
| **Lig@O4** | Ser469@OG | 2.71 | 164.02 | 29.64 |
| **Lig@O5** | Gln470@N | 2.81 | 161.27 | 29.18 |
| **Lig@O5** | Arg365@NH2 | 2.76 | 153.71 | 16.57 |
| **Lig@O5** | Arg365@NE | 2.83 | 149.57 | 12.90 |
| **Ser468@O** | Lig@N4 | 2.84 | 153.32 | 20.26 |
| **Ser446@O** | Lig@O1 | 2.85 | 150.23 | 14.06 |
| **Ser446@OG** | Lig@O1 | 2.83 | 145.24 | 13.35 |
| | | **CMNPD23066** | | |
| **Lig@O4** | Arg365@NH2 | 2.78 | 152.00 | 95.63 |
| **Lig@O4** | Arg365@NE | 2.85 | 148.29 | 67.11 |
| **Lig@O5** | Gln470@N | 2.89 | 165.20 | 39.20 |
| **Lig@O5** | Lys369@NZ@HZ2 | 2.80 | 151.24 | 22.22 |
| **Lig@O4** | Lys369@NZ@HZ1 | 2.83 | 151.36 | 22.18 |
| **Lig@O5** | Lys369@NZ@HZ1 | 2.81 | 148.71 | 20.39 |
| **Lig@O4** | Lys369@NZ@HZ2 | 2.83 | 151.50 | 20.19 |
| **Lig@O5** | Lys369@NZ@HZ3 | 2.81 | 150.16 | 14.35 |
| **Lig@O4** | Lys369@NZ@HZ3 | 2.83 | 151.65 | 13.37 |
| **Asp368@OD2** | Lig@N2 | 2.81 | 155.37 | 71.89 |
| **Glu373@OE2** | Lig@N4 | 2.76 | 156.10 | 55.04 |
| **Glu373@OE1** | Lig@N4 | 2.76 | 156.03 | 38.57 |
| **Asp453@OD2** | Lig@N3 | 2.83 | 154.51 | 38.35 |
| | | **CMNPD8620** | | |
| **Lig@O3** | Arg465@NH2 | 2.77 | 155.49 | 39.47 |
| **Lig@O2** | Gln470@N | 2.86 | 164.30 | 32.50 |
| **Lig@O3** | Gln470@N | 2.87 | 166.23 | 28.66 |
| **Lig@O2** | Arg365@NH2 | 2.78 | 156.62 | 22.75 |
| **Lig@O3** | Arg365@NE | 2.86 | 148.53 | 21.77 |
| **Lig@O2** | Ser469@OG | 2.69 | 163.38 | 19.10 |
| **Lig@O3** | Ser469@OG | 2.67 | 164.59 | 14.84 |
| **Lig@O3** | Lys369@NZ@HZ2 | 2.78 | 160.19 | 12.76 |
| **Lig@O3** | Lys369@NZ@HZ3 | 2.78 | 159.60 | 12.24 |
| **Lig@O3** | Lys369@NZ@HZ1 | 2.78 | 159.97 | 12.15 |
| **Lig@O2** | Lys369@NZ@HZ2 | 2.78 | 158.80 | 11.76 |
| **Lig@O2** | Lys369@NZ@HZ3 | 2.78 | 158.78 | 11.57 |
| **Asp368@OD2** | Lig@N4 | 2.81 | 159.33 | 50.89 |

**Supplementary Table S5.4:** Residue-wise binding free energy (kcal/mol) decomposition of the crucial contributing residues.

| Residue | $E_{vdW}$ (kcal/mol) | $E_{elec}$ (kcal/mol) | $G_{pol}$ (kcal/mol) | $G_{np}$ (kcal/mol) | $G_{total}$ (kcal/mol) |
|---|---|---|---|---|---|
| | | **CONTROL** | | | |
| **Ligand** | -19.4043 | -36.1621 | 38.81032 | 0 | -16.7561 |
| **ARG 441** | -4.01449 | -15.8985 | 16.09836 | 0 | -3.81464 |
| **GLU 373** | -1.42837 | -16.8741 | 14.5904 | 0 | -3.71204 |
| **TYR 442** | -0.97338 | -1.87827 | 1.685274 | 0 | -1.16637 |
| **LEU 438** | -1.52945 | 1.351421 | -0.85288 | 0 | -1.03092 |
| | | **CMNPD23062** | | | |
| **Ligand** | -19.3821 | -31.3251 | 46.44513 | 0 | -4.26204 |
| **SER 469** | -0.29889 | -11.061 | 5.732874 | 0 | -5.62701 |
| **VAL 471** | -1.49277 | -2.94824 | 1.712795 | 0 | -2.72822 |
| **GLN 470** | -1.83576 | -1.99978 | 1.582546 | 0 | -2.253 |
| **VAL 450** | -1.54909 | 0.024203 | -0.21314 | 0 | -1.73803 |
| | | **CMNPD23066** | | | |
| **Ligand** | -17.796395 | -72.793391 | 78.74897 | 0 | -11.8408 |
| **LYS 369** | -0.068157 | -22.612129 | 14.68777 | 0 | -7.992512 |
| **ARG 365** | -1.471158 | -17.192092 | 10.78259 | 0 | -7.880663 |
| **VAL 450** | -2.18269 | -0.677366 | 0.343009 | 0 | -2.517047 |
| **ASP 368** | -0.35551 | -17.255905 | 15.25645 | 0 | -2.3555008 |
| **GLN 470** | -1.637962 | -4.679357 | 4.019432 | 0 | -2.297887 |
| **GLU 373** | 0.123009 | -14.737026 | 12.761022 | 0 | -1.852995 |
| **ALA 436** | -1.43752 | 0.009866 | 0.075515 | 0 | -1.352134 |
| | | **CMNPD8620** | | | |
| **Ligand** | -18.7514 | -51.8569 | 62.25895 | 0 | -8.34932 |
| **LYS 369** | -1.15074 | -20.9064 | 16.60362 | 0 | -5.45351 |
| **ASP 368** | -0.806 | -18.4015 | 14.0942 | 0 | -5.11325 |
| **ARG 365** | -0.79108 | -11.9352 | 10.08165 | 0 | -2.64458 |
| **GLN 470** | -1.5754 | -5.09842 | 4.38669 | 0 | -2.28712 |
| **SER 469** | -0.45189 | -4.7234 | 2.905713 | 0 | -2.26957 |
| **VAL 450** | -1.27156 | -0.061 | -0.22412 | 0 | -1.55669 |